Defining the surface proteome of apoptotic cell-derived extracellular vesicles

Rachel Butler

Doctor of Philosophy

Aston University

September 2024

Defining the surface proteome of apoptotic cell-derived extracellular vesicles

Rachel Butler

Doctor of Philosophy

Aston University

2024

Abstract

The release of extracellular vesicles is essential for intercellular communication and transport of molecular cargo. During apoptosis, cells release a significant quantity of apoptotic cell-derived extracellular vesicles (ACdEVs), which play a critical role in regulating inflammation by attracting immune cells for apoptotic cell clearance and enhancing their pro-resolving functions, thus promoting tissue homeostasis. Despite their abundance, the molecular mechanisms governing ACdEV interactions with recipient immune cells remain poorly understood. This project aimed to elucidate the surface proteome of ACdEVs to identify key surface molecules involved in immune cell engagement, with only CX3CL1 and ICAM-3 identified to date.

ACdEVs from various immune cell sources and apoptotic timepoints revealed fundamental differences in physical and molecular properties, highlighting their heterogeneity. Data mining of in-house mass spectrometry proteomic ACdEV datasets led to the selection of adhesion proteins and known immunomodulators CD31, CD47, CD49d, and CD166, for investigation. Notably, these proteins were lost from the apoptotic cell surface and detected on ACdEVs. The interactions of ACdEVs with macrophages, key regulators of apoptotic cell clearance, were also examined to assess their influence on macrophage migration, binding, internalisation, and phenotype.

Strikingly, ACdEVs were chemoattractive to macrophages, but this property was abolished by size-exclusion chromatography, suggesting disruption of a functional chemoattractive ACdEV corona. Antibody blockade enabled the functional assessment of individual proteins at the ACdEV surface. Together, these data indicated a ‘don't eat me’ function exerted by CD47 and ‘eat me’ functions exerted by CD31 and CD49d, highlighting their roles in regulating ACdEV surface interactions. Furthermore, the four adhesion proteins did not appear to modulate macrophage phenotype. This research, therefore, identifies surface proteins involved in the interactions between ACdEVs and recipient macrophages that do not affect phenotypic changes, thereby enhancing our understanding of the molecular mechanisms that facilitate ACdEV interactions with recipient cells and their role in immunomodulation.

Keywords: apoptosis, extracellular vesicle, macrophage, surface proteome, inflammation

Acknowledgments

Professional acknowledgements

I would like to thank my fantastic supervisors, especially Professor Andrew Devitt, for his invaluable guidance, unwavering support, and immense enthusiasm throughout my PhD journey; and also Professor Alan Goddard, for his continuous encouragement, for always providing an additional perspective, and for giving me a job(!). I feel very lucky to have had them as my supervisors. I would also like to thank Dr Ewan Ross for his invaluable advice, for always being a friendly face in the lab and for his encouragement to apply for this PhD project in the first place! I also thank Dr Ivana Milic for donation of proteomic datasets that were used in this project, donation of primary T cell samples used for cryoTEM analysis, as well as general lab training. I am grateful, as well, to Dr Annaïg Rozo, Dr Jimmy Gavin, Dr Jake Moorse and Dr Tom Page for their help around the lab.

I must also thank Dr Dimitri Aubert, who has been an ever-present mentor the beginning of my PhD, and all colleagues at NanoFCM, giving a special mention to Dr Ben Peacock, Dr Alice Law and Rebecca Lees. I am incredibly grateful for the time they dedicated to my training during my industrial placement, as well as their continued support throughout my PhD.

We acknowledge Dr Saskia Bakker at the Midlands Regional Cryo-EM Facility, hosted at the Warwick Advanced Bioimaging Research Technology Platform, for use of the JEOL 2100Plus, supported by MRC award reference MC_PC_17136.

We also acknowledge Dr Caterina Severi and Dr Mehdi Madi from Abbelight and Dr Alexandre Kitching from Nanometrix for their collaboration and assistance with single molecule localisation microscopy.

This work was supported by the Biotechnology and Biological Sciences Research Council (BBSRC) and Aston University funded Midlands Integrative Biosciences Training Partnership (MIBTP) [grant number BB/T00746X/1].

Personal acknowledgements

To Jaspreet, Calum and Alice who have made my Aston experience so much fun - thank you Jaspreet for your endless help and advice in the lab but most importantly, the special friendship we have built over the last few years. Thank you Calum for being a continual source of encouragement and inspiration and getting me into running! I will miss our morning walks into uni. And thank you Alice for keeping me sane, you are a constant inspiration and I'm so grateful we had each other during those first few months in the lab!

Finally, I am forever grateful to my family for always believing in me, being there for me and praying for me. And to Ash, who I would not have met if weren't for this PhD program, it has been so special to share this experience together. Thank you for being there for me through the ups and downs. I'm proud of all our hard work and can't wait to see where it takes us next.

Table of Contents

List of abbreviations

ACdEV	Apoptotic cell-derived extracellular vesicle
APC	Allophycocyanin
ATP	Adenosine triphosphate
BODIPY Maleimide	BODIPY™ FL N-(2-Aminoethyl)) Maleimide
BSA	Bovine serum albumin
CryoTEM	Cryo- transmission electron microscopy
CX3CL1	C-X3-C motif chemokine ligand 1
EDTA	Ethylenediaminetetraacetic acid
DAMP	Damage-associated molecular pattern
dSTORM	direct Stochastic Optical Reconstruction Microscopy
ESCRT	Endosomal Sorting Complex Required for Transport
EV	Extracellular vesicle
FBS	Foetal bovine serum
FC	Fold change
FITC	Fluorescein isothiocyanate
FSC	Forward scatter
GM-CSF	Granulocyte macrophage colony-stimulating factor
GO	Gene ontology
ICAM	Intercellular adhesion molecule
IFN-γ	Interferon gamma
IgG1, κ	Immunoglobulin G subclass 1, kappa light chain
IgG2b, κ	Immunoglobulin G subclass 2b, kappa light chain

IL	Interleukin
LAMP	Lifestyle-associated molecular pattern
LPC	Lysophosphatidylcholine
LPS	Lipopolysaccharide
MHC	Major histocompatibility complex
PAMP	Pathogen-associated molecular pattern
PBS	Phosphate-buffered saline
PECAM	Platelet-endothelial cell adhesion molecule
PERCP	Peridinin-Chlorophyll-Protein complex
PI	Propidium iodide
PMA	Phorbol 12-myristate 13-acetate
PS	Phosphatidylserine
S1P	Sphingosine-1-phosphate
SDS	Sodium Dodecyl Sulphate
SDS-PAGE	Sodium Dodecyl Sulfate Polyacrylamide Gel Electrophoresis
SEC	Size exclusion chromatography
SEM	Standard error of the mean
sfRPMI	Serum-free RPMI
SMLM	Single molecule localisation microscopy
SSC	Side scatter
SIRPα	Signal regulatory protein alpha
TNF	Tumour necrosis factor
UC	Ultracentrifugation
UTP	Uridine triphosphate

UV	Ultraviolet
VD3	1,25-dihydroxyvitamin D3

List of figures

Supplementary figures

List of tables

Supplementary tables

Chapter 1 Introduction

The release of extracellular vesicles (EVs) is a fundamental and highly conserved mechanism that cells use for communication. EVs are membrane-bound compartments that carry and present complex molecular cargo, which they can use to signal with recipient cells or transfer materials. This mechanism plays a crucial role in facilitating cellular interactions in a wide range of physiological and pathological conditions. Among the various forms of cell death, apoptosis is a tightly regulated process that is fundamental for maintaining tissue homeostasis. During apoptosis, cells release significant quantities of EVs, which include larger apoptotic bodies (>1 μm) and smaller apoptotic cell-derived extracellular vesicles (ACdEVs) (<1 μm) (Grant *et al.,* 2019; Aktin-Smith & Poon, 2017).

There is growing recognition of the role that ACdEVs play as critical regulators of immune and inflammatory responses (Grant *et al.,* 2019; Caruso & Poon, 2018). ACdEVs from various cell sources have demonstrated the ability to effectively attract immune cells to sites of apoptotic cell death and promote the efficient clearance of apoptotic cells from tissues (Torr *et al.,* 2011; Truman *et al*., 2008; Segundo *et al.,* 1999). This clearance process is essential for promoting the resolution of inflammation, which is a key step in returning tissues to homeostasis (Poon *et al.,* 2014b). Furthermore, multiple studies have shown that ACdEVs can actively modulate the behaviour and phenotype of immune cells, promoting their anti-inflammatory and pro-resolving functions (Zhu *et al*., 2023; Li *et al.,* 2022; Liu *et al.,* 2020; Shen *et al*., 2017; Fehr *et al*., 2013). This modulatory capacity allows ACdEVs to influence immune responses, making them significant players in immune regulation.

Despite the abundance and significance of ACdEVs in apoptosis and inflammation, there is still limited understanding of their biogenesis, surface composition, and interactions with recipient cells (Grant et al., 2019; Caruso & Poon, 2018). The mechanisms involved in the clearance of apoptotic cells might mirror how ACdEVs are processed, offering valuable insights. Due to their rapid release and ability to modulate immune responses, ACdEVs serve as an ideal model to enhance our understanding of EV biology in general, which can inform studies across various cell types.

1.1 Apoptotic cell clearance

Apoptosis, first described by Kerr *et al*. in 1972, is a major form of programmed cell death in which cells undergo controlled dismantlement (Kerr *et al.,* 1972). Clearance of apoptotic cells by phagocytes is essential for maintaining tissue homeostasis, to allow replacement of old, senescent or damaged cells with new, functional cells (Poon *et al*., 2014b). Furthermore, this removal process is important to prevent the release of potentially harmful intracellular contents, which could lead to chronic inflammation. As such, efficient apoptotic cell clearance is essential in ensuring the timely removal of dying cells and returning to tissue homeostasis.

Inflammation is a fundamental immune response to injury or infection; the innate immune system responds rapidly, with tissue resident immune cells acting as the 'first responders' to danger signals presented by pathogens or damaged cells, referred to as 'pathogen-associated molecular patterns' (PAMPs) and 'damage-associated molecular patterns' (DAMPs), respectively (Figure 1.1). More recently, the term 'lifestyle-associated molecular patterns' (LAMPs) has been coined to describe the presence of immune-stimulatory molecules as a symptom of poor lifestyle-associated diseases, *e.g.* cholesterol crystals are a symptom of cardiovascular disease (Zindel & Kubes, 2020). Leukocytes (typically short-lived neutrophils) are recruited from circulation, a hallmark of inflammation, undergoing transendothelial migration, in which they undergo a characteristic rolling and extravasation, mediated by endothelial selectins and leukocyte integrins (Zindel & Kubes, 2020; Nourshargh & Alon, 2014). The recruited leukocytes rapidly remove pathogens or damaged cells by phagocytosis, leading to their subsequent degradation and recycling of cellular components, before undergoing apoptosis and themselves requiring phagocytic removal (Figure 1.1) (Zindel & Kubes, 2020). In fact, the process of phagocytosis triggers their own apoptosis; this is believed to offer a dual layer of protection by enabling the phagocytic digestion of apoptotic neutrophils that contain pathogens, LAMPs or cells displaying DAMPs (Poon *et al.,* 2014b). Apoptotic leukocytes release a variety of signals that attract other phagocytes, such as macrophages, initiating the clearance process (Figure 1.1). Importantly, efficient apoptotic cell clearance prevents the progression of cells undergoing apoptosis to secondary necrosis, in which potentially harmful intracellular contents are released into the extracellular environment, which can lead to exposure of autoantigens and promote persistent inflammation (Poon *et al*., 2014b). Moreover, efficient removal of apoptotic cells contributes to the release of specialised pro-resolving factors, facilitating resolution of inflammation (Figure 1.1) (Soehnlein & Lindbom, 2010).

Pro-resolving signals actively inhibit further leukocyte infiltration and promote apoptotic cell clearance (Figure 1.1) (Soehnlein & Lindbom, 2010). The time-dependent regulation of the release of specific lipid mediators during different stages of inflammation is central to this process; the initial release of pro-inflammatory lipid mediators, prostaglandins and leukotrienes, is followed by the release of anti-inflammatory lipid mediators, including various lipoxins, resolvins and protectins (Soehnlein & Lindbom, 2010; Levy *et al.,* 2001). For example, lipoxin A4 was shown to selectively inhibit neutrophil recruitment and promote monocyte recruitment (circulatory macrophage pre-cursors) (Maddox *et al.,* 1997). As well as various lipid mediators and cytokines, the protein annexin A1 has been shown to localise to the plasma membrane of apoptotic neutrophils, promoting apoptosis and clearance and inhibiting further recruitment of neutrophils (Ortega-Gómez *et al.,* 2013). Furthermore, macrophages transition from a pro-inflammatory phenotype to an anti-inflammatory, pro-resolving phenotype, referred to as 'M1' and 'M2' phenotypes, demonstrating their dynamic plasticity (Ortega-Gómez *et al.,* 2013). They are characterised based on their release of pro-inflammatory cytokines and anti-inflammatory cytokines, tumour necrosis factor α (TNFα) and IL-1β or transforming growth factor (TGF)-β and IL-10, respectively (Ortega-Gómez *et al.,* 2013; Fadok *et al.,* 1998). In addition, differential gene expression in arachidonic pathway enzymes (the precursor to pro-inflammatory prostaglandins and leukotrienes, and anti-inflammatory lipoxins) has been observed in M1 and M2 macrophages (Martinez *et al.,* 2006). More recently, it has been revealed one of the major underlying mechanisms governing macrophage function is metabolism (Stunault *et al.,* 2018). Upon phagocytic uptake of apoptotic cells, phagocytes contain an abundance of apoptotic cell membrane-derived lipids which contribute to metabolic reprogramming of macrophages; transcription of anti-inflammatory cytokine IL-10 was shown to be dependent on fatty acid oxidation, beta oxidation (fatty acid metabolism inside the mitochondria) and the activity of a specific enzyme, sirtuin 1 (Zhang *et al.*, 2019; Stunault *et al.*, 2018).

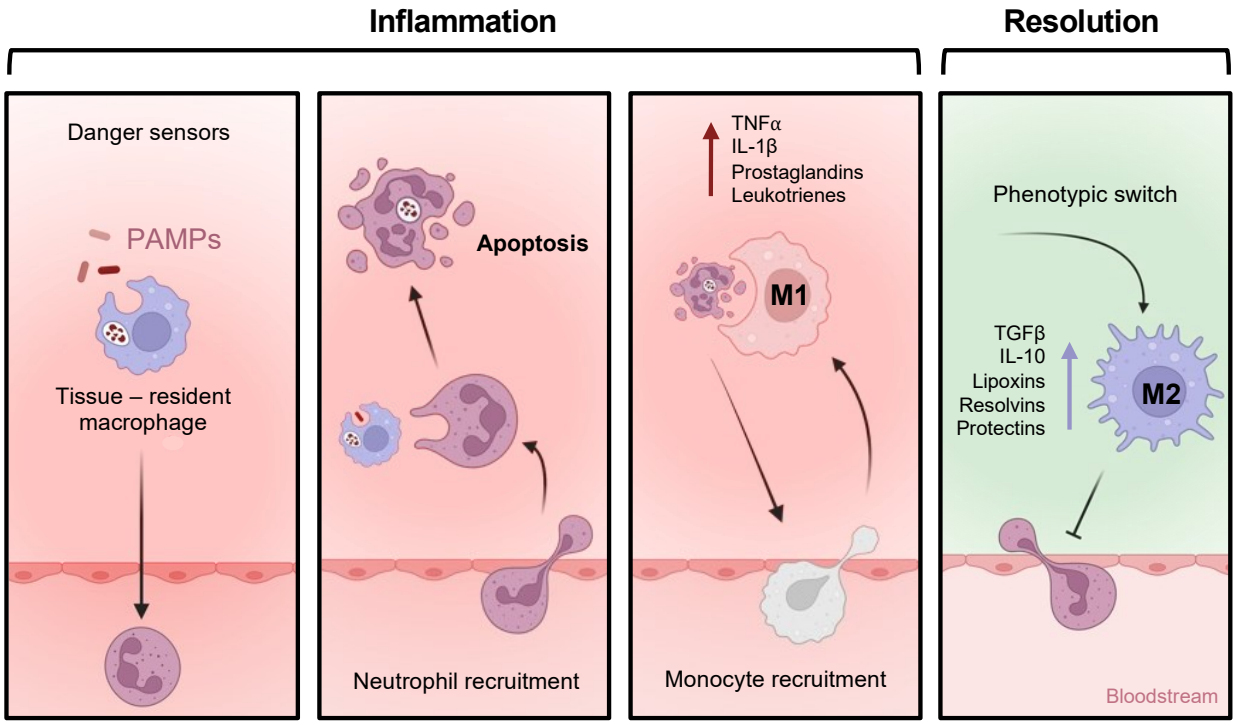

Figure 1.1: Apoptotic cell clearance. Tissue-resident phagocytes sense and respond to danger signals, including DAMPs (shown), PAMPs and LAMPs, and recruit peripheral immune cells, predominately neutrophils (Zindel & Kubes, 2020; Poon *et al*., 2014b). Recruited neutrophils rapidly phagocytose damaged cells and/or pathogens, or the danger signals themselves, and undergo apoptosis. Apoptotic neutrophils release signals that recruit peripheral monocytes. Recruited monocytes differentiate into M1 activated macrophages and release a variety of pro-inflammatory mediators which promotes vasodilation, further recruitment of monocytes and activation of macrophages (Ortega-Gómez *et al.,* 2013). M1 cells phagocytose apoptotic neutrophils and subsequently, undergo a crucial phenotypic switch to an M2 phenotype (Ortega-Gómez *et al.,* 2013). M2 cells release a variety of anti-inflammatory, pro-resolving mediators that act to inhibit neutrophil recruitment and promote macrophage-mediated phagocytic clearance of apoptotic cells which results in resolution of inflammation (Soehnlein & Lindbom, 2010). Figure made in Biorender.

Apoptosis occurs as a natural part of cell turnover, yet apoptotic cells are rarely detected in healthy tissues (Poon *et al.,* 2014b). For example, in the thymus, widespread apoptosis of immature T cells takes place, but histological sections show few apoptotic cells (King *et al.,* 2002; Scott *et al.,* 2001). This indicates that apoptotic cell clearance is rapid and highly efficient. Consequently, the presence of detectable apoptotic cells in tissues is generally regarded as an indicator of defective clearance processes (Gardai *et al.,* 2006). Impaired apoptotic cell clearance has been shown to be implicated in several pathologies, including atherosclerosis,

systemic lupus erythematosus, various lung diseases, cancer and is also important for transplantation, as reviewed by Poon *et al.* (2014b).

Atherosclerosis exhibits many of the classic symptoms of inflammation without resolution (Zindel & Kubes, 2020). Atherosclerosis involves the impaired clearance of apoptotic macrophages, which contributes to the formation and rupture of plaques. Atherosclerotic plaques are composed of fatty deposits, calcium, connective tissue, and dead cells. Monocytes are attracted to oxidised lipoproteins, a type of LAMP, within arterial walls (Zindel & Kubes, 2020). Once recruited, monocytes differentiate into macrophages and engulf large amounts of oxidised lipoproteins, resulting in the formation of 'foam cells', named after their characteristic lipid droplets (Gui *et al.,* 2022). Activated foam cells proliferate and attract further immune cells, causing chronic localised inflammation (Robbins *et al.,* 2013). Impaired clearance of foam cells coinciding with their accumulation leads to the release of their lipid content, exacerbating plaque formation and increasing the risk of plaque rupture (Gui *et al.,* 2022). Plaque rupture disrupts blood flow, leading to a higher risk of heart attacks, strokes, or peripheral artery disease. The mechanism underlying impaired clearance of apoptotic foam cells is not yet fully defined. However, oxidised lipoproteins bind CD14 preventing macrophage-mediated recognition and promoting their persistent activation, rho kinase (an activator of phagocytic inhibitors, the Rho-associated protein kinases (ROCKs)) is upregulated in atherosclerotic plaques and cholesterol efflux (a process in which lipids are exported to the liver) may be impaired (Poon *et al.,* 2014b; Miller *et al.,* 2003). Together, these features contribute to impaired apoptotic cell clearance and promote the progression of atherosclerosis.

Understanding the molecular mechanisms regulating apoptotic cell clearance and resolution of inflammation is crucial for developing therapeutic strategies aimed at controlling these processes in the context of various chronic inflammatory diseases. This is particularly important in the context of LAMPs, which the immune system has not evolved to appropriately tackle, therefore leading to chronic inflammation (Zindel & Kubes, 2020).

1.2 Apoptosis – morphological features

Apoptosis is induced by two major apoptotic pathways: permeabilisation of the outer mitochondrial membrane and release of cytochrome C, termed the 'intrinsic pathway' or activation of cell surface death receptors, termed the 'extrinsic pathway' (Lossi, 2022). The intrinsic pathway is triggered in response to intracellular prompts such as DNA damage, reactive oxygen species (ROS), or a

depletion in pro-survival factors (Roos *et al.,* 2015; Brumatti *et al.,* 2010). Whereas, the extrinsic pathway is initiated by immune cells, activated to eliminate infected, damaged, or abnormal cells, that bind death receptors exposed at the extracellular cell surface, inducing apoptosis (Lossi, 2022). Importantly, both pathways converge to a conserved panel of apoptosis effector proteins, irrespective of the initial apoptotic stimuli.

Once a cell has committed to apoptosis, it undergoes a controlled process of structural dismantlement, which is predominantly regulated by the caspases (Figure 1.2). Apoptotic cells exhibit several major morphological features, including loss of cell attachment, cell shrinkage, chromatin condensation, nuclear fragmentation, membrane blebbing, apoptotic cell protrusions and release of apoptotic bodies (Atkin-Smith & Poon, 2017; Kerr *et al*., 1972). Caspase 3 is a protease that is central in controlling apoptosis and has several characterised roles in mediating controlled cellular dismantlement during apoptosis.

Catenins are a family of adaptor proteins that complex with cadherins, a group of adhesion receptors, that provide a link between the intracellular actin cytoskeleton and the extracellular environment (Miller & Moon, 1996). Caspase 3-mediated cleavage of β-catenin renders it unable to complex with α-catenin (Brancolini *et al.,* 1997). This was observed alongside the reorganisation of the actin cytoskeleton, in which apoptotic cells reveal loss of stress fibres and attachment between viable and apoptotic cells. In addition, cadherin proteins are no longer localised to the cell membrane and apoptotic cells exhibit a loss of cell-to-cell contact (Brancolini *et al.,* 1997). Further to this, caspase 3 cleaves focal adhesion-associated proteins resulting in the disassembly of focal adhesions, disrupting cellular attachment to the extracellular matrix (ECM) (Levkau *et al.,* 1998).

Caspase 3 also indirectly activates caspase-activated deoxyribonuclease (CAD) by performing proteolytic cleavage of its inhibitor ICAD, which releases CAD to translocate into the nucleus and break down DNA (Figure 1.2) (Enari *et al.,* 1998). In addition, mitochondrial-derived endonucleases translocate to the nucleus and degrade DNA, independently of caspases (Li *et al.,* 2001). The collective activity of caspases and endonucleases that perform DNA fragmentation, combined with breakdown of the nuclear envelope by the cleavage of laminins, histone modifications and subsequent chromatin condensation, lead to the incorporation of uniform chromatin fragments and DNA into apoptotic bodies (Füllgrabe *et al.,* 2010; Oberhammer *et al.,* 1994; Kerr *et al.,* 1972).

The release of apoptotic bodies is a major feature of apoptosis in many cell types (Atkin-Smith & Poon, 2017). Apoptotic bodies are large membrane-enclosed compartments that are released from the apoptotic cell into the extracellular environment (Figure 1.2). Apoptotic bodies are classified as the largest type of extracellular vesicle (> 1 μm in size) and as such, can encapsulate entire organelles (Jiang *et al.,* 2017). They are formed in concert with plasma membrane blebbing and the formation of characteristic thin membrane protrusions, from which apoptotic bodies separate and bud off.

Plasma membrane blebbing is facilitated by contraction of actin filaments and polymerisation of microtubules, which regulate the release of apoptotic bodies, as well as preserve the plasma membrane integrity to prevent permeabilisation (Atkin-Smith & Poon, 2017; Moss et al., 2006). Caspase 3–mediated cleavage of Rho-associated kinase I (ROCK I) results in constitutive kinase activity, correlating with an increased presence of phosphorylated myosin light chain in apoptotic cells (Sebbagh *et al.,* 2001; Coleman *et al.*, 2001). This facilitates actin-mediated dismantlement of the cell membrane by membrane blebbing and the release of apoptotic bodies (Figure 1.2). Furthermore, a non-cleavable mutant of ROCK I was shown to downregulate phosphorylated myosin light chain, alter morphology of apoptotic cell disassembly and delay apoptotic cell clearance (Julian *et al.*, 2021). The effect on apoptotic body formation was not determined. Overall, the expression of non-cleavable ROCK I led to an increased release of intracellular contents and inflammation in mice, highlighting the important role of ROCK I in aiding tissue homeostasis (Julian *et al.,* 2021). Caspase-mediated activation of two other kinases, LIMK1 and PAK2, have also been implicated in membrane blebbing, although their mechanism is less well defined (Atkin-Smith & Poon, 2017). Furthermore, independent of caspases, microtubules assemble into an ‘apoptotic microtubule network’ (AMN), characterised by localisation to the plasma membrane (Sánchez-Alcázar *et al.,* 2007). The AMN stabilises the plasma membrane and prevents premature permeabilisation and necrosis (Figure 1.2). The AMN has also been suggested to support the process of membrane blebbing through interaction with the actin cytoskeleton (Atkin-Smith & Poon, 2017; Moss *et al.,* 2006).

In addition to plasma membrane blebbing, apoptotic cells also form several types of characteristic thin protrusions, microtubule spikes, apoptopodia / beaded apoptopodia, from which apoptotic bodies separate and bud off (Figure 1.2). Microtubule spikes are protrusions that are enriched in microtubule networks that facilitate the packaging of condensed chromatin fragments into apoptotic bodies (Moss *et al.,* 2006). Apoptotic bodies were suggested to localise along the length

or at the end of the microtubule spike, promoting their release independent of actin-mediated plasma membrane blebbing (Moss *et al.,* 2006).

Apoptopodia are described as 'string-like' structures that extend from the apoptotic cell surface (Poon *et al.,* 2014a). The mechanism behind apoptopodia formation remains undefined. However, caspase-mediated activation of pannexin 1, a receptor that facilitates the release of attractive signalling nucleotides to phagocytes, was shown to inhibit apoptopodia formation (Figure 1.2) (Poon *et al.,* 2014a; Chekeni et al., 2010). Atkin-Smith *et al.* suggested the inverse relationship in function of pannexin 1 indicates apoptotic cells may prefer one method of removal over another: direct phagocytic clearance of the entire apoptotic cell versus disassembly into fragments (Atkin-Smith & Poon, 2017). The activity of pannexin 1 may enable apoptotic cells to modulate the mechanism of apoptotic cell clearance.

Another form of apoptopodia, termed 'beaded apoptopodia' refers to a structure in which nuclear material is specifically omitted from the intraluminal contents of apoptotic bodies, revealing an active sorting mechanism (Atkin-Smith *et al*., 2015). Interestingly, differences between Jurkat T cell and THP-1 monocyte cell types were observed, whereby Jurkat T cells generally produced larger apoptotic bodies (> 5 μm) from non-beaded apoptopodia and monocytes produced a higher abundance of smaller apoptotic bodies (1-3 μm) derived from beaded apoptopodia (Atkin-Smith *et al*., 2015). This was attributed to either plasma membrane blebbing and apoptopodia formation occurring simultaneously, was was in the case of Jurkat T cells, or independently, such as in THP-1 monocytes which simply formed apoptopodia followed by beaded-apoptopodia (Atkin-Smith *et al*., 2015). Together, this work revealed the interplay between mechanisms of apoptotic cell disassembly in regulating the size and composition of apoptotic body release. Despite this, the specific molecules that mediate how apoptotic bodies are formed and released remains ill-defined.

Together, the structural dismantlement of an apoptotic cell, via the disassembly mechanisms that have been discussed, may simply reflect a loss of cell function or, may actively promote tissue homeostasis by aiding phagocytic clearance of apoptotic cells. The release of apoptotic bodies may ease the physical challenge of engulfing a cell larger than the phagocyte (Atkin-Smith & Poon, 2017). Furthermore, apoptotic cell protrusions (microtubule spikes, and apoptopodia / beaded apoptopodia) have been suggested to be a mechanism for an apoptotic cell to present apoptotic bodies to neighbouring phagocytes to aid their clearance, given that apoptotic bodies associate along the length of the protrusion structures (Atkin-Smith & Poon, 2017). Indeed, inhibition of plasma membrane blebbing and microtubule polymerisation decreased phagocytic engulfment

and direct apopototic cell – phagocytes interactions, respectively (Witasp *et al.,* 2007; Moss *et al.,* 2006).

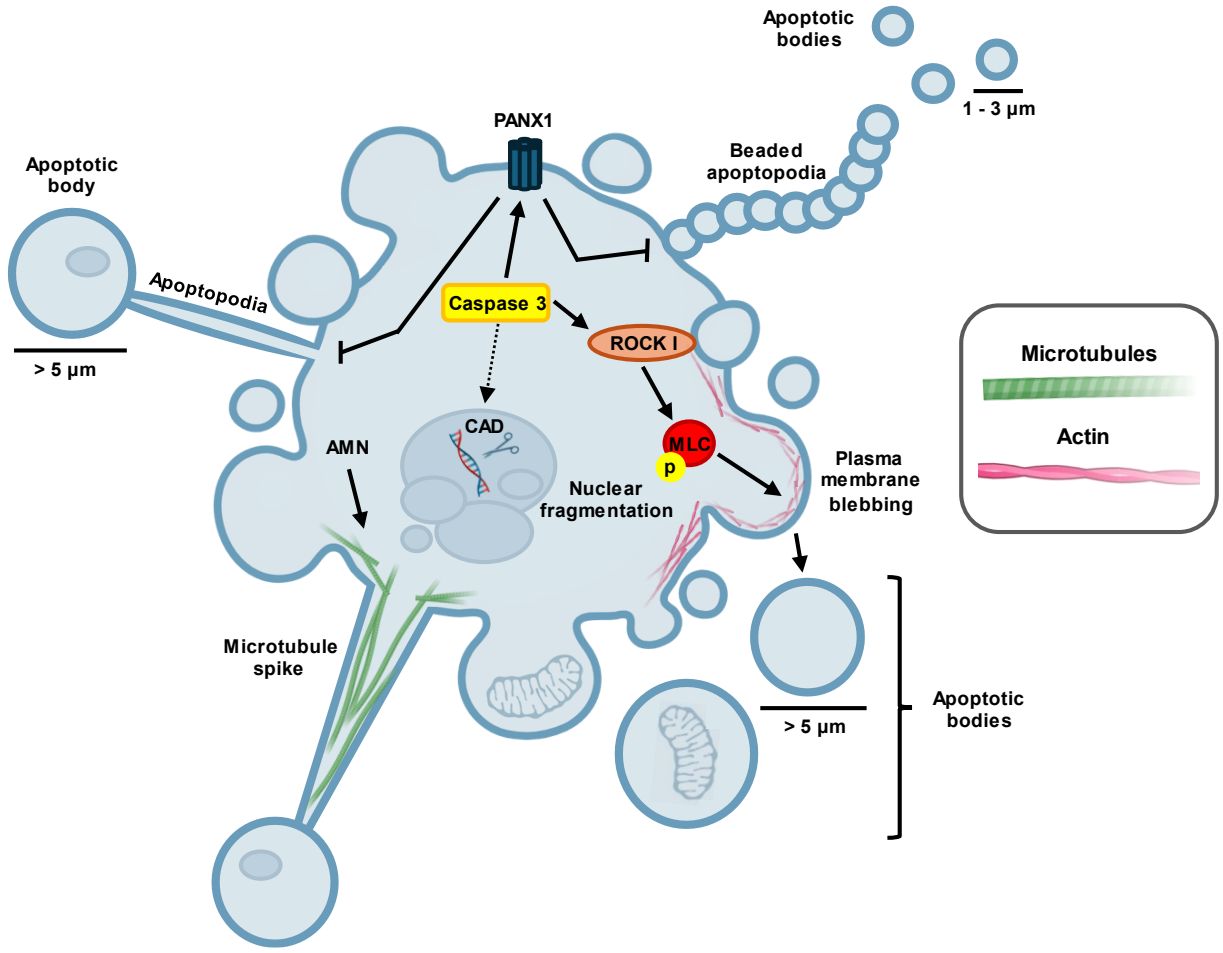

Figure 1.2: Structural disassembly of an apoptotic cell. Typical morphological characteristics of an apoptotic cell include nuclear fragmentation, plasma membrane blebbing, the formation of microtubule spikes and apoptopodia / beaded apoptopodia, and the release of apoptotic bodies. Caspase 3 indirectly activates caspase-activated deoxyribonuclease (CAD), upon which it translocates to the nucleus and digests DNA, contributing to nuclear fragmentation (Enari *et al.,* 1998). Caspase 3 also proteolytically cleaves Rho-associated kinase I (ROCK I), rendering it constitutively active (Coleman *et al.*, 2001). Activated ROCK I upregulates the phosphorylation of myosin light chain (MLC), thus promoting actin cytoskeleton contraction resulting in plasma membrane blebbing and release of apoptotic bodies (Sebbagh *et al.,* 2001). In addition, caspase 3 negatively regulates the formation of apoptopodia and beaded apoptopodia through activation of pannexin 1 (PANX1) by a mechanism that remains elusive (Atkin-Smith & Poon, 2017). Beaded apoptopodia specifically sorts apoptotic body cargo to exclude nuclear material (Atkin-Smith *et al*., 2015). Furthermore, independently of caspase activity, microtubules organise into an apoptotic microtubule network (AMN) which stabilises the plasma membrane and form microtubule spikes, from which apoptotic bodies can be released from the spike end (Moss *et al.,* 2006). Figure made using Biorender.

1.3 'Find me' and 'eat me' signals released by apoptotic cells

Besides structural characteristics, apoptotic cells release or display various molecular signals, with caspase 3 often playing a key role. These signals are divided into two categories: the expression of 'find me' signals, which chemotactically attract phagocytes, and 'eat me' signals, which facilitate their uptake by phagocytes. 'Find me' signals are released by apoptotic cells into the extracellular environment to attract phagocytes to the site of apoptosis (Figure 1.3). These include soluble factors such as nucleotides, adenosine triphosphate (ATP) and uridine triphosphate (UTP), and the chemokine CX3CL1, that are released during the early stages of apoptosis and therefore, may function as an early trigger warning to local phagocytes to activate a large-scale clearance response (Elliott *et al.,* 2009, Truman *et al*., 2008). Specifically, caspase 3 or caspase 7 activates the pannexin 1 receptor which facilitates the transport of nucleotides, ATP and UTP, from inside the cell to the extracellular environment (Chekeni *et al.,* 2010). ATP and UTP bind the $PY2_2$ purinergic receptors expressed by phagocytic cells, which in turn, enables directional migration towards the apoptotic cell to promote apoptotic cell clearance (Elliott *et al.,* 2009). CX3CL1 is proteolytically cleaved, either directly or indirectly by the activation of caspases, and released from the surface of apoptotic cells, acting as a 'find me' chemokine (Truman *et al*., 2008). Its receptor, CX3CL1R, is expressed by phagocytes; upon ligand binding, phagocytes are directed towards the site of the apoptotic cell.

Other 'find me' signals include the release of lipids such as sphingosine-1 phosphate (S1P) and lysophosphatidylcholine (LPC) (Figure 1.3) (Gude *et al.,* 2008; Lauber *et al*., 2003). Caspase 3 was shown to activate calcium-independent phospholipase A2, which then enzymatically breaks down phosphatidlycholine into arachidonic acid (AA) and LPC, leading to the release of both bioactive biproducts (Lauber *et al.,* 2003; Atsumi *et al*., 2000; Atsumi *et al.,* 1998). The receptor for LPC has not yet been confirmed; G2A G-protein coupled receptor (GPCR) was initially proposed as an LPC receptor but was later shown to act as an antagonist of G2A signalling, leading to uncertainty about its role (Murakami *et al.,* 2004). Furthermore, whilst AA isn't defined as a 'find me' signal, it is a precursor to several bioactive eicosanoids, including prostaglandins and leukotrienes, and therefore, the activity of calcium-independent phospholipase A2 serves multiple purposes (Atsumi *et al.,* 1998).

During apoptosis, the expression of sphingosine kinase I is upregulated, likely by caspase activation, which results in the conversion of sphingosine into S1P and promotes rapid S1P release (Gude *et al.,* 2008). S1P binds to S1P receptors expressed by phagocytes which promotes phagocytic migration and recruitment towards the apoptotic cell (Figure 1.3) (Gude *et*

al., 2008). Furthermore, S1P -S1P receptor binding has been shown to induce macrophage erythropoietin signalling by upregulating hypoxia inducible factor-1α, a subunit of the transcription factor responsible for transcription of erythropoietin (Herr *et al.,* 2009). Erythropoeitin signalling, originally known for its role in governing haematopoiesis, was shown to be central to regulating phagocytic uptake of apoptotic cells and actively downregulated the phagocytic expression of pro-inflammatory cytokines (Luo *et al.,* 2016). Interestingly, the concentration of S1P is higher in circulation than in local tissues, where apoptotic cell clearance most commonly occurs, suggesting phagocytes may respond to localised changes in S1P concentration (Hochreiter-Hufford & Ravichandran, 2013).

The rapid release of a diverse array of 'find me' signals by apoptotic cells indicates the significance of efficient apoptotic cell clearance. Although it remains unclear if and how these signals interact, the presence of multiple mechanisms likely provides apoptotic cells with the flexibility needed to ensure the appropriate response from nearby phagocytes.

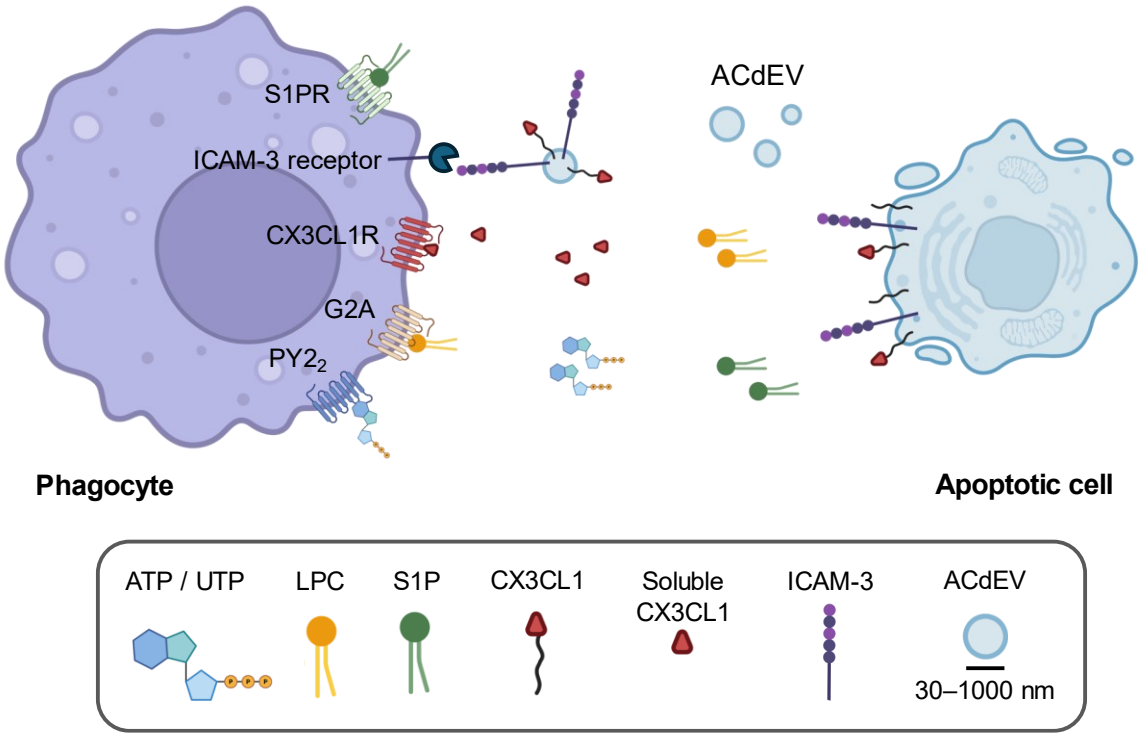

Figure 1.3: 'Find me' signals released by apoptotic cells actively recruit phagocytes for apoptotic cell clearance. Nucleotides (ATP and UTP), proteolytically cleaved chemokines (CX3CL1), and lipid by-products (lysophosphatidylcholine (LPC) and sphingosine-1 phosphate (S1P), are released into the extracellular environment and bind to phagocyte-expressed receptors, $PY2_2$ purinergic receptors, chemokine receptors (e.g. CX3CL1R), and LPC/S1P receptors, respectively (Elliott *et al.,* 2009; Truman *et al*., 2008; Gude *et al.,* 2008; Lauber *et al*., 2003). Evidence has suggested the G2A G-protein coupled receptor (GPCR) may be a receptor for LPC (Murakami *et al.,* 2004). Furthermore, bioactive 'find me' signals can be transported at the surface of ACdEVs; CX3CL1 and ICAM-3, at the surface of ACdEVs, potently attracted macrophages (Torr *et al.*, 2011; Truman *et al.,* 2008). Figure made using Biorender.

Once in close proximity, phagocytes must correctly distinguish between viable cells and apoptotic cells through a process of recognition, before engulfment and digestion of an apoptotic cell. This is regulated by a finetuned balance of 'eat me' and 'don't eat me' signals (Figure 1.4). A well-established feature of apoptosis is cell surface exposure of phosphatidylserine (PS). PS is a phospholipid typically found on the inner leaflet of the plasma membrane in viable cells. Its asymmetrical distribution is maintained by phospholipid flippases, which actively transport PS from the outer to the inner leaflet by hydrolysing ATP (Segawa *et al.,* 2016). During apoptosis, activation of caspase 3 promotes PS exposure by activating phospholipid scramblases like XKR8, which facilitate PS externalisation, and inhibiting phospholipid flippases like ATP11A/ATP11C,

which normally translocate PS to the inner membrane leaflet (Suzuki *et al*., 2016) (Segawa *et al.,* 2016) (Suzuki *et al*., 2014). PS can directly bind to several phagocyte receptors, including multiple promiscuous scavenger receptors, several members of T cell immunoglobulin mucin domain (TIM) family, or brain-specific angiogenesis inhibitor 1 (BAI1), the first PS receptor to be discovered (Vorselen, 2022) (Park *et al.,* 2007).

PS can also act as a bridging molecule to bind other molecules which then bind to their respective receptors at the phagocyte cell surface (Figure 1.4) (Vorselen, 2022). One example is the protein calreticulin, which can either bind PS directly or complex with complement component C1q to facilitate PS-mediated phagocytic uptake by binding the phagocyte receptor CD91 (Wijeyesakere *et al.,* 2016; Ogden *et al*., 2001). Calreticulin is a soluble protein known for its role in calcium signalling in the endoplasmic reticulum, but is able to translocate to the plasma membrane by association with PS, establishing it as a marker of apoptosis (Wijeyesakere *et al.,* 2016; Gardai *et al.,* 2005).

Some molecules have dual 'find me' and 'eat me' signalling functions; CX3CL1, which can also directly bind phagocyte receptors, and ICAM-3 (Figure 1.3 and 1.4) (Torr *et al.,* 2011; Truman *et al*., 2008). ICAM-3 is an immunoglobulin superfamily member expressed by apoptotic leukocytes that was shown to potently attract phagocytes (Torr *et al.,* 2011). Its chemoattractive property combined with the ability for it to bind directly to macrophages, together promote apoptotic cell clearance (Moffatt *et al.,* 1999). Notably, ICAM-3 is also expressed at the surface of viable cells. Ig-like domain 1 was shown to exhibit an altered preferential binding from lymphocyte function-associated antigen 1 (LFA-1) to an alternative receptor that remains unidentified (Moffatt *et al*., 1999). It has been proposed that during apoptosis, modifications to the apoptotic cell surface may alter the function of ICAM-3, such as changes in glycosylation patterns or protein conformation, allowing these alterations to be recognised by its receptor (Torr *et al*., 2011). In addition, the expression of inhibitory 'don't eat me' signals are rapidly lost which may allow 'eat me' signals to prevail.

CD47, an integrin-associated receptor, interacts with signal regulatory protein α (SIRPα) on phagocytes to prevent the phagocytosis of viable cells (Figure 1.4) (Oldenborg, Gresham, and Lindberg, 2001). SIRPα binds to the extracellular IgV-like domain of CD47, activating Src homology-2 domain-containing protein tyrosine phosphatase (SHP), which suppresses the cytoskeleton-driven process of phagocytosis, thus regulating immune responses (Kaur *et al.,* 2016). However, during apoptosis, CD47-SIRPα signalling is disrupted, preventing this interaction. This disruption is thought to arise from substantial plasma membrane reorganisation during

apoptosis, driven by the breakdown of cholesterol-enriched lipid rafts (Dufour *et al.,* 2023; Lv *et al.,* 2015). This process may alter the conformation of CD47, resulting in a loss of its ability to bind SIRPα.

Another group reported caspase-dependent shedding of 'don't eat me' signal CD46 during apoptosis, a complement regulatory protein, which led to opsonisation of the apoptotic cell with complement component C3b (Elward *et al.,* 2005). Furthermore, CD31 is an immunoglobulin-like superfamily member (IgSF) that is reported to undergo a functional switch during apoptosis, from a 'don't eat me' signal to an 'eat me' signal (Brown *et al.,* 2002). On the surface of viable cells, CD31 engages in homophilic interactions with CD31 on the phagocyte surface, signalling for active detachment and preventing phagocytic uptake. In contrast, on apoptotic cells, CD31 similarly interacts homophilically but instead promotes strong binding between the apoptotic cell and the phagocyte (Figure 1.4) (Brown *et al.,* 2002). This is achieved through the activation of α5β1 integrin and prolonged phagocyte membrane depolarisation (Vernon-Wilson *et al.*, 2007; Vernon-Wilson *et al.,* 2006).

More recently, the presence of a 'glycocalyx', a layer of glycan-decorated molecules associated to the cell surface, was shown to inhibit phagocytic receptor engagement by acting as both a physical and electrostatic barrier to 'find me' molecules at the apoptotic cell surface or 'find me' receptors on the phagocyte surface (Imbert *et al.,* 2021). Interestingly, Le *et al.* very recently demonstrated late apoptotic bodies to have lost the glycolcalyx coat, hypothesised to be due to the actin cytoskeleton dismantlement, thereby exposing 'eat me' signals and promoting their phagocytic uptake (Le *et al.,* 2024). Notably, early apoptotic bodies retained the glycolcalyx coat, highlighting compositional time-dependent differences between early and late apoptotic bodies that may modulate their function. Kelley and Ravichandran postulated that the glycolcalyx coat may act to preserve the bioactivity of early apoptotic bodies to propagate 'find me' signals for a longer duration (Kelley and Ravichandran, 2024).

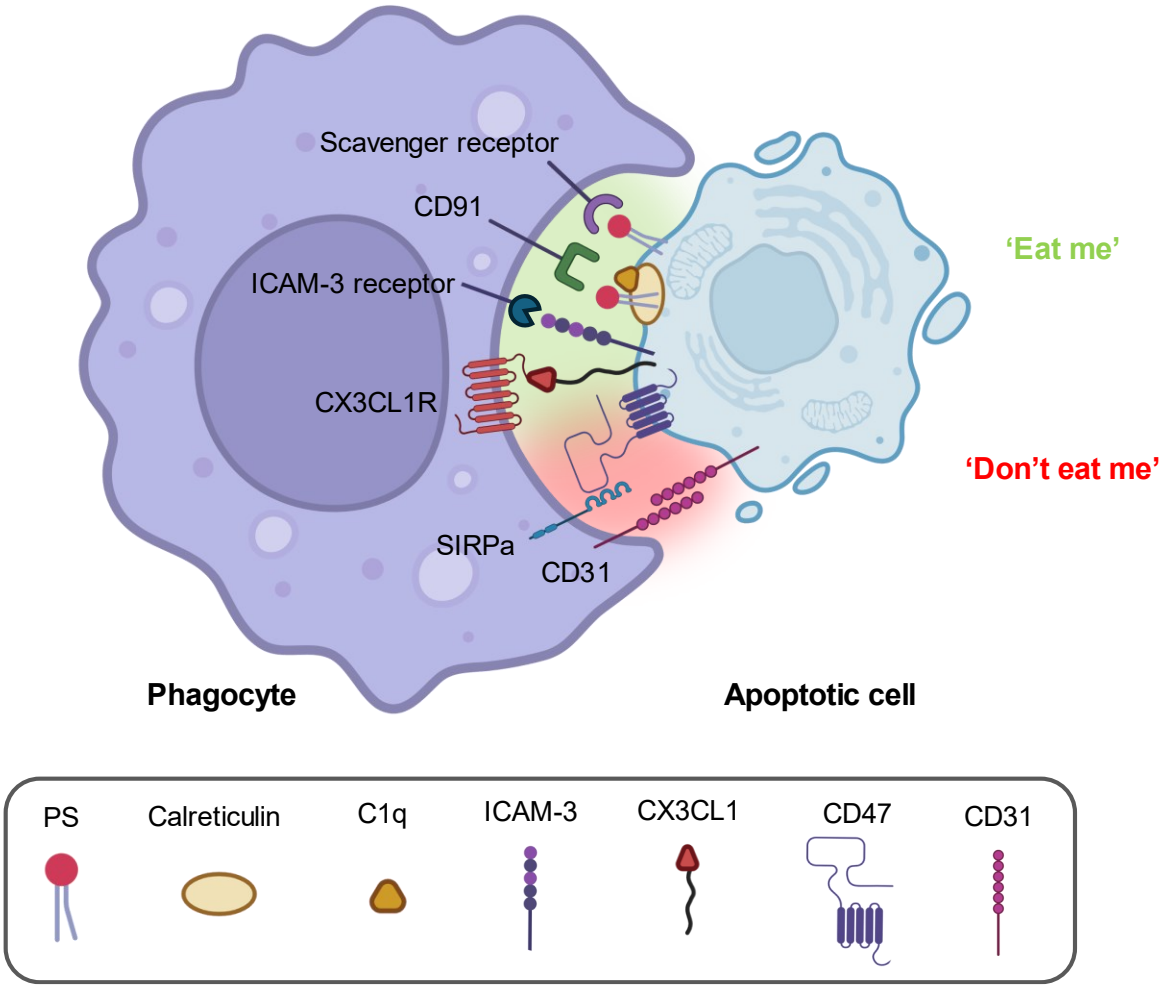

Figure 1.4: Apoptotic cells express 'eat me' signals and 'don't eat me' signals which promote or inhibit phagocytosis, respectively. Phosphatidylserine (PS), alone or complexed with calreticulin and complement factor C1q, is a potent 'find me' signal that binds multiple phagocyte receptors (Wijeyesakere *et al.,* 2016; Park *et al.,* 2007; Ogden *et al*., 2001). CX3CL1 and ICAM-3 also function as 'eat me' signals at the surface of apoptotic cells (Torr *et al.,* 2011; Truman *et al.,* 2008). CD47 is a potent 'don't eat me' signal that binds signal regulatory protein α (SIRPα) (Oldenborg, Gresham, and Lindberg, 2001). CD31 undergoes a functional switch from a 'don't eat me' signal to an 'eat me' signal, during apoptosis (Brown *et al.,* 2002). Together, the balance of 'eat me' versus 'don't eat me' signals determines the occurrence of phagocytosis. Figure made using Biorender.

1.3.1 The role of ACdEVs in apoptotic cell clearance

'Find me' and 'eat me' signals are also shed via the release of ACdEVs (Figure 1.3). EVs are membrane-bound particles released into the extracellular environment that can transport a variety of proteins, lipids and nucleic acids, both within the intravesicular lumen and exposed on the surface (Figure 1.6). EVs can transport information locally or to different tissues by entering circulation and are therefore, powerful mediators of communication. 'ACdEVs' is sometimes used as an umbrella term referring to several subsets of EV types: apoptotic bodies (> 1 μm in size) (which have already been described), microvesicles (100 -1000 nm) and exosomes (30 – 200 nm) (Caruso *et al.,* 2018). However, there is currently no widely accepted agreement of terminology, method of ACdEV isolation or easy discrimination between the smaller subsets of EVs, microvesicles and exosomes (Welsh *et al.,* 2024; Caruso *et al.,* 2018). In this thesis, 'ACdEVs' will be used to describe all EVs released by apoptotic cells that are < 1 μm in size and EVs released by apoptotic cells that are > 1 μm in size will be referred to as apoptotic bodies.

ACdEVs have been shown to attract phagocytes to the site of apoptosis and promote apoptotic cell clearance (Segundo *et al.,* 1999). However, the molecular components that facilitate interactions between ACdEVs and phagocytes remain largely unexplored. Just two functional molecules associated with ACdEVs have been defined in this context thus far, 'find me' signals CX3CL1 and ICAM-3 (Truman *et al.,* 2008; Torr *et al*., 2011). Interestingly, the majority of released CX3CL1 was found to be associated to ACdEVs, termed 'microparticles', showing ACdEVs to be a major player in CX3CL1-mediated chemotaxis (Truman *et al.,* 2008). Similarly, ICAM-3 was shown to be functional at the surface of ACdEVs by potently attracting macrophages (Torr *et al.*, 2011). 'Don't eat me' signals have also been reported to be associated with ACdEVs; CD46 was rapidly lost from the apoptotic cell surface, facilitating the release of 'CD46-enriched microparticles' (Elward *et al.,* 2005). Therefore, apoptotic cells may release ACdEVs to propagate 'find me' signals to promote recruitment of immune cells and to shed inhibitory 'don't eat me' signals, making apoptotic cells more 'appetising' to phagocytes.

So far, apoptotic bodies have been described as EVs that are > 1μm in size and act as a structural disassembly mechanism utilised by apoptotic cells, thought to enable them to be engulfed more efficiently by phagocytes (Atkin-Smith & Poon, 2017; Witasp *et al.,* 2007). In addition to this, like ACdEVs, apoptotic bodies also provide a mechanism for communication between apoptotic cells and recipient cells by carrying bioactive molecules at the surface or inside as cargo. For example, apoptotic bodies were shown to display chemokines bound to their surface via interaction with PS (Pontejo & Murphy, 2021). Apoptotic bodies can chemotactically recruit phagocytes via

chemokine activity, likely through the binding of chemokine receptors on phagocytes, as demonstrated by reduced chemotaxis when chemokine inhibitors are present (Pontejo & Murphy, 2021). Apoptotic bodies have also been shown to promote wound healing in a mouse model of acute lung injury through modulation of macrophages; uptake of human umbilical cord MSC-derived apoptotic bodies by macrophages induced polarisation towards an anti-inflammatory phenotype (Jiang *et al.,* 2023). This effect was mediated by inhibition of glycolysis through interaction of PDL1 at the surface of apoptotic bodies and PD1 expressed by macrophages (Jiang *et al.,* 2023).

Whilst there is growing evidence of the role apoptotic bodies and ACdEVs play in communicating with the innate immune system, particularly in the context of apoptosis, many details remain unclear. Much is still to be discovered about their biosynthesis, structure, and function, both for EVs in general and those originating from apoptotic cells. Apoptotic bodies and ACdEVs carry diverse molecular cargo, but understanding how these molecules collectively communicate and exert their effects remains a key challenge. Moreover, ACdEVs are smaller than apoptotic bodies and may, therefore, distribute more easily or travel greater distances, making them more effective in recruiting phagocytes, while larger apoptotic bodies might be more involved in local immunomodulation.

1.4 EV biogenesis

EVs are broadly categorised into three main types: exosomes, microvesicles (MVs), and apoptotic bodies (Welsh *et al.,* 2024). Exosomes, the smallest EV subtype, range from 30-150 nm in size and originate from the endosomal pathway. They are formed when multivesicular bodies (MVBs) fuse with the plasma membrane, releasing their intraluminal vesicles (ILVs) as exosomes. Microvesicles are larger, ranging from 100-1000 nm, and are formed through the outward budding of the plasma membrane. Apoptotic bodies, the largest EV subtype at > 1000 nm, are released during the late stages of apoptosis (Atkin-Smith & Poon, 2017). As previously described, these apoptotic bodies contain cellular debris, including DNA, entire organelles, and cell fragments, and are recognized by phagocytes for clearance, aiding in the removal of dying cells (Jiang *et al.,* 2017; Atkin-Smith & Poon, 2017). Notably, apoptotic cells also release ACdEVs, which may comprise of a mixture of exosome and microvesicle populations or may represent a unique population of EVs that have a distinct mode of biogenesis (Caruso & Poon, 2018).

As each type of EV have distinct biogenesis pathways, they may serve distinct roles in cellular communication, homeostasis, and disease processes. Most cells likely release both plasma membrane- and endosome-derived vesicles, but evidence for the origin of biogenesis is often lacking due to the difficulty of distinguishing them from other vesicles (Welsh *et al.,* 2024).

1.4.1 Exosome biogenesis - endosomal pathway

The endosome plays a central role in the formation of exosomes, which are small extracellular vesicles involved in intercellular communication (Colombo *et al.,* 2014). The process begins when the plasma membrane invaginates to form early endosomes, which are membrane-bound compartments. These endosomes are formed as the cell internalises extracellular molecules, receptors, and membrane components through endocytosis. Early endosomes undergo maturation into late endosomes, during which the endosomal membrane can undergo inward budding to form ILVs. ILVs can be actively packaged with specific molecular cargo and are commonly enriched in CD63, LAMP-1 and LAMP-2 (Colombo *et al.,* 2014). The accumulation of ILVs leads to these structures being referred to as MVBs. An MVB has two possible fates: the MVB can fuse with lysosomes where their contents are degraded and recycled, or fuse with the plasma membrane for release of ILVs by exocytosis (Colombo *et al.,* 2014). Once ILVs are released in the extracellular environment, they are referred to as ‘exosomes’.

To date, two main mechanisms driving ILV formation have been described: ESCRT-dependent and ESCRT-independent pathways. ESCRT, an acronym for ‘endosomal sorting complex required for transport’, describes a group of approximately 30 proteins that organise into four main complexes: ESCRT-0-III (Colombo *et al.,* 2014). In the ESCRT-dependent endosomal pathway, ESCRT-0 binds ubiquitinylated endosomal membrane proteins, ESCRT-I and ESCRT-II induce membrane curvature and budding for ILV formation and ESCRT-III is responsible for scission and release of ILVs into the MVB lumen (Colombo *et al.,* 2014). Hepatocyte growth factor–regulated tyrosine kinase substrate (HRS), a member of ESCRT-0, is responsible for sorting ILV cargo (Dixson *et al.*, 2023). HRS also acts to recruit TSG101, a member of ESCRT-I complex, which results in the sequential recruitment of ESCRT-II and ESCRT-III. Additionally, the ESCRT complex contains enzymes that can remove ubiquitin tags from the ILV cargo. Alternatively, ESCRT-I can interact with ALIX to recruit ESCRT-III (Colombo *et al*., 2014). ALIX is an ESCRT accessory protein that interacts with TSG101 (a member of ESCRT-I), syndecan 1 (a membrane protein that binds various signalling molecules), syntenin (a scaffold protein) and CD63 (tetraspanin) as an additional method of cargo sorting (Dixson *et al.,* 2023).

Additionally, ILVs can be formed via an ESCRT-independent pathway, possibly mediated by lipid rafts that are rich in lipids capable of inducing membrane curvature due to their inherent structure (Dixson *et al.,* 2023). EVs are typically enriched with specific lipid species such as ceramide, phosphatidylcholine, phosphatidylserine, sphingomyelin, and cholesterol, which are less abundant in host cell membranes (Dixson *et al.,* 2023). As such, the lipid composition has drawn attention as it may represent a key mechanism in EV biogenesis. An ESCRT-independent pathway of exosome biogenesis shown initially during investigation of proteolipid protein (PLP) (Trajkovic *et al.,* 2008). Inhibition of neutral sphingomyelinase 2 (nSMase2), an enzyme that converts sphingomyelin into ceramide, has been shown to prevent the formation of ILVs containing PLP and typical exosome-enriched proteins and therefore, ceramide is concluded to be an essential part of this process (Colombo *et al*., 2014; Trajkovic *et al.,* 2008). Moreover, transport of ceramide from the endoplasmic reticulum to the endosome actively promotes ILV formation (Dixson *et al.,* 2023). In addition, the role of S1P signalling with S1P receptor (S1PR) was shown to mediate endosome maturation and regulate the packaging of cargo into ILVs, independent of the ESCRT machinery (Kajimoto *et al.,* 2013).

Also important in ESCRT-independent formation of exosomes are tetraspanin-enriched domains (TEMs). TEMs are specific microdomains in the membrane which are enriched with tetraspanins, such as CD9, CD63, and CD81, along with other proteins including integrins. TEMs are implicated in EV biogenesis and can organise the packaging of TEM-associated proteins (Dixson *et al.,* 2023). Like ceramide, TEMs exhibit a distinct structure that promotes membrane curvature (Dixson *et al.,* 2023). Furthermore, cholesterol was shown to be able to bind CD81 via a unique intramembrane cavity (Zimmerman *et al.,* 2016). Therefore, TEMs and lipids may interact to induce membrane curvature and vesicle budding. Notably, the presence of CD9, CD63, or CD81 does not indicate the origin of EVs, as these proteins can also be expressed on the plasma membrane (Dixson *et al.,* 2023). Therefore, they cannot be reliably used as markers to distinguish exosomes from microvesicles.

Both the ESCRT-depedent and ESCRT-independent pathway rely on the activity of Rab GTPases in enabling transport of MVBs to the plasma membrane (Yu *et al.,* 2024). In addition, molecular machinery, such as the SNARE complex, are essential for mediating MVB plasma membrane fusion for subsequent release of exosomes (Yu *et al.,* 2024).

1.4.2 Microvesicle biogenesis

The biogenesis of microvesicles is referred to as ‘ecotocytosis’; as such, microvesicles are often referred to as ‘ectosomes’ (Dixson *et al.,* 2023). Most of the molecular machinery used for the

biogenesis and release of microvesicles is the same as exosomes, except microvesicles are released directly from the plasma membrane surface by a process of 'budding' (Dixson *et al.,* 2023). Specific components of the ESCRT complex, such as TSG101, localise to the plasma membrane where they act in concert with arrestin domain-containing protein 1 (ARRDC1) and tetraspanins to mediate budding, altering the local protein composition of the plasma membrane (Colombo *et al*., 2014). Tetraspanins are connected to the actin cytoskeleton which can induce complex rearrangements of membrane and cytoskeletal components and direct the packaging of specific EV cargo (Yu *et al.,* 2024). Importantly, specific ESCRT proteins are not involved in microvesicle biogenesis, including HRS, and therefore the presence of HRS may be a useful marker of exosomes (Colombo *et al*., 2014).

Despite significant advances in understanding the biogenesis pathways of exosomes and microvesicles, the exact molecular mechanisms of biogenesis, including cargo sorting and the triggers for vesicle formation, are still not fully understood. The interplay between different pathways (ESCRT-dependent and independent), the influence of lipids, and how various stimuli regulate EV release remain unclear. Additionally, distinguishing between different types of EVs and understanding their physiological relevance in different contexts are ongoing challenges in the field (Dixson *et al.,* 2023).

One such context, is apoptosis, in which the role of ACdEVs is still not fully understood. As the formation of apoptotic bodies by plasma membrane blebbing, microtubule spike formation and apoptopodia / beaded-apoptopodia formation has already been described, the limited knowledge surrounding biogenesis of ACdEVs will now be introduced.

1.4.3 ACdEV biogenesis

Overall, it remains unclear whether ACdEVs are produced by similar or unique mechanisms to exosome and microvesicle biogenesis. However, details of a few unique molecular regulators have been discovered in recent years; caspase 3 activation is a key event regulating the release of apoptotic exosome-like vesicle (Beillevaire *et al*., 2022; Park *et al.,* 2018; Dieudé *et al.,* 2015). Furthermore, one seminal paper revealed the S1P/S1P receptor (S1PR) pathway as essential for apoptotic exosome-like vesicle biogenesis (Park *et al.,* 2018). In particular, sphingosine kinase 2 was revealed as an essential mediator of this process, in which it localised to the plasma membrane and increased the local concentration of S1P. S1P was able to bind and activate S1PR1 and S1PR3 which led to downstream regulation of the actin cytoskeleton to induce membrane deformation and subsequent endocytosis. The endosome, enriched in S1PR and CD63, produced ILVs, transitioning it to a MVB, which could then fuse to the plasma membrane

and release apoptotic exosome-like vesicles. Together with genetic knockouts of specific ESCRT machinery, this revealed apoptotic exosome-like vesicles were, in this instance, produced independently of ESCRT machinery (Park *et al.,* 2018). Notably, different EV biogenesis pathways are activated in various contexts, and their regulation is not yet fully understood (Dixson *et al.,* 2023; Tucher *et al.,* 2018). Therefore, the possibility that ACdEVs utilise ESCRT machinery in their biogenesis cannot be ruled out. Interestingly, the same study reported apoptotic exosome-like vesicles to be localised to 'spindle-like' structures enriched in actin that relied on S1P-S1PR signalling and structurally mimicked apoptopodia (Park *et al.,* 2018; Atkin-Smith *et al.,* 2015). Therefore, some of the mechanisms regulating formation of ACdEVs and apoptotic bodies may overlap.

Another mechanism of apoptotic exosome-like vesicles formation has been described, involving fusion of autolysosomes at the plasma membrane (Beillevaire *et al*., 2022). Inhibition of caspase 3 disrupted fusion of the autolysosome with the plasma membrane, revealing its role in modulating fusion events (Beillevaire *et al*., 2022). This provided the first link between apoptosis and autophagy, a process in which cells degrade and recycle their intracellular contents, in biogenesis of ACdEVs.

Importantly, ACdEVs are distinct from apoptotic bodies in molecular composition, indicating different modes of biogenesis; ACdEVs contain S1PRs and lysosomal protein LAMP-1 (Beillevaire *et al*., 2022; Park *et al.,* 2018). They are also enriched in heat-shock protein 70 (HSP70), proteosome subunits and high-mobility group box 1 (HMGB1), exosomal markers CD9, CD63 and TSG101 and immunostimulatory non-ribosomal non-coding RNA transcripts (Hardy *et al.,* 2019; Tucher *et al.,* 2018).

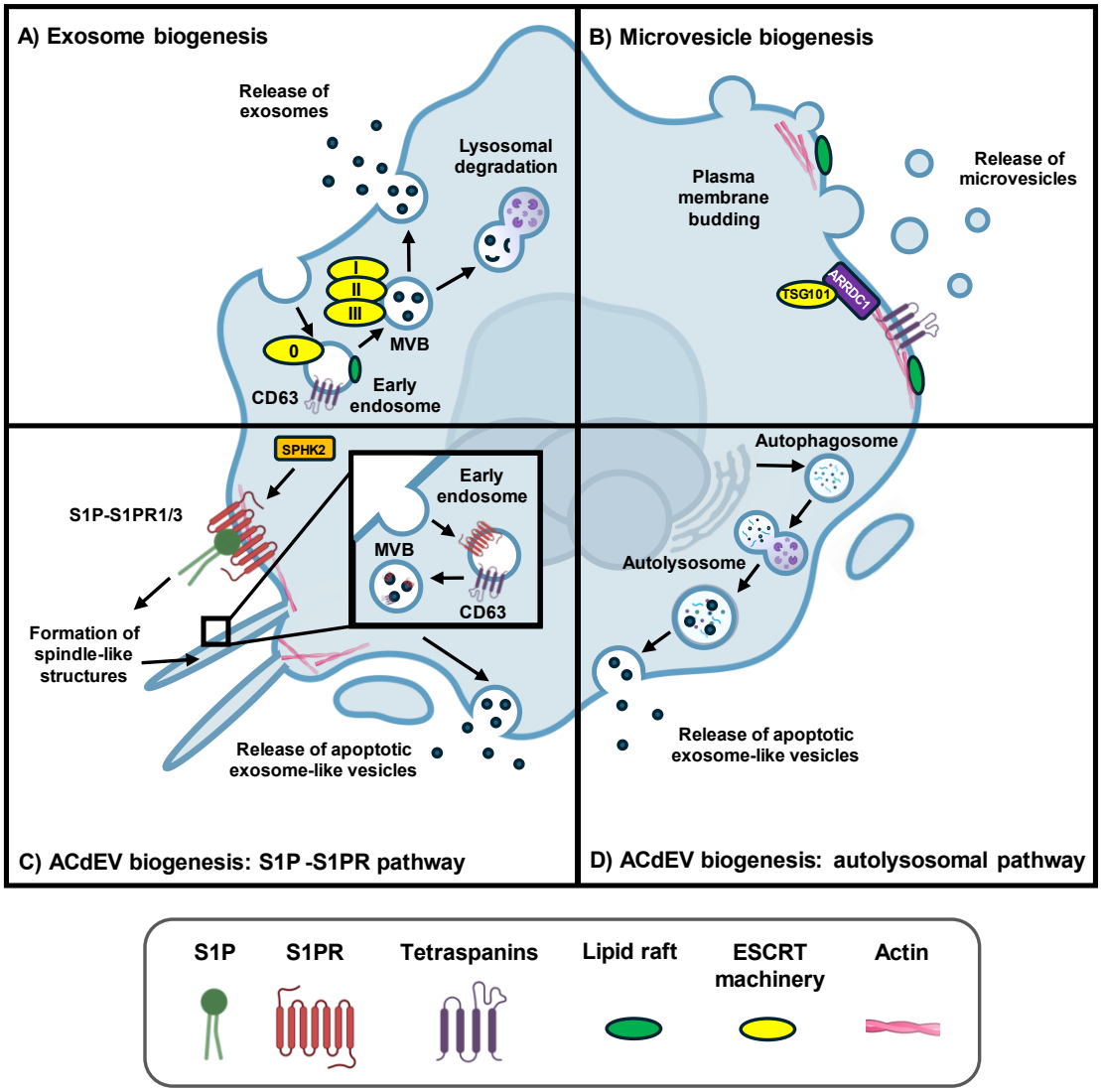

Figure 1.5: Viable cell-derived EV and ACdEV biogenesis pathways. A) The endosomal pathway leads to the release of exosomes (Colombo *et al.,* 2014). The process begins with the formation of early endosomes which mature into late endosomes and undergo inward budding to form intraluminal vesicles (ILVs), which are commonly enriched in tetraspanin CD63 and accumulate to form multivesicular bodies (MVBs). MVBs either fuse with lysosomes for degradation or with the plasma membrane to release ILVs as exosomes into the extracellular environment. This pathway either relies on the ESCRT complexes or alternative mechanisms, such as lipid rafts or tetraspanin-enriched domains (TEMs) (Dixson *et al.,* 2023).B) Microvesicles are released directly from the plasma membrane through budding, a process mediated by arrestin domain-containing protein 1 (ARRDC1), tetraspanins, lipid rafts and certain ESCRT machinery components including tumor susceptibility gene 101 (TSG101) (Dixson *et al.,* 2023). These connect to the actin cytoskeleton, driving membrane rearrangement and selective EV cargo packaging. C) Spingosine-1-phosphate (S1P)-S1P receptor 1 and 3 (S1PR1/3) plays a key role in release of apoptotic exosome-like vesicles; sphingosine kinase 2 (SPHK2) increases the S1P concentration at the plasma membrane (Park *et al.,* 2018). S1P activates S1PR1 and S1PR3, leading to actin cytoskeleton regulation, formation of 'spindle-like' structures, and endocytosis (Park *et al.,* 2018). This process produces endosomes enriched in S1PRs and CD63, which mature into MVBs that release exosome-like vesicles upon fusion with the plasma membrane. D) Autophagosomal fusion to lysomes, forming 'autolysosomes', has been reported to harbour ILVs which are then released as apoptotic exosome-like vesicles upon fusion to the plasma membrane (Beillevaire *et al*., 2022). Figure produced using Biorender.

1.5 Mechanisms of EV communication

A major focus in EV research is understanding how EVs communicate with recipient cells. Much of the attention has centred on the intracellular uptake of EVs via endocytosis, possibly driven by the wide interest in their potential for therapeutic cargo delivery (Sun *et al.,* 2023; Kim & Kim, 2017). However, EVs can signals with recipient cells via many mechanisms: EV surface-cell surface binding interactions activating receptors and associated intracellular signalling cascades or facilitating direct transfer of membrane-associated molecules, or EV modulation of the ECM (Buzás *et al.,* 2019). Furthermore, the cell source and dose of EVs have been shown to induce differential phenotypic changes in recipient cells, revealing the process of EV communication is complex and multifaceted (Hagey *et al.,* 2023).

1.5.1 EV surface

The ‘EV surface refers to the properties of the EV surface and is comprised of the phospholipid bilayer membrane and a diverse array of membrane-embedded molecules including proteins, lipids and nucleic acids (Buzás *et al.,* 2019). Together, the different components of the EV surface governs the initial interaction between EVs and their environment, dictating EV uptake by recipient cells, surface-to-surface signalling, modulation of the ECM, and the directional movement of EVs.

The ability to probe the EV surface has led to the identification of several common surface-expressed EV markers: most famously tetraspanins CD9, CD63, CD81, which are used in several commercial immunocapture methods of EV isolation and detection (Welsh *et al.,* 2024). The presence of several other proteins has also been noted: adhesion molecules, complement proteins, heat-shock proteins, MHC II and various cell surface receptors (Buzás *et al.,* 2019). Lipidomics analysis has revealed the majority of EVs are enriched in specific lipid species PS, glycosphingolipids, sphingomyelin and cholesterol (Skotland *et al.,* 2020). Furthermore, the EV lipidome is an indication of biogenesis, method of cargo sorting, and can also impact downstream EV communication (Fyfe *et al.,* 2023). The EV lipidome is not merely the structural building block of an EV, but also acts as a bioactive lipid platform that can signal with its surrounding environment; EVs can contain enzymes required to catalyse lipid precursors, such as arachidonic acid and polyunsaturated fats, into bioactive mediators, such as eicosanoids (Fyfe *et al.,* 2023). Notably, the ability to discern molecules associated with the EV membrane surface versus intraluminal cargo remains an ongoing challenge (Fyfe *et al.,* 2023). Despite several conserved EV molecules, the EV surface is incredibly diverse and depends on the originating cell type, mode of EV biogenesis and the microenvironment (Buzás *et al.,* 2019).

The EV surface is comprised of bioactive molecules (Buzás *et al.,* 2019). The functional activity of the EV surface has been demonstrated and implicated in many settings: as previously discussed, apoptotic cells release EVs (ACdEVs) which act as chemotactic mediators by displaying 'find me' signals, CX3CL1 and ICAM-3, to attract phagocytes to the site of apoptosis for efficient removal (Truman *et al.,* 2008; Torr *et al*., 2011). Viable cell derived-EVs from activated T cells can also induce apoptosis of recipient cells by presenting Fas ligand or TRAIL ligands which bind to death receptors and activate the extrinsic apoptosis pathway (Rivoltini *et al.,* 2016; Monleón *et al.,* 2001). EVs have been shown to engage in antigen presentation to immune cells via their MHC II expression; B cells release EVs that displayed peptide-bound MHC II at their surface and are able to induce T cell responses, revealing that EVs can instigate immune responses through surface binding interactions with recipient immune cells (Raposo *et al.,* 1996). The EV surface can also direct EVs to specific sites; various tumour cells were shown to release EVs that accumulated at specific tissue sites depending on the EV surface expression of specific integrins (Hoshino *et al.,* 2015). This directional EV homing allowed prediction of organ-specific metastasis (Hoshino *et al.,* 2015). Indeed, a significant amount of work is continued to be invested in organotropic drug delivery and engineering EVs to enhance this trait for more efficient targeted drug delivery (Busatto *et al*., 2019).

More recently, increasing attention is being given to the impact of the surface 'corona' on EV function, a loosely attached layer of molecules that adsorb to the EV surface and vary in composition depending on the surrounding environment (Buzás, 2022). The formation of a corona at the surface of artificial nanoparticles (*e.g.* lipid nanoparticles, liposomes) has been well established and implicated in the efficacy of drug delivery phosphatidylserine (PS), phosphatidylethanolamine (PE), phosphatidylcholine (PC), sphingolipids (SM), ceramide (a byproduct of the sphingolipid, sphingomyelin) and cholesterol (Skotland *et al.,* 2020; Xiao & Gao, 2018). However, the composition of an EV corona is not well characterised, especially *in vivo* (Buzás, 2022). To date, most studies have characterised the protein content of EV coronas formed by exposure to plasma or serum and therefore, are reported to comprise of proteins commonly present in plasma, including apolipoproteins and immunoglobulins (Tóth *et al,* 2021). However, the EV corona is comprised of a diverse array of molecules, including lipids, glycans and nucleic acids, that is likely to form spontaneously, depending on the microenvironment, by a combination of electrostatic interactions and receptor-ligand interactions (Yerneni *et al.,* 2022; Buzás, 2022). Notably, EV surfaces tend to be negatively charged, and thus, may preferentially attract positively charged molecules (Richter *et al.,* 2021). The importance of EV corona on downstream EV function was first highlighted by E. Tóth *et al* in 2021, where they observed

differential cytokine release induced in recipient dendritic cells, when incubated with plasma-coated THP-1-derived EVs versus uncoated THP-1-derived EVs (Tóth *et al*, 2021). Therefore, in addition to the EV surface, the EV corona also dictates EV function.

The EV surface is also important for intracellular uptake of EVs, with the surface composition likely influencing the pathway of uptake (Mulcahy *et al.,* 2014). Protein and sugar interactions are thought to be particularly important in initiating uptake, such as tetraspanins, adhesion molecules, proteoglycans, glycans and lectins (Williams *et al.,* 2019; Mulcahy *et al.,* 2014). Furthermore, the presence of a protein corona can enhance or inhibit EV uptake (Liam-Or *et al.,* 2024; Dietz *et al.,* 2023). One study found that serum-coated EVs had coronas enriched in albumin, which inhibited phagocytic uptake by hepatic macrophages while enhancing uptake by hepatocytes and other liver cells (Liam-Or *et al.,* 2024). This suggests that the corona can retarget EVs to specific recipient cells, highlighting the dynamic nature of the EV surface. Most recently, the presence of a glycocalyx coat on early apoptotic bodies hints at exciting functional differences between early and late apoptotic bodies (Kelly and Ravichandran, 2024; Le *et al.,* 2024). Future work should aim to determine the presence and functional relevance of glycocalyx coats on the surface of ACdEVs.

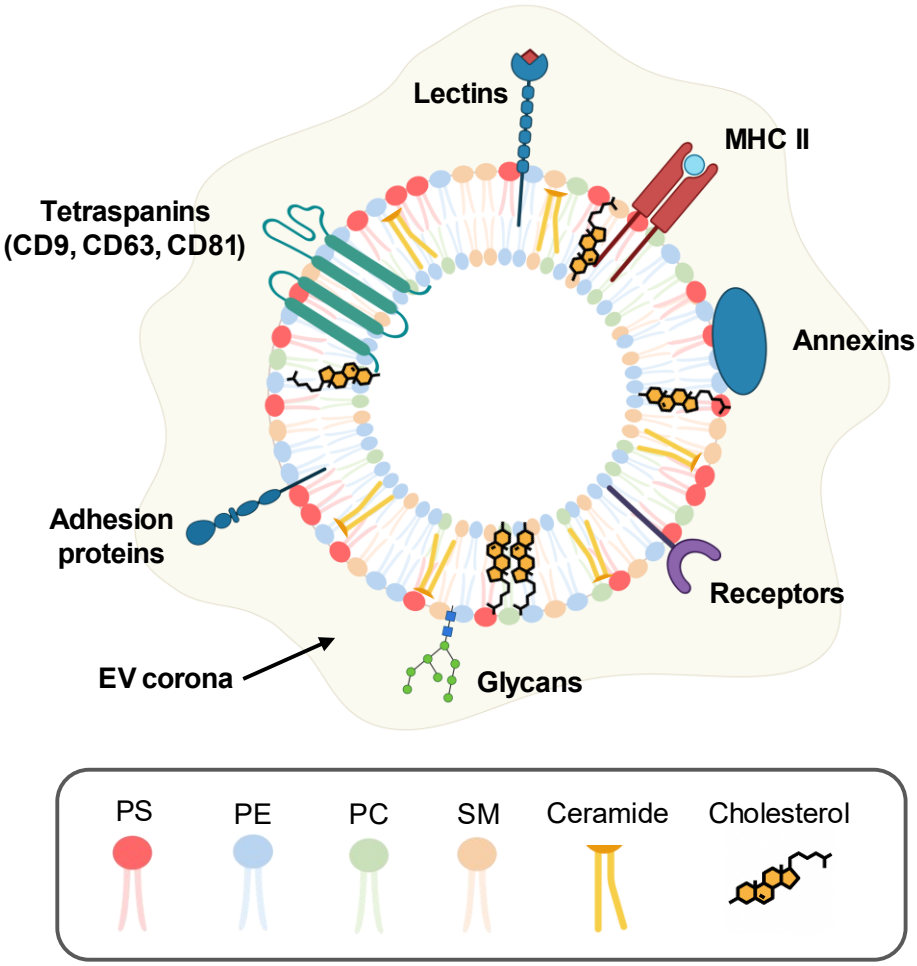

Figure 1.6: The EV surface. EVs commonly display tetraspanins, adhesion proteins, glycans, cell surface receptors, annexins, MHC II and lectins (Buzás *et al.,* 2019). EVs are enriched in EVs also have a dynamic corona layer comprised of proteins, lipids and nucleic acids, that spontaneously adsorb to the EV surface depending on the microenvironment (Yerneni *et al.,* 2022; Buzás, 2022). Figure made using Biorender.

1.5.2 EV uptake

EVs have been shown to enter cells by several different active mechanisms: clathrin-mediated endocytosis, direct membrane fusion, phagocytosis, caveolin-mediated endocytosis, micropinocytosis and lipid raft-mediated endocytosis (Mulcahy *et al.*, 2014). Notably, several variations of endocytosis are noted; endocytosis refers to the intracellular trafficking of material to the endosomal compartment, of which there are several known mechanisms that cells are able to internalise material and traffic to the endosome. Each mechanism will be briefly described.

Clathrin-mediated endocytosis (CME) can be briefly defined as: the early recruitment of clathrin, induction of membrane curvature, selective recruitment of cargo, clathrin cage assembly, formation of clathrin-coated pits, dynamin 2-mediated scission, followed by trafficking to the endosomal compartment. Here, the vesicle undergoes uncoating, upon which disassembled clathrin cages and adaptor proteins undergo recycling and the EV fuses to the endosome membrane and releases its cargo (McMahon and Boucrot, 2011). Notably, clathrin does not directly bind to the vesicle membrane, but instead depends on the recruitment of adapter proteins that form the interface between the clathrin coat and the vesicle membrane (McMahon and Boucrot, 2011). This intermediatory step provides an additional level of control, in which adaptors selectively recruit cargo receptors and coat components, such as clathrin. For example, AP-2, the evolutionary conserved adaptor complex, is comprised of four subunits and functions to initiate membrane curvature, localisation of clathrin and other adaptor proteins (Boucrot *et al.,* 2010).

Caveolin-mediated endocytosis is characterised by the presence of caveolae, small membrane indentations that resemble clathrin-coated pits. They are enriched in caveolin proteins, sphingolipids and cholesterol, highlighting the likely interplay between proteins and lipids (Mulcahy *et al.*, 2014). Caveolae can enclose extracellular material, such as EVs, and transport them intracellularly to the endosomal compartment. The full array of molecular machinery is yet to be determined, however, dynamin 2 may also be involved in vesicle fission, as in CME (Mulcahy *et al.*, 2014).

Lipid rafts can both aid CME and caveolin-mediated endocytosis and mediate an alternative clathrin/caveolin independent mechanism of endocytosis (Sapoń *et al.,* 2023). Lipid rafts are localised microdomains that are comprised of a unique lipid composition, enriched in sphingolipids and cholesterol (Mulcahy *et al.*, 2014). Lipid rafts alter the membrane fluidity and can regulate the distribution of proteins, such as the formation of highly ordered clusters of protein molecules. One example of this is the localisation of flotillin proteins at the cytoplasmic inner region of lipid rafts; flotillins have been shown to mediate membrane curvature and invagination by oligomerisation, leading to the subsequent formation of intracellular vesicles (Sapoń *et al.,* 2023; Frick *et al.,* 2007). In addition, calveolin has been demonstrated to directly bind cholesterol within lipid rafts, which triggers the formation of caveolin membrane indentations (Sapoń *et al.,* 2023; Murata *et al.,* 1995).

Phagocytosis is a process undertaken by professional or non-professional phagocytes; the terms ‘professional’ and ‘non-professional’ refer to efficiency of phagocytosis capability *e.g* macrophages, neutrophils and dendritic cells or epithelial cells, endothelial cells, and fibroblasts, respectively (Gordon, 2016). Generally, phagocytosis is associated with the engulfment of cellular

material (> 0.5 μm) such as, apoptotic bodies or entire cells (Gordon, 2016). However, it may also be a mechanism in which phagocytes internalise EVs (Mulcahy *et al.*, 2014). Phagocytosis is governed by receptor-mediated interactions, referred to as 'eat me' signals, which have been previously described (see section 1.4). Notably, EVs are enriched in surface-exposed PS which may facilitate their phagocytic uptake, given that PS exposure on cells is an indication of apoptosis (Buzás *et al.,* 2019). Furthermore, the EV surface is described to consist of immunoglobulins and complement proteins, both of which are ligands to a variety of phagocyte receptors and may promote their uptake (Sun *et al.,* 2024).

Phagocytosis involves the formation of an internal phagosome, a membrane-bound compartment that engulfs the target material (Gordon, 2016). The actin cytoskeleton plays a crucial role in extending the phagocyte membrane during this process. Upon engulfment, the phagosome fuses with the lysosome, allowing enzymatic degradation of the ingested material (Gordon, 2016). As phagocytosis is known to be a degradative process, it is unclear whether EVs can transmit messages or induce phenotypic changes after being phagocytosed, or whether their components are simply degraded. From a therapeutic drug delivery perspective, efforts have been made to engineer EVs to evade phagocytic uptake and promote site-directed delivery, such as by coating EVs with factors that inhibit phagocytosis (Sun *et al.,* 2024).

Macropinocytosis is another type of endocytosis, associated with the intracellular uptake of extracellular fluid via the extension of characteristic membrane 'ruffles' (Mulcahy *et al.*, 2014). Driven by the actin cytoskeleton, cells extend membrane ruffles which can trap extracellular fluid containing EVs and re-fuse with the plasma membrane. This facilitates the engulfment of large intracellular vesicles termed 'macropinosomes' (Mulcahy *et al.*, 2014). Cholesterol mediates the recuitment of the GTPase, Rac1, a major player of macropinocytosis, functioning to regulate actin cytoskeletal rearrangement (Grimmer *et al.*, 2002). Notably, macropinocytosis is not receptor-mediated and as such, is less specific.

Another method of EV internalisation is direct fusion of the EV membrane to the recipient cell membrane, functioning to release the EV intraluminal contents into the cytoplasm of the cell (Prada & Meldolesi, 2016). Evidence suggests that membrane fusion may be promoted at a low pH, such as the environment of the endosome (Parolini *et al.,* 2009). Due to the breadth of knowledge surrounding endocytic pathways, it is unlikely membrane fusion is the main mechanism EVs enter cells (Mulcahy *et al.*, 2014).

Importantly, how the cargo or membrane component of the internalised EV is processed will dictate its downstream function in the recipient cell, *i.e.* whether the cargo contents are degraded, recycled or remain bioactive. To date, little is understood about the intracellular processing pathways except that the endosome is predicted to be the primary destination for most EVs (Mulcahy *et al.*, 2014). Therefore, future work should aim to understand how the processing of EV cargo is regulated and what governs whether EV cargo is degraded, recycled or preserved.

1.6 Harnessing EVs for therapy

There is great interest in EVs as promising candidates for therapeutic applications due to their ability to efficiently cross biological membranes and their abundance in biological fluids and engineering of EVs for optimal loading and delivery with various therapeutic cargos, such as synthetic drugs or nucleic acid therapies (Kumar *et al.,* 2024) (Wang *et al.,* 2023) (Richter *et al.,* 2021). EVs also have low immunogenicity, making them less likely to trigger immune responses, and their ability to preserve cargo from degradation could be utilised to increase the therapeutic half-life (Wang *et al.,* 2023). One of the most notable advantages of EVs is their ability to cross the blood-brain barrier, a major challenge in treating neurological conditions (Ramos-Zaldívar *et al.,* 2022). Moreover, EVs can be engineered to target specific cell types; this was first done by Alvarez-Eviti *et al.,* where they targeted exosomes to deliver siRNA to brain tissue (Alvarez-Erviti *et al.,* 2011). Site-directed delivery may improve drug efficacy and minimise off-target effects, leading to fewer side effects. Indeed, several ongoing clinical trials are investigating the potential of mesenchymal stem cell (MSC)-derived EVs, as they have been shown to induce similar anti-inflammatory effects to MSCs (Mendt *et al.,* 2019). However, it has been noted that upon implantation, MSCs rapidly undergo apoptosis and release ACdEVs, which may be responsible for their therapeutic functions (Zhu *et al.,* 2023). Indeed, MSC-derived ACdEVs have been shown to promote tissue regeneration in skin, bone, muscle and the vasculature (Zhu *et al.,* 2023). MSC-derived ACdEVs and apoptotic bodies can also promote M2 polarisation and proliferation (Zhu *et al.,* 2023; Li *et al.,* 2022; Liu *et al.,* 2020). Furthermore, ACdEVs, derived from several other cell types, have shown therapeutic potential by enhancing apoptotic cell clearance, supressing further activation of immune cells and promoting macrophages to exert anti-inflammatory, pro-resolving functions (Liu *et al.,* 2020; Shen *et al.,* 2017; Fehr *et al.,* 2013; Segundo *et al.,* 1999).

From a therapeutic perspective, EVs may not even require loading with drugs; their surface properties alone can interact with cell receptors to trigger signalling cascades (Buzás *et al.,* 2019).

In addition, since the EV surface is external and accessible for direct probing, it offers a valuable opportunity to identify novel biomarkers. Indeed, much research is dedicated to detecting novel disease-associated biomarkers for diagnosis and prognosis (Kumar *et al.,* 2024). With EVs present in all bodily fluids, they present an opportunity for accessible and non-invasive diagnostic methods. For example, endothethial-derived ACdEVs have been proposed as biomarkers of coronary heart disease (Zacharia *et al.,* 2020; Berezin *et al*., 2019).

Furthermore, functionalisation of EV surfaces via incorporation of membrane-associated proteins, such as TRAIL, has been shown to be significantly enhance their potency than soluble recombinant forms, likely due to the lipid environment supporting protein structure and function (Yuan *et al.,* 2017). As previously described, ACdEVs have been shown to recruit phagocytes via surface expression of CX3CL1 and ICAM-3 (Torr *et al*., 2011; Truman *et al.,* 2008). Therefore, it may be possible to engineer EVs to mimic ACdEVs by expressing a high concentration of 'find me' and 'eat me' signals at the EV surface to enhance their inherent pro-resolving functions. Genetic manipulation of cell lines can be implemented to cause overexpression of 'find me'/'eat me' signals, which one would expect to result in an increased abundance of the proteins at the EV surface. Alternatively, if a desired protein is not normally present at EV surfaces, the desired protein can be fused to a protein known to be highly expressed at EV surfaces by genetic engineering; indeed, this has been done with lysosome-associated membrane protein 2 isoform B (LAMP2B) or GPI anchor signal peptides (Richter *et al.,* 2021). Other methods of engineering EV surfaces include fusion of EVs with artificial liposomes, insertion of lipids and controlled adsorption of molecules to the EV surface (Richter *et al.,* 2021).

Given the ongoing challenges with drug delivery efficiency, the EV surface may be a promising area for focus; EVs have a large surface membrane area: volume ratio which presents a platform of opportunity for EV-cell interactions, and therefore, engineering of the EV surface offers great therapeutic potential (Buzás *et al.,* 2019).

1.7 Technical challenges in studying EVs

Of the EVs that are released by apoptotic cells, most research has concentrated on characterising apoptotic bodies, the largest EV population, likely because they were discovered first and present fewer technical challenges for study (Poon *et al.,* 2014b). Due to their nanoscopic size, heterogeneity and overlapping characteristics with other types of biological nanoparticles, ACdEVs (and EVs in general) remain challenging to characterise.

Firstly, isolation and purification of EVs is challenging due to the risk of co-isolation of several other biological nanoparticles that overlap in size and density *e.g.* lipoproteins and protein aggregates. Some of the most common methods used are differential ultracentrifugation (dUC), size exclusion chromatography (SEC) and tangential flow filtration (TFF). Each have their caveats: for instance, dUC causes aggregation of EVs due to the high centrifugal force (100,000 xg) exerted on them, SEC dilutes EV samples and TFF is generally time consuming, requires large volumes and specialised equipment (Welsh *et al.,* 2024) (Linares *et al.,* 2015). Furthermore, dUC and SEC can disrupt the EV corona (Welsh *et al.,* 2024).

To identify confirm the presence of EVs and the absence of contaminating co-isolated nanoparticles, researchers often use a panel of common EV markers, most often the tetraspanins CD9, CD63 and CD81. However, this is flawed as not all EVs express these markers and indeed some EVs have been shown to express none of these three tetraspanins (Welsh *et al.,* 2024). In addition, exosomes, microvesicles and apoptotic bodies lack unique markers that distinguish each EV subpopulation from one another (Welsh *et al.,* 2024). Distinguishing between these subtypes and understanding their specific roles remains a significant challenge. This has led to ongoing debate surrounding appropriate classification and use of nomenclature (Welsh *et al.,* 2024). To date, most researchers refer to vesicles derived from the endosomal biogenesis pathway as ‘exosomes’, vesicles that bud directly from the plasma membrane as ‘microvesicles’ and large vesicles (> 1000 nm) released from apoptotic cells as ‘apoptotic bodies’ (Welsh *et al.,* 2024). As previously described, ‘ACdEVs’ is the generic term used in this thesis to refer to EVs that are < 1000 nm released from apoptotic cells, that may contain a mixture of microvesicle-like and exosome-like EVs or those that have a distinct mode of biogenesis.

Due to their nanoscopic size and often low yield, accurate quantification and characterisation of EVs is technically challenging (Welsh *et al.,* 2024). Common techniques used include nanoparticle tracking analysis (NTA), dynamic light scattering (DLS) and tunable-resistive pulse sensing (TRPS) which characterise the physical traits of EVs *e.g.* size, concentration, surface charge. Techniques that characterise the biochemical EV composition include western blotting, ELISA, fluorescent NTA, single molecule localisation super resolution microscopy (SMLM), nano-flow cytometry. Due to their small size, EV samples push the limit of detection for most characterisation techniques; indeed, most EVs are below the diffraction limit and therefore, require high resolution microscopy methods for imaging, such as SMLM or transmission electron microscopy (TEM) (Welsh *et al.,* 2024).

Nano-flow cytometry is a popular method chosen for the characterisation of EVs due to it offering multiparametric single-EV measurements, providing information of biochemical composition, size and concentration (Welsh *et al.,* 2023). Flow cytometry is a technique that implements hydrodynamic focusing to direct cells or nanoparticles into single file, enabling them to be interrogated by lasers one at a time. Most flow cytometers are designed to detect cells, which are orders of magnitude bigger in size than the smallest EVs, and therefore emit a much bigger light scatter or fluorescence signal. To effectively separate EVs from background noise, flow cytometers require highly sensitive detectors (Welsh *et al.,* 2023). In addition, a sufficiently slow flow rate is required to ensure single particle interrogation. To report size and concentration, standards are required; often these are beads made of polystyrene or silica, which will inevitably scatter light differently to EVs, described by refractive index (RI). Silica has a RI which is similar to EVs (~1.45 and ~1.40, respectively, compared to polystyrene which has a RI of ~1.605) (Welsh *et al.,* 2023). Therefore, differently sized silica nanoparticle populations can be used to produce a standard curve and calculate the relevant size of each detected EV. In addition, a concentration standard (*i.e.* a bead or nanoparticle with a known concentration) can be used to determine flow rate, which is used to calculate sample concentration. Importantly, how EVs are defined by nano-flow cytometry should be carefully considered. The most sensitive flow cytometers can reach a limit of detection of particles < 40 nm. As such, nano-flow cytometric readings can be easily obscured by contaminating particles such as protein aggregates, salt precipitate or bubbles. To overcome this, EVs can be labelled with a fluorescent probe. The choice of probe is important as it must effectively label the entire EV population. Antibodies targeting specific molecules will fail to label EVs lacking that particular marker, leading to undetected populations (Welsh *et al.,* 2023). Conversely, dyes are less specific, but many tend to aggregate, which can produce false positive events being recorded (Welsh *et al.,* 2023). To mitigate this, a clean-up step is necessary, or alternatively, self-quenching dyes, such as MemGlow™ (Cytoskeleton, Inc.), can be used to minimise false positive fluorescent events. Overall, nano-flow cytometry offers an effective way to probe the surface of EVs for molecules of interest, obtaining information of molecular localisation in addition to confirming their presence.

EVs also contain heterogeneous intraluminal cargo, consisting of proteins, lipids, and nucleic acids, which vary depending on the cell of origin, biogenesis pathway and physiological conditions. Advanced omics technologies (proteomics, genomics, lipidomics) can detail the presence and enrichment of EV cargo in different conditions. However, these techniques require a high concentration of EVs which often exceeds the native EV concentration in biological fluids/tissues,

making additional concentration steps necessary (Welsh *et al.,* 2024). Furthermore, identifying whether molecules are located inside the EV lumen or localised to the EV surface is challenging.

Defining the functional role of EVs is complex; different methods of isolation and sample preparation can affect EV structure, concentration and molecular composition (*e.g.* EV corona) (Welsh *et al.,* 2024). Furthermore, attributing a particular function to EVs is challenging due to the difficulty in separation from contaminating nanoparticles. Additionally, EV dose can alter the functional output of EVs in recipient cells, highlighting the importance of considering physiologically relevant EV concentrations (Hagey *et al.,* 2023).

1.8 Project aims and objectives

This project seeks to address key gaps in our understanding of the composition and function of ACdEVs in modulating immune cell responses. Despite their importance, several key aspects of ACdEV biology, and EV biology in general, remain poorly understood. For instance, the regulation of ACdEV release, particularly why they are more abundantly released during apoptosis, is not fully elucidated. There is limited knowledge regarding how their composition is regulated, including the active packaging of cargo observed in structures like apoptopodia (Aktin-Smith *et al*, 2015). Additionally, the molecular mechanisms governing how ACdEVs interact with and are taken up by recipient cells remain largely unknown, leaving a significant gap in our understanding of their communication with the immune system.

Furthermore, it is unclear how the cargo of ACdEVs is processed upon internalisation by recipient cells and how this processing influences immune cell phenotypes, especially in terms of promoting pro-resolving activity. Given that the ACdEV surface is the first point of contact with recipient cells, it is particularly crucial in determining the nature of ACdEV-cell interactions. Therefore, this thesis focuses on the surface properties of ACdEVs, emphasising their proteomic composition.

While ACdEVs are known to facilitate apoptotic cell clearance and promote anti-inflammatory, pro-resolving functions in immune cells, the precise molecular mechanisms that regulate their communication with the immune system remain unclear (Liu *et al.,* 2020; Segundo *et al.,* 1999). To date, only two ACdEV surface molecules, CX3CL1 and ICAM-3, have been characterised (Torr *et al.,* 2011; Truman *et al.,* 2008), with ICAM-3 being limited to expression on leukocytes (Torr *et al.,* 2011). There is an ongoing need to identify additional functionally active molecules present on the surface of ACdEVs and to investigate whether their composition and function vary

at different stages of apoptosis. Additionally, determining whether ACdEV surface interactions alone can initiate immune responses may provide insights that could inform the design of engineered EV surfaces, potentially leading to novel therapeutic strategies. Together, this research aims to enhance our understanding of the regulatory roles ACdEVs play in immune system processes and the molecular mechanisms that govern their interactions with recipient cells.

This project aimed to:

i. Establish a method for inducing apoptosis and collecting ACdEVs. This included characterisation of their physical and biochemical properties by comparing size, concentration, and expression of common EV markers across ACdEVs from different immune cell types and stages of apoptosis.

ii. Identify the protein composition of ACdEVs through data mining of mass spectrometry proteomic datasets and identify key candidate proteins based on their predicted surface localisation and functional relevance. Surface localisation was confirmed by nano-flow cytometry.

iii. Investigate how the ACdEV surface proteome modulates immune cell activity. Specifically, the functions of key candidate proteins were assessed using an antibody blockade strategy to identify their roles in immune cell migration, uptake or binding, and phenotype.

Chapter 2 Materials and methods

2.1 Materials

2.1.1 Reagents

Reagent	Manufacturer
RPMI 1640 Medium (With L-glutamine and sodium bicarbonate, liquid, sterile-filtered, suitable for cell culture)	Sigma Aldrich
Foetal bovine serum (FBS) of South American origin	Gibco (Thermo Fisher Scientific)
Penicillin – streptomycin	Sigma Aldrich
Dimethyl sulphoxide (DMSO)	Thermo Fisher Scientific
Dulbecco's phosphate buffered saline	Gibco (Thermo Fisher Scientific)
1α,25-Dihydroxyvitamin D_3 (VD3)	Enzo Life Sciences
Phorbol 12-myristate-13-acetate (PMA)	Sigma Aldrich
Recombinant Human IL-4	R&D Systems
Recombinant Human IL-13	R&D Systems
Recombinant Human Granulocyte-Macrophage colony-stimulating factor (GM-CSF)	R&D Systems
Recombinant Human Interferon Gamma (IFNγ)	R&D Systems
Lipopolysaccharide from *E.coli* (LPS)	Sigma Aldrich
RosetteSep™ Human Monocyte Enrichment Cocktail	STEMCELL Technologies
Lymphoprep™ Density Gradient Medium	STEMCELL Technologies
ACK Lysing buffer	Gibco (Thermo Fisher Scientific)
Staurosporine	Thermo Fisher Scientific

Table 2.1: Cell culture reagents

Reagent	Manufacturer
Bovine Serum Albumin (BSA)	Roche
Ethylenediaminetetraacetic acid (EDTA)	Invitrogen (Thermo Fisher Scientific)
qEVoriginal Columns, generation 1	Izon (no longer supplied)
Amicon filter (30 kDa)	Merck
FITC Annexin V Apoptosis Detection Kit with Propidium Iodide (PI) and Annexin V binding buffer	BioLegend
BODIPY™ FL N-(2-Aminoethyl)) Maleimide	Invitrogen (Thermo Fisher Scientific)
MemGlow™ 488	Cytoskeleton, Inc.
MemGlow™ 640	Cytoskeleton, Inc.
NanoFCM™ Silica Nanoparticles Cocktail S16M-Exo	NanoFCM
Quality Control Nanosphere series	NanoFCM
Pierce™ Coomassie Brilliant Blue Dyes	Thermo Fisher Scientific
Pierce™ Prestained Protein MW Marker	Thermo Fisher Scientific
Thermo Scientific Chemicals Laemmli SDS sample buffer, reducing (4X)	Thermo Fisher Scientific
Acylamide	Thermo Fisher Scientific
SDS micro-pellets	Melford
N,N,N′,N′-Tetramethylethylenediamine (TEMED)	Melford
Ammonium persulphate	Merck

Table 2.2: Assay reagents

2.1.2 Antibodies

Target	Isotype	Fluorophore	Manufacturer / Cat. No.
CD9	Mouse IgG1, κ	FITC	Abcam (ab18241)
CD63	Mouse IgG1, κ	FITC	Abcam (ab18235)
CD63	Mouse IgG1, κ	APC	Abcam (ab319310)
CD81	Mouse IgG1, κ	FITC	Antibodies.com (A86716)
N/A	Mouse IgG1, κ	FITC	Abcam (ab106163)
CD31	Mouse IgG1, κ	APC	Invitrogen (17-0319-42)
CD47	Mouse IgG1, κ	APC	Invitrogen (17-0479-42)
CD49d	Mouse IgG1, κ	APC	BioLegend (304308)
CD166	Mouse IgG1, κ	APC	BioLegend (343906)
N/A	Mouse IgG1, κ	APC	Invitrogen (17-4714-82)
CD11b	Rat IgG2b, κ	BV750™	BioLegend (101267)
N/A	Rat IgG2b, κ	BV750™	BioLegend (402607)
CD14	Mouse IgG1, κ	APC/Fire™ 750	BioLegend (367120)
N/A	Mouse IgG1, κ	APC/Fire™ 750	BioLegend (400196)
CD40	Mouse IgG1, κ	APC	BioLegend (334310)
N/A	Mouse IgG1, κ	APC	BioLegend (400120)
CD64	Mouse IgG1, κ	BV421™	BioLegend (305020)
N/A	Mouse IgG1, κ	BV421™	BioLegend (400158)
CD86	Mouse IgG2b, κ	Super Bright™ 600	Invitrogen (63-0869-42)
N/A	Mouse IgG2b, κ	Super Bright™ 600	Invitrogen (63-4732-82)
CD206	Mouse IgG1, κ	PerCP-eFluor™ 710	Invitrogen (46-2069-42)
N/A	Mouse IgG1, κ	PerCP-eFluor™ 710	Invitrogen (46-4714-82)
CD209	Rat IgG2b, κ	FITC	Invitrogen (11-2099-42)
N/A	Rat IgG2b, κ	FITC	Invitrogen (11-4321-80)

Table 2.3: Antibodies and isotype-matched controls.

Target	Clone	Manufacturer / Cat. No.	References for antibody blockade
CD31	HEC7	Invitrogen (MA3100)	(Rahman *et al.*, 2021) (Williams *et al.*, 2009) (Chandrasekaran *et al.*, 2000) (Gröger *et a*l., 1999) (Luscinskas *et al.*, 1996)
CD47	B6H12	Invitrogen (14-0479-82)	(Reed-Geaghan *et al.*, 2009)
CD49d	TA-2	Invitrogen (MA49D7)	(Brennan et al., 2008) (Davies *et al.*, 1999) (Issekutz, 1991)
CD166	3A6	BD Biosciences (559260)	(Castro *et al.*, 2007)

Table 2.4: Blocking antibodies.

2.1.3 Equipment

- GelDoc Go Imaging System (Bio-Rad, USA)
- Cytation 5 automated cell imaging reader (Biotek, USA)
- CytoFLEX S (Beckman Coulter, USA)
- EVOS™ FL Digital Inverted Microscope (Invitrogen, UK)
- Ix83 inverted microscope (Olympus (Evident) Japan) equipped with a SMLM module SAFe MN360 (Abbelight, France).
- JEOL2200FS Transmission Electron Microscope (Jeol Ltd., Japan)
- Multiskan™ GO Microplate Spectrophotometer (Fisher Scientific, UK)
- NanoAnalyzer (NanoFCM, China)
- UVP Chromato-vue C71 light box cabinet and UVX radiometer (UV-PInc, USA)

2.2 Methods

2.2.1 Cell culture

2.2.1.1 Cell lines

A human monocyte cell line THP-1 (TIB-202, ATCC) and a human Jurkat T cell line (CRL-2900, LGC Standards) were maintained at a density of 5 x 10^5 cells/mL in RPMI-1640 medium, supplemented with 10% (v/v) foetal bovine serum (FBS), 2 mM L-glutamine, 100 U/ml penicillin, and 100 µg/ml streptomycin. Cell cultures were kept at 37°C in a humidified environment with 5% CO2.

THP-1 monocytes were differentiated into macrophages either by a 48 hour treatment with 100 nM dihydroxyvitamin D3 (Enzo Life Sciences™, UK) or a 1 hour treatment with 10 ng/mL phorbol 12-myristate 13-acetate (PMA, Sigma Aldrich). For both treatments, THP-1 cells were left to differentiate for 48 hours. THP-1 macrophages were polarised into M1 macrophages by a 48 hour treatment with 10 ng/mL lipopolysaccharide (LPS) (R&D) and 0.32 ng/mL interferon-γ (IFN-γ) (R&D), and M2 macrophages by a 48 hour treatment with 20 ng/mL interleukin-4 (IL-4) (R&D) and 20 ng/mL interleukin-13 (IL-13) (R&D).

2.2.1.2 Primary human monocytes

Concentrated blood cones (500 mL concentrated to 7 mL) were collected from four healthy donors from the Queen Elizabeth hospital in Birmingham, UK (NHS Blood and Transplant). Primary monocytes were collected by a negative-selection cocktail (RosetteSep™ Human Monocyte Enrichment Cocktail). Briefly, 7 mL blood was topped up to 10 mL with wash buffer (containing 2% heat-inactivated FBS and 1 mM EDTA). 500 µL RosetteSep™ Human Monocyte Enrichment Cocktail was added and incubated at room temperature for 30 minutes. The blood sample was then topped up to 20 mL with wash buffer and loaded onto 20 mL Lymphoprep™ density gradient medium, followed by centrifugation at 1200 x g for 20 minutes at room temperature. The monocyte-enriched layer was collected and resuspended in wash buffer, followed by centrifugation at 300 x g for 5 minutes. To lyse contaminating erythrocytes, ACK lysing buffer was incubated with the cell pellets for 5 minutes at room temperature. Cell pellets were washed once again (300 x g, 5 minutes) and the pelleted primary monocytes were resuspended in complete RPMI medium and left to settle in a T75 cm^2 flask (non-tissue culture treated). After 3 hours, floating monocytes were removed and seeded into a second T75 cm^3 flask and allowed to adhere. Primary monocytes were treated with 20 ng/mL granulocyte-macrophage colony-stimulating

factor (GM-CSF) for six days to differentiate into primary human monocyte-derived macrophages (pM0s). pM0 cells were polarised into M1 macrophages (pM1) and M2 macrophages (pM2) using the same 48 hour treatments as the THP-1 model: 10 ng/mL LPS and 0.32 ng/mL IFN-γ, and 20 ng/mL IL-4 and 20 ng/mL IL-13, respectively. In addition, pM0 cells were incubated with ACdEVs (unblocked and antibody-blocked) for 48 hours (Supplementary Table 5.1).

2.2.2 Induction of apoptosis

To remove FBS-contaminant EVs, cells were washed in sterile PBS and resuspended at 4 x 10^6 cells/mL in serum-free phenol red-free RPMI-1640 medium (supplemented with 2 mM L-glutamine, 100 U/ml penicillin, and 100 µg/ml streptomycin). Apoptosis was induced by exposure to 310 nm ultraviolet light in a Chromato-Vue C-71 viewing cabinet. The UV dosage was measured using a UVP radiometer connected to a UVX-31 detector, and the cells were exposed to a UV-B dose of 100 mJ/cm^2, in line with our previous established protocol (Torr *et al.,* 2011).

2.2.3 Preparation of apoptotic cell secretome and apoptotic cell-derived extracellular vesicles (ACdEVs)

Apoptotic cells were pelleted and discarded by centrifugation at 300 x g for 5 minutes at room temperature. To remove debris and large apoptotic bodies, the supernatant was subjected to centrifugation at 2000 x g for 20 minutes at 4°C. The 2000 x g supernatant is referred to as ‘apoptotic secretome’ and was used in several assays.

2.2.3.1 Size-exclusion chromatography

ACdEVs were collected by size exclusion chromatography (SEC) using a qEVoriginal/70 nm column (Izon). The column was first warmed to room temperature and primed with 10 ml PBS. The apoptotic secretome (2000 x g supernatant) was concentrated to < 500 µL by centrifugation (3200 x g, 4°C) using a 30 kDa molecular weight cut-off Amicon filter (Merck). Upon sample loading, a 3 mL void volume fraction was discarded before collection of the 3.5 mL ACdEV fraction. Following this, the column was rinsed with 20 mL of PBS for regeneration, and the qEV columns were reused up to 5 times following the manufacturer's instructions.

2.2.3.2 Ultracentrifugation

Apoptotic secretome was concentrated accordingly by centrifugation (3200 x g, 4°C) using a 30 kDa molecular weight cut-off Amicon filter (Merck). Concentrated secretome was ultracentrifuged for 1 hour to pellet ACdEVs (100,000 x g, 4°C).

2.2.4 Flow cytometry

Flow cytometry was performed on a CytoFLEX S fitted with a 405 nm, 488 nm, 561 nm, and 638 nm laser and the following bandpass filters: 525/40, 585/42, 660/10, 712/25, 780/60, 585/42, 610/20, 690/50, 780/60, 450/45, 525/40, 610/20, 660/10 (Beckman Coulter).

For staining with antibodies, cells were pelleted (300 x g, 5 minutes) and washed with 0.1% w/v BSA in PBS. To block Fc receptors and prevent non-specific antibody binding, cells were resuspended in 10% v/v human serum in PBS. 1 µL of each antibody was incubated per 1 x 10^5 cells in 100 µL. Antibodies were incubated on ice in the dark for 1 hour (for antibody information see Table 2.2). Cells were washed and resuspended in 0.1% w/v BSA in PBS before analysing on the flow cytometer. To measure apoptosis, 2 x 10^5 cells were added to 500 µL of annexin V binding buffer (BioLegend) and incubated with 5 µL of annexin V-FITC and 10 µL propidium iodide. Cells were measured after incubation on ice for 15 minutes.

Flow cytometry data was analysed in FlowJo v10.9.0. Singlets were gated for (FSC-A vs FSC-H) and live cells were gated for (FSC-A vs SSC-A) (apart from the apoptosis assay) (Dive *et al.,* 1992). For antibody staining, gates were set from the isotype-matched control with a maximum 2% false positive allowance and the median fluorescence intensity (MFI) was calculated by subtraction of the isotype-matched control MFI.

2.2.5 Nano-flow cytometry

ACdEVs were measured on the NanoAnalyzer flow cytometer (NanoFCM Inc., Nottingham, UK), fitted with a 488 nm and 640 nm laser and single-photon counting avalanche photodiode detectors. Manufacturer recommended laser settings were implemented with bandpass filters 488/10 (SSC channel); 525/40; 670/30. Side scatter-based triggering allowed for detection of nanoparticles > 40 nm in diameter; trigger threshold was automatically set three standard deviations above the mean background noise. Between 2000-10,000 events were collected per sample during a 1 minute sample acquisition, at a sampling pressure of 1.0 kPa, to ensure an optimal event rate.

2.2.5.1 Setting up concentration and size standards

To determine particle concentration, a 250nm silica bead standard (1.99E+10 particles/mL, NanoFCM Inc., 250nm Std FL SiNP) was used to calibrate flow rate. Particle size distributions were calculated using a polydisperse mixture of non-fluorescent silica nanoparticles (3E+10 particles/mL, sizes: 68, 91, 113 and 155 nm) (NanoFCM Inc., S16M-Exo). A standard curve was plotted within the NanoFCM Profession V2.0 software using nonlinear regression to represent the relationship between the side scatter intensity values with particle size (Figure 2.1).

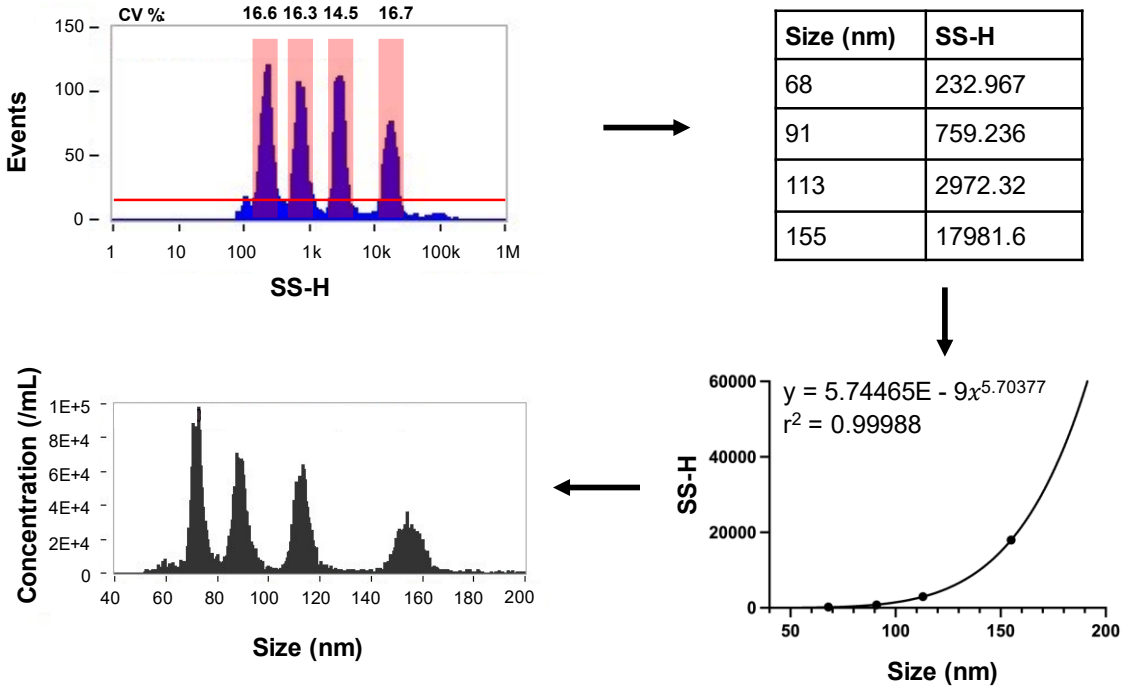

Figure 2.1: Representative standard curve of a polydisperse mixture of silica nanoparticles that were 68, 91, 113 and 155 nm in size (NanoAnalyzer, NanoFM). The equation was used to calculate individual particle sizes from the side scatter signal (SS-H). These beads were measured each time system alignment was performed and the start of each day.

2.2.5.2 ACdEV labelling

To determine the percentage particles (that exceeded the side scatter trigger threshold) that were ACdEVs, ACdEVs were fluorescently labelled with antibodies or dyes. All antibody labelling or labelling with Annexin V-FITC was performed at a particle concentration of 2E+10 particles / mL

(as determined by nano-flow cytometry). Antibody titrations were carried out to determine the optimal incubation to ensure epitope saturation whilst minimising background noise (Figure 2.2). The optimised dilutions were as follows: CD9-FITC (1:50), CD63-FITC (1:50), CD63-APC (1:10), CD81-FITC (1:50), CD31-APC (1:200), CD47-APC (1:100), CD49d-APC (1:100), CD166-APC (1:200), Annexin V-FITC (1:200).

For labelling ACdEVs with dyes, 5 µM BODIPY™ FL Maleimide (Invitrogen) was incubated for 1 hour on ice, or 100 nM MemGlow™ 488 (Cytoskeleton, Inc.) was incubated for 30 minutes at 4°C. BODIPY™ FL Maleimide labelling was followed by SEC (qEV, Izon) (see section 2.3) or processing by spin columns (Vesi-SEC micro, Vesiculab) to remove excess dye (Figure 2.3). MemGlow™ 488 is a self-quenching dye so no post-incubation clean-up step was necessary. Labelling with each dye was optimised so that the background noise was minimised.

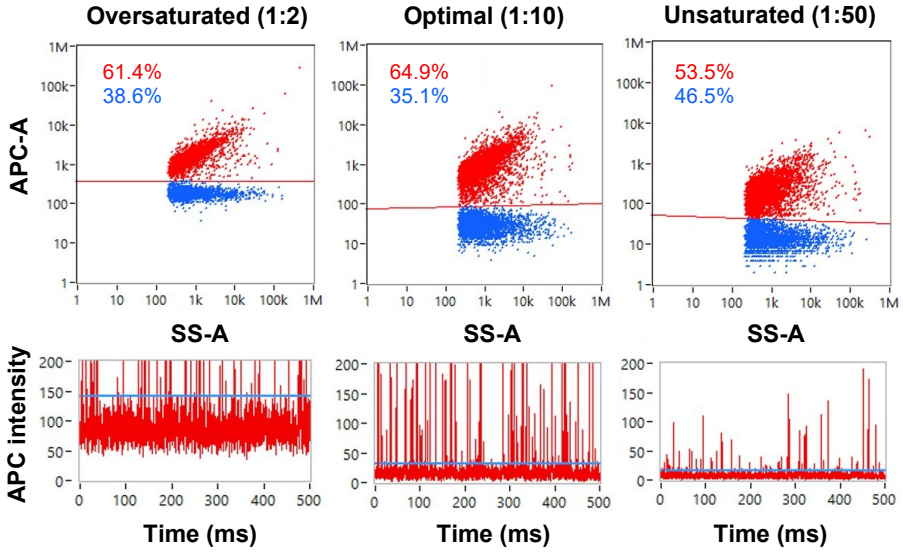

Figure 2.2: Representative antibody titration. 1 µL of CD63-APC (diluted 1:2, 1:10, or 1:50 in PBS) was incubated with 9 µL of ACdEVs (1E+10 particles/mL) for 30 minutes at 4°C. The titration results for this particular antibody indicated that the optimal dilution for incubation of CD63-APC is 1:10. A 1:2 dilution caused excessive background noise and an elevated baseline (blue line on bottom three graphs), whilst a 1:50 dilution failed to label the entire CD63-positive population effectively. Both oversaturation and undersaturation led to inaccurate detection of the true CD63-positive population (N = 1).

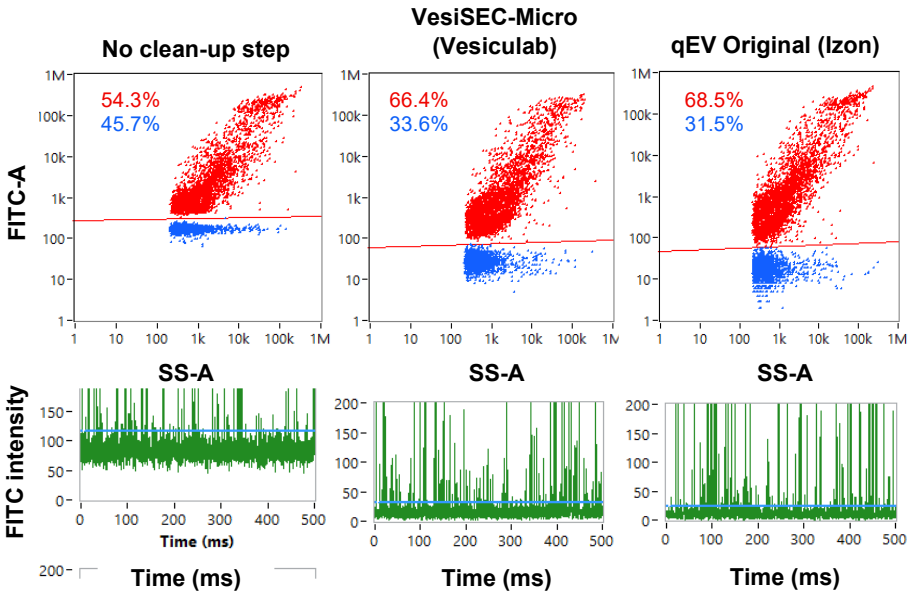

Figure 2.3: Removal of excess unbound BODIPY™ FL Maleimide dye (Invitrogen) by spin column (Vesi-SEC micro, Vesiculab) or SEC (qEV Original, Izon). Implementation of a post-labelling clean-up step decreased fluorescent background noise, revealing an increased number of BODIPY™ FL Maleimide-positive particles. Representative flow plots and event burst traces shown above (N = 1).

2.2.6 Cryo-electron microscopy

A 5 µL droplet of ACdEV sample was loaded onto a lacey mesh carbon grid (EM Resolutions - LC300Cu100) that had previously been treated in a glow-discharger (ELMO Cordouan) to minimize the hydrophobicity. The droplet was converted into a thin surface layer with an absorbent filter paper and immediately plunge-frozen in liquid ethane (-183°C) using a Leica GP2. Once the grid was frozen it was kept under liquid nitrogen. The grid was imaged with a JEOL2200FS TEM fitted with a Gatan K2 Summit camera, at 200kV. Images were captured at 20,000X magnification.

2.2.7 Bradford assay

ACdEV protein concentration was determined by a Bradford assay employing the Bio-Rad Protein Assay Kit II. A standard curve was generated by serially diluting BSA from 30 to 0.12 µg/mL. 200 µL of dye solution was mixed with 25 µL of either the standard or the sample and incubated for 5 minutes at room temperature. Absorbance at 595 nm was measured using a MultiskanTM GO Microplate Spectrophotometer (Thermo Scientific).

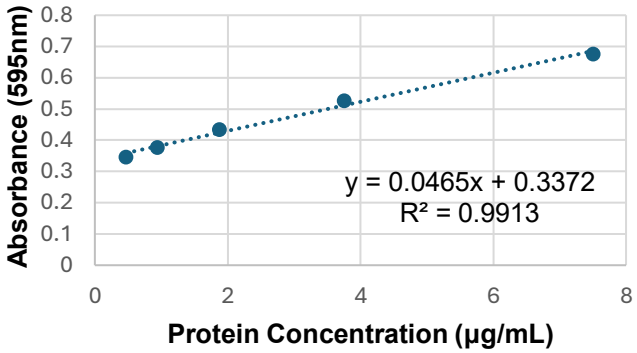

Figure 2.4: Representative plot of BSA standards used for Bradford assay.

2.2.8 SDS-PAGE

0.5 mL SEC fractions were collected using a qEVoriginal/70 nm column (Izon) (as described in 2.3: Preparation of apoptotic secretome and apoptotic cell-derived extracellular vesicles (ACdEVs)). Fractions were frozen at –20 °C until the day of running the SDS-PAGE. Samples were prepared by mixing 12 µL of each fraction with 4 µL 4X reducing buffer and then denatured by heating at 95°C for 5 minutes. 15 µL of each sample was loaded. SDS-PAGE was performed using a 10% acrylamide gel. Electrophoresis was carried out at a voltage of 180V for 1 hour. Gels were gently agitated in Coomassie blue staining solution for 4 hours. Then the gels were rinsed with dH_20 and gently agitated until the background was sufficiently clear and the protein bands were distinctly visible. The stained gels were then visualised using a lightbox imaging system (Bio-Rad) using a white tray and imaging parameters automatically set for Coomassie blue-stained protein gel.

2.2.9 Single molecule localisation microscopy (SMLM)

SMLM experiments were performed on an Olympus Ix83 inverted microscope (Evident) equipped with a SMLM module SAFe MN360 (Abbelight). The setup was with a 100X 1.49NA TIRF objective (Evident) Detection, an Orca Flash 4.0 sCMOS camera (Hamamatsu). Samples were excited with a 640 nm laser (500 mW, Oxxius) and a 405 nm laser (50 mW, Oxxius).

2.2.9.1 Staining with tetraspanin cocktail

ACdEVs were diluted 1:100 in PBS and immobilised to a 1.5H glass coverslip for single-molecule imaging using the Smart EVs Kit (Abbelight). ACdEV samples were incubated with a tetraspanin antibody cocktail (anti-CD9, anti-CD63, and anti-CD81) for 2 hours at room temperature and at 4°C overnight. The immobilised ACdEVs were washed and incubated for 2 hours with a tetraspanin antibody cocktail (anti-CD9, anti-CD63, and anti-CD81) each conjugated to AlexaFluor 647. The labelled ACdEVs were then mounted in dSTORM buffer (SMART-Kit, Abbelight). Imaging was performed by capturing two regions of interest (ROIs) of 80 x 80 µm for each experimental condition.

2.2.9.2 Staining for CD47

As before, ACdEVs were diluted 1:100 in PBS and immobilised on a 1.5H glass coverslip for single molecule imaging by using Smart EVs Kit (Abbelight). This time, the ACdEV samples were incubated on a cocktail of Wheat Germ Agglutinin and Concanavalin A for 2 hours at room temperature and at 4°C overnight, then the samples were washed and stained with a tetraspanin antibody cocktail (anti-CD9, anti-CD63 and anti-CD81) conjugated with Alexa Fluor 647 (Smart EVs Kit, Abbelight) and an antibody against CD47 conjugated with CF680 (Mix'n'Stain, Biotium) (diluted 1:2000) for 2 hours. The sample was mounted in dSTORM buffer (SMART-Kit, Abbelight). Imaging was performed by capturing two regions of interest (ROIs) of 80 x 80 µm for each experimental condition.

Given their close spectral proximity, AF647 and CF680 were excited and imaged simultaneously using the same dSTORM buffer and laser. Imaging was conducted with a dual-camera setup, where a long-pass dichroic mirror was used to separate fluorescence from individual emitters onto the two cameras. Spectral demixing was then applied to differentiate the signals from the two fluorophores. SMLM videos were captured using Abbelight NEO live imaging, at a 25 ms exposure time for 10,000 frames. Excitation was performed at 640 nm (60% intensity) and 405 nm (uniform ramp from 0 to 40% during acquisition).

2.2.9.3 Post-processing

The SMLM videos were processed using Abbelight NEO_analysis to extract the sub-diffraction xy coordinates of the blinking events, with drift correction applied via cross-correlation. The coordinate tables were filtered by removing the first 1,000 frames, excluding localisations with uncertainties greater than 25 nm, and discarding any localisations that persisted for 10 consecutive frames or more. Single ACdEV segmentation was performed in Nanometrix software

using DBSCAN clustering (with a search radius of 50 nm and a minimum of 20 points per cluster). Additionally, single-cluster calculations were conducted to determine parameters such as cluster diameter, biomarker positivity, and the number of localisations per cluster.

2.2.10 Vertical transwell migration assay

THP-1 monocytes were differentiated into macrophages by a 48 hour treatment with 100 nM dihydroxyvitamin D3 (VD3) (Enzo Life Sciences™, UK). 8 x 10^4 cells were seeded on top of the insert in the upper chamber in a 300µl volume suspended in serum-free RPMI medium. 700 µL apoptotic secretome was placed in the bottom chamber of each well. Cells were incubated at 37°C in a humidified environment with 5% CO2, and migration of cells through an 8 µm pore transwell insert into the bottom chamber was assessed over a 12 h period. Each blocking antibody was incubated with apoptotic secretome at a concentration of 10 µg/mL for 30 minutes at room temperature prior to seeding of cells. Four images were captured per well every 30 minutes at 4X magnification. Images were automatically stitched and manually plugged for regions where the inserts were not obstructing the field of view (FOV) (Figure 2.1). Cell segmentation was performed within the BioTek Gen5 software (Cytation 5, Gen5 software, Biotek).

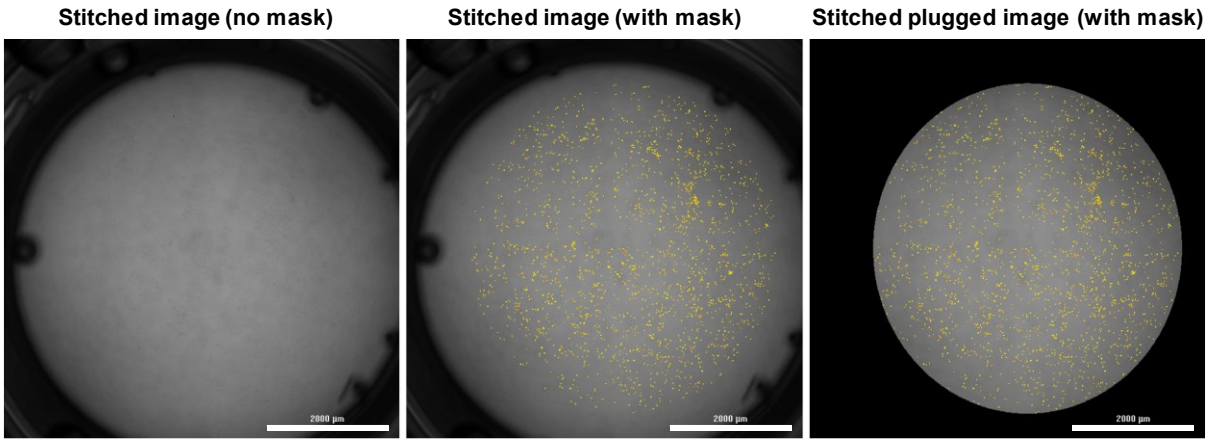

Figure 2.5: Defining the region for counting migrated MΦs in the vertical transwell migration assay. For each well, four images were taken at 4X magnification and automatically stitched together. The stitched images were manually plugged to exclude the sides of the transwell insert and any bubbles. Cell segmentation was applied to just cells included in the plugged image (Cytation 5, Gen5 software, Biotek). Scale bar ~ 2000 µm.

2.2.11 ACdEV interaction assay

Apoptotic secretome was collected and concentrated as described earlier (2.3: Preparation of apoptotic secretome and apoptotic cell-derived extracellular vesicles (ACdEVs)). The concentrated apoptotic secretome was incubated with 5 μM BODIPY™ FL Maleimide at 4°C overnight before loading onto the SEC qEVoriginal/70 nm column (Izon) to remove excess unbound dye (Figure 2.3). The standard 3.5 mL ACdEV fraction was collected. BODIPY™ FL Maleimide-labelled ACdEVs were measured by nano-flow cytometry (see 2.5 Nano-flow cytometry) to determine concentration and incubated with VD3-treated THP-1 macrophages at a 500 ACdEVs : 1 cell ratio at 4°C, 20°C or 37°C for 2 hours, unless otherwise specified. After incubation, cells were washed in 0.1 % BSA in PBS and measured on the flow cytometer (CytoFLEX S, Beckman Coulter). THP-1 macrophages alone were used to set the gate.

2.2.12 Statistical analysis

Statistical analysis was performed using GraphPad Prism v10.2.0. The statistical tests applied are described in the figure legends.

Chapter 3 Characterisation of apoptotic cell-derived extracellular vesicles (ACdEVs)

3.1 Introduction

EVs released by cells are membrane-bound nanoparticles that facilitate intercellular signalling. Whilst there is great interest in harnessing EVs as biomarkers or for the delivery of therapeutics, there remains a fundamental lack of understanding in EV biogenesis, packaging of EV cargo and mechanisms of EV signalling. To date, just two pathways have been described that regulate the release of apoptotic exosome-like vesicles: the S1P/S1PR pathway, involving the formation of 'spindle-like structures', and the autolyososomal pathway, revealing the first link between autophagy and ACdEV release (Beillevaire *et al*., 2022; Park *et al.,* 2018). The packaging of cargo of viable cell-derived EVs is thought to be regulated by ESCRT-0, tetraspanins, and S1P-S1PR signalling (Dixson *et al.*, 2023; Kajimoto *et al.,* 2013). ACdEVs may utilise similar mechanisms of cargo sorting. In addition, beaded apoptopodia were reported to actively sort the cargo of apoptotic bodies and therefore, it is possible ACdEV cargo is regulated in a similar way, such as by the formation of 'spindle-like structures' observed as part of the S1P/S1PR pathway (Park *et al.,* 2018; Atkin-Smith *et al*., 2015).

Moreover, the function of ACdEVs and the mechanisms by which they modulate immune responses remain poorly understood (Caruso & Poon, 2018). It has been reported that ACdEVs promote the phagocytic clearance of apoptotic cells and drive the polarisation of macrophages toward an anti-inflammatory, pro-resolving M2 phenotype (Li *et al.,* 2022; Segundo *et al.,* 1999). This indicates that ACdEVs play a crucial role in the resolution of inflammation. So far, just two 'find me'/'eat me' molecules, CX3CL1 and ICAM-3, have demonstrated functional activity at the surface of ACEVs (Torr *et al.,* 2011; Truman *et al.,* 2008). However, further research is necessary to elucidate the molecular components involved in ACdEV-phagocyte interactions, in order to harness the therapeutic potential of ACdEVs.

To characterise ACdEVs, it is necessary to validate a method of apoptosis induction. This project used UV irradiation as it potently induces apoptosis by multiple conserved pathways including DNA damage, mitochondrial release of cytochrome C and direct activation of death receptors (Kulms & Schwarz, 2000). As a result, UV is a valuable tool for studying downstream products of

UV-induced apoptosis, such as ACdEVs. Furthermore, UV irradiation can rapidly and synchronously induce apoptosis across all cells by simultaneous exposure.

It is also important to consider the method of ACdEV collection. Currently, there is no standardised method of EV collection recommended (Welsh *et al.,* 2024). This is because EVs are a heterogeneous population that vary greatly in size, density and molecular composition and are, therefore, notoriously challenging to separate from other types of nanoparticles commonly present in biological samples. Therefore, the most appropriate EV collection method is dependent on the nature of the sample and the downstream applications.

Upon collection, characterisation of ACdEV samples is required to confirm the presence of ACdEVs, determine the abundance of ACdEVs and define characteristics such as size, shape, surface composition and intraluminal cargo to understand ACdEV function. Due to heterogeneity in size, molecular composition, and an inability of several techniques to distinguish between EVs and non-EV nanoparticles, it is recommended by the MISEV guidelines to use several techniques to measure several components of EVs (Welsh *et al.,* 2024).

3.2 Aims and Objectives

Here, this chapter aims to establish UV irradiation as a method of inducing apoptosis and confirm the kinetics of UV-induced apoptosis in human immortalised cell lines: Jurkat T cells and THP-1 monocytes. These immune cell lines were chosen as an apoptosis model for collection of apoptotic cell-derived extracellular vesicles (ACdEVs).

Differential centrifugation combined with size-exclusion chromatography (SEC) was chosen for ACdEV collection because this approach provides highly pure EV samples while minimising the risk of EV aggregation that can occur with high centrifugal forces (Welsh *et al.,* 2024). This chapter aimed to validate this method to confirm the separation of ACdEVs from soluble protein present in apoptotic cell culture medium and characterise the ACdEVs from each cell line based on concentration, size, shape and presence of EV markers using a variety of complementary techniques.

3.3 Results

3.3.1 Induction of apoptosis by UV irradiation

In this study, Jurkat T cells and THP-1 monocytes were the human immortalised cell lines used for induction of apoptosis and collection of apoptotic cell-derived extracellular vesicles (ACdEVs). To confirm UV irradiation was an effective method of inducing apoptosis, Jurkat T cells and THP-1 monocytes were incubated with Annexin V-FITC and propidium iodide (PI) at 0 h, 6 h and 18 h post-exposure to UV (Figure 3.1, Supplementary Figure 3.1). The timepoints chosen were in line with previously established methods (Grant, 2022; Cameron, 2018). Annexin V binds to phosphatidylserine (PS) in the presence of calcium, a phospholipid that is under the control of a family of enzymes, the flippases. In viable cells, PS is maintained in the inner leaflet of the phospholipid bilayer by flippase activity, which requires ATP hydrolysis (Segawa *et al.,* 2016). During apoptosis, caspase 3 deactivates flippases and activates phospholipid scramblases, which together, leads to the irreversible translocation of PS to the outer leaflet (Suzuki *et al*., 2016; Segawa *et al.,* 2016). As such, PS is exposed at the apoptotic cell surface and accessible for annexin V to bind; this is a hallmark sign of early-stage apoptosis. PI binds and intercalates with deoxyribose nucleic acid (DNA) and therefore will only label cells that no longer have an intact cell membrane and nuclear envelope, allowing the dye to enter intracellularly and bind DNA. Cells positive for PS and PI labelling are indicative of late-stage apoptosis.

In Jurkat T cells, an average of 54.1% of cells were in the early apoptotic stage, while 21.3% were in the late apoptotic or early necrotic stage 6 hours after UV exposure (Figure 3.1C, 3.1D). A significantly higher number of cells were in the early apoptotic stage at 6 hours post-exposure compared to 0 hours post UV exposure (Figure 3.1D). By 18 hours post-UV exposure, nearly all cells were apoptotic, displaying characteristics typical of late apoptosis or early necrosis, such as membrane blebbing observed via brightfield microscopy (Figure 3.1B). At this time point, an average of 35.3% of cells were early apoptotic, and 61.7% were late apoptotic, with significantly more cells in the late apoptotic stage compared to 6 hours post-exposure (Figure 3.1D). A similar pattern was observed in the THP-1 monocytic cell line (Supplementary Figure 3.1). Therefore, UV irradiation served as an effective method of apoptosis induction for the downstream enrichment and collection of ACdEV.

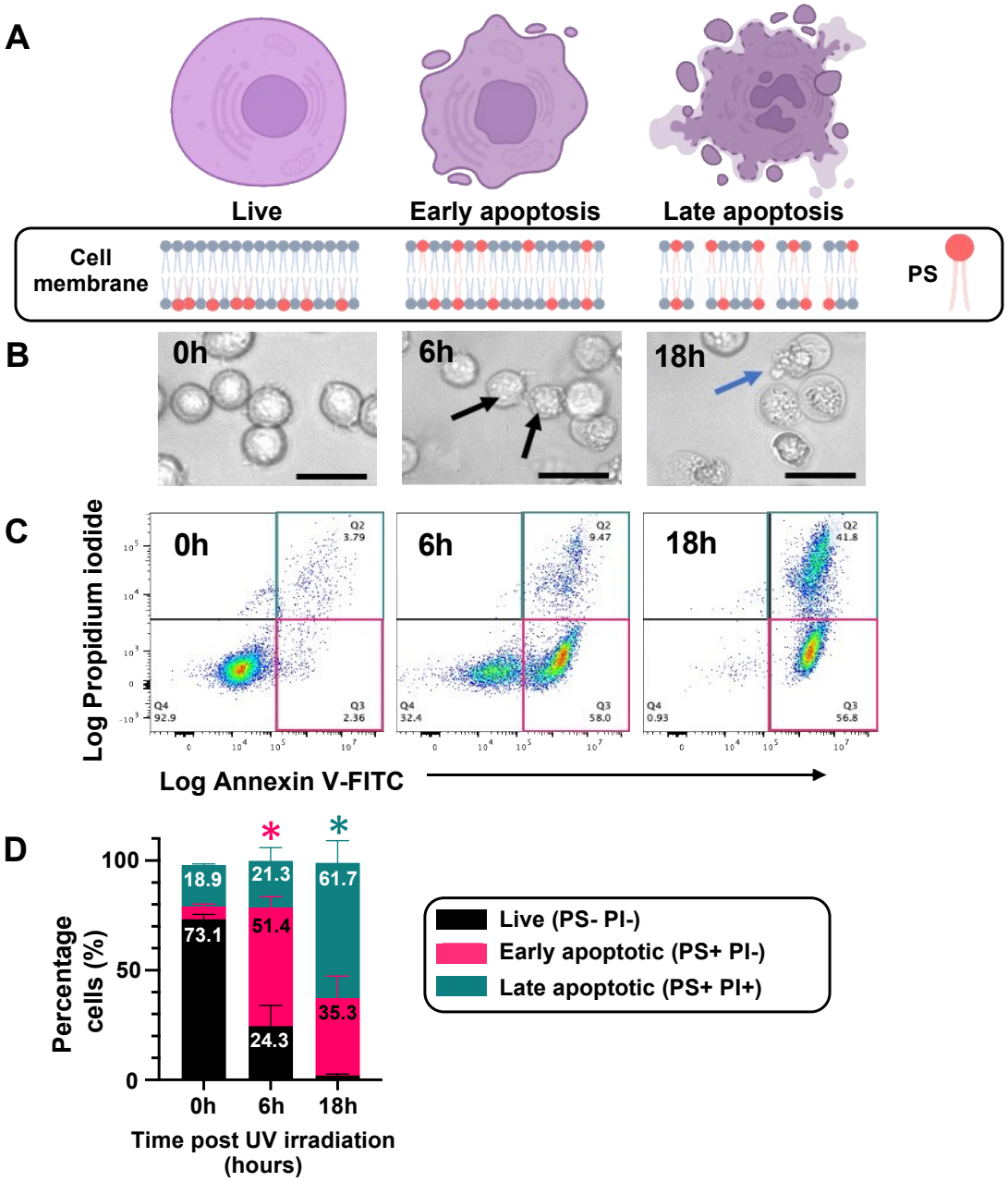

Figure 3.1: A cell death model – synchronous induction of apoptosis by UV irradiation. Jurkat T cells were UV irradiated (100 mJ/cm^2 dose) and labelled with apoptosis markers annexin V-FITC and propidium iodide (PI). A) Graphical depiction of cell progressing through apoptosis including surface exposure of phosphatidylserine (PS), blebbing and leakage of intracellular components (created with Biorender). B) Representative microscopy images of Jurkat cells at 0, 6 and 18 hours post UV irradiation. Black arrows indicate apoptotic blebbing and blue arrow indicates loss of cell membrane integrity. Scale bar ~25 µm. C) Representative flow plot of UV irradiated Jurkat cells measured 0, 6 and 18 hours post UV irradiation. D) Percentage live, early apoptotic and late apoptotic cells at 0, 6 and 18 hours post UV irradiation, determined by flow cytometric gates (mean (shown as text on bars) ± SEM, N = 3. Two-way ANOVA was performed with Tukey's Multiple Comparison test comparing 'Early apoptotic' and 'Late apoptotic' cells at 0h, 6h and 18h post-UV irradiation. *$p < 0.05$, *(magenta) = early apoptotic cells compared at 0 and 6h, *(green) = late apoptotic cells compared at 6h and 18h.)

3.3.2 Validation of method of ACdEV collection

Cells release a variety of soluble factors, including protein, lipids, cytokines and EVs into the extracellular environment. In an *in vitro* setting, soluble factors are released into the cell culture medium, which, in this study, is termed 'secretome'. To elucidate unique ACdEV-specific functions, it is necessary to separate ACdEV from the remaining soluble factors for use in downstream assays. To do this, a combination of differential centrifugation and size-exclusion chromatography (SEC) was used to separate particles by density and size, respectively.

ACdEVs were collected by a combination of differential centrifugation and size-exclusion chromatography (SEC) (as outlined in section 2.2.3). Briefly, prior to apoptosis induction, cells were washed and resuspended in serum-free medium to prevent contamination of ACdEV samples with viable cell-EVs and foetal bovine serum (FBS)-derived EVs. Apoptotic cell secretome (collected at either 6 hours or 18 hours post UV irradiation) was subjected to differential centrifugation to pellet and allow for the removal of apoptotic cells, cellular debris and large apoptotic bodies (>1 μm in size) (Figure 3.2A). The secretome was concentrated with an Amicon filter with a 30 kDa molecular weight cut-off, before loading onto a SEC column (qEV Original, Izon). To identify the SEC fractions containing ACdEVs and validate the collection method, the concentrated secretome was stained with thiol-binding dye BODIPY™ FL maleimide. This stained sample was then loaded onto the SEC column to simultaneously separate ACdEVs from soluble factors and any unbound dye. Each 0.5 mL fraction was collected, and ACdEVs were quantified using nano-flow cytometry, while protein content was measured via protein assays and visualised using Coomassie blue-stained SDS-PAGE (Figure 3.2B – F).

For characterisation by nano-flow cytometry, ACdEVs were defined as particles that exceeded the side scatter trigger threshold and emitted a positive signal in the FITC channel (in this case, by labelling with BODIPY™ FL maleimide) (Figure 3.2B-C). The thresholds for both channels were automatically set and indicated particles that were > 40 nm in size (NanoFCM). Most protein aggregates are unlikely to exceed 40 nm and therefore, particles that passed this dual threshold were considered ACdEVs.

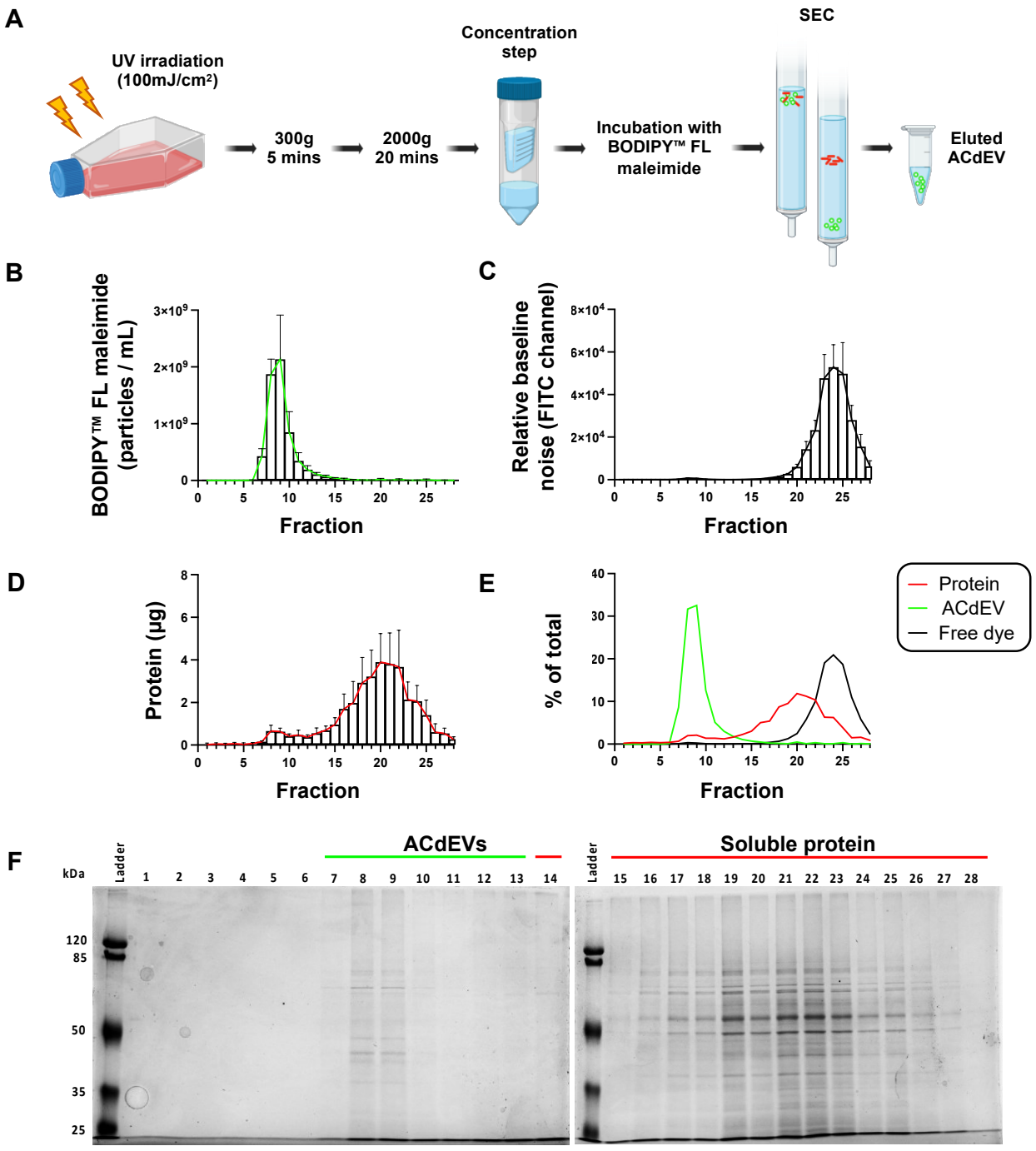

Figure 3.2: Validation of ACdEV enrichment via differential centrifugation and size-exclusion chromatography (SEC) using Jurkat-derived late ACdEV (qEV Original, Izon). A) Method of ACdEV collection and staining with BODIPY™ FL maleimide (created with Biorender). B) BODIPY™ FL maleimide – positive particles per 0.5 mL fraction, measured by nano-flow cytometry (Nanoanalyzer, NanoFCM) (Mean ± SEM, N = 3). C) Relative baseline level of fluorescence detected in the FITC channel per 0.5 mL fraction, indicating the presence of free dye (Mean ± SEM, N = 3). D) Protein per 0.5 mL fraction, measured by Bradford assay (Mean ± SEM, N = 3). E) Overlay of each parameter, presented as percentage of the total (Mean, N = 3). F) Protein per 0.5 mL fraction was observed by Coomassie blue-stained PAGE gel (10%) (N = 1).

BODIPY™ FL maleimide+ particles, considered ACdEVs, were detected by nano-flow cytometry in fractions 7-13 (Nanoanalyzer, NanoFCM) (Figure 3.2B). BODIPY™ FL maleimide+ particles were defined by side scatter triggering and an accompanying BODIPY™ FL maleimide signal detected in the FITC channel (525/40 lens) (*i.e.* SSC+ BODIPY™ FL maleimide+ dual-positive events). For a detailed explanation of the nano-flow cytometry set up, refer to the Methods secion.

Fractions 18-28, measured by nano-flow cytometry, detected a negligible concentration of BODIPY™ FL maleimide+ particles but exhibited a large increase in baseline noise in the FITC channel, by up to 4 orders of magnitude (Figure 3.2C). This is typically a symptom of excess unbound fluorophore and therefore, indicated unbound BODIPY™ FL maleimide dye eluted in the later fractions of the SEC column. Notably, the presence of BODIPY™ FL maleimide-labelled soluble protein was also detected, as seen in Figure 3.2D, and therefore, will have also contributed to increased baseline noise.

The protein present in each 0.5 mL fraction was quantified by Bradford protein assay. Protein was detected in fractions 7-28, peaking at approximately 5 µg protein between fractions 15-25 (Figure 3.2D). A similar trend was observed visually by Coomassie blue-stained SDS-PAGE, in which fractions 17-25 visibly contained more intense protein bands (Figure 3.2F). It is assumed that fractions 15-25 contained the majority of soluble protein that was expected to be present in the crude secretome.

Each quantification per fraction of BODIPY™ FL maleimide+ particles / mL, 525/40 baseline noise and protein (µg) was normalised to ‘percentage of total’ and overlaid (Figure 3.2E). This revealed a clear separation between the early elution of ACdEV in fractions 7-13 and the late elution of protein and unbound dye in fractions 15-28. As such, fractions 7-13 were pooled and used in all future SEC-isolated ACdEV experiments.

For further validation, Bradford protein assay was used to quantify the reduction of soluble protein from the concentrated secretome to the pooled SEC-isolated ACdEV fractions, which will now be referred to as simply ACdEVs (*i.e.* ACdEVs collected post-SEC) (Figure 3.3A and 3.3B). In addition, secretome and ACdEVs were stained with membrane-intercalating dye, MemGlow™ 488, and measured by nano-flow cytometry (Figure 3.3C and 3.3D) (NanoFCM). This time, MemGlow™ 488 was chosen for labelling ACdEVs, as it self-quenches and therefore, doesn’t require a clean-up step prior to sample measurement (Cytoskeleton, Inc.). This was most

important for accurately characterising the protein concentration in the secretome without additional processing steps.

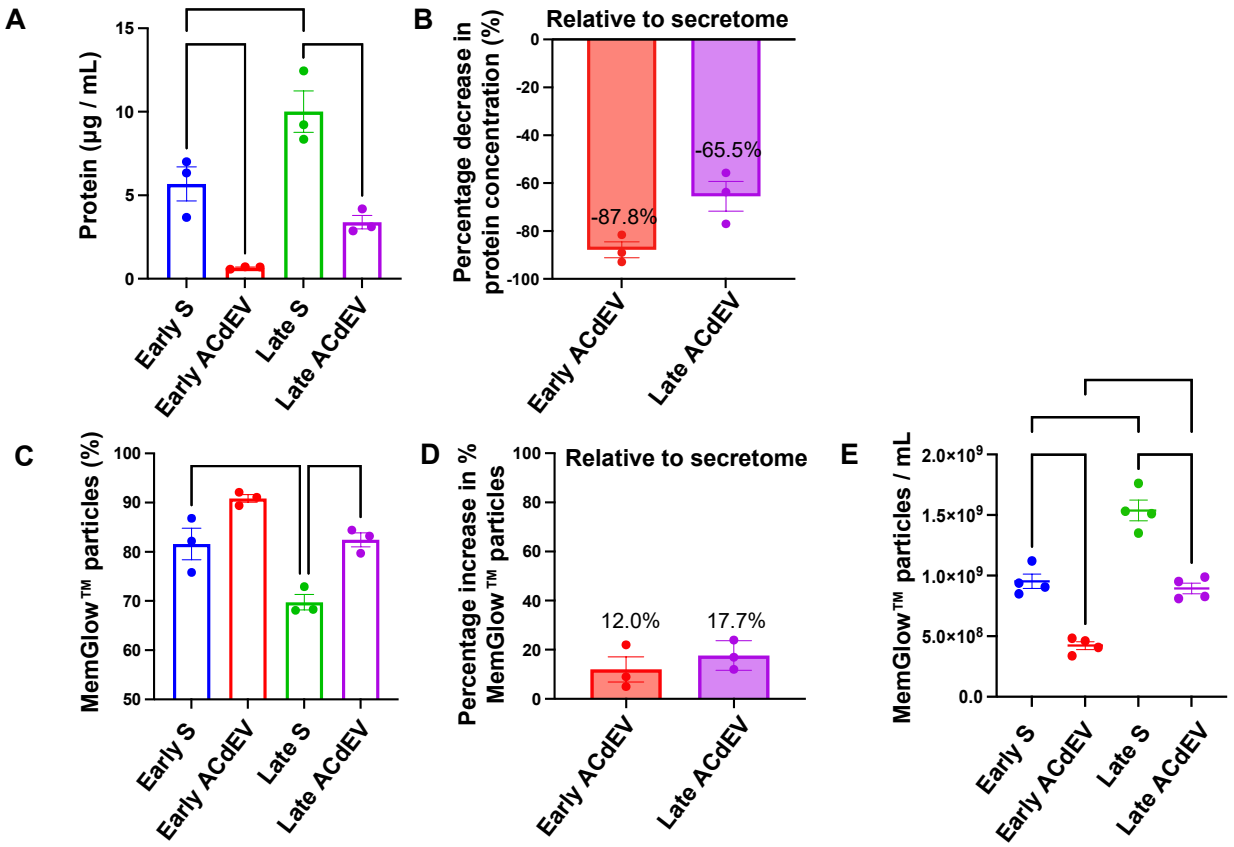

Figure 3.3: Soluble protein concentration is significantly reduced, proportion of MemGlow™ - positive particles are enriched and concentration of MemGlow™ - positive particles are decreased, post-processing by SEC. Secretome was harvested from UV-irradiated Jurkat cells at indicated time points ('early S' and 'late S') and ACdEV were isolated from this prior to further analysis of secretome or ACdEV by protein assay and nano-flow cytometry. A) Protein concentration, quantified by Bradford assay, was significantly decreased in SEC-isolated ACdEVs, compared with early and late apoptotic secretome. B) Percentage decrease in protein concentration between secretome and ACdEVs collected at early and late apoptotic timepoints. C) Secretome and ACdEV samples were labelled with membrane-intercalating dye MemGlow™ 488 and measured by nano-flow cytometry (NanoFCM). SEC-isolated ACdEVs contained a higher percentage of MemGlow™ - positive particles compared to early and late apoptotic secretome. D) Percentage increase in percentage MemGlow™ - positive particles between secretome and ACdEVs collected at early and late apoptotic timepoints. E) Absolute concentration of MemGlow™ - positive particles, measured by nano-flow cytometry (Mean ± SEM, N = 3, ordinary two-way ANOVA with Tukey's multiple comparison test, *P < 0.05, **P < 0.01).

A mean decrease of 87.8% and 65.5% in protein was observed at the early and late apoptotic timepoints, respectively, when comparing the cell secretome to ACdEVs (Figure 3.3B). A higher concentration of protein was detected in both secretome and ACdEVs collected at the late apoptotic timepoint compared to the early apoptotic timepoint (Figure 3.3A). It is likely that this was due to an accumulation of ACdEVs and soluble factors released into the secretome over a longer duration of time (18 hours compared to 6 hours).

Secretome and ACdEVs were then labelled with membrane-intercalating dye MemGlow™ 488 and measured by nano-flow cytometry (Figure 3.3C). MemGlow™ 488 labelling revealed an enrichment of ACdEV in the SEC-isolated ACdEV samples compared to the ACdEV-containing secretome, with a mean increase of 12.0% and a statistically significant mean increase of 17.7% in percentage of MemGlow™ 488+ particles, at the early and late apoptotic timepoints, respectively (Figure 3.3D). The percentage of MemGlow™ 488+ particles compared to total particles was significantly lower in the secretome collected at the late apoptotic timepoint compared to the early apoptotic timepoint, possibly due to the aggregation of soluble proteins that were detected as non-fluorescent particles or due to a decreased rate of ACdEV release during the later stages of apoptosis (Figure 3.3C). As anticipated, the absolute concentration of MemGlow™ 488+ particles per mL was decreased post processing by SEC (Figure 3.2E). Furthermore, the concentration of MemGlow™ 488+ particles per mL was increased in both the late apoptotic secretome and late ACdEVs compared to the early apoptotic timepoint, which is attributed to the accumulation of ACdEVs released over the extended duration (Figure 3.2E).

3.3.3 Physical characterisation of ACdEVs

As two human immortalised immune cell lines were chosen to model apoptosis and used as a source of ACdEVs, we sought to characterise the ACdEVs released by each cell line in line with the MISEV 2024 guidelines, and compare the ACdEV populations for similarities and differences in concentration, size, structure and biochemical composition (Welsh *et al.,* 2024). This characterisation will form the remainder of this chapter.

The concentration of ACdEVs, defined as MemGlow™ 488+ particles / mL, was measured by nano-flow cytometry using a concentration bead standard supplied by the manufacturer (see Methods) (Nanoanalyzer, NanoFCM). With the same number of apoptotic cells, THP-1 monocytes consistently released a significantly greater quantity of ACdEVs (approximately a 2-3 fold difference) than Jurkat T cells (Figure 3.4).

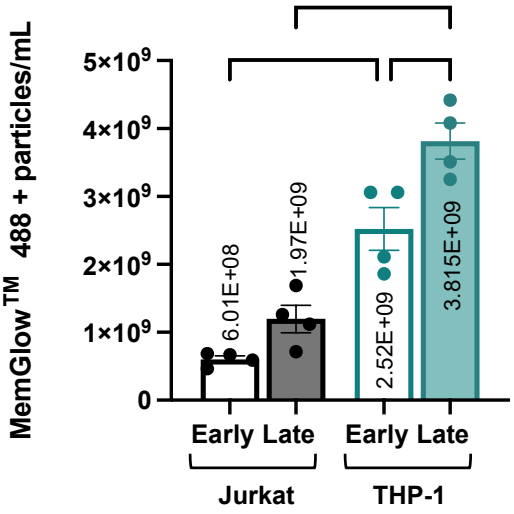

Figure 3.4: The concentration of ACdEVs released is cell line-dependent and for apoptotic THP-1 monocytes, time-dependent. 2 x 10^7 cells Jurkat T cells and THP-1 monocytes in 5 mL RPMI culture medium were UV irradiated to induce apoptosis. ACdEV were stained with MemGlow™ 488 and measured by nano-flow cytometry (NanoFCM). THP-1 monocytes released significantly more ACdEVs than Jurkat T cells at both early and late apoptosis. The concentration of THP-1-derived ACdEVs was significantly higher at 18 h post UV-induced apoptosis compared to 6 h (mean (shown as text on bars) ± SEM N = 4. Ordinary two-way ANOVA with Tukey's multiple comparison test, ***$p < 0.001$, **$p < 0.01$, *$p < 0.05$).

Jurkat ACdEVs and THP-1 ACdEVs were also measured by single molecule localisation microscopy (SMLM, Abbelight). This technology, applicable to just a subset of fluorophores, implements a unique method of fluorophore excitation that causes them to enter an intermediate activation state where they rapidly and randomly switch 'on' and 'off'. The sequential 'blinking' of fluorophores allows for the full reconstruction of a super-resolution image, revealing the spatial localisation of individual molecules using direct Stochastic Optical Reconstruction Microscopy (dSTORM). To image via SMLM, EVs must be immobilised. Here, ACdEVs were immobilised by and stained for a cocktail of commonly expressed tetraspanins: CD9, CD63 and CD81.

Both SMLM and nano-flow cytometry provide single-EV characterisation, by dSTORM and light scattering, respectively. Together SMLM and nano-flow cytometry provide a comprehensive overview of size, biochemical composition, and spatial arrangement of epitopes on the surface of EVs.

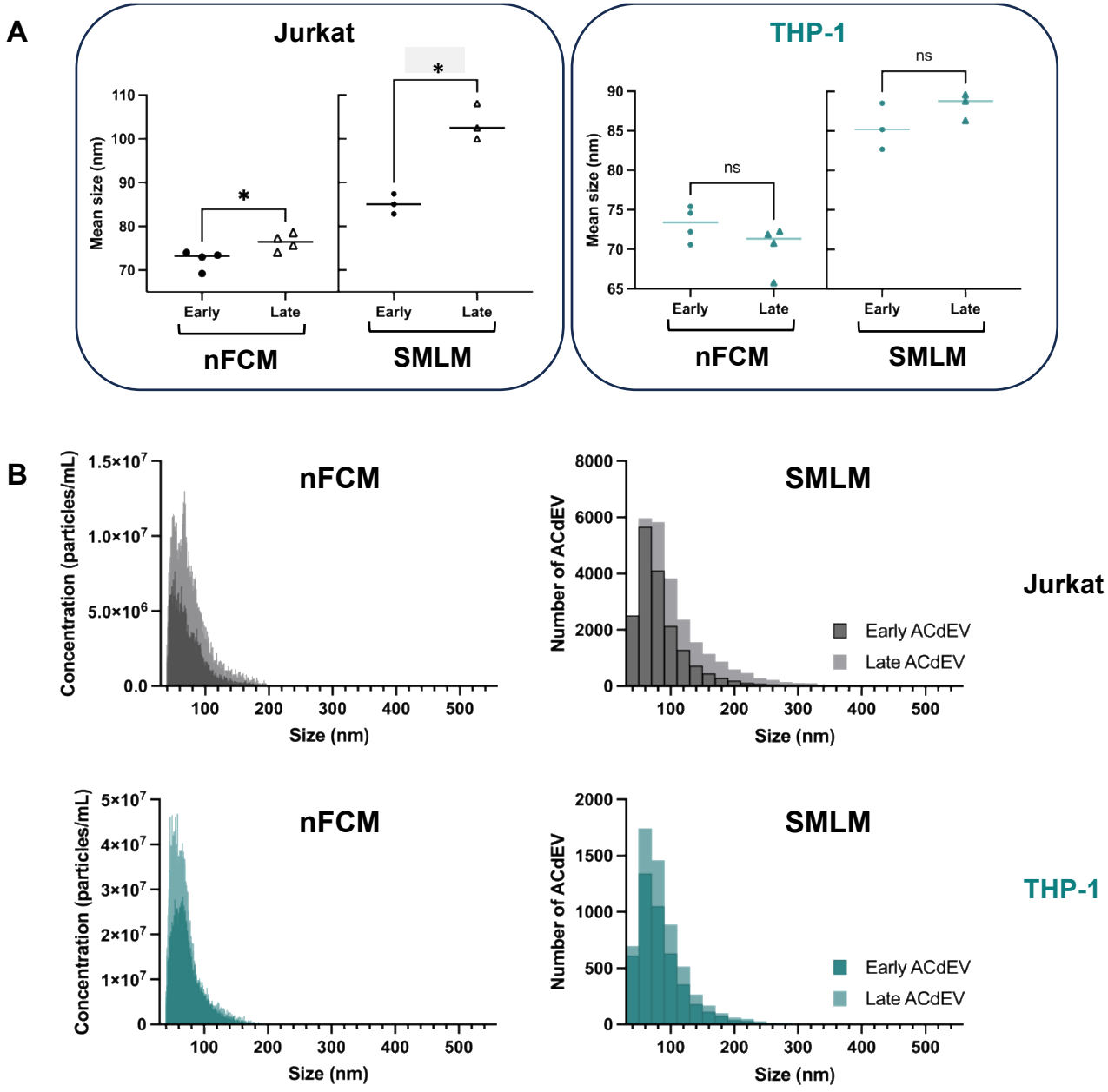

Figure 3.5: Comparing the size distribution of ACdEVs collected from different cell lines and apoptotic timepoints. ACdEV were measured by nano-flow cytometry (NanoFCM) and stained with Memglow™ 488, or by single molecule localisation super-resolution microscopy (SMLM, in collaboration with Abbelight) and stained with antibodies against tetraspanins CD9, CD63 and CD81. A) Mean size of ACdEV derived from Jurkat and THP-1 cells at early (6 h) or late (18 h) apoptosis (Paired t test, *$p < 0.05$, ns = $p > 0.05$). B) Size distribution of ACdEV derived from Jurkat and THP-1 cells at early (6h) or late (18h) apoptosis (Nano-flow cytometry N = 4, SMLM N = 3).

With both methodologies, Jurkat late ACdEVs were, on average, significantly bigger in diameter than early ACdEVs (Figure 5A). Interestingly, this trend was not observed in THP-1 ACdEVs; there was no significant difference in mean diameter for THP-1 early and late ACdEV. Similarly, with both methodologies, a shift in the size distribution of Jurkat late ACdEVs was observed, which was not observed for THP-1 ACdEVs (Figure 5B).

Notably, ACdEVs were reported as bigger in diameter by SMLM than nano-flow cytometry: by nano-flow cytometry, Jurkat ACdEV were reported to have a mean average diameter of 72.4 nm and 76.4 nm for early and late ACdEV, respectively. By SMLM, Jurkat ACdEV were reported to have a mean average diameter of 85.1 nm and 103.6 nm, for early and late ACdEV, respectively. This disparity also applied to the THP-1-derived ACdEV, in which nano-flow cytometry reported THP-1 ACdEV had a mean average diameter of 73.2 nm and 70.2 nm, for early and late ACdEV, respectively. Whereas SMLM reported THP-1 ACdEV to have a mean average diameter of 85.5 nm and 88.3 nm, for early and late ACdEV, respectively.

To provide insight into the native shape of Jurkat and THP-1 ACdEVs, cryo-transmission electron microscopy (cryoTEM) was performed (Figure 3.6). The cryopreservation method better preserves the native EV structure, unlike conventional TEM in which the dehydration step during sample preparation leads to a stereotypical cup-shape artefact. Here, early and late ACdEVs from Jurkat T cells and THP-1 monocytes were compared to ACdEVs collected from human primary T cells (donated by Dr Ivana Milic, Aston University).

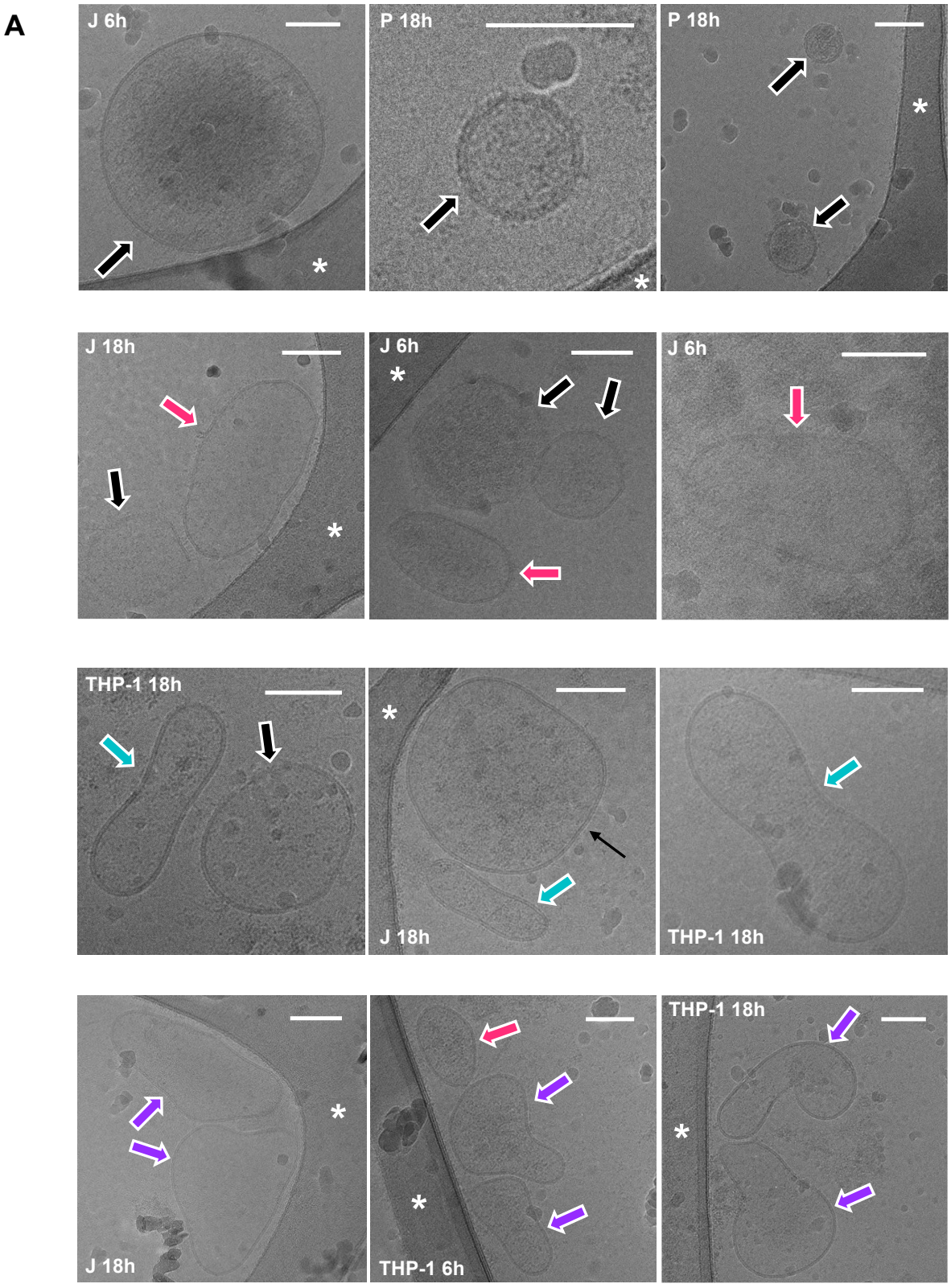

[Figure 3.6 continues onto next page]

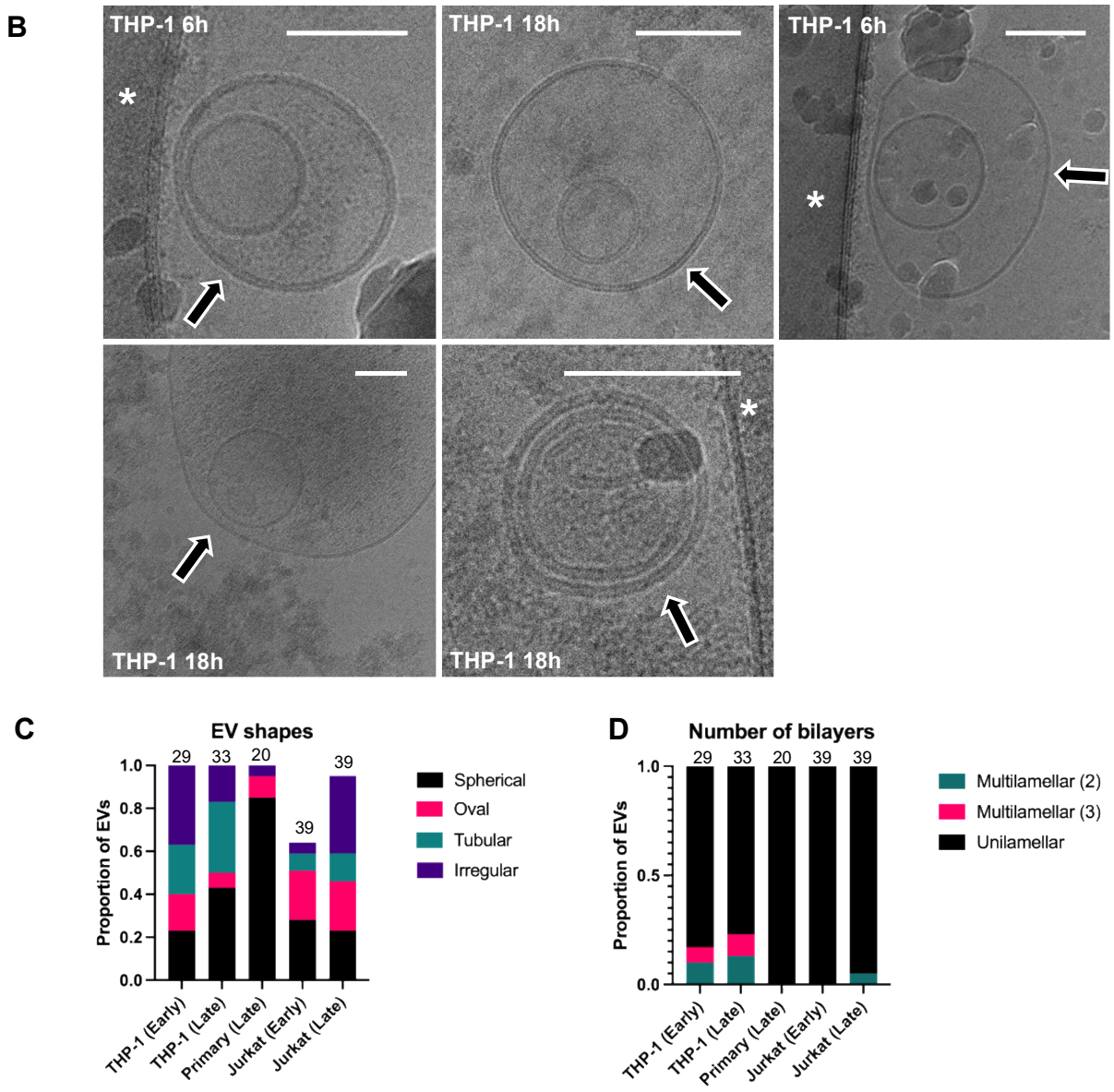

Figure 3.6: Morphology of early and late ACdEVs derived from Jurkat T cells, THP-1 monocytes, and human primary T cells. Apoptosis was induced by standard UV irradiation (100mJ/cm^2) for Jurkat and THP-1 cells, and by 18 h treatment with cycloheximide (20 µg/mL, Sigma Aldrich) and anti-Fas antibody (1/10000, CH11, Merck Millipore) for primary T cells (Primary T cell ACdEVs were donated by Dr Ivana Milic, Aston University). ACdEVs were collected by SEC at indicated apoptotic timepoints and imaged by cryo-transmission electron microscopy. A) Representative images of ACdEVs from each cell type (J = Jurkat, P = primary T cell). (Black arrow: spherical, magenta arrow: oval, green arrow: tubular, purple arrow: irregular, white asterisk highlights the TEM grid). Scale bar ~100 nm. B) Representative images of multilamellar ACdEVs. Scale bar ~100 nm. C) Proportion of ACdEVs exhibiting various morphologies. Primary T cell-derived ACdEVs were predominantly spherical. D) ACdEVs derived from THP-1 cells had the highest proportion of multilamellar structures (N numbers, shown at the top of each bar, indicate the number of ACdEVs in which the structure was fully captured). CryoTEM done in collaboration with Dr Saskia Bakker at the Univeristy of Warwick.

ACdEVs presented in a variety of shapes and sizes, some with multiple membranes (Figure 3.6A and 3.6B). ACdEVs were categorised into four groups describing shape: spherical; oval; tubular; irregular (Figure 3.6C). ACdEVs were only counted if the entire structure was captured and therefore the shape could be defined.

Jurkat-derived early and late ACdEVs were diverse in shape, with roughly an equal proportion of spherical and oval ACdEVs (Figure 3.6C). A higher proportion of irregular-shaped ACdEVs were identified in late ACdEVs. A similar trend was observed for THP-1 ACdEVs, except tubular-shaped ACdEVs dominated oval-shaped ACdEVs. Strikingly, primary T cell ACdEVs were mostly spherical in shape, with just one irregular-shaped and two oval ACdEVs identified (Figure 3.6C) (Supplementary Table 7.1).

The number of ACdEV bilayers were also counted per ACdEV (Figure 3.6C) (Supplementary Table 7.2). For all cell types and apoptotic timepoints, unilamellar ACdEVs were the most common – that is, an ACdEV comprised of a single phospholipid bilayer. Interestingly, THP-1 early and late ACdEVs had notable population of multilamellar ACdEVs with two and three bilayers (Figure 3.6B). Whereas, Jurkat-derived ACdEVs were almost exclusively unilamellar ACdEVs and no primary T cell-derived multilamellar ACdEVs were observed.

The lumen of certain ACdEVs appeared darker in intensity and was therefore more densely packed with protein than other ACdEVs. An example of a densely packed ACdEV versus an ‘empty’ ACdEV is the top left and bottom left panel (Figure 3.6A).

Of note, the majority of the ACdEVs imaged were larger than 100 nm in diameter. Larger ACdEVs are easier to identify on the cryo-TEM grid at a low resolution. Therefore, this size range may have been preferentially represented in this cryo-TEM dataset.

3.3.4 Biochemical characterisation of ACdEVs

As discussed in the introduction, despite EVs lacking a universal marker, tetraspanins remain the most used surface proteins as markers of EVs (Welsh *et al*., 2024). Therefore, antibodies against CD9, CD63 and CD81 were incubated with ACdEVs and measured by nano-flow cytometry (Figure 3.7).

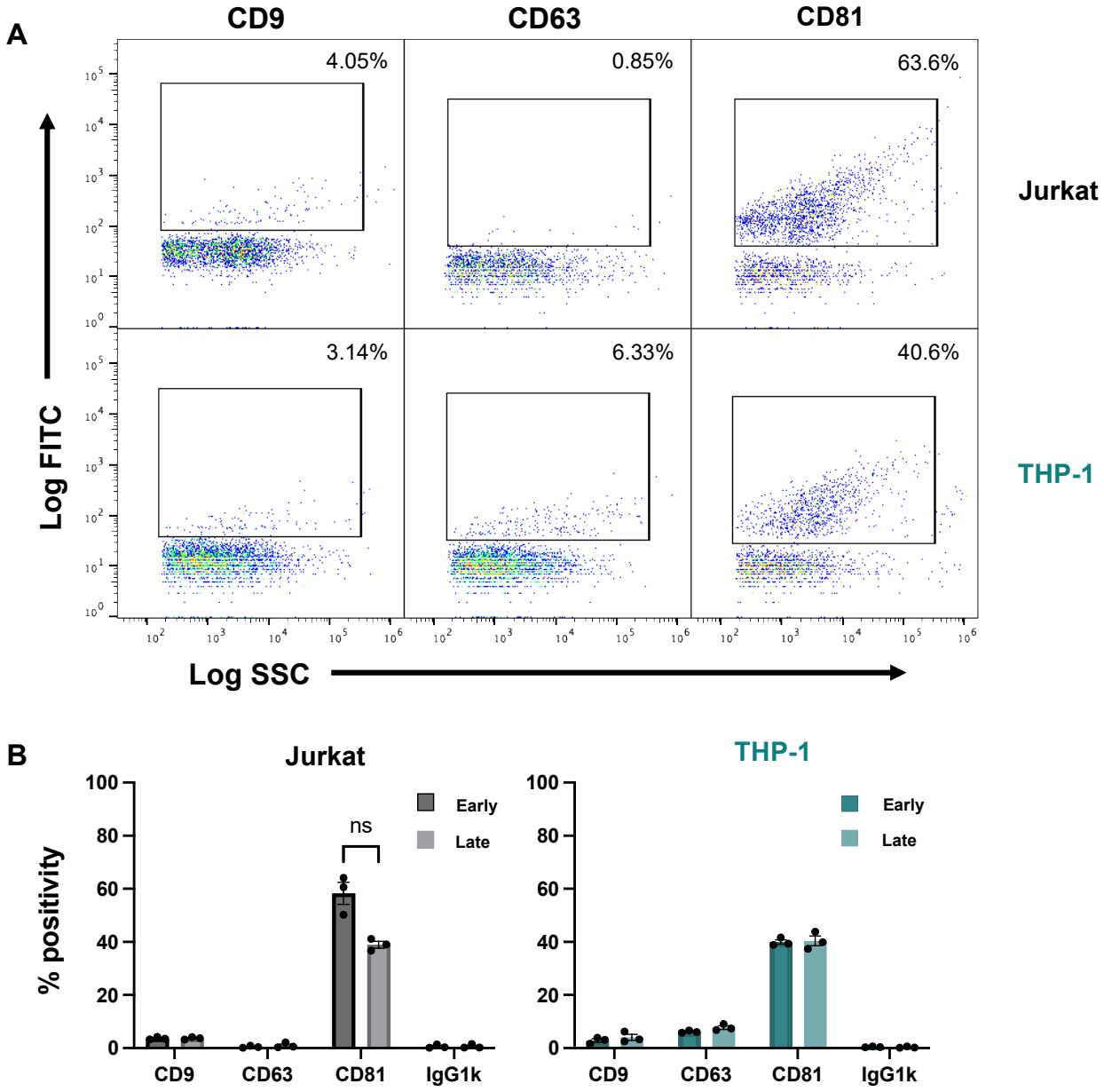

Figure 3.7: Tetraspanins CD9, CD63 and CD81 were detected on the surface of ACdEV by nano-flow cytometry (NanoFCM). A) Representative flow plots of antibody-labelled Jurkat and THP-1 ACdEV (N = 1). B) CD81 was present on the largest percentage of ACdEV for both Jurkat and THP-1 cell lines. There was a non-significant decrease in the percentage of Jurkat-derived late ACdEV positive for CD81 compared to early ACdEV (mean ± SEM, multiple paired t test, ns = $p > 0.05$, N = 3).

For early and late ACdEVs derived from both Jurkat and THP-1 cell lines, CD81 was present on the highest proportion of ACdEVs compared to tetraspanins CD9 and CD63 (Figure 3.7). Interestingly, there was a notable decrease (non-significant) in the proportion of late ACdEV positive for CD81 compared to early ACdEV in the Jurkat cell line (Figure 3.7B).

Approximately 4% Jurkat-derived early and late ACdEVs were positive for CD9, whereas negligible numbers of Jurkat-derived ACdEVs were detected as positive for CD63 (< 1%) (Figure 3.7B). Conversely, at both apoptotic timepoints, approximately 3% THP-1-derived ACdEVs were positive for CD9 and approximately 6% THP-1-derived ACdEVs were positive for CD63.

Whilst nano-flow cytometry can reveal the proportion of EVs that may express an epitope, it is unable to report on the spatial arrangement of epitopes. It is possible to estimate the number of epitopes expressed per EV with beads with molecules of equivalent soluble fluorophore (MESF) (Welsh *et al.,* 2020). However, these rely on several assumptions surrounding the mechanism of antibody binding and are therefore, an estimation (Welsh *et al.* (2020) and Davis *et al.* (1998)). By harnessing the power of SMLM via dSTORM, this technique was able to provide the number of individual tetraspanin molecules localised per ACdEV and visualise the distribution of tetraspanin molecules across the ACdEV surface, providing unique insight into potential signalling mechanisms harnessed by tetraspanins.

The number of tetraspanin molecules per ACdEV was linked to size (Figure 3.8). As expected, fewer tetraspanin molecules were detected on smaller ACdEVs compared to larger ACdEVs (Figure 3.8). Interestingly, there were clear observable differences between Jurkat-derived ACdEV and THP-1-derived ACdEVs: whilst both showed a positive correlation between ACdEV size and number of tetraspanins, small THP-1-derived ACdEVs (< 200 nm) carried more tetraspanin molecules per ACdEV than Jurkat-derived small ACdEVs (as indicated by the circles in Figure 3.8). No obvious difference was observed between timepoints, except for a larger abundance of ACdEVs and a higher frequency of bigger Jurkat-derived ACdEVs, as previously reported (Figure 3.5). The majority of ACdEVs (>70%) from both cell lines carried fewer than 100 tetraspanin molecules per ACdEV (Supplementary Figure 3.2).

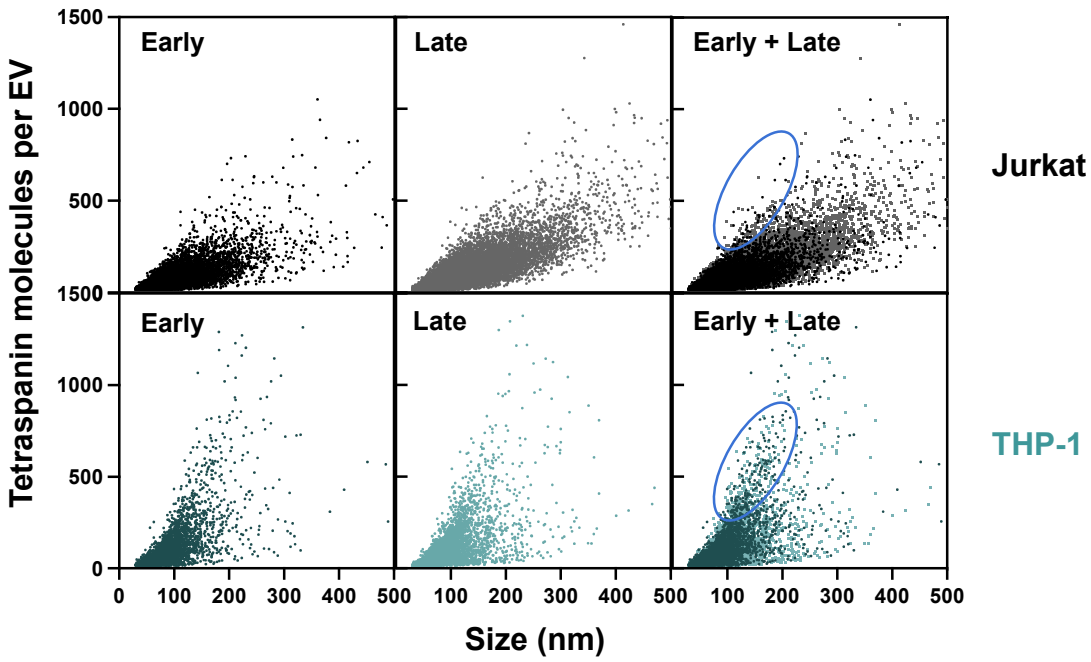

Figure 3.8: Larger ACdEVs displayed a higher number of tetraspanin molecules per ACdEV. Early and late ACdEVs from Jurkat and THP-1 cells were immobilised by antibody capture (against tetraspanins CD9, CD63 and CD81), labelled with a tetraspanin antibody cocktail (CD9, CD63 and CD81) and imaged by SMLM (in collaboration with Abbelight). There was a positive correlation between the number of tetraspanin molecules per ACdEV and ACdEV size (diameter, nm). Different populations of ACdEVs were observed in Jurkat and THP-1-derived ACdEVs (highlighted by circles): THP-1-derived ACdEVs < 200 nm in size were enriched in tetraspanins, compared to Jurkat-derived ACdEVs (N = 3 technical replicates).

Using an artificial intelligence (AI) – driven segmentation algorithm, ACdEVs were categorised as ‘distributed or ‘ring-like’, depending on the spatial arrangement of tetraspanins (Figure 3.9A) (Nanometrix). ‘Distributed’ ACdEVs had tetraspanins distributed evenly across the surface, whereas ‘ring-like’ ACdEVs had tetraspanins arranged in specialised ring structures across the ACdEV surface, as seen in Figure 3.8A. The majority of Jurkat and THP-1-derived ACdEVs imaged had a ‘distributed’ formation of tetraspanins (Figure 3.9B). 10.07% Jurkat-derived ACdEVs were categorised as ‘ring-like’, whereas just 5.42% THP-1-derived ACdEVs were categorised as ‘ring-like’. On average, ‘ring-like’ ACdEVs were larger in diameter than ‘distributed’ ACdEVs, derived from both cell lines (Figure 3.9C).

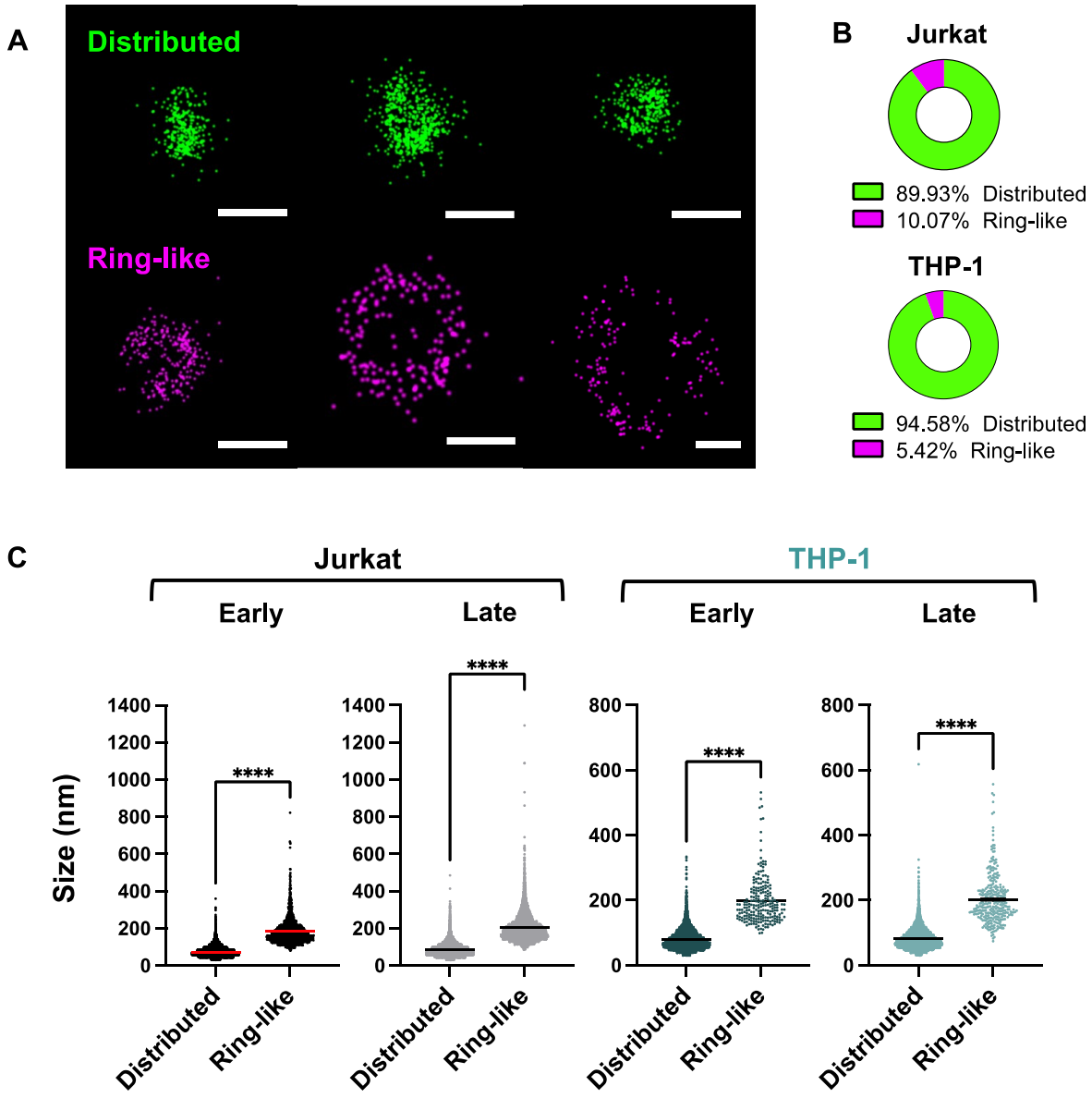

Figure 3.9: Spatial arrangement of tetraspanins CD9, CD63 and CD81, at the surface of ACdEVs. Early and late ACdEVs from Jurkat and THP-1 cells were immobilised by antibody capture (against tetraspanins CD9, CD63 and CD81), labelled with a tetraspanin antibody cocktail (CD9, CD63 and CD81) and imaged by SMLM (Abbelight). ACdEVs were categorised into 'distributed' or 'ring-like' according to the spatial arrangement of tetraspanins CD9, CD63 and CD81, by implementation of an AI-driven segmentation algorithm (in collaboration with Nanometrix, Abbelight). A) Representative images of ACdEVs with 'distributed' or 'ring-like' formations of tetraspanins. Scale bar ~100 nm. B) The percentage of ACdEVs, out of the total population, categorised based on tetraspanin arrangement as either 'distributed' or 'ring-like'. C) ACdEVs with a 'ring-like' arrangement of tetraspanins were, in general, larger in size than ACdEVs with 'distributed' tetraspanin expression (Mean ± SEM, unpaired t test, ****$p < 0.0001$, N = 3 technical replicates).

3.4 Discussion

3.4.1 UV irradiation as a model of apoptosis

Jurkat T cell and THP-1 monocyte cell lines were the human immune cell lines chosen to collect ACdEVs and model ACdEV : macrophage interactions. Due to a rapid rate of proliferation (every 2 - 3 days Jurkat T cells triple and THP-1 monocytes double in number) the use of immortalised cell lines allowed for efficient scale up of experiments. This enabled the collection of highly concentrated ACdEVs from large populations of apoptotic cells (in a typical experiment ~40 million cells were exposed to UV irradiation). As such, all ACdEV samples were freshly prepared for each experiment, preventing the need to explore methods of ACdEV preservation. Additionally, prior mass spectrometry analysis (discussed in Chapter 4) provided insights into the proteomic composition of ACdEVs derived from various immune cell lines, including Jurkat T cells and THP-1 monocytes (Grant L.R., 2022). Therefore, use of these cell lines enabled the continuation of previous work.

As with use of any immortalised cell line, there are caveats that must be considered during data interpretation. Immortalised cell lines are inherently cancerous and can be passaged extensively without any obvious abnormalities in cell morphology. Cell lines contain genetic mutations, most often associated with cancer, but also involved in other cell signalling pathways. For example, the Jurkat T cell line was shown to have a mutation in C1GALT1C1 which causes disrupted *O*-linked glycosylation (Gioia *et al.*, 2018). This could fundamentally alter the surface composition of ACdEVs. Additionally, differences in cytokine release and sensitivity to polarising treatments have been observed in THP-1 monocytes compared to primary monocytes, showing cellular behaviour is altered (Schildberger *et al.,* 2013). Therefore, it is possible cell line mutations may alter functional characteristics of ACdEVs and recipient cell responses.

UV irradiation was the chosen method of apoptosis induction, as it potently and synchronously induces apoptosis (Figure 3.1, Supplementary Figure 3.1) (Salucci *et al.,* 2012). Specifically, UV irradiation achieves induction of apoptosis by the activation of multiple pathways: direct DNA damage causing cell cycle arrest by activation of p53, and activation of cell surface-expressed death receptors, such as Fas (Kulms & Schwarz, 2000). The kinetics of UV-mediated apoptosis induction were measured by flow cytometry (Figure 3.1, Supplementary Figure 3.1). In both cell lines, cells had entered the early apoptotic stage 6 hours post UV exposure, marked by PS exposure. At 18 hours post UV exposure, cells had entered the late apoptotic, marked by loss of

membrane integrity in addition to PS exposure (Figure 3.1, Supplementary Figure 3.1). As such, EVs collected from cells at either apoptotic stage were termed ‘early ACdEV’ or ‘late ACdEV’.

It is important to consider the biological relevance of UV irradiation as a method of apoptosis induction, as immune cells would not be exposed to UV irradiation *in vivo*. However, studies have demonstrated that the function of ACdEVs remains consistent regardless of whether apoptosis is induced by UV irradiation or chemical methods. For example, ACdEVs collected from cells treated with UV irradiation conserve the ability to drive phagocyte recruitment, as reported when apoptosis occurs spontaneously in culture or is induced by, staurosporine (protein kinase inhibitor), actinomycin (RNA synthesis inhibitor) (Torr *et al.,* 2011; Truman *et al.,* 2008; Segundo *et al.,* 1999). In addition, as apoptosis is a convergent pathway, this led us to the hypothesis that ACdEV functions are conserved irrespective of the method of apoptosis induction. However, more work is needed to confirm this. It would be insightful to compare the molecular composition of ACdEVs to evaluate the effect of different methods of apoptosis induction on ACdEV biogenesis, cargo packaging and release kinetics. Notably, UV irradiation is highly oxidising which could impact the functional activity of individual molecules, as well as, reduce the availability of free thiol groups for labelling with BODIPY™ FL maleimide, as thiol groups are susceptible to oxidation, limiting their ability to react with thiol-binding dyes.

3.4.2 ACdEV collection and enrichment

As this project aimed to understand ACdEV-specific functions in immune interaction, a protocol was established to attempt to separate ACdEV from all other apoptotic cell-secreted factors, such as large apoptotic bodies, soluble proteins (e.g. chemokines, cytokines), lipid mediators and nucleotides. There is an ongoing lack of standardisation in the EV field, one aspect of which is method of EV collection (Welsh *et al.,* 2024). The most common methods are ultracentrifugation, SEC and TFF, all of which have their disadvantages including, EV aggregation, dilution of precious EV samples and loss of EV sample (Linares *et al.,* 2015; Welsh *et al.,* 2024). As detailed in the Methods section (see Chapter 2), a combination of differential centrifugation and SEC was chosen to collect ACdEVs. This protocol successfully separated ACdEVs from most of the apoptotic cell-secreted soluble protein (Figure 3.2, Figure 3.3A and 3.3B). Notably, it is possible some of these soluble proteins may normally be loosely adhered to the ACdEV surface, forming part of an EV corona - a layer of surface molecules that spontaneously adsorb to the EV surface and impart functionality (Buzás, 2022). Notably, SEC has been previously reported to disrupt the EV corona and therefore, may have impacted ACdEV composition and function (Welsh *et al.,* 2024). This topic will be discussed further in Chapter 5. Additionally, apoptosis was induced in

serum-free conditions to eliminate FBS-derived vesicles that would contaminate downstream ACdEV characterisation. However, it cannot be completely ruled out that negligible amounts of bovine contaminants might have been present in ACdEV preparations potentially altering the composition and functions of ACdEVs.

ACdEVs were defined as particles that exceeded the side scatter trigger threshold and emitted a positive signal in the FITC channel (by either labelling with BODIPY™ FL maleimide or MemGlow™ 488) (Figure 3.2B-C and Figure 3.3C-D). Highly elevated background noise was detected in the FITC channel for fractions 15 – 28 (Figure 3.2C and 3.2E). This was attributed to unbound dye that had eluted in the later fractions. As BODIPY™ FL maleimide labels free thiol groups on proteins, it was expected that the peak in FITC background noise and protein signal would align more closely (Figure 3.2F). However, whilst both peaks overlapped, the peak signal for FITC background noise was in fraction 24 and the peak signal for protein was in fraction 20. This suggested that in addition to BODIPY™ FL maleimide – labelled soluble protein, there was significant excess unbound BODIPY™ FL maleimide that eluted after the soluble protein.

Low levels of protein were still detected in what was considered the 'ACdEV fractions', fractions 7-13 (Figure 3.2D and 3.2F), and the pooled ACdEV sample (Figure 3.3C-D). This was attributed to the presence of ACdEVs, as ACdEVs carry protein both internally in the EV lumen and exposed at the surface as membrane-embedded proteins or loosely adhered surface proteins. Notably, the protein concentration calculated by Bradford protein assay may be an underestimation of the true ACdEV protein concentration, depending on the accessibility of the Bradford reagent to the intraluminal proteins (as no ACdEV lysis step was performed). Future work should determine this by comparing the protein concentration of intact versus lysed EVs. Overall, the concentration of protein post-SEC was significantly reduced (Figure 3.3C-D). Furthermore, the percentage of ACdEVs (indicated by MemGlow™ 488) out of total detected unstained particles was increased post-SEC, suggesting the ACdEV collection method simultaneously removed soluble protein and enriched ACdEVs (Figure 3.3).

Unexpectedly, the percentage ACdEVs (out of total particles) at the late apoptotic timepoint was reduced, significantly in late apoptotic secretome and non-significantly in late ACdEVs, when compared to the early apoptotic timepoint (Figure 3.3C). This may have been the result of an accumulation of large protein aggregates overtime, emitting a sufficiently large side scatter signal to exceed the side scatter trigger threshold, thereby skewing the proportion of ACdEVs, here defined as MemGlow™ 488-positive particles. Future work may be able to confirm this by carrying out cryoTEM analysis to identify the increased presence of protein aggregates in late apoptotic

secretome and late ACdEVs. As expected, the absolute concentration of ACdEVs significantly increased, comparing early versus late apoptotic timepoints, due to an accumulation of ACdEV release over time (Figure 3.3E). Importantly, late ACdEVs contain a mixture of early and late ACdEVs, and therefore, have an overlapping composition, which must be considered during future data interpretation. Furthermore, ACdEV release was not linear between early and late apoptotic timepoints, indicating that the rate of ACdEV release decreases throughout apoptosis (Figure 3.3E). This may reflect a loss of regulation as the cell enters a highly dismantled state.

The functional implications of EV 'separation' or 'isolation' must be considered given that EVs do not exist in isolation *in vivo.* As mentioned, soluble factors or loosely adsorbed factors, termed 'corona', have been shown to contribute to EV functionality; the presence of an EV corona has been shown to directly promote EV uptake and thus, cellular processing of EV cargo (Tóth et al., 2021; Dietz et al., 2023). Considering this, it is increasingly difficult to define what is an 'isolated' EV and which method of EV collection may provide the most representative EV sample. As such, crude apoptotic secretome and ACdEVs processed by SEC are both valuable samples and were used to investigate ACdEV function in this project.

3.4.3 ACdEV physical characterisation

Having set up an ACdEV collection workflow, ACdEVs from Jurkat T cells and THP-1 monocytes were collected and assessed for several characteristics, including concentration, size and presence of common EV markers. THP-1 monocytes consistently released a higher concentration of ACdEVs than Jurkat T cells, at both apoptotic timepoints (Figure 3.4). This suggested that cell source dictates regulation of ACdEV release. Indeed, the cell source and its activation state, dictates the composition and function of EVs (Dixon *et al.,* 2023; Hagey *et al.,* 2023). The underlying mechanism explaining why certain cell types release more EVs than others is not yet fully understood. In the context of apoptosis, given that ACdEVs are an important attractant for phagocytes, it is somewhat surprising that ACdEV release differs between cell types, given that all dying cells require clearance by phagocytic cells (Poon *et al.,* 2014b). Given that apoptotic cells release a variety of 'find me' signals, ACdEV release may represent an additional regulatory mechanism that is flexible and dependent on cell type. For instance, cells that pose the greatest risk of causing damage if not efficiently cleared may release a higher quantity of ACdEVs to ensure prompt phagocytic removal. In the context of neutrophils and monocytes, it is possible that these cell types are programmed for rapid and abundant ACdEV release upon mass infiltration at an inflammation site. Sequential release of ACdEVs may facilitate long distance signalling for the recruitment and activation of waves of neutrophils, followed by macrophages (Poon *et al.,* 2014b).

This process could help rapidly resolve inflammation, minimising unnecessary damage to the local tissue. Alternatively, T cells undergo rapid apoptosis during thymic selection (Wang & Zúñiga-Pflücker, 2022). Phagocytes reside in large numbers in the thymus to assist this process. Therefore, apoptotic T cells may not require abundant ACdEV release to facilitate their rapid removal. More work is needed to understand the intrinsic differences in regulation of ACdEV release between cell types, and indeed, EV release from viable cells.

The majority of ACdEVs were less than 100 nm in size for both cell lines, highlighting the ongoing need for characterisation of the most abundant ACdEV population (Figure 3.5). Interestingly, late Jurkat-derived ACdEVs were significantly larger than early Jurkat ACdEVs, suggesting late apoptotic Jurkat T cells release bigger ACdEVs (Figure 3.5A). This may be due to the late apoptotic cells having lost membrane integrity, leading to the release of larger apoptotic blebs. However, this was not observed in THP-1 ACdEVs, with early and late ACdEVs showing no significant difference in size (Figure 3.5A). Therefore, apoptotic THP-1 cells release a high abundance of small ACdEVs throughout early and late apoptosis, highlighting cell type-specific features of ACdEV release.

There was significant disparity in the ACdEV size reported by nano-flow cytometry versus SMLM (NanoFCM, Abbelight). In each sample, SMLM reported the mean ACdEV size as at least 10 nm bigger than nano-flow cytometry (Figure 3.5). This is partly because the limit of detection of both methodologies is different: nano-flow cytometry was calibrated to detect particles between 40 – 200 nm, and SMLM detected particles down to 30 nm with no upper limit. Therefore, the larger ACdEVs captured by SMLM will have skewed the mean average sizes recorded. That said, there are key differences in EV measurements made by both techniques; whilst SMLM is a direct measure of ACdEV size, nano-flow cytometry relies on an indirect measurement of light scatter. A series of silica nanoparticles of set sizes are used to produce a standard curve, that EVs measurements are fitted to (Figure 2.1). As silica nanoparticles refract light differently to EVs, this measurement is an estimation of size (Welsh *et al.,* 2023). This could also account for the difference in reported ACdEV sizes by nano-flow cytometry and SMLM. Furthermore, whilst nano-flow cytometry measured all ACdEVs within the limit of detection (40 – 200 nm), SMLM immobilised ACdEVs for imaging by antibodies against tetraspanins CD9, CD63 and CD81, therefore only representing the tetraspanin-positive subpopulation of ACdEVs which may have unique subpopulation-specific characteristics, such as size.

CryoTEM is one of the most accurate techniques for sizing EVs as it provides a direct measurement of size whilst preserving the native structure of the EV, and unlike other methods,

doesn't rely on the assumption of particle sphericity (Welsh *et al.,* 2024). Previously, conventional TEM was more commonly used but the requisite dehydration step introduces a cup-shaped distortion of the EV structure and therefore, is unable to provide an accurate representation of EV size and shape. In this project, between 20 – 39 ACdEVs were imaged per sample by cryoTEM, which was considered insufficient to perform statistical sizing analysis (Supplementary Table 3.1 and Supplementary Table 3.2). However, it has provided unique insight into ACdEV shape and structure that alternative techniques could not achieve (Figure 3.6).

Interestingly, cell line-derived ACdEV shape was heterogeneous but human primary T cell ACdEVs were mostly spherical with just 3 individual ACdEVs identified having an alternative shape (Figure 3.6B, Supplementary Table 3.1). This could suggest cell lines have intrinsic differences in the pathways that lead to the production and release of ACdEVs, compared to primary cells. Importantly, donor variability could impact ACdEV structure and therefore, many more replicates of primary T cell-derived ACdEVs should be carried out to confirm this result.

The ice thickness must be considered as a limiting factor in terms of ACdEV size – large ACdEVs exceeding the ice thickness will inevitably be compressed to 'fit' within the ice or may rupture, destroying the native EV structure. If large ACdEVs were compressed but not destroyed, this could have altered their structure causing ACdEVs to appear oval, tubular or irregular in shape. It is possible the cell line-derived ACdEVs had a higher frequency of bigger ACdEVs, causing this heterogeneity in ACdEV shape to be preferentially represented. The exact ice thickness is unknown and will inevitably vary across the TEM grid but was estimated to be approximately ~200 nm (personal communication with Dr Saskia Bakker, University of Warwick). Therefore, it is challenging to determine if the different ACdEV shapes reported are representative of native ACdEV structures or an artefact of the ice thickness. However, this study and others have reported the presence of oval and tubular-shaped EVs inside spherical EVs, forming multilamellar structures, and therefore, cannot have formed as the result of the freezing procedure (Figure 3.6B) (Höög & Lötvall, 2015). As such, it is possible the formation of oval or tubular EV structures may depend on the membrane composition, such as the presence of curvature-inducing proteins or lipid rafts. Future work should aim to better characterize the smallest and most prominent population of ACdEVs < 100 nm in size (Figure 3.5).

The frequency of multilamellar ACdEVs was noticeably increased in THP-1-derived ACdEVs compared to Jurkat and primary T cell-derived ACdEVs (Figure 3.6B). Due to challenges in separating multilamellar EVs from unilamellar EVs, the mode of biogenesis and the significance of multiple bilayers on EV function remains unexplored (Broad *et al.,* 2023). However, in the field

of liposome-mediated drug delivery, multi-layered liposomes are routinely engineered to aid targeted delivery and control drug release (Chaurasiya *et al.,* 2021). The presence of multiple bilayers delays the release of intraluminal cargo and can be modulated for the sequential release of cargo in response to specific stimuli, such as temperature or pH (Boyer & Zasadzinski, 2007; Peyret *et al.,* 2017; Seong *et al.,* 2018). Therefore, apoptotic cells may benefit by the release of multilamellar ACdEVs for their preservation for long-distance delivery of cargo. Additionally, the presence of multiple bilayers could fundamentally change the mechanism of cargo delivery; direct fusion of a unilamellar ACdEV with the recipient cell plasma membrane results in cytoplasmic cargo release, whereas, a multilamellar ACdEV might result in the cytoplasmic release of a 'luminal' ACdEV by sequential 'shedding' of outer bilayers (Broad *et al.,* 2023; Prada & Meldolesi, 2016). Furthermore, one study showed THP-1 monocytes treated with lipopolysaccharide (LPS) responded by the increased release of multilamellar EVs that had increased expression of immunomodulatory membrane protein, glucose transporter-1 (GLUT1) (Yang *et al.,* 2022). Therefore, cells may utilise the increased capacity of multiple bilayers to transport a higher abundance of membrane-associated proteins. In the case of apoptotic cells, this could facilitate the long-distance display of 'eat me' signals to immune cells, and the uptake of membrane protein-rich ACdEV to modulate the inflammatory status of immune cells.

3.4.4 Tetraspanin profiling of ACdEVs

There is no universal marker of EVs which makes it challenging to distinguish between EVs and other nanoparticles that can be co-isolated during EV collection (Welsh *et al.,* 2024). Often, co-isolation is due to overlapping sizes and/or densities (such as lipoproteins - a common contaminant of plasma-derived EV samples). Therefore, probing for a combination of EV proteins provides confidence in the presence of EVs.

For this project, ACdEVs were probed for the presence of the most commonly expressed tetraspanins: CD9, CD63 and CD81. CD81 was present on the largest percentage of Jurkat and THP-1-derived ACdEVs, compared to CD9 and CD63 which were only present on a small population of <10 % ACdEVs (Figure 3.7). Additionally, Jurkat-derived late ACdEVs displayed noticeably less CD81 than early ACdEVs (not statistically significant) (Figure 3.7). This data provided further evidence that tetraspanins are not present on all EVs and expression may change in response to different cellular states. Therefore, tetraspanins are a poor marker of EVs when used in isolation (Welsh *et al*., 2024). This is particularly important when interpreting results gained from EV collection methods or characterisation techniques that implement antibody-mediated immobilisation of EVs, most often targeting tetraspanins, as only subpopulations of EVs

will be represented. This includes well-known EV technologies such as the ExoView (not used in this project) and the SMLM data presented in this chapter (Abbelight) (Figure 3.5, Figure 3.8, Figure 3.9).

As previously described, SMLM reported the spatial localisation of individual tetraspanin molecules using dSTORM (Lelek *et al.,* 2021). As expected, larger ACdEVs carried a higher number of individual tetraspanin molecules, likely because they have a bigger membrane surface area (Figure 3.8). However, factors other than surface area must also determine the number of tetraspanins loaded into ACdEVs, as a population of smaller (< 200 nm) THP-1-derived ACdEVs carried more tetraspanins than smaller Jurkat-derived ACdEVs (Figure 3.8). Tetraspanins play a key role in EV biogenesis and cargo selection, and their abundance on EVs may influence function. It is not known whether viable cell-derived EVs and ACdEVs carrying different numbers of tetraspanin molecules and how this could impact their downstream function. One study found that plasma EVs from breast cancer patients were significantly larger and exhibited higher tetraspanin expression than those from control patients, with a mean of < 40 tetraspanin molecules per EV (Jiang *et al.,* 2024). This suggests that disease state, along with EV size, can influence tetraspanin expression at the EV surface. Understanding this complex relationship could provide valuable insight into EV regulation.

Interestingly, several ACdEVs showed tetraspanins to be organized into ring-like structures across the EV surface and this correlated with an increased ACdEV size (Figure 3.9). Therefore, a minimum EV membrane surface area may be required in order for tetraspanins to form higher order ring-like structures. Given that CD81 was the tetraspanin identified on the highest percentage of ACdEVs, it can be assumed that the majority of tetraspanin localisations identified by SMLM are CD81. Indeed, it has been reported that tetraspanins can organise into localised clusters in the plasma membrane, termed ‘tetraspanin enriched domains’ (TEMs) (Huang & Yu, 2022) (Zuidscherwoude *et al.,* 2015). Spatial reorganisation into TEMs facilitates signalling in complex with other signalling proteins or lipids, including MHC II, integrins, immunoglobulin-like superfamily members, cholesterol and gangliosides. Some tetraspanin interactions have been shown to participate in immune cell activation, such as localised clustering of MHC II along with tetraspanins CD9, CD63 and CD81 that, together, participate in antigen presentation to T cells via a high affinity immunological synapse interaction (Vogt *et al.,* 2002). It has been suggested that tetraspanins may act to coordinate and stabilise the clustering of MHC II (Anderson & Roche, 2015). Indeed, the presence of tetraspanins prevents diffusion of TEM partner molecules, such as CD19 to stabilise B cell receptor signalling (Mattila *et al*., 2013) .

It is therefore intriguing that this work has identified high order spatial organisation of tetraspanins on the surface of ACdEVs, indicating their potential to engage in high affinity, immunological synapse-like interactions with immune cells. One group recently identified nanoscale rings of CD81 present at the surface of activated lung-derived macrophage EVs (Ambrose *et al.,* 2020). However, it is unclear whether CD81 was evenly distributed across the EV surface or organised into ring-like structures, as identified here. Notably, the ring-like structures identified in this project were only identified on a small population of ACdEVs (10.07% Jurkat ACdEV and 5.42% THP-1 ACdEV) (Figure 3.9). Notably, ACdEVs were immobilised using anti-tetraspanin antibodies for SMLM imaging. The affinity of these antibodies may have affected the natural spatial organisation of tetraspanins on the ACdEV surface. Further research is required to determine the native arrangement of tetraspanins and to understand the significance of a highly ordered distribution at the surface of ACdEVs.

3.4.5 Conclusions

Overall, this chapter demonstrated UV irradiation to be an effective method of apoptosis induction. Jurkat T cells and THP-1 monocytes progressed to 'early apoptosis' 6 hours post UV irradiation, defined by PS exposure, and 'late apoptosis' 18 hours post UV irradiation, defined by membrane permeabilisation (*i.e.* capacity of propidium iodide to bind DNA) in addition to PS exposure (Figure 3.1). In addition, the combination of differential centrifugation and SEC was validated as an effective method of ACdEV collection (Figure 3.2 and 3.3). This approach allowed the collection of early and late ACdEVs to observe time-sensitive changes in physical and biochemical features of ACdEVs.

Characterisation of ACdEVs was conducted to confirm their presence in sample preparations and assess concentration, size, morphology, and tetraspanin expression. Furthermore, the role of cell source and apoptotic timepoint in governing characteristics of ACdEVs was questioned. The majority of ACdEVs from Jurkat T cells and THP-1 monocytes were below 100 nm in size and displayed the commonly expressed tetraspanin, CD81 (Figure 3.5 and 3.7). As ACdEV size increased, the number of tetraspanin molcules displayed at the ACdEV surface increased (Figure 3.8). Ring-like structures of tetraspanins were observed in a minority population of ACdEVs from both cell lines, suggesting ACdEVs may have the ability to signal via high affinity interactions (Figure 3.9). However, several different characteristics were observed in ACdEVs dependent on parental cell line or apoptotic timepoint. Apoptotic THP-1 monocytes released a higher quantity of small ACdEVs, whereas apoptotic Jurkat T cells released fewer ACdEVs (Figure 3.4 and 3.5). Furthermore, late apoptotic Jurkat T cells released ACdEVs that were significantly larger than

early ACdEVs, whereas THP-1-derived ACdEVs remained consistent in size during apoptosis (Figure 3.5). THP-1-derived ACdEVs also presented a notable population of multilamellar EVs compared to Jurkat T cells and primary T cells, possibly reflecting different modes of biogenesis (Figure 3.6).

Taken together, this chapter reinforced the widely reported heterogeneity of EVs and raised several intriguing questions regarding the influence of cell source and apoptotic timepoint on the regulation of ACdEV biogenesis and release, as well as ACdEV structure and expression of tetraspanins. Going forward, this work provided a basis for targeted characterisation of the ACdEV surface proteome and the downstream immunomodulatory function of ACdEVs.

3.5 Supplementary Data

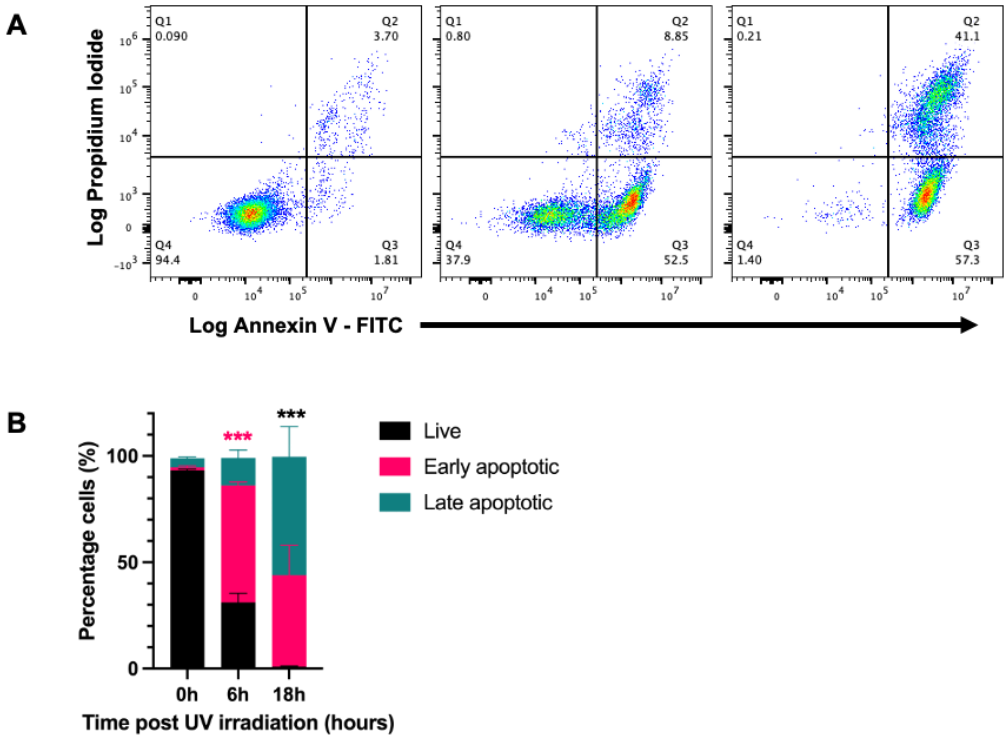

Supplementary Figure 3.1: Induction of apoptosis by UV irradiation in THP-1 monocytes. A) Representative flow plots of cells labelled with Annexin V-FITC and propidium iodide at 0 h, 6 h and 18 h post UV irradiation. B) Percentage live, early apoptotic and late apoptotic / early necrotic cells at 0, 6 and 18 hours post UV irradiation, determined by flow cytometric gates (Mean ± SEM, N = 3. Two-way ANOVA was performed with Tukey's Multiple Comparison test comparing 'Early apoptotic' and 'Live' cells between 0 h and 6 h, and 0 h and 18 h post-UV irradiation, respectively. Early apoptotic cells (magenta) ***P < 0.001, Late apoptotic cells (green) ***P <0.001).

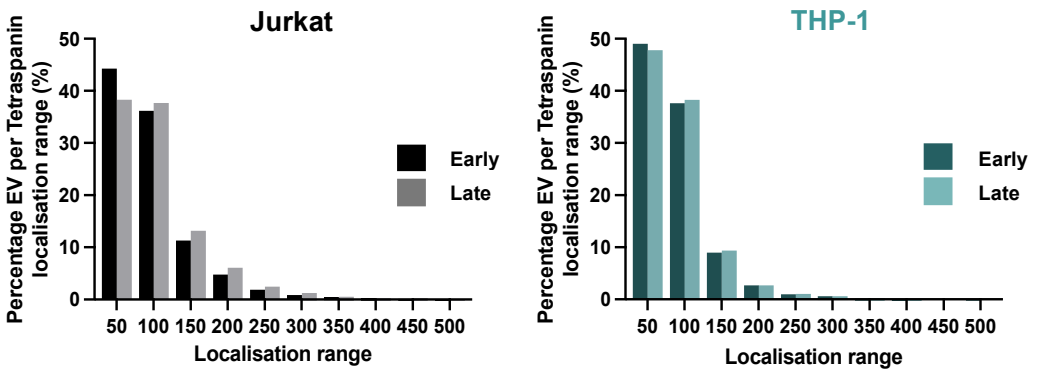

Supplementary Figure 3.2: The majority of ACdEVs carried fewer than 100 tetraspanin molecules. Early and late ACdEVs from Jurkat and THP-1 cells were immobilised by antibody capture (against tetraspanins CD9, CD63 and CD81), labelled with a tetraspanin antibody cocktail (CD9, CD63 and CD81) and imaged by SMLM (in collaboration with Abbelight). Over 70% of ACdEVs had 100 tetraspanin localisations or less (N = 3 technical replicates).

Chapter 4 Characterising the ACdEV surface proteome

4.1 Introduction

Cells release EVs that engage in communication with recipient cells through various mechanisms, including direct surface-to-surface interactions. The EV surface is heterogeneous, comprising proteins, lipids, glycans, and nucleic acids. It is often enriched in characteristic EV proteins such as tetraspanins (CD9, CD63, and CD81) but can also resemble the originating cell membrane by expressing cell-specific proteins (Lara *et al.,* 2020; Buzás *et al.,* 2018). These surface molecules, which can be anchored or embedded in the EV membrane, help direct EVs to specific tissue sites or engage with the microenvironment to promote cell motility (French *et al.,* 2017; Sung *et al.,* 2015). The EV surface can also be modified by the microenvironment, where molecules can weakly and spontaneously adsorb, forming what is known as the EV 'corona' (Buzás, 2022). The EV corona has been shown to dictate specificity of uptake by recipient cells, as well as functional outcomes such as inducing differential cytokine release (Liam-Or *et al.,* 2024; Tóth *et al.*, 2021).

ACdEVs promote the clearance of apoptotic cells by attracting immune cells chemotactically by displaying CX3CL1 and ICAM-3 at the ACdEV surface (Torr *et al.,* 2011; Truman *et al.,* 2008). ACdEVs have also shown therapeutic potential by promoting anti-inflammatory, pro-repair responses in immune cells, however, it remains unclear whether these immunomodulatory effects are driven by surface interactions, the delivery of ACdEV cargo, or a combination of both (Liu *et al.,* 2020; Shen *et al.,* 2017; Fehr *et al.,* 2013). Understanding the precise mechanisms of EV surface-mediated communication is crucial for understanding how recipient cells receive and respond to these messages.

Research in this field faces technical challenges, particularly in probing the EV surface due to the nanoscale size and heterogeneity of EVs. Current methodologies often use ensemble approaches to estimate characteristics of a population of particles or rely on indirect measurements, such as dynamic light scattering and nanoparticle tracking analysis. Techniques like tunable resistive pulse sensing provide direct single-particle analysis but are limited to parameters like size and charge. In contrast, nano-flow cytometry offers extensive multiparametric analyses (size, concentration, and biochemical composition) at the single-particle level, allowing unprecedented detail in probing the EV surface across a broad size range (Welsh *et al.,* 2023).

4.2 Aims and objectives

As the first point of contact between ACdEVs and recipient cells, we hypothesise that the surface proteome plays a crucial role in governing early ACdEV-cell interactions. This chapter aims to characterise the molecular composition of the surface proteome of ACdEVs, which remains relatively unexplored.

Mass spectrometry proteomic analysis was previously performed on ACdEVs isolated from early and late apoptotic cells of three human immortalised cell lines: Jurkat T cells, THP-1 monocytes, and Mutu B cells, a cell line derived from Burkitt's lymphoma (Grant L. R., 2022). ACdEVs collected during early and late apoptosis, defined by early exposure of phosphatidylserine (PS) and late membrane permeabilisation, respectively, identified time-sensitive changes in protein composition that may infer changes in ACdEV function (Grant L. R., 2022). In this project, these proteomics datasets will be reanalysed using a new gene ontology analysis approach and cross-referenced with updated Vesiclepedia and UniProt databases. Candidate proteins will be selected based on their predicted surface localisation, ensuring accessibility to immune cells, and their reported functions in processes relevant to apoptotic cell clearance, maximising the likelihood of their involvement in ACdEV-driven immune modulation.

To confirm surface localisation, the ACdEV surface will be probed at high resolution for the candidate proteins by nano-flow cytometry. Together, this data will contribute to establishing a comprehensive atlas of the surface proteome of ACdEVs.

4.3 Results

4.3.1 Proteomic profile of ACdEVs

In-house liquid chromatography tandem mass spectrometry (LC-MS/MS) was previously performed on early and late ACdEVs derived from Jurkat T cells, THP-1 monocyte and Mutu B cell lines by Grant (2022). Apoptosis was induced chemically by cycloheximide and anti-Fas and ACdEVs were collected by the same differential centrifugation / SEC method described in this thesis (see Methods). Label-free relative quantification was performed in Progenesis QI (v4.1) to identify differences in ACdEV proteomes between immune cell lines and apoptotic timepoints (Grant, L. R., 2022). The proteomic datasets published in the doctoral thesis of Grant (2022) were kindly donated to this project for further data mining (Grant, L. R., 2022). Here, updated gene ontology analysis was carried out to select a new panel of candidate proteins for investigation.

When cross-referencing the proteomic ACdEV datasets with Vesiclepedia, an openly accessible encyclopaedia of proteins reported in EVs, 232 proteins were uniquely identified that had not been previously identified in T cells, B cells or monocytes (Figure 4.1) (Appendix, Table 7.3). This had decreased from 596 proteins that were previously uniquely identified using this dataset by Grant (2022), showing the rapid advancement in EV studies and reporting of EV data (Grant, L. R., 2022). 417 proteins were conserved across Jurkat T cell, THP-1 monocyte and Mutu B cell lines – this was higher than reported by Grant (2022) (Appendix, Table 7.7) (Grant, L. R., 2022). This was because UniProt IDs that failed to be automatically mapped to gene names (format required by Vesiclepedia for cross-referencing) were converted and mapped manually in this study. 313 of the conserved proteins were associated to the gene ontology (GO) term ‘Exosomes’, as reported by Grant (2022). Just 6 conserved proteins (down from 17 conserved proteins reported by Grant (2022)) had not been previously reported in Vesiclepedia: cytochrome c oxidase subunit 2, serine/threonine-protein kinase Nek9, small ribosomal subunit protein, RNA-splicing ligase RtcB homolog, protein SETSIP and Zinc finger protein 500. Additionally, of the all proteins that were identified: 358 proteins were specific to Jurkat-derived ACdEVs; 407 proteins were specific to THP-1-derived ACdEVs; 89 proteins were specific to Mutu-derived ACdEVs (Appendix, Table 7.4-6).

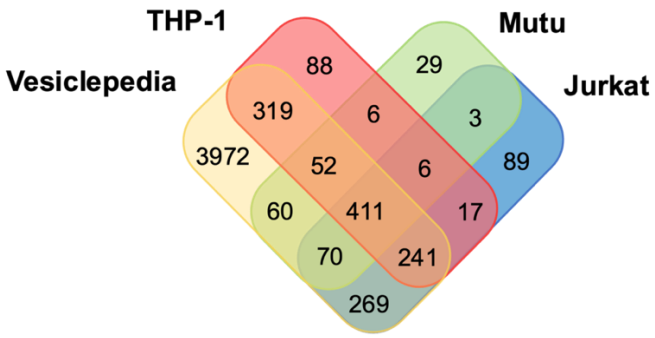

Figure 4.1: Updated comparison with Vesiclepedia revealed the number of proteins uniquely identified from the LC-MS/MS datasets had decreased from 596 proteins, as reported by Grant (2022), to 238 proteins. 417 proteins were conserved in ACdEVs collected from three immune cell lines: Jurkat T cells, THP-1 monocytes and Mutu B cells (Appendix, Table 7.7). Analysis performed in FunRich v3.1.4 on 1.07.24 (Pathan *et al.,* 2017).

4.3.2 Selection of candidate proteins

To select novel candidate proteins for further investigation and functional characterisation, proteins of interest were extracted by a combination of gene ontology analysis and cross-referencing with Vesiclepedia and UniProt databases (Figure 4.2). The candidate proteins were chosen from the pool of 417 conserved proteins, as it was hypothesised that proteins important in facilitating apoptotic cell clearance and immune responses may be conserved across different cell types.

As this project is focussed on the function of the ACdEV surface proteome, the aim was to select proteins predicted to be localised to the ACdEV surface. Gene ontology analysis was performed which led to the extraction of 244 proteins associated with the following cellular component terms: ‘Apical membrane’; ‘Cell surface’; ‘Extracellular’; ‘Extracellular region’; ‘Extracellular space’; ‘Extrinsic to membrane’; ‘Extrinsic to plasma membrane’; ‘Integral to membrane’; ‘Integral to plasma membrane’; ‘Membrane’; ‘Membrane fraction’; ‘Plasma membrane’; ‘Plasma membrane enriched fraction’ (Figure 4.2).

These proteins were further shortlisted based on their reported association with processes relevant to apoptotic cell clearance and modulation of the immune system. Gene ontology analysis was performed which led to the extraction of 69 proteins associated with the following biological process terms: ‘Apoptosis’; ‘Cell communication’; ‘Cell migration’; ‘Immune cell migration’; ‘Immune response’; ‘Regulation of immune response’; ‘Signal transduction’; ‘Transport’ (Figure 4.2).

It was predicted that proteins commonly detected in EVs derived from different cell types (including viable cells) would not have unique functions relevant to apoptotic cell clearance. 16 proteins were identified in the filtered proteomics dataset that were reported in the ‘Top 100’ most reported EV proteins on Vesiclepedia (Appendix, Table 7.8). A further 16 proteins were members of the same protein families reported in the ‘Top 100’ most reported EV proteins on Vesiclepedia (Appendix, Table 7.9). These proteins were removed which left 37 proteins of interest. A further 10 proteins were eliminated based on their predicted cellular localisation being ‘Centromere’, ‘Chromosome’, ‘Cytoplasm’, ‘Cytosol’, ‘Endoplasmic reticulum’, ‘Nucleus’, ‘Secreted’, ‘Spindle pole’, as reported by UniProt (Figure 4.2) (Appendix, Table 7.10). This led to a final list of 27 proteins of interest (Table 4.1).

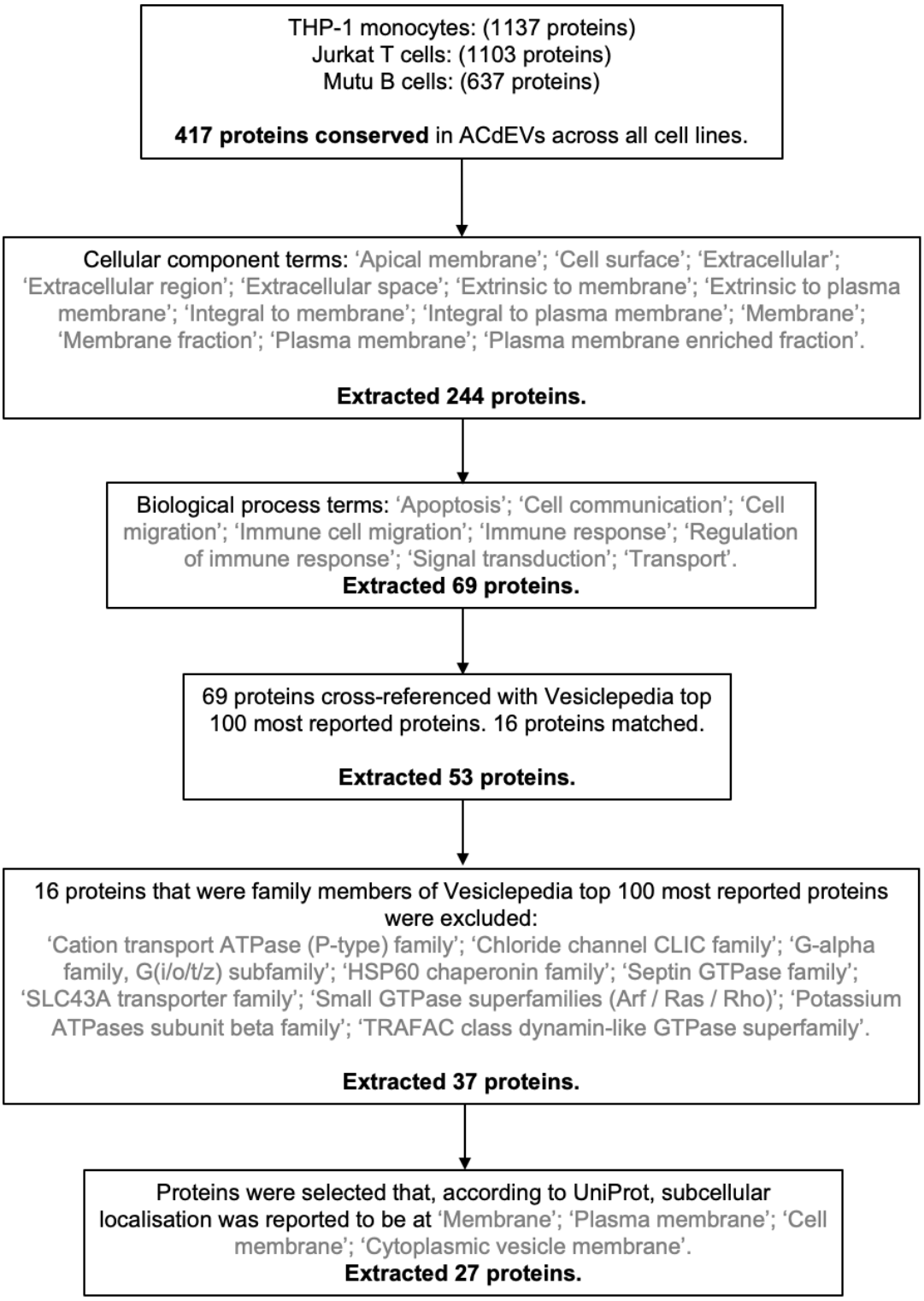

Figure 4.2: Flow diagram showing method of protein extraction via gene ontology analysis and cross-referencing with Vesiclepedia and UniProt databases. Gene ontology analysis was done using FunRich v3.1.4 on 25.01.22 (Pathan *et al.,* 2017). Cross-referencing with Vesiclepedia and UniProt was done on 01.07.24.

Gene symbol	Protein	Protein family
ABCC1 / MRP1	ABC transporter C family member 1	ABC transporter
ALCAM / CD166	Activated leukocyte adhesion molecule	Immunoglobulin (Ig) superfamily member
ELMO1	Engulfment and motility protein 1	ELMO-domain containing protein family
EPB41L2	Band 4.1-like protein 2	Protein 4.1 superfamily
IAP / CD47	Integrin-associated protein	Immunoglobulin (Ig) superfamily member
ITA4 / CD49d	Integrin alpha 4 subunit	Integrin alpha chain family
ITGB1	Integrin beta 1 subunit	Integrin beta chain family
MARCKSL1	MARCKS-related protein	MARSCKS family
NPTN / SDR-1	Neuroplastin / Stromal cell-derived receptor 1	Immunoglobulin (Ig) superfamily member
PECAM1 / CD31	Platelet endothelial adhesion molecule 1	Immunoglobulin (Ig) superfamily member
PLP2	Proteolipid protein 2	Myelin basic protein (MBP) family
PTPRC	Receptor-type tyrosine protein phosphatase C	Protein-tyrosine phosphatase family
SLC16A1	Monocarboxylate transporter 1	Major facilitator superfamily, Monocarboxylate porter family
SLC1A4	Neutral amino acid transporter A4	Dicarboxylate/amino acid:cation symporter family
SLC1A5	Neutral amino acid transporter A5	Dicarboxylate/amino acid:cation symporter family
SLC29A1	Equilibritave nucleoside transporter 1	SLC29A/ENT transporter family
SLC2A1 / GLUT1	Glucose transporter member 1	Major facilitator superfamily, Sugar transporter family
SLC44A1	Choline transporter-like protein 1	Choline transporter-like family
SLC7A1	High affinity cationic amino acid transporter 1	Cationic amino acid transporter family
SLC7A5	Large neutral amino acids transporter small subunit 1	L-type amino acid transporter family
SNAP23	Synaptosomal-associated protein 23	SNAP25 family
STX4	Syntaxin 4	Syntaxin family
SYNGR2	Synaptogyrin 2	Synaptogyrin family
SYPL1	Synaptophysin-like protein 1	Synaptophysin / synaptobrevin family
TMED10	Transmembrane emp24-domain containing protein 10	EMP24 / GP25L family
VDAC1	Voltage-dependent anion selective channel protein 1	Eukaryotic mitochondrial porin family
VDAC2	Voltage-dependent anion selective channel protein 2	Eukaryotic mitochondrial porin family

Table 4.1: 27 proteins of interest predicted to be localised to the membrane surface and have roles in biological processes likely relevant to apoptotic cell clearance and inflammation.

Several transporters, involved in the transport of amino acids, ions, nucleotides, glucose and choline, were identified which have been reported to be enriched in mammalian EVs and can alter the metabolism of recipient cells (Appendix, Table 7.7) (Fonseca *et al.*, 2016; Choi *et al.,* 2014). ATP binding-cassette (ABC) transporter C1 is known to transport sphingosine – 1 – phosphate (S1P) into the extracellular space (Mitra *et al*., 2006). S1P is a potent 'find me' signal released by apoptotic cells that chemotactically recruits phagocytic immune cells to sites of apoptosis (Gude *et al.,* 2008). In addition, SLC transporters have several reported roles in immunomodulation (Sheng *et al.,* 2022). SLC7A1 facilitates the transport of arginine to maintain T cell function and SLC7A5 may be involved in cytokine production by macrophages (Sheng *et al.,* 2022; Yoon *et al.,* 2018). SLC1A5 is important for the activation of T cells and was shown to be essential for IFNγ release by Natural Killer cells (Jensen *et al.,* 2017; Nakaya *et al*., 2014).

Syntaxin-2 and snaptosomal-associated protein 23 are core members of the SNARE complex – the molecular machinery that carries out vesicle fusion (Teng *et al*., 2001; Castle *et al.,* 2002). Synaptogryins and synaptophysins are proteins historically associated with regulation of synaptic vesicle release and are enriched in synaptic vesicles (Sugita *et al.,* 1999). However, expression of synaptogyrin-2 is widespread (Janz & Südhof, 1998). Generally, synaptogyrins and synaptophysins are thought to interact with the SNARE complex to inhibit exocytosis but the exact mechanism remains unclear (Raja *et al.,* 2019).

Four immunoglobulin superfamily (IgSF) members were present in the shortlisted dataset: CD31, CD47, CD166 and neuroplastin (Table 4.1). These proteins contain one or more immunoglobulin-like (Ig-like) domains which are characterised by β-sheets that are organised into a sandwich-like structure stabilised by conserved disulfide bonds (Williams & Barclay, 1988). IgSF members play diverse roles in the immune system, cell adhesion, and recognition processes.

CD31 (PECAM-1) is comprised of six Ig-like domains and plays a critical role in the diapedesis of leukocytes to a site of inflammation (Schenkel *et al.,* 2004; Muller *et al.,* 1993). Ig-like domain 1 and 2 facilitate homophilic binding, which in turn, facilitates migration of several cell types (Paddock *et al*., 2016). As such, CD31 activity has been associated with several pro-inflammatory actions including adhesion, migration and infiltration of immune cells (Privratsky *et al.,* 2010). CD31 also functions as an inhibitory 'don't eat me' signal that was shown to mediate detachment of viable cells from phagocytes by homophilic binding (Brown *et al.,* 2002). Moreover, on apoptotic cells CD31 functionally switches to an 'eat me' signal by facilitating attachment of apoptotic cells to phagocytes. This is achieved by homophilic binding which actively maintains membrane

depolarisation through inhibition of *ether-à-go-go*-related gene (ERG) and results in the activation of integrins (Vernon-Wilson *et al.,* 2007; Vernon-Wilson *et al.,* 2006).

CD47 is a glycoprotein surface receptor that has 5 transmembrane domains, making it unique to the IgSF. CD47 can bind thrombospondin-1, which acts to mobilise cells for migration by interaction with integrins (Liu *et al.,* 2001; Wang & Frazier, 1998; Gao *et al.*, 1996). CD47 can also bind signal regulatory protein α (SIRPα). This interaction functions as a 'don't eat me' signal, preventing live cells from being engulfed by phagocytes (Barclay & Van Den Berg, 2014). SIRPα binds to the extracellular IgV-like domain of CD47 which activates Src homology-2 domain-containing protein tyrosine phosphatase (SHP) and suppresses the cytoskeleton-driven process of phagocytosis, thereby regulating immune responses (Kaur *et al*., 2016).

CD166, otherwise known as activated leukocyte adhesion molecule (ALCAM), is a cell surface receptor that has 5 extracellular Ig-like domains. It is widely expressed on a variety of cell types including haematopoietic stem cell progenitors, endothelial cells, mesenchymal stromal cells and T lymphocytes, and has a variety of reported functions including involvement in haematopoiesis, leukocyte infiltration, migration and T cell activation (von Lersner *et al*., 2019; Jeannet *et al.,* 2013; Cayrol *et al.,* 2007; Hassan *et al.*, 2004). CD166 can signal via weak homophilic interactions or higher affinity heterophilic interactions with CD6 (Hassan *et al*., 2004). CD166-CD6 binding is essential for T cell activation, by stabilising T cell – antigen presenting cell (APC) immunological synapses, and migration of leukocytes across the blood-brain barrier (BBB) (Cayrol *et al.,* 2007; Hassan *et al.*, 2004).

Neuroplastin is predominantly known for its involvement in the regulation of neuronal synapses (Ilic *et al.,* 2021). It exists as two isoforms, Np55 and Np65, named according to their relative molecular mass (M_r kDa), which have two or three Ig-like domains, respectively (Langnaese *et al.,* 1998). Neuroplastin mediates neuronal adhesion and network formation, regulates neuronal migration and Ca^{2+} influx for synaptic transmission (Ilic *et al.,* 2021). Whilst its role outside of neural tissues is largely unexplored, neuroplastin has been shown to regulate keratinocyte proliferation and has been implicated in cancer, with its upregulated expression correlated with increased tumour growth, invasion and metastasis (Sumardika *et al*., 2019; Sakaguchi *et al.,* 2016; Rodriguez-Pinto *et al.,* 2008). Together, this suggests neuroplastin may have a potential role in survival and migration.

Integrin subunits alpha 4 (CD49d) and beta 1 (ITGB1) were also identified in the final shortlist of 27 proteins (Table 4.1). Integrins mediate adhesion of a cell to the extracellular matrix or other

cells and transmit signals bi-directionally from inside the cell to the extracellular environment (inside-out) or from the extracellular environment to the inside of a cell (outside-in) (Hynes, 2002). This dynamic signalling enables integrins to coordinate cell migration through engagement of the intracellular cytoskeleton with the extracellular environment, promote proliferation and survival (Koopman *et al.,* 1994; Taichman *et al.,* 1991), and determine the fate of differentiating stem cells (Kadry & Calderwood, 2020). Integrins are made up of alpha and beta subunits that heterodimerise; CD49d is an integrin alpha subunit that can only dimerise with integrin subunits beta 1 (ITGB1) and beta 7 (ITGB7) – of which just ITGB1 was identified in proteomic datasets (Grant L.R, 2022). ITGB1 can dimerise with integrin alpha subunits 1-11. CD49d and ITGB1 dimerise to form Very Late Antigen-4 (VLA-4) which facilitates adhesion and extravasation of circulating leukocytes to inflamed tissue sites through binding with vascular cell adhesion molecule 1 (VCAM-1) and fibronectin (Taichman *et al.,* 1991). VLA-4 has also been shown to promote the survival of B lymphocytes (Koopman *et al.,* 1994).

Because of their reported roles in inhibiting viable cell: phagocyte interactions, CD31 and CD47 were two major proteins of interest. Furthermore, with surface interactions as the focus and the likelihood for adhesion molecules to be important in ACdEV-immune cell interactions and the interlinked relationship between IgSFs and integrins, CD49d and CD166 were also chosen for further investigation. CD49d was chosen over ITGB1 because of its limited choice of beta subunits to dimerise with, and therefore, higher specificity in targeting VLA-4, a known immunomodulator (Koopman *et al.,* 1994; Taichman *et al.,* 1991). This formed a panel of 4 candidate proteins, in which the surface expression and function in ACdEVs will be investigated for the remainder of this thesis: CD31, CD47, CD49d and CD166 (Figure 4.3).

A

Proteins of interest	Reported function
CD31 (PECAM-1)	Adhesion and migration of leukocytes (Schenkel et al., 2004) (Muller et al., 1993) 'Don't eat me' signal / 'eat me' signal (Vernon-Wilson et al., 2006) (Brown et al., 2002)
CD47 (IAP)	Adhesion (Liu et al., 2001) Integrin-associated (Wang & Frazier, 1998) 'Don't eat me' signal (Barclay & Van Den Berg, 2014)
CD49d (Integrin α4 subunit)	Localises with integrin subunits β1 to form VLA-4 (Kadry & Calderwood, 2020) Adhesion and migration of leukocytes (Taichman et al., 1991)
CD166 (ALCAM)	Adhesion and migration of leukocytes (von Lersner et al., 2019) (Cayrol et al., 2007) T cell activation (Hassan et al., 2004)

B

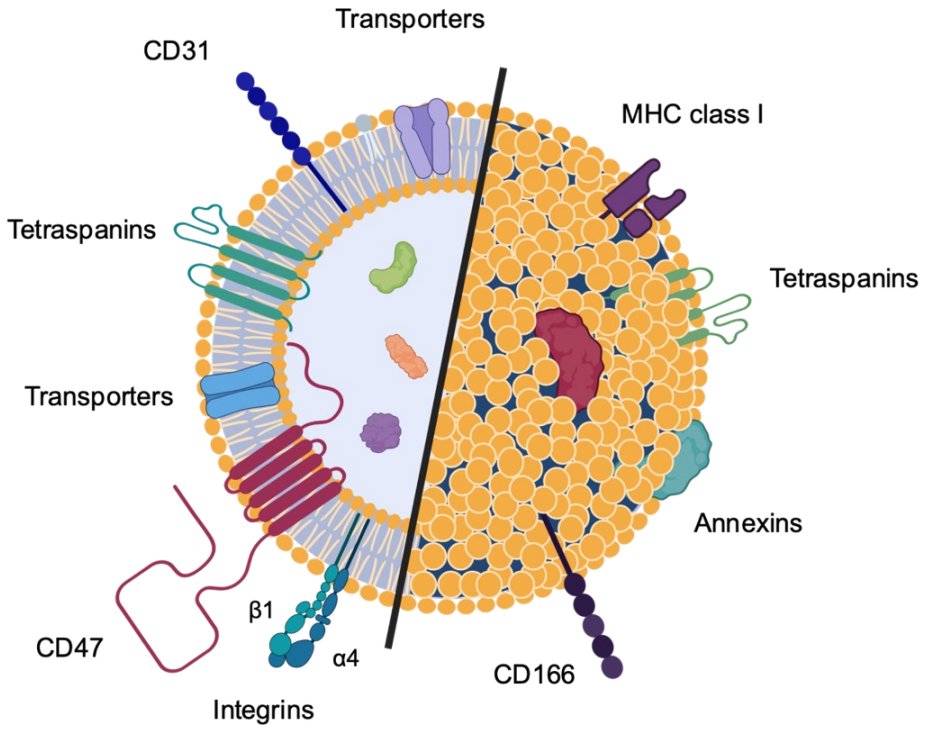

Figure 4.3: Four proteins of interest chosen for further investigation: CD31, CD47, CD49d and CD166. A) Reported protein functions according to the literature. B) Visual depiction of ACdEV proteome, displaying CD31, CD47, CD49d (integrin α4 subunit) and CD166 at the surface along with other common EV protein families identified via mass spectrometry and reported by Vesiclepedia. Figure made in Biorender.

4.3.3 Relative enrichment of candidate proteins during apoptosis

To compare the relative protein enrichment of the candidate proteins in early versus late ACdEVs, the datasets were presented as volcano plots (Figure 4.4). As the same LC-MS/MS datasets were analysed and presented by Grant (2022), the volcano plot profiles of each cell line are identical to those previously reported and show proteins were significantly differentially enriched depending on the apoptotic timepoint of ACdEV collection, though now highlighting the prioritised proteins of interest from Figure 4.3 (Figure 4.4) (Grant L. R., 2022). By highlighting the position of the candidate proteins, it revealed the relative enrichment of CD31, CD47, CD49d and CD166 in early versus late ACdEVs was dependent on the cell line. CD31 was significantly enriched in late THP-1 with the highest fold change in relative abundance of 6.76 (Figure 4.4B). However, there was no significant enrichment between Jurkat and Mutu-derived early and late ACdEVs. CD47 was significantly enriched in early Jurkat and THP-1-derived ACdEVs and late Mutu-derived ACdEVs. CD49d was significantly enriched in late THP-1 and Mutu-derived ACdEVs but there was no significant enrichment in Jurkat-derived ACdEVs. CD166 was significantly enriched in early Jurkat-derived ACdEVs and late THP-1 and Mutu-derived ACdEVs.

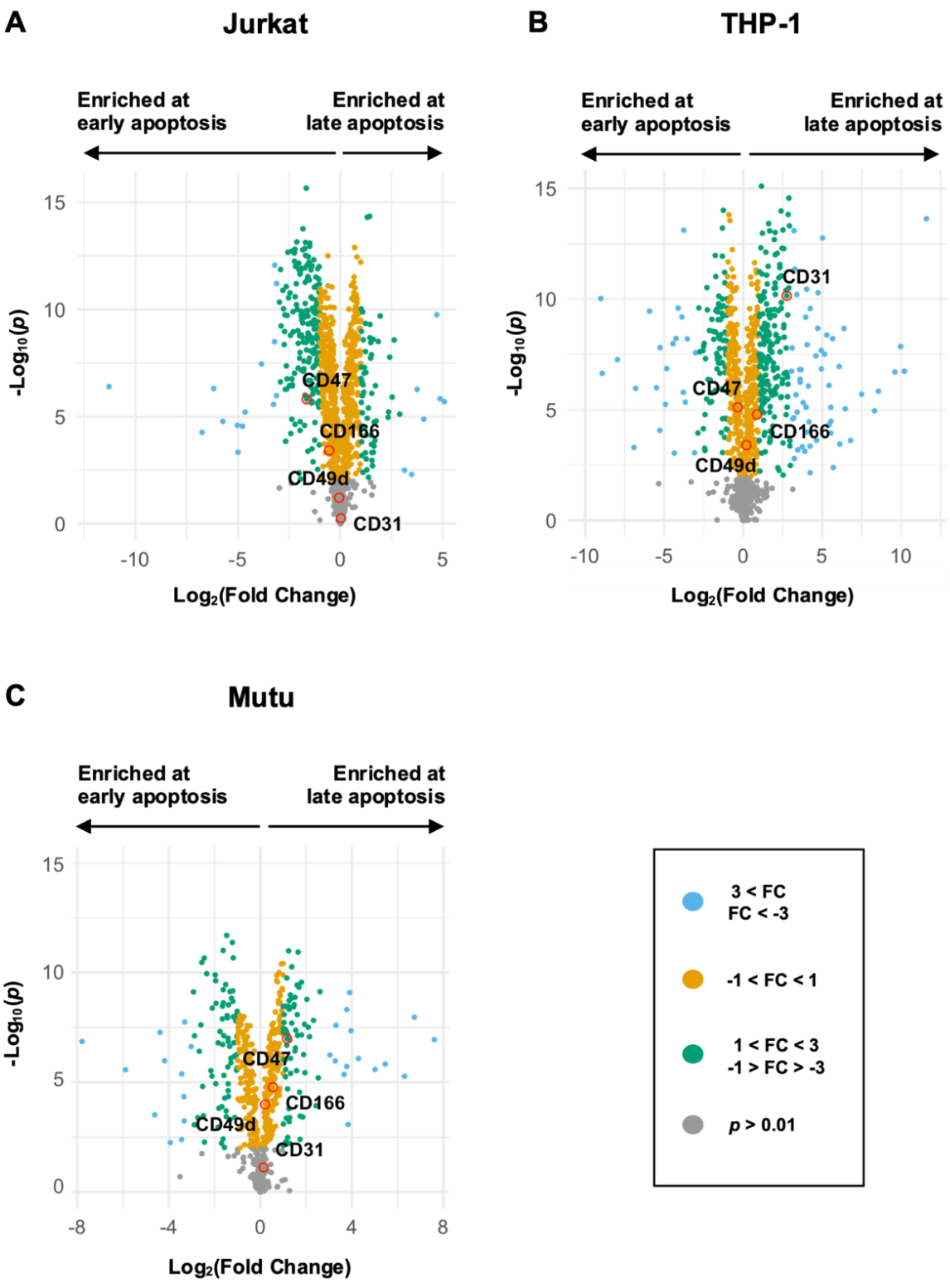

[Figure 4.4 continues onto next page]

D

Candidate protein	Jurkat		THP-1		Mutu	
	Enriched in early or late ACdEV	Max fold change	Enriched in early or late ACdEV	Max fold change	Enriched in early or late ACdEV	Max fold change
CD31	Late	1.02 (ns)	Late	6.76 (****)	Late	1.11 (ns)
CD47	Early	1.33 (****)	Early	1.27 (****)	Late	2.25 (****)
CD49d	Early	1.04 (ns)	Late	1.15 (***)	Late	1.16 (***)
CD166	Early	1.45 (***)	Late	1.83 (****)	Late	1.46 (****)

Figure 4.4: Candidate proteins CD31, CD47, CD49d and CD166 were differentially expressed in early versus late ACdEVs from each cell line, determined by LC-MS/MS analysis performed by Grant (2022) (datapoints circled in red) (Grant L.R., 2022). Volcano plots presenting differentially expressed proteins in [A] Jurkat-derived ACdEVs, [B] THP-1-derived ACdEVs and [C] Mutu-derived ACdEVs. Proteins that were non-significant ($p > 0.01$) coloured grey. Fold change (FC) in abundance: FC > 3 or FC < -3 (blue), 1 < FC < 3 and -1 > FC > -3 (green), -1 > FC < 1 (orange). Plots generated using gg(plot) package in R Studio. D) Values coloured by FC. Statistical analysis of fold change enrichment of each candidate protein. (ANOVA, ****P < 0.0001, ***P < 0.001, ns (non-significant) P > 0.01, N = 5) (Grant L. R., 2022).

4.3.4 Apoptotic cell surface expression of candidate proteins

As differences in the relative enrichment of CD31, CD47, CD49d, and CD166 in ACdEVs from early versus late apoptotic cells were observed, this led to questioning if and how cell surface expression may change during apoptosis. Cells were induced to undergo apoptosis by UV irradiation and dual stained with apoptosis marker, annexin V-FITC, and primary conjugated antibodies against each candidate protein (Figure 4.5). Apoptotic cells were measured at 0, 6 (early apoptosis) and 18 (late apoptosis) hours post induction of apoptosis, as previously defined in Chapter 3 (Figure 3.1). CD31 was measured on apoptotic THP-1 monocytes and CD47, CD49d and CD166 on apoptotic Jurkat T cells. This was because THP-1 monocytes more highly expressed CD31 than Jurkat T cells and it was hypothesised this may translate to THP-1-derived ACdEVs displaying more CD31 molecules at the surface (data not shown) (NB. Mutu B cells were not tested due to inaccessibility to this cell line).

All candidate proteins revealed a decrease in cell surface expression during apoptosis (Figure 4.5). Indeed, cell surface expression of CD31 and CD166 was significantly reduced in late

apoptotic THP-1 monocytes and Jurkat T cells, respectively (Figure 4.5B). Furthermore, a rapid (non-significant) loss of CD31 was observed from the surface of early apoptotic THP-1 monocytes (Figure 4.5B). Considering the LC-MS/MS data, it is clear the loss of cell surface expression of each candidate protein is, at least partially accounted for, by shedding via the release of ACdEVs.

A

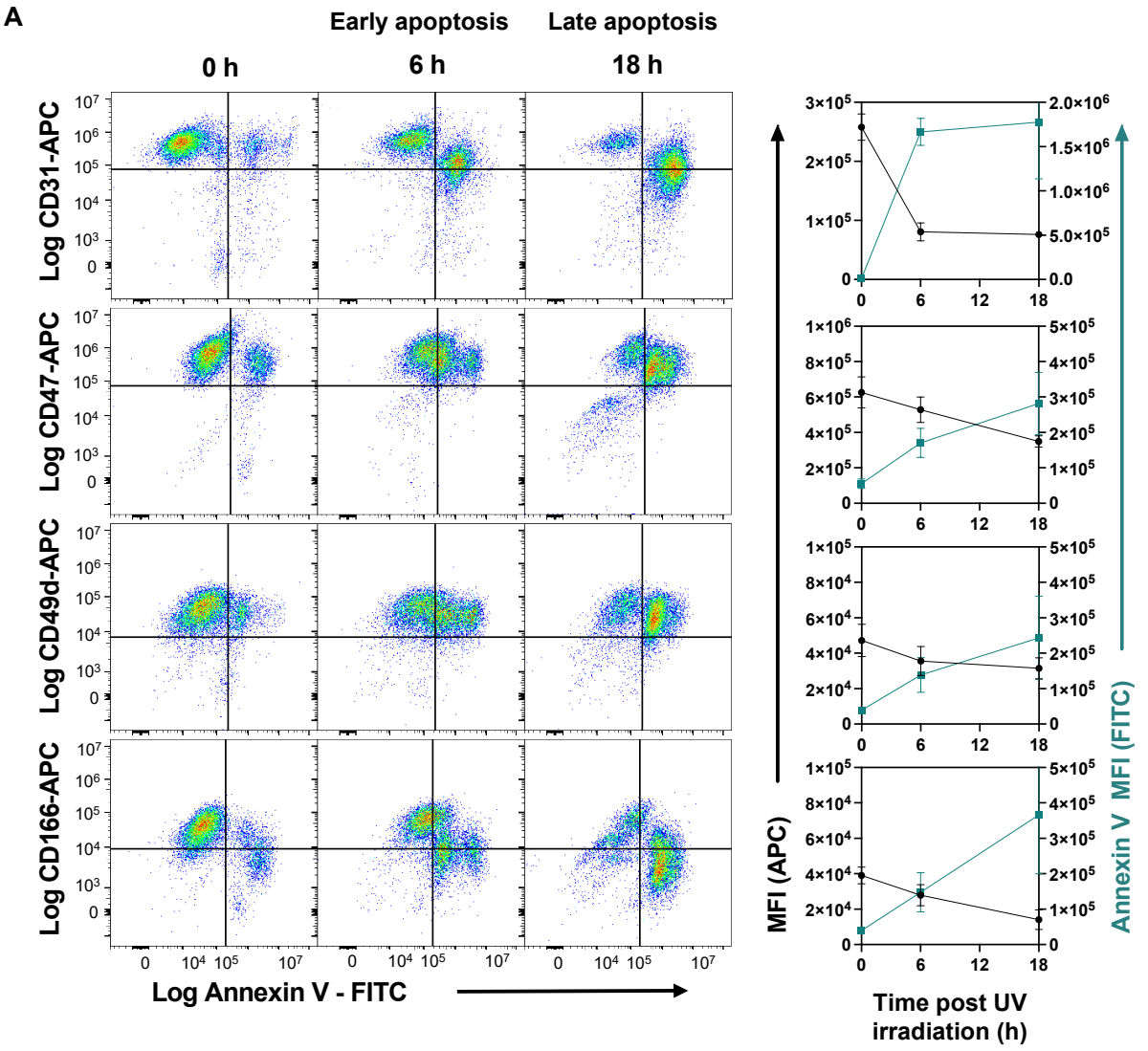

B

	Adjusted P value		
Protein target	**0 h vs 6 h**	**0 h vs 18 h**	**6 h vs 18 h**
Anti - CD31	0.075 (ns)	0.030 (*)	0.951 (ns)
Anti - CD47	0.071 (ns)	0.183 (ns)	0.293 (ns)
Anti - CD49d	0.087 (ns)	0.085 (ns)	0.354 (ns)
Anti - CD166	0.315 (ns)	0.031 (*)	0.061 (ns)

Figure 4.5: Cell surface expression of each candidate protein decreased during apoptosis. Cells were measured by flow cytometry at 0 hours, 6 hours and 18 hours post UV-mediated induction of apoptosis for externalisation of phosphatidylserine (marked by Annexin V-FITC) and surface expression of CD31, CD47, CD49d, CD166 (CytoFLEX S, Beckman Coulter). CD31 was measured on THP-1 cells and CD47, CD49d and CD166 were measured on Jurkat T cells. A) Representative flow plots (N = 1) and median fluorescence intensity (MFI) plots (Mean ± SEM, N = 3). B) Statistical table of adjusted P values from two – way ANOVA with Tukey's multiple comparison test of MFI values (N = 3). Acknowledgement to Alice Wigington for performing the experiment to measure CD31 on the surface of apoptotic THP-1 monocytes (top three flow plots in part [A]).

4.3.5 Probing the ACdEV surface

Based on the gene ontology analysis and literature searching, the candidate proteins were predicted to be localised to the surface of ACdEVs and therefore, were predicted to be accessible to immune cells and may actively engage in immunomodulation. To confirm their localisation, nano-flow cytometry was performed to directly probe the ACdEV surface with primary conjugated antibodies against each candidate protein (Table 2.3) (Figure 4.6). Annexin V-FITC was used to label the 'total' ACdEV population as PS is commonly exposed at the surface of both viable and non-viable/apoptotic cell-derived EVs (Buzás *et al.,* 2018). Annexin V-FITC didn't aggregate in solution or spillover in spectral emission in the APC channel, unlike BODIPY™ FL Maleimide and MemGlow™ 488, respectively (data not shown). As such, annexin V-FITC was suitable for dual staining with antibodies conjugated to APC. Annexin V-FITC efficiently labelled most particles detected by nano-flow cytometry (Figure 4.6B).

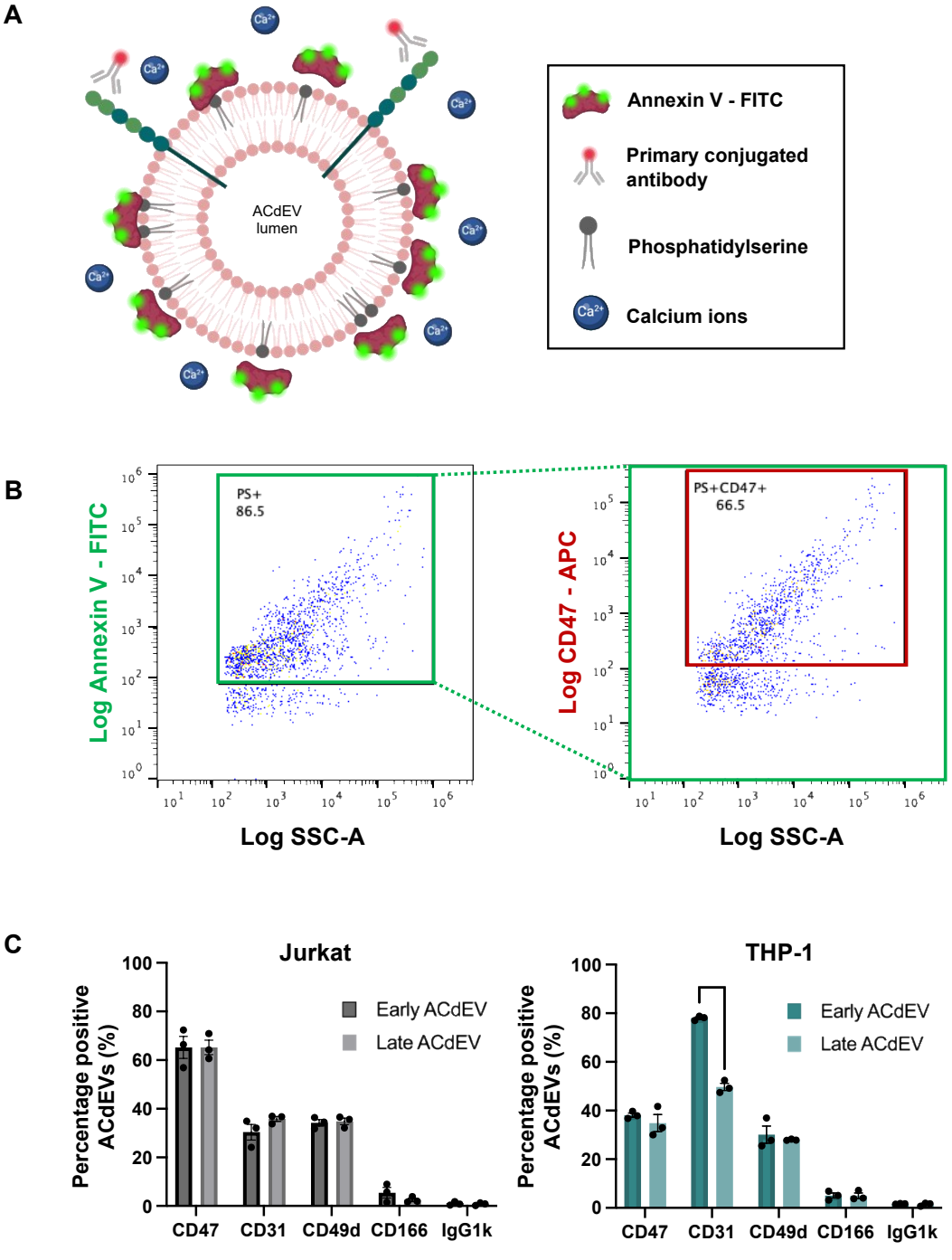

Figure 4.6: Candidate proteins were detected at the surface of ACdEVs by nano-flow cytometry (Nanoanalyzer, NanoFCM). A) ACdEV staining strategy: ACdEVs were labelled with Annexin V – FITC, a marker of phosphatidylserine (PS), and primary conjugated antibodies. B) Particles that were positive for PS were considered ACdEVs – here showed as 86.5% particles displayed PS. ACdEVs were dual stained with antibodies probing for the candidate proteins, this example showing CD47 on the surface of 66.5% Jurkat-derived early ACdEVs (N = 1). C) Percentage of ACdEVs displaying candidate protein at the ACdEV surface, comparing early versus late ACdEVs in Jurkat and THP-1-derived ACdEVs (multiple paired t tests with Holm-Šídák multiple comparisons test, $*p < 0.05$, mean ± SEM, N = 3).

Surface exposed CD47 and CD49d were detected on a significantly higher percentage of late ACdEVs derived from Jurkat T cells compared to THP-1 monocytes (Figure 4.6C) (Supplementary Table 4.1). Whereas a significantly higher percentage of THP-1-derived ACdEVs displayed CD31 compared to Jurkat-derived ACdEVs (Supplementary Table 4.1). Interestingly, significantly fewer THP-1-derived ACdEVs were positive for CD31 at the late apoptotic timepoint compared to the early apoptotic timepoint, reduced from approximately 78.0% to 49.7%. A further 3 replicate experiments were done for CD31 ACdEV labelling to ensure this result was correct (Supplementary Figure 4.1). CD166 was present on a small population of ACdEVs (< 10%) for both cell lines, but a larger population was detected in late THP-1-derived ACdEVs compared to late Jurkat-derived ACdEVs (non-significant), approximately 5.0% and 2.53%, respectively (Supplementary Table 4.1).

To estimate the size of ACdEVs by nano-flow cytometry, a series of silica nanoparticles were used as size standards, given that silica is reported to have a similar refractive index to EVs (Figure 2.1) (Welsh *et al.,* 2023). When comparing the size distribution of each ACdEV population (*ie.* ACdEVs positive or negative for a candidate protein) a surprising trend was observed; ACdEVs positive for each candidate protein were, on average, significantly bigger than ACdEVs that were negative for each candidate protein (Figure 4.7). This included ACdEVs positive for CD166 despite it being a minority population (Figure 4.7D). CD47+ ACdEVs were also significantly bigger at late apoptosis than early apoptosis, in line with the apoptotic timepoint-dependent size difference observed Jurkat-derived ACdEVs in the previous chapter (Figure 4.7B and Figure 3.5).

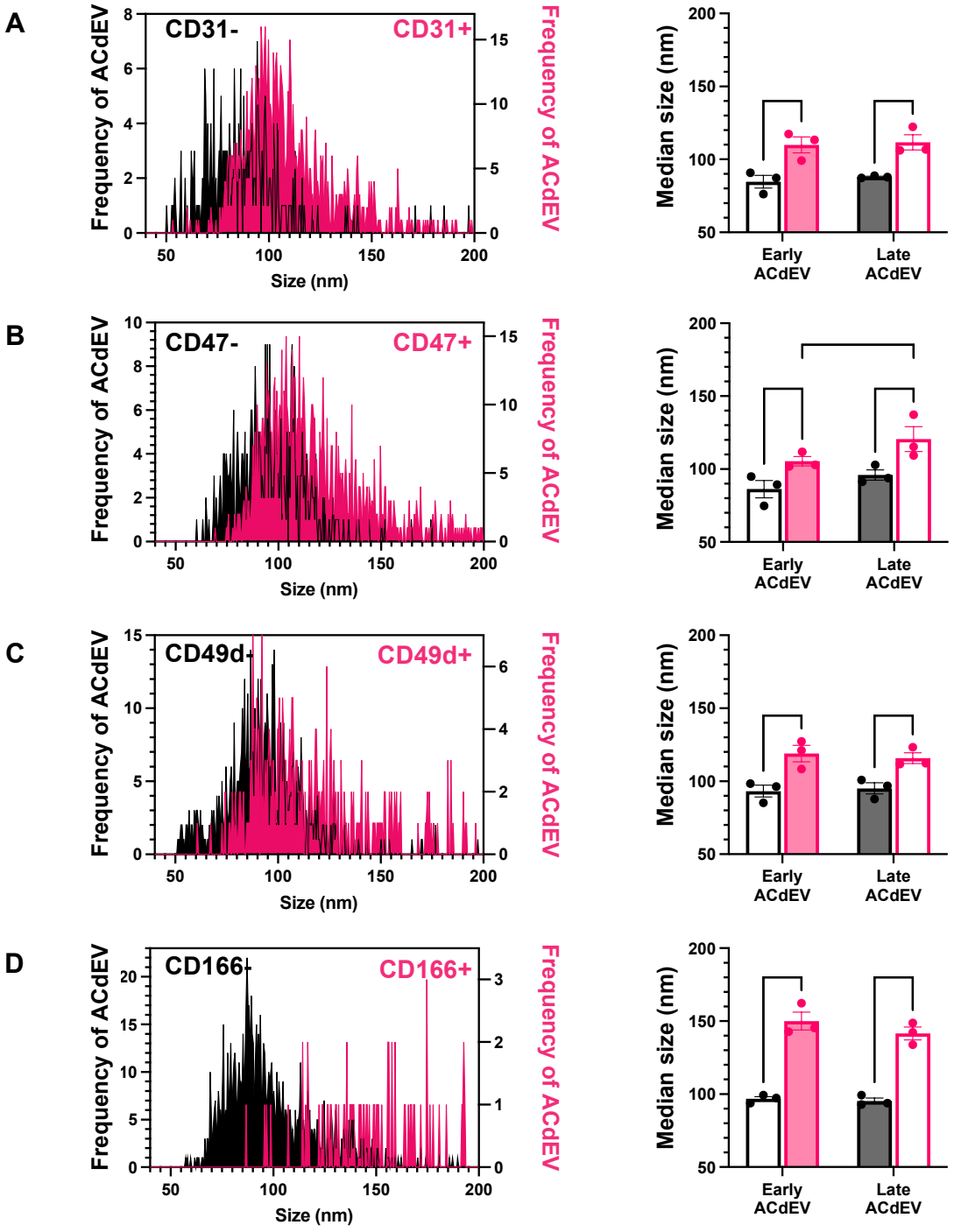

Figure 4.7: ACdEVs that display candidate proteins CD31, CD47, CD49d or CD166, are bigger in size, estimated by nano-flow cytometry (Nanoanalyzer, NanoFCM). Representative size distribution plot of early ACdEVs (each bin = 1 nm, N = 3) [left] and median size of ACdEVs (mean ± SD, N = 3) [right] positive or negative for candidate proteins A) CD31, B) CD47, C) CD49d and D) CD166. Plots presenting CD31 and CD166 are THP-1-derived ACdEVs and plots presenting CD47 and CD49d are Jurkat-derived ACdEVs (Two-way ANOVA, ***$p < 0.001$, **$p < 0.005$, *$p < 0.05$, mean ± SEM, N = 3).

As previously discussed, nano-flow cytometry cannot provide information on the spatial distribution of molecules on the ACdEV surface. In collaboration with Abbelight, ACdEVs were immobilised by lectins (Wheat Germ Agglutinin and Concanavalin A) and CD47, in combination with a tetraspanin cocktail (probing for CD9, CD63 and CD81), were imaged at the ACdEV surface by single molecule localisation microscopy (SMLM) (Figure 4.8).

SMLM revealed the same size trend observed by nano-flow cytometry; ACdEVs that were positive for CD47 were, on average, bigger than ACdEVs that lacked CD47 (Supplementary Figure 4.2). SMLM also revealed that CD47 could be arranged in punctate clusters or distributed evenly across the ACdEV surface (Figure 4.8A). Just a minority population of ACdEVs had CD47 molecules localised in clusters at the surface – 8.31% and 7.56% of CD47-positive early ACdEVs and late ACdEVs, respectively (Figure 4.8B). Interestingly, CD47 appeared to cluster more readily on late ACdEVs that were below 250 nm in size, compared to early ACdEVs (Supplementary Figure 4.3).

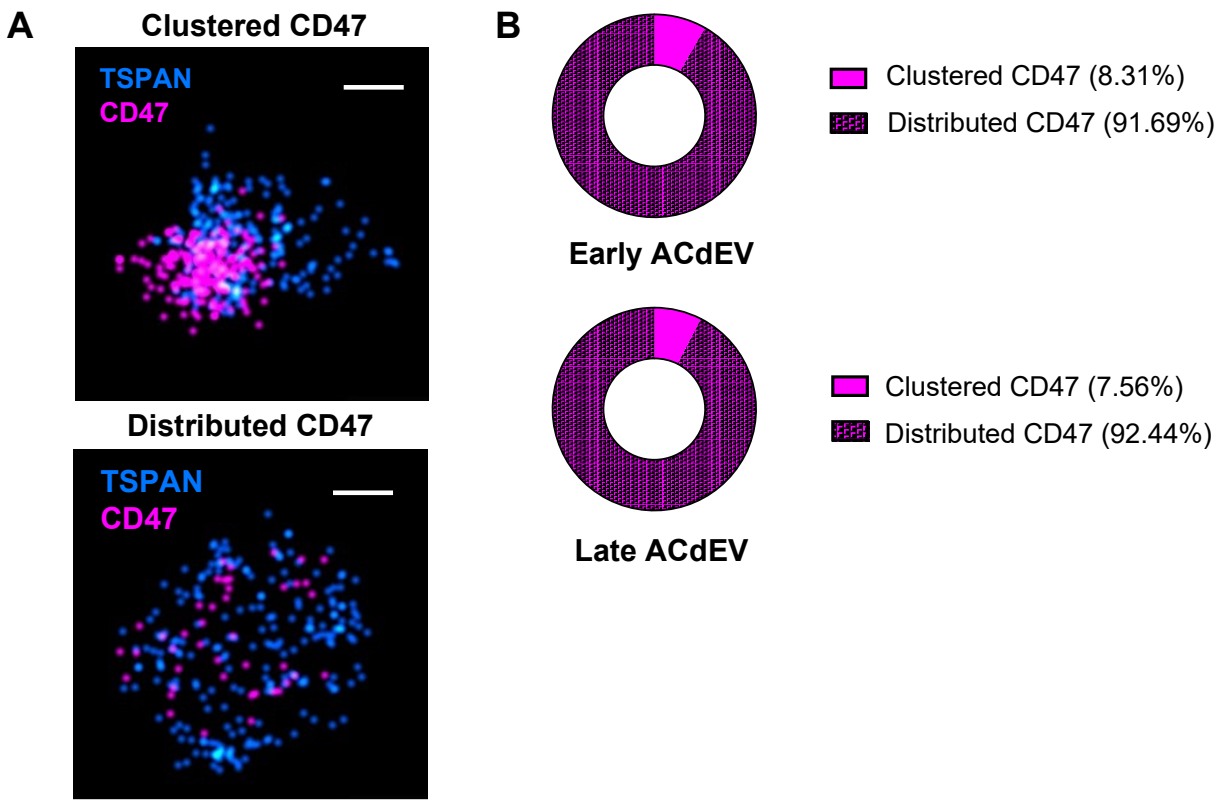

Figure 4.8: CD47 is spatially distributed across the surface of the majority of early and late ACdEVs, imaged by SMLM (Abbelight). Jurkat-derived early and late ACdEVs were immobilised by lectins, Wheat Germ Agglutinin and Concanavalin A, and dual stained for tetraspanins CD9, CD63, CD81 (antibody cocktail - blue) and CD47 (magenta), and imaged by SMLM (Abbelight). ACdEVs were categorised into 'clustered' or 'distributed' CD47 by implementation of an AI-driven segmentation algorithm (Nanometrix, Abbelight). A) Representative images of CD47 arranged in 'clustered' and 'distributed' formation. Scale bar ~100 nm. B) CD47 appeared clustered in 8.31% early CD47+ ACdEVs and 7.56% late CD47+ ACdEVs (N = 3 technical replicates).

4.4 Discussion

LC-MS/MS proteomic datasets provided a detailed breakdown of the total proteins detected in ACdEVs collected from immune cell lines undergoing apoptosis: Jurkat T cells, THP-1 monocytes and Mutu B cells (Grant L. R., 2022). As described by Grant (2022), apoptosis was chemically induced using cycloheximide, a protein synthesis inhibitor, and anti-Fas, a death receptor ligand mimetic (Grant L. R., 2022). As such, it is possible the ACdEVs represented in the proteomics datasets had an altered composition compared to the UV-induced ACdEVs characterised in this thesis. However, as discussed in Chapter 3 (section 3.4.2), ACdEV function has been shown to be conserved across various apoptosis induction methods, in the context of phagocytic recruitment (Torr *et al.,* 2011; Truman *et al.,* 2008; Segundo *et al.,* 1999). Of course, this may not include all ACdEV-associated functions and the molecular composition of ACdEVs may still differ depending on the method of apoptosis induction. Nevertheless, if certain proteins are conserved across ACdEV populations induced by different apoptosis methods, it may indicate their importance.

Updated cross-referencing with Vesiclepedia, an openly accessible database of EV proteomics data, revealed a decrease in the number of uniquely identified proteins in this experiment from 596 to 238 (analysis done in 2022 and 14.06.24, respectively) (Grant L. R., 2022). This simultaneously highlighed the rapid advancements in EV studies and reporting of EV data over the last two years and the need for ongoing EV proteomic characterisation. Several proteins were identified that were unique to each cell line but overall, 417 proteins were conserved across cell lines (Supplementary Figure 7.7). This pool of conserved proteins formed the basis for selection of the candidate proteins, as it was hypothesised these proteins may provide the most important functions. Following a gene ontology-based selection process, 27 proteins were extracted sequentially based on their predicted localisation to membrane surfaces and predicted functions in biological processes important in inflammation and apoptotic cell clearance (Figure 4.2) (Table 4.1). Proteins and protein family members that are commonly associated with EVs (reported in Vesiclepedia top 100) were excluded, as they were thought unlikely to exert unique functions on the surface of ACdEVs versus other types of EV populations. The main limitation of this approach is the reliance on previously reported protein functions. Consequently, novel protein functions on the surface of ACdEVs will have gone undetected.

A range of transporters were identified, implicated in the transport of various signalling molecules including amino acids, ions, nucleotides, glucose and S1P. ABCC1, a transporter identified in the proteomic datasets, facilitates the transport of bioactive lipids, such as S1P—a potent 'find me' signal—into the extracellular space (Mitra et al., 2006; Gude et al., 2008) (Table 4.1). Additionally, work within the group has previously shown ACdEVs can carry active lipoxygenase enzymes that generate bioactive eicosanoids, such as pro-resolving lipoxins (unpublished data). ABCC1 may also transport these bioactive lipids from the lumen of an ACdEV to the extracellular space, potentially playing a role in controlling inflammation. GLUT-1, a transporter of glucose that was identified in the proteomics datasets, has been shown to be enriched in EVs secreted by endotoxin-stressed THP-1 monocytes, which in turn, promoted an inflammatory phenotype in human umbilical vein endothelial cells (HUVECs) (Table 4.1) (Yang *et al.,* 2022). The presence of transporters has previously been reported in a wide range of mammalian EVs, though little is known about their function in EVs (Choi *et al.,* 2014).

Synaptophysin-like protein 1 is implicated in synaptic vesicle release (Sugita *et al.,* 1999). As the ACdEVs are not synaptic in origin, it may serve a similar regulatory function in vesicle release that is not unique to synaptic vesicles. Furthermore, synaptogryin-2 is widely expressed but its function remains unclear (Janz & Südhof, 1998). The presence of members of the SNARE complex, Syntaxin-2 and SNAP23, may represent the mechanism of ACdEV release or be important for the fusion and uptake of ACdEVs to recipient cells. Though these proteins weren't reported in the Vesiclepedia top 100, it is likely they are common to many EV subtypes and don't have ACdEV-unique functions. This raises an important question about whether ACdEVs possess distinct functional properties compared to EVs from viable cells. Although viable cell-derived EVs and ACdEVs share some overlapping roles - such as involvement in antigen presentation, anti-tumor immunity, and the promotion of tissue regeneration and wound healing by stem cell-derived EVs (Liu *et al.,* 2020; Casado-Díaz *et al.,* 2020; Gebara *et al.,* 2020; Caruso & Poon, 2018), there are notable differences in their characteristics. ACdEVs have a distinct protein and RNA composition from viable cell-derived EVs (Than *et al.,* 2018; Tucher *et al.,* 2018; Crescitelli *et al*., 2013). Apoptosis has been shown to promote the release of EVs compared to viable cells, resulting in a higher abundance of ACdEVs (Skovronova *et al*., 2021). This increased production during apoptosis suggests that ACdEVs may more potently exert EV-associated functions, potentially enhancing their influence on immune regulation, tissue repair, and other biological processes.

Multiple adhesion molecules were also identified in the proteomics datasets, including integrins and immunoglobulin superfamily (IgSF) members (Table 4.1). Adhesion molecules are proteins, normally located on the cell surface, that facilitate the binding of cells to each other and to the extracellular matrix. Adhesion molecules allow cells to communicate with their environment and respond to various signals. As such, these molecules play crucial roles in a variety of processes, including tissue formation, immune responses, wound healing, and cell signalling. As the focus of this project is modulation of immune cells by interaction with the ACdEV surface, adhesion molecules were of particular interest and consequently, 4 adhesion molecules were chosen as the focus of the remainder of the thesis: CD31, CD47, CD49d and CD166 (Figure 4.3).

CD31, CD47 and CD166 are all IgSF members which are characterised by the presence of at least one immunoglobulin-like (Ig) domain and play key roles in various processes, including cell recognition, adhesion, and communication in the immune system (Barclay, 2003). In addition, ICAM-3 is an IgSF member found at the surface of ACdEVs and was previously demonstrated to mediate chemoattraction and binding of phagocytes, promoting apoptotic cell clearance (Torr *et al.,* 2011). Indeed, ICAM-3 was detected in our ACdEV proteomic datasets for the Jurkat T cell and Mutu B cell lines (L. R. Grant, 2022).

The presence of CD47 on the surface of T cell-derived EVs has been implicated in the activation of immune cells, alteration of VEGF signalling and modulation of gene expression in recipient cells (Kaur *et al.,* 2014). Jurkat T cell-expressed CD47 was shown to regulate the packaging of RNAs into the lumen of Jurkat-derived EVs (Kaur *et al.,* 2014). As such, CD47 may indirectly modulate recipient cells through the activity of intraluminal RNAs (Kaur *et al.,* 2014). If ACdEV-expressed CD47 maintains the capacity to bind SIRPα, it may be able to exert a ‘don’t eat me’ signal to recipient cells. This could provide two functions for the apoptotic cell: firstly, CD47 may protect the ACdEVs from being engulfed by phagocytes enabling ACdEVs to carry signals for a longer duration and distance. Indeed, this has been suggested by data comparing the retention of CD47-expressing EVs to liposomes (Kamerkar *et al.,* 2017). Secondly, shedding of the inhibitory ‘don’t eat me’ signal from the cell surface via the release of ACdEVs may make the apoptotic cells more ‘edible’ to phagocytes to promote their clearance. This mechanism was previously suggested for apoptotic cells that showed abrogated CD47/SIRPα signalling correlated with calreticulin-mediated recognition and engulfment (Gardai *et al.,* 2005).

CD31 is another IgSF member that can exert a ‘don’t eat me’ signal, this time by homophilic binding. However, CD31 is unique in that it can functionally switch to promote an ‘eat me’ signal on the surface of apoptotic cells (Brown *et al.,* 2002). This functional switch involves prolonged

phagocyte membrane depolarisation, caused by CD31 inhibiting the activity of voltage-gated potassium channel ERG, which facilitates the β1 integrin-dependent attachment of apoptotic cells to phagocytes (Vernon-Wilson *et al.*, 2007; Vernon-Wilson *et al.,* 2006). ACdEV surface-exposed CD31, along with soluble factors, may promote phagocyte membrane depolarisation via homophilic binding, which would thereby prime phagocytes for clearance of apoptotic cells.

CD166 is important in stabilising high affinity immunological synapses, functioning to activate T cells in response to antigen presentation (Hassan *et al.,* 2004). There is evidence that EVs can engage in immunological synapses - it has been shown that EVs enriched in T cell receptor (TCR) are released at the immunological synapse and maintain the ability to bind peptide-major histocompatibility complex (pMHC) and as such, may be able to modulate the activity of B cells (Choudhuri *et al.,* 2014). Therefore, it is possible CD166 is shed from the apoptotic cell surface by a similar mechanism, allowing CD166-expressing ACdEVs to engage in high affinity binding to CD6 on recipient immune cells for their activation.

As a major family of adhesion proteins that have several reported immunomodulatory functions, of which ICAM-3 and CD47 functions have already been associated with EVs, it seems likely that IgSF members could be key modulators of inflammation at the surface of ACdEVs (Kaur *et al.,* 2014; Torr *et al.,* 2011). It is possible that different IgSF members may perform a conserved function, with a degree of redundancy allowing one member to substitute for another, regardless of the specific IgSF member involved. This mechanism may simply rely on the presence of an Ig-like domain, rather than the unique features of individual members. Interestingly, IgSF members have few highly conserved residues at the primary amino acid sequence level but form highly conserved structural folds, characterised by the presence of several beta sheets that are stabilised by disulphide bonds (Barclay, 2003). Ig-like domains are one of the most common domains identified in the human genome and are most commonly present in proteins involved in the immune system. Indeed, as mentioned, ICAM-3, known to potently attract and bind phagocytes, is expressed by leukocytes and therefore, unsurprisingly was detected in the Jurkat T cell and Mutu B cell-derived ACdEVs, but not THP-1-derived ACdEVs, based off our proteomics analysis (L. R. Grant, 2022; Torr *et al.,* 2011). However, several other IgSF members were identified in ACdEVs derived from the THP-1 monocyte line, which may facilitate chemoattraction or surface interactions and therefore, should be investigated in future work (Appendix, Table 7.11) (L. R. Grant, 2022). In addition, germinal centre B cell-derived ACdEVs were shown to be chemoattractive and contained IgSF members: CD21 (complement receptor 2), CD22 (sialic acid-binding Ig-like lectin) and CD54 (ICAM-1) (the presence of ICAM-3 was not determined) (Segundo

et al., 1999). CD54 was identified in THP-1-derived ACdEVs according to the proteomic datasets (Appendix, Table 7.11).

CD49d is a member of the integrin family of cell adhesion molecules. CD49d is limited in that it can only heterodimerise with ITGB1 and ITGB7 (Hynes, 2002). As just ITGB1 was identified in the proteomics datasets, we hypothesise that CD49d and ITGB1 may dimerise, forming VLA-4 at the ACdEV surface. However, as EVs lack a cytoskeleton, it is unlikely integrins would have the ability to perform bi-directional signalling in EVs. Nevertheless, it is feasible that ACdEVs that display VLA-4 at the surface may direct ACdEVs to tissues where ligands for VLA-4 are highly expressed (*e.g*. VCAM-1) or *vice versa*, attract immune cells towards ACdEVs that may be localised close to the originating apoptotic cell(s). It has been shown that VLA-4 at the surface of EVs can bind to fibronectin, a key protein component of the extracellular matrix (Rieu *et al.,* 2000). Furthermore, EV-integrin engagement promotes cell motility (Sung *et al.,* 2015). Therefore VLA-4-expressing EVs may have the capacity to modulate the local microenvironment with may promote the motility of local immune cells.

The proteomics datasets reported the relative enrichment of proteins at early and late apoptosis, providing valuable insight into potential time-dependent functions of ACdEVs. As reported by Grant (2022), proteins were differentially enriched in early and late ACdEVs in all three cell lines (Figure 4.4A) (Grant, L.R., 2022). Apoptotic cells may actively package specific proteins in ACdEVs during early apoptosis to promote the rapid clearance of apoptotic cells and prevent the release of inflammatory autoantigens (a symptom of necrosis). The changes in ACdEV protein composition towards late apoptosis may reflect a loss of cellular regulation resulting in stochastic, passive sorting and loading of cargo in ACdEVs. As previously highlighted, the mechanism of ACdEV biogenesis and cargo packaging is poorly understood (see section 1.4). Furthermore, changes in ACdEV composition could also occur upon release in response to a new microenvironment. For example, differences in physicochemical conditions, such as pH, charge or salt concentrations could impact protein conformation, and as such, protein activity, including enzymes. Notably, enrichment of a protein at one or the other time point may not be necessary for function; its presence may be sufficient. Furthermore, it is possible the enrichment observed by the LC-MS/MS proteomics experiment may simply reflect the biological variation of samples, which may be negated with additional replicates (Grant, L.R., 2022).

Changes in relative protein abundance between early and late ACdEVs led us to question whether these changes were a mimic of the originating apoptotic cell. As the candidate proteins are normally cell surface expressed, flow cytometry was used to track changes in cell surface

expression during apoptosis (Figure 4.5). This revealed that cell surface expression of all candidate proteins decreased during apoptosis. This, coupled with the LC-MS/MS proteomics data, showed apoptotic cells lose surface expression of proteins via the release of ACdEVs. This has previously been shown for various adhesion molecules, including ICAM-3, which was lost from the surface of apoptotic leukocytes via the release of ACdEVs, termed 'microparticles' (Torr *et al.,* 2011; Segundo *et al.,* 1999). As discussed earlier, this may be the result of active packaging into ACdEVs or reflect passive shedding of ACdEVs that resemble the host cell surface. Importantly, the apoptotic cell surface expression of the candidate proteins may also have been lost by endocytic uptake and recycling/degradation or by proteolytic cleavage and soluble release of protein domains, the latter of which has been reported for all 4 candidate proteins (von Lersner *et al.,* 2019; Hebron *et al.,* 2018; Fornasa *et al.,* 2010; Maile *et al.,* 2008; Ilan *et al.,* 2001; Teixidó *et al.,* 1992). Therefore, the function of the candidate proteins may be propagated in several ways, not just by ACdEV release. However, packaging into ACdEVs may preserve the bioactivity of proteins to protect from enzymatic degradation and maintain the proteins in a native membrane, likely to be the candidate proteins' favoured environment. Beyond surface protein activity, the ACdEV structure, featuring a lumen, can carry various types of bioactive molecular cargo, enabling the transmission of multiple signals to recipient cells.

As the localisation of the candidate proteins at the ACdEV surface relied on gene ontology predictions and UniProt reports, it was important to confirm their surface localisation by nano-flow cytometry (Figure 4.6). A higher proportion of ACdEVs were positive for CD47 and CD49d in the Jurkat T cell line, whereas a higher proportion of THP-1-derived ACdEVs were positive for CD31 (Figure 4.6C) (Supplementary Table 4.1). Despite CD166-displaying ACdEVs being a minority population in both cell lines, a bigger population was identified in THP-1-derived late ACdEVs than Jurkat-derived late ACdEVs. As such, going forwards, Jurkat-derived ACdEVs will be used to study CD47 and CD49d activity and THP-1-derived ACdEVs will be used to study CD31 and CD166 activity, as there will be a higher likelihood of observing changes in functional effects in the presence of inhibitors – this will form the majority of Chapter 3.

Further to confirmation of surface localisation, the known epitope-binding site of each antibody revealed insight into the orientation and accessibility of each protein to their respective ligands. The CD47 antibody (clone: B6H12) binds to the extracellular IgV-like domain and therefore suggested the binding site for SIRPα is exposed at the surface of ACdEV (Fenalti *et al.,* 2021). CD31 has 6 Ig-like domains, domain 1 being the most membrane distal. During proteolytic cleavage, all six Ig-like domains are released as a soluble fragment (Ilan *et al.,* 2001). The CD31

antibody (clone: WM-59) was mapped to the Ig-like domain 2, thereby marking the presence of non-cleaved CD31 and, therefore, ACdEV-expressed CD31 may be able to engage in homophilic binding (Fawcett *et al.,* 1995).

The exact epitope binding site of the antibody against CD49d (clone: 9F10) is not defined, therefore the presence of cleaved or non-cleaved form of CD49d at the ACdEV surface could not be determined. Both forms (cleaved / non-cleaved) maintain the ability to bind the β1 integrin subunit, which forms VLA-4, and show no difference in the functional outputs of VLA-4 in the context of cell adhesion (Teixidó *et al.,* 1992). However, T cell activation is associated with increased cleavage of CD49d, suggesting a potential link with CD49d cleavage and cell activation (Blue *et al.,* 1993). Therefore, further research is needed to fully understand the implications of CD49d proteolytic cleavage.

The epitope binding site for the anti-CD166 antibody (clone: 3A6) has also not been defined and therefore, the presence of the intact or cleaved form of CD166 at the surface of ACdEVs also could not be determined. CD166 was readily detected at the apoptotic cell surface, and significantly reduced during apoptosis (Figure 4.5), but was only detected at the surface of a minority population of ACdEVs (Figure 4.6). One hypothesis is that loss of CD166 at the apoptotic cell surface may be facilitated by release of soluble cleaved CD166 into secretome and that the antibody is unable to bind to the remaining cell membrane-embedded fragment. Interestingly, two isoforms of CD166 can be expressed and are proteolytically cleaved by different proteases. Isoform 1 is shed at a slower rate and maintains cell adhesion, whereas, isoform 2 (lacking exon 13) is shed 10x more rapidly and resulted in loss of cell adhesion (Hebron *et al.,* 2018). This showed CD166 can be regulated at the level of post-transcriptional splicing which can modulate cellular activity by the rate of cleavage and release (von Lersner *et al.,* 2019). Furthermore, cell surface-expressed CD166 has been shown to be endocytosed as part of a clathrin-independent endocytic pathway, which in turn, reduced the adhesive properties of the cells and promoted migration (Renard *et al.,* 2020). Therefore, a second hypothesis is that apoptotic cells lost surface expression of CD166 by intracellular uptake for recycling or lysosomal degradation. Of course, it could be a combination of these processes.

Overall, these data confirmed each candidate protein is released from the parental cell and exposed at the ACdEV surface, accessible to immune cells and could hypothetically signal and modulate immune cell behaviour through direct interaction.

Interestingly, there was a significant decrease in the proportion of THP-1-derived late ACdEVs displaying CD31 at the surface, compared to early ACdEVs (Figure 4.6C). This was unexpected as CD31 was significantly enriched in THP-1-derived late ACdEVs, detected by LC-MS/MS (Figure 4.4). A further 3 repeats of the nano-flow cytometry experiment were done to confirm this result (Supplementary Figure 4.1). LC-MS/MS measures the total abundance of protein in ACdEVs, including surface membrane proteins and intraluminal cargo proteins. In contrast, the nano-flow cytometry performed here simply reported the proportion of ACdEVs that displayed at least 1 accessible epitope of a protein (instrument capable of single fluorophore detection), thereby providing a binary categorisation of individual ACdEVs: positive or negative for a protein of interest. Together, these techniques reveal different possibilities of protein expression and localisation and lead to three main hypotheses: it may be that only a specific ACdEV subpopulation is loaded with CD31 and during late apoptosis, a lower proportion of that ACdEV population is released but carry more CD31 molecules at a higher density. Alternatively, late ACdEVs may carry more CD31 as intraluminal cargo that is not accessible to antibody-mediated detection. As CD31 is typically a membrane protein, it may be enriched in the inner layers of multilamellar ACdEVs – indeed, cryo-TEM revealed multilamellar EVs were most frequent in THP-1 late ACdEVs (Figure 3.6). Finally, as previously described, the CD31 antibody binds to Ig-like domain 2. Therefore, if cleaved CD31 is presented at the surface of ACdEVs, the antibody would fail to bind and detect this population. Based on the nano-flow cytometry data, this could suggest CD31 is cleaved during late apoptosis on the surface of ACdEVs (Figure 4.6C). Notably, cleavage and shedding of CD31 results in the loss of homophilic binding, and subsequently, loss of the inhibitory ‘don’t eat me’ signal (Fornasa et al., 2010). This further supports the hypothesis that apoptotic cells may lose expression of inhibitory ‘don’t eat me’ signals, possibly by shedding via ACdEVs or proteolytic cleavage, to facilitate their efficient uptake by phagocytes. Future work should determine the presence of uncleaved/cleaved CD31 at the surface of ACdEVs by probing with a combination of antibodies that target non-cleavable Ig-like domain 6 and cleavable Ig-like domains 1-5.

Interestingly, nano-flow cytometry revealed that ACdEVs carrying each candidate protein were, on average, larger than ACdEVs that were negative for each candidate protein (Figure 4.7). This trend was also confirmed for CD47 by SMLM, reinforcing the conclusions made by both approaches (Supplementary Figure 4.2) (Abbelight). This may suggest the ACdEVs positive for each candidate protein represent a specialised subpopulation. It is unknown whether ACdEVs would ‘benefit’ from a size difference of between ~50 - 100 nm; an EV of a larger size increases the surface area of the EV membrane, increasing the capacity of surface interactions with

recipient cells, as well as a larger capacity to transport cargo. An expanded membranous platform with potential for surface interactions could enable the ACdEV to be taken up by recipient cells more readily. Or the size difference may reflect different ACdEV populations generated by different biogenesis pathways, as exosomes, formed by the endosomal pathway, are typically smaller in size than microvesicles, formed by plasma membrane budding. The exact mechanisms underlying ACdEV biogenesis unclear but it is plausible, given that viable cells simultaneously release exosomes and microvesicles, that apoptotic cells may simultaneously release ACdEVs by multiple biogenesis pathways.

Another important consideration is membrane curvature. The presence of proteins can influence membrane curvature in several ways, such as embedding into and deforming the membrane, forming scaffolds or oligomers, imposing tertiary structure constraints (*i.e.* if the protein has an inherent curvature), or through an abundance of localised proteins, termed 'protein crowding' (Kirchhausen, 2012; Stachowiak *et al.,* 2012). It is intriguing that the candidate proteins are only present in a population of ACdEVs that is, on average, larger than other ACdEVs (Figure 4.7) (Supplementary Figure 4.2). This led us to question the individual spatiotemporal properties of these proteins and their influence on the ACdEV membrane. Local deformation of the membrane can be induced simply by exceeding a high enough surface density of protein (Stachowiak *et al.,* 2012). Indeed, all 4 candidate proteins have been shown to localise into distinct high density clusters, which in various ways may regulate signalling (Dufour *et al.,* 2023; Lv *et al.,* 2015; Calderwood *et al.,* 2013; Gilsanz *et al.,* 2012; Fornasa *et al.,* 2010; Nelissen *et al.,* 2000).

CD47 molecules were observed to be evenly distributed across most CD47+ Jurkat-derived ACdEV surfaces by SMLM (Figure 4.8). This was expected as CD47 is reportedly evenly distributed across apoptotic cell surfaces (Dufour *et al.,* 2023; Lv *et al.,* 2015). However, a notable population of Jurkat-derived ACdEVs exhibited clusters of CD47, accounting for approximately 7-8% of CD47+ ACdEVs (Figure 4.8). Interestingly, Lv *et al.* reported CD47 expression didn't decrease during apoptosis, directly conflicting with the results observed in this thesis (Figure 4.5); instead they reported that CD47 spatially redistributed from punctate clusters localised to lipid rafts on the surface of viable cells, into a less clustered, more even distribution on the surface of apoptotic cells, due to dismantlement of lipid rafts, and this reduced the ability for CD47 to bind SIRPα (Lv *et al.,* 2015). They used an almost identical approach to this project, using UV irradiation to induce apoptosis, labelling with Annexin V-FITC as a marker of apoptosis and antibody probing CD47 with the same clone (B6H12), except for use of different cell lines: HT-29, T47D, and MCF7 cells (Lv *et al.,* 2015). Therefore, it is possible CD47 activity may be disrupted

by different mechanisms according to the cell type. The CD47- SIRPα interaction is essential for mediating the 'don't eat me' signal, and disruption of this signal makes apoptotic cells more susceptible to phagocytosis (Oldenborg, Gresham, and Lindberg, 2001). A more recent study confirmed that binding of CD47 is to SIRPα is reliant on the presence of cholesterol but not a clustered formation (Dufour *et al.,* 2023). The authors further hypothesised that cholesterol reorganisation during apoptosis may destabilise CD47, leading to a conformational change that prevents it from binding to SIRPα (Dufour *et al.,* 2023). Notably, apoptotic blebs displaying CD47 also failed to bind SIRPα, hypothesised to be caused by the dynamic membrane reorganisation that occurs during apoptotic cell membrane blebbing (Dufour *et al.,* 2023). Therefore, the presence of clustered CD47 at the surface of ACdEvs may indicate a small population of ACdEVs maintain a level of membrane organisation that may preserve the ability of CD47 to signal. Future work should confirm whether CD47 at the ACdEV surface is also localised to cholesterol-rich domains and whether ACdEV-associated CD47 maintains the ability to bind SIRPα. In addition, the presence of clustered CD47 on the surface of ACdEVs should be explored to determine whether it exhibits a higher affinity interaction compared to distributed CD47, similar to what was observed in cells (Lv *et al.,* 2015). This could be achieved by solubilising ACdEV membranes using polymer nanodisc technology, such as styrene-maleic acid (SMA), and purifying the CD47-containing nanodiscs through immunopurification. This approach would allow for the analysis of the local lipid composition surrounding CD47 and the ability of the CD47-containing nanodiscs to bind SIRPα. Notably, this SMLM experiment utilised lectins, Wheat Germ Agglutinin and Concanavalin A, for ACdEV immobilisation (see Methods). CD47 is heavily glycosylated with 5 N-linked glycosylation sites within the IgV-like domain, alone (Zhang *et al.,* 2024). Therefore, it is possible Wheat Germ Agglutinin and Concanavalin A could bind CD47 which may have altered its spatial arrangement in ACdEV membranes.

CD166 also spatially clusters in the cell membrane. Clustering of CD166, mediated by the tetraspanin CD9, enhances homophilic CD166 signalling and promotion of cell adhesion and T cell activation (Gilsanz *et al.,* 2012; Nelissen *et al.,* 2000). A similar sized population of CD9+ and CD166+ ACdEVs were identified (mean average of 4% and 5%, respectively) (Figure 3.7, Figure 4.6); future work should determine if these are dual positive populations and whether these molecules are colocalised at the ACdEV surface. This would provide insight into whether CD9 also mediates the spatial organisation of CD166 in ACdEVs and if ACdEVs can engage in homophilic CD166-mediated adhesion.

Clustering of integrins upon activation by ligand binding is well-established (Calderwood *et al.,* 2013). Clustering regulates the affinity of integrin-ligand interactions, allowing cells to finetune the level of cell adhesion. Therefore, the formation of CD49d clusters is likely to be reliant on accessibility to ligands (as well as ability to dimerise with integrin beta subunits e.g. ITGB1), which in the case of VLA-4, is VCAM-1 and fibronectin.

There is also evidence for CD31 clustering; one study investigating proteolytic cleavage and shedding of CD31 showed the remaining cleaved CD31 fragment (comprised of just Ig-like domain 6 and the cytoplasmic portion of CD31) would reorganise into distinct clusters, upon rescue of signalling with a synthetic peptide and TCR activation (Fornasa *et al.,* 2010). This would suggest that non-cleaved CD31 may rearrange into clusters upon TCR activation. Furthermore, a high density of surface CD31 promotes homophilic signalling which has been suggested may be facilitated by clustering (DeLisser *et al.,* 1997). However, it remains unclear what regulates the spatial distribution of CD31.

Future work should determine whether CD31, CD49d or CD166 arrange into a clustered formation at the surface of ACdEVs. If they do, this may strengthen the hypothesis that a specific membrane curvature is necessary to host higher order structures, linking ACdEV structure to function, and shedding light on the potential signalling mechanisms initiated by ACdEVs.

4.4.1 Conclusions

In summary, proteomic profiling revealed the diverse molecular composition of ACdEVs from different originating cell sources, collected at early and late apoptotic timepoints. Four candidate proteins were chosen based on their known roles in cell-to-cell communication, adhesion and immunomodulation: CD31, CD47, CD49d and CD166. Loss of cell surface expression of each candidate protein during apoptosis was, at least partially, accounted for by shedding into and release of ACdEVs. Additionally, each candidate protein was localised to the ACdEV surface, with the signalling portion of CD31 and CD47 confirmed accessible by antibody binding. Clustering of CD47 was observed at the surface of Jurkat-derived ACdEVs, leading to hypotheses of the mechanism of CD47- SIRPα signalling. This, coupled with reported molecular clustering for CD31, CD49d and CD166, led to several hypotheses of ACdEV-mediated signalling and involvement in immunomodulation.

4.5 Supplementary Data

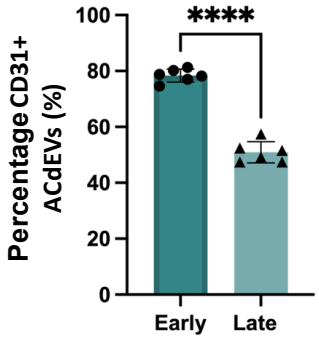

Supplementary Figure 4.1: The percentage of THP-1-derived ACdEVs displaying CD31 was significantly reduced in late ACdEVs compared to early ACdEVs. (Unpaired t test, ****p < 0.0001, mean ± SD, N = 6).

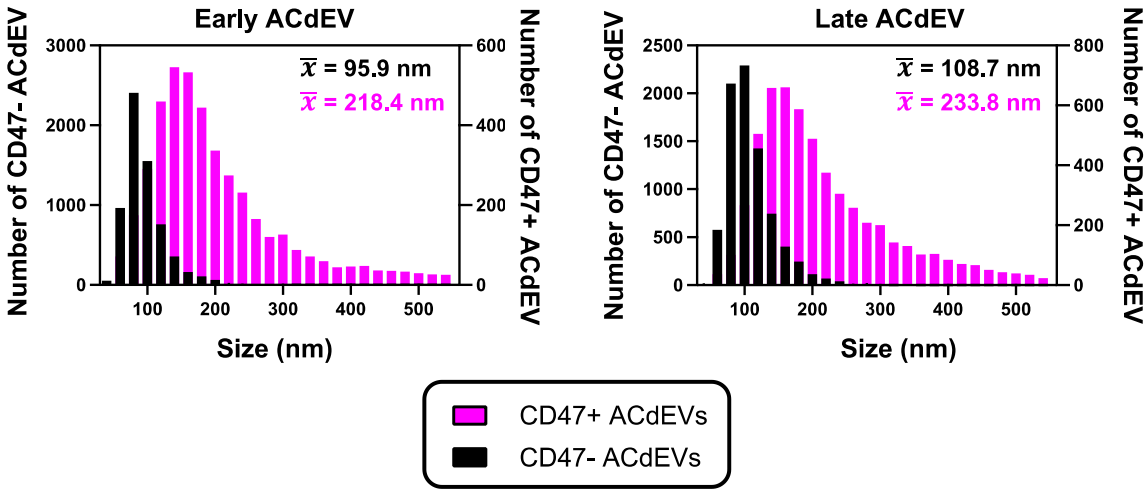

Supplementary Figure 4.2: ACdEVs that display CD47 at their surface are, on average, bigger than ACdEVs that lack CD47. Jurkat-derived early and late ACdEVs were immobilised by lectins, Wheat Germ Agglutinin and Concanavalin A, stained for CD47, and imaged by SMLM (Abbelight). $\bar{x}$ = mean average size. (N = 3 technical replicates).

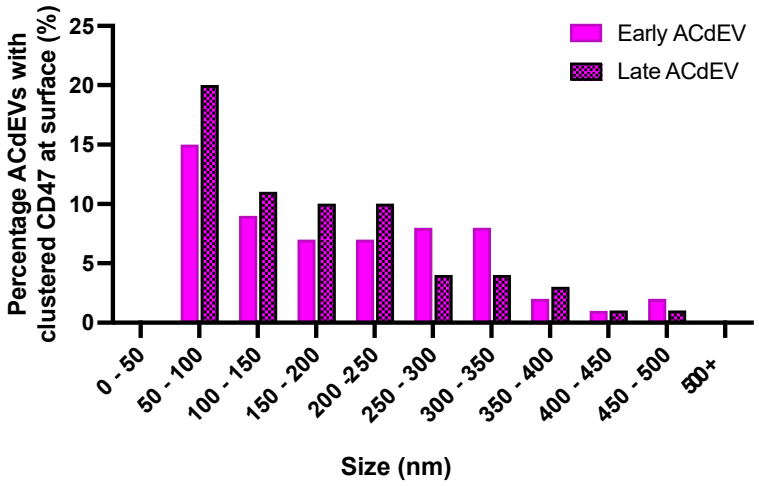

Supplementary Figure 4.3: CD47 clustered more readily on late ACdEVs that are below 250 nm in size, determined by SMLM (Abbelight). Jurkat-derived early and late ACdEVs were immobilised by lectins, Wheat Germ Agglutinin and Concanavalin A, stained for CD47, and imaged by SMLM (Abbelight) (N = 3 technical replicates).

	Early ACdEV (6h)		Late ACdEV (18h)	
Candidate protein	Enriched at surface of Jurkat or THP-1-derived ACdEVs	Adjusted *p* value	Enriched at surface of Jurkat or THP-1-derived ACdEVs	Adjusted *p* value
CD31	THP-1	0.001275 (**)	THP-1	0.012752 (*)
CD47	Jurkat	0.028318 (*)	Jurkat	0.021907 (*)
CD49d	N/A	0.586602 (ns)	Jurkat	0.046144 (*)
CD166	N/A	0.885952 (ns)	N/A	0.503597 (ns)

Supplementary Table 4.1: Statistical table of adjusted P values from multiple unpaired t tests with Holm-Šídák multiple comparisons test comparing percentage ACdEVs positive for each candidate protein derived from Jurkat T cells versus THP-1 monocytes (ns = non-significant, N = 3).

Chapter 5 The ACdEV surface in relation to macrophage function

5.1 Introduction

ACdEVs show evidence of promoting the clearance of apoptotic cells and therefore, may be important regulators in resolving inflammation (Grant *et al.,* 2019; Caruso & Poon, 2018). Macrophages are innate immune cells central to detecting, responding to, and resolving immunological challenges. During inflammation, macrophages and other phagocytes detect apoptotic cells, triggering their activation, and efficiently clear apoptotic material (Poon *et al.,* 2014b). Throughout this process, macrophages undergo several phenotypic changes, including alterations in cell surface expression, transcription, metabolism, and the release of soluble factors, such as cytokines (Stunault *et al.,* 2018; Ortega-Gómez *et al.,* 2013; Martinez *et al.,* 2006).

Macrophages can polarise into two major phenotypic states: pro-inflammatory, termed 'M1', and anti-inflammatory/pro-resolving, termed 'M2', phenotypes. M1 cells respond to lipopolysaccharide (LPS) or interferon-gamma (IFNγ), release reactive oxygen and nitrogen species, and produce pro-inflammatory cytokines such as IL-12, IL-23, and TNFα (Basu Mallik *et al.,* 2018). Most macrophages are polarised as M1 cells at the onset of inflammation, but M1 cells phenotypically switch to M2 polarised cells throughout an inflammatory response, eventually exceeding the number of M1 cells (Basu Mallik *et al.,* 2018). M2 cells are activated by anti-inflammatory cytokines IL-4 and IL-13, highly express scavenger receptors, and release growth factors like TGF-β and IGF (Sica & Mantovani, 2012). The ability of macrophages to switch from pro-inflammatory M1 to anti-inflammatory/pro-repair M2 is essential for resolving inflammation, highlighting the importance of macrophage plasticity in pathological settings (Hristodorov *et al.,* 2015; Sindrilaru *et al.,* 2011). Notably the 'M1/M2' model of macrophage polarisation oversimplifies the complexity macrophage biology, which is regulated by a combination of tissue-specific spatiotemporal exposure to microenvironmental signals and macrophage ontogeny (Ginhoux *et al.,* 2015). Several M2 subtypes have been described which show differences in surface expression and function, including differential activation of T cells and cytokine release (Edwards *et al.,* 2006).

Efficient clearance of apoptotic cells is paramount for preventing persistent, chronic inflammation (Poon *et al*., 2014b). To achieve this, apoptotic cells release soluble factors, including ATP, UTP,

S1P, and LPC, which have been well characterised (Poon *et al.,* 2014b). Additionally, they release apoptotic bodies (>1 μm in size) and apoptotic cell-derived extracellular vesicles (ACdEVs) (30 – 1000 nm). Phagocytic uptake of apoptotic cells is enhanced when apoptotic body formation is promoted (Tixeira *et al.,* 2019). Apoptotic bodies have also been shown to promote immune cell chemoattraction by the surface presentation of chemokines and the phenotypic switching of M1 to M2 cells through surface binding via PDL1–PD1 (Jiang *et al.,* 2023; Pontejo & Murphy, 2021).

The role of ACdEVs in regulating inflammation and apoptotic cell clearance remain poorly understood (Grant *et al.,* 2019; Caruso & Poon, 2018). Apoptotic bodies differ from ACdEVs in size and molecular composition, suggesting they may exert distinct functions (Hardy *et al.,* 2019). One study suggested that ACdEVs act as damage-associated molecular patterns (DAMPs), promoting macrophages to release pro-inflammatory cytokines IL-1β via S1P receptor-mediated NF-κB signaling (Park *et al.,* 2018). Endothelial-derived ACdEVs were also shown to activate the NF-κB pathway, promoting wound healing and inhibiting apoptosis in endothelial cells (Migneault *et al.,* 2020). Further work is needed to characterise and harness the immunomodulatory function of ACdEVs.

5.2 Aims and objectives

This project focuses on four major proteins identified from ACdEV proteomic profiling of three immune cell lines, confirmed to be expressed at the ACdEV surface by nano-flow cytometry and single molecule localisation microscopy (SMLM): CD31, CD47, CD49d, and CD166 (see Chapter 4). These proteins have known immunomodulatory roles, and so far, CD47, CD49d and CD166 have been reported to mediate immunomodulation at the EV surface (Dufour *et al.,* 2023; Kamerkar *et al.,* 2017; Kaur *et al.,* 2014; Choudhuri *et al*., 2014; Sung *et al.,* 2015). This project aims to understand their function at the ACdEV surface in relation to macrophages, a major innate immune cell that is essential for resolution of inflammation.

The molecular mechanisms by which ACdEVs communicate with immune cells are vital for understanding the apoptotic cell clearance process, a process known for its immunological silence (Poon *et al.,* 2014b). This project will investigate ACdEVs' functional role in macrophage migration, a timely process which is carefully balanced to promote efficient clearance of apoptotic cells and prevent persistent infiltration of immune cells, which can drive chronic inflammation (Poon *et al.,* 2014b). Additionally, determining whether ACdEV interactions with macrophages are mediated by surface binding or internalisation will be key to understanding how these interactions drive phenotypic changes in recipient cells, whether through cargo delivery or the activation of

intracellular signaling pathways via surface receptors. Finally, characterisation of macrophage phenotype in response to ACdEVs will provide insight into how ACdEVs influence immune responses and inflammation. Antibody-mediated blockade will be used to assess the involvement of each candidate protein, potentially revealing molecular mechanisms by which ACdEV communicate with the immune system, advancing knowledge of immune regulation and highlighting potential therapeutic targets.

5.3 Results

5.3.1 The role of ACdEVs in chemotaxis

For apoptotic cells to be efficiently cleared, phagocytes must be recruited in a timely manner (Poon *et al.,* 2014b). Apoptotic cells release a series of chemoattractive factors, including ACdEVs (Torr *et al.,* 2011; Truman *et al.,* 2008; Segundo *et al.,* 1999). To establish a method of monitoring macrophage migration and evaluate the chemotactic properties of ACdEVs collected from our apoptotic immune cell model, a vertical transwell assay was conducted (Figure 5.1). THP-1 macrophages (MΦs) were differentiated by treatment with 100 nM 1,25-dihydroxyvitamin D3 (VD3), which is marked by the upregulated expression of CD14, a macrophage pattern recognition receptor (PAMP sensor) for lipopolysaccharide (LPS) and active 'tetherer' of apoptotic cells which facilitates their clearance by phagocytosis (Devitt *et al.,* 2004; Hmama *et al.,* 1999; Landmann *et al.,* 1996) (Supplementary Figure 5.2B). VD3 treatment of THP-1 cells also preserves their monocytic-like weakly-adherent properties, meaning the cells retain the ability to migrate through the transwell membrane in response to a chemoattractant (Torr *et al.,* 2011).

Macrophages (MΦs) were seeded in the upper chamber of a vertical transwell assay and exposed for 12 hours to various conditions placed in the lower chamber: Jurkat-derived early and late apoptotic secretome (2000 x g supernatant, as defined in Chapter 3.3), Jurkat-derived early and late ACdEVs (isolated by SEC), and serum-free RPMI medium, which served as a negative control. Secretome and ACdEV samples were collected from equal numbers of apoptotic Jurkat T cells: 4 x 10^7 cells. Notably, late apoptotic secretome and late ACdEV samples contained an accumulation of factors released over a longer timeframe (18 hours versus 6 hours post UV irradiation) and inevitably, were more concentrated. MΦs that migrated into the lower chamber of the vertical transwell assay were counted every 30 minutes over 12 hours (Figure 5.1).

In the presence of a non-chemoattractive sample, such as serum-free RPMI medium (sfRPMI) which served as a negative control, few MΦs migrated through the transwell membrane (Figure 5.1B). Similarly, ACdEVs isolated by SEC induced a low percentage of MΦ migration, comparable to sfRPMI, indicating that SEC-isolated ACdEVs are not chemoattractive to MΦs. In contrast, apoptotic secretome induced most MΦs to migrate, with percentage migrated cells peaking at approximately 4.5 hours (Figure 5.1B). There was no significant difference in MΦs chemotaxis induced by secretome collected at early versus late apoptosis (Figure 5.1B). The percentage of migrated MΦs decreased gradually after 4.5 hours (Figure 5.1B). This was because clumping of

the cells prevented the cell segmentation algorithm from accurately counting the cells (Supplementary figure 5.3).

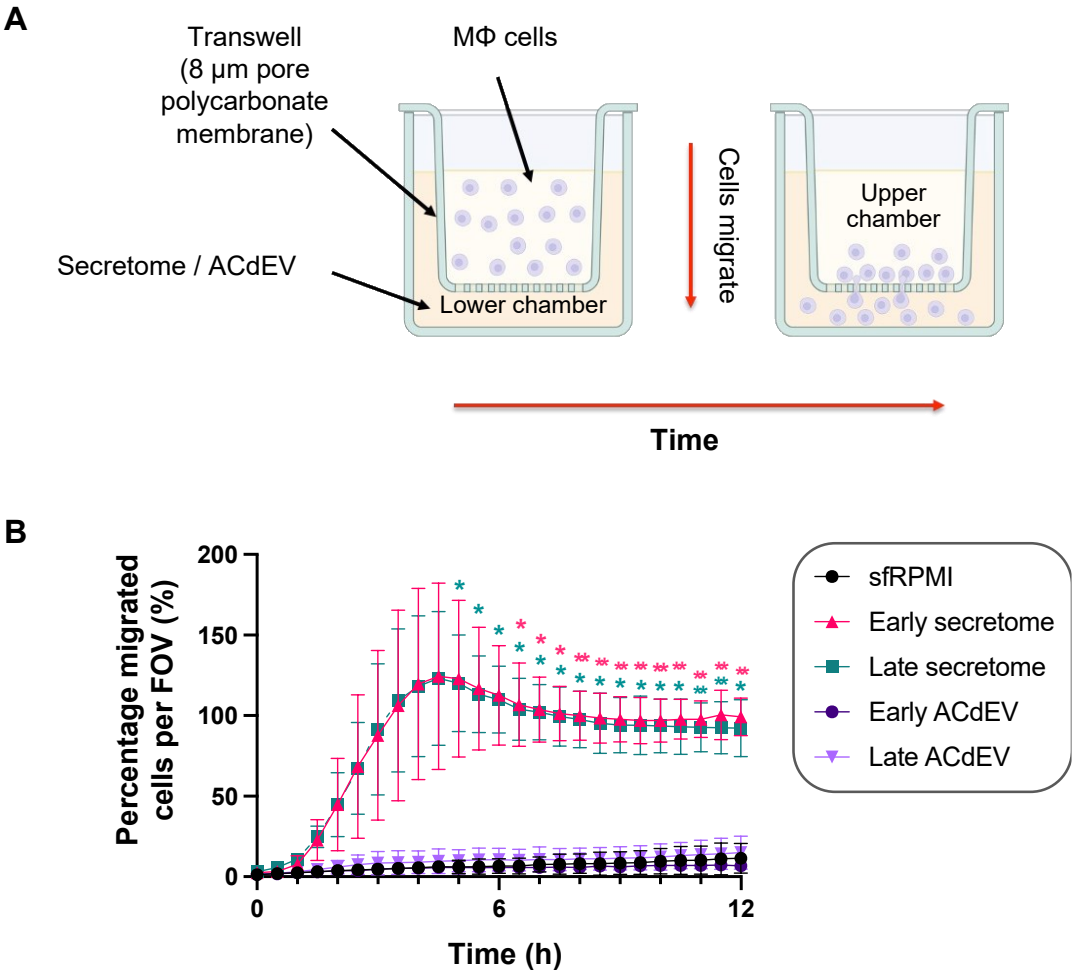

Figure 5.1: THP-1 macrophages (MΦs) migrated towards Jurkat-derived apoptotic secretome but not size-exclusion chromatography (SEC)-isolated ACdEVs. 8 x 10^4 MΦ cells were seeded into a transwell with apoptotic secretome, SEC-isolated ACdEVs or serum-free RPMI medium plated at the bottom of the wells. The number of MΦs that migrated into the lower chamber of the vertical transwell assay were counted per field of view (FOV) after 12 hours and normalised to a well containing MΦs only (no transwell). A) Cartoon depiction of vertical transwell migration assay set-up. B) MΦs migrated towards early and late Jurkat-derived apoptotic secretome but not Jurkat-derived ACdEVs collected by SEC. Cells were counted by in-built cell segmentation algorithm in the accompanying microscope software (Cytation 5 Cell Imaging Multimode Reader, Biotek). (Two-way ANOVA with Dunnett's multiple comparison test comparing sfRPMI (black) with all other conditions: ns = non-significant, *$p < 0.05$, **$p < 0.01$. mean ± SEM, N = 3).

This led to the questioning of whether ACdEV-depleted secretome is as chemoattractive as ACdEV-containing secretome. Previous work by Grant (2022) demonstrated that ACdEVs collected by ultracentrifugation (UC) were chemoattractive to THP-1 MΦs (L. R. Grant, 2022). However, it was hypothesised whether a combination of soluble factors and ACdEVs might exert an additive, or indeed synergist, chemoattractive effect. As such, a preliminary experiment was carried out observing the migration of MΦs towards SEC-isolated ACdEVs, SEC soluble protein fractions, UC-pelleted ACdEVs, and UC supernatant (see Supplementary Figure 5.1). Protein concentration and ACdEV particle concentration (particles/mL) were not normalised and therefore the potency of chemoattraction between samples cannot be directly compared. Nonetheless, the preliminary experiment revealed that MΦs migrated towards UC-pelleted ACdEVs, UC supernatant and pooled SEC soluble protein fractions, but, in agreement with previous work, not SEC-isolated ACdEVs (Supplementary Figure 5.1). In addition, to determine whether the chemoattractive properties of ACdEVs could be restored, 're-coating' SEC-isolated ACdEVs with chemoattractive soluble factors was attempted, to investigate whether the chemoattractive properties arise from the assembly of a functional corona. SEC-isolated ACdEVs were incubated in pooled SEC fractions 14-28 or the UC supernatant, that were enriched in soluble protein and likely, other soluble factors (Figure 3.2). The 'coated' ACdEVs were then re-purified by an additional round of ultracentrifugation. However, the 'coated' ACdEVs did not induce migration of MΦs, suggesting that the chemoattractive molecule(s) had been lost or were no longer functional (Supplementary Figure 5.1).

Having established a method to assess macrophage migration, the next aim was to determine whether candidate proteins CD31, CD47, CD49d and CD166, played a role in the chemoattraction of macrophages. To investigate this, antibody-mediated blockade was implemented to block protein activity and determine protein function. Antibodies were selected that had previously been reported as effective inhibitors of protein activity (see Table 2.4 for antibody information). As SEC-isolated ACdEVs were not chemoattractive to macrophages (Figure 5.1), blocking antibodies were incubated against apoptotic secretome by incubation in the lower chamber (Figure 5.2A). As previously discussed, the functional activity of CD47 and CD49d was assessed using Jurkat-derived secretome and the activity of CD31 and CD166 was assessed using THP-1-derived secretome, due to a higher proportion of ACdEVs displaying the respective proteins at the ACdEV surface (see Chapter 4, Figure 4.6). This applies to SEC-isolated ACdEVs used later in this chapter.

All blocking antibodies significantly delayed migration (Figure 5.2B and 5.2C). There was no significant difference between the percentage of migrated MΦs between unblocked secretome and blocked secretome by 5 hours with anti-CD47, 2 hours with anti-CD49d, 1.5 hours with anti-CD31 and 2 hours with anti-CD166 (Figure 5.2B and 5.2C). Therefore, CD47-blocked Jurkat-derived secretome most significantly delayed MΦ migration (Figure 5.2B). Notably, SIRPα and thrombospondin, CD47 binding partners, were not present in the proteomic datasets, therefore suggesting this effect is CD47-mediated (Grant L. R., 2022). As before, the cell segmentation algorithm failed to accurately count clumped cells and therefore reported a false decrease in the percentage of MΦs that migrated towards unblocked Jurkat-derived secretome after 4 hours (Supplementary figure 5.3).

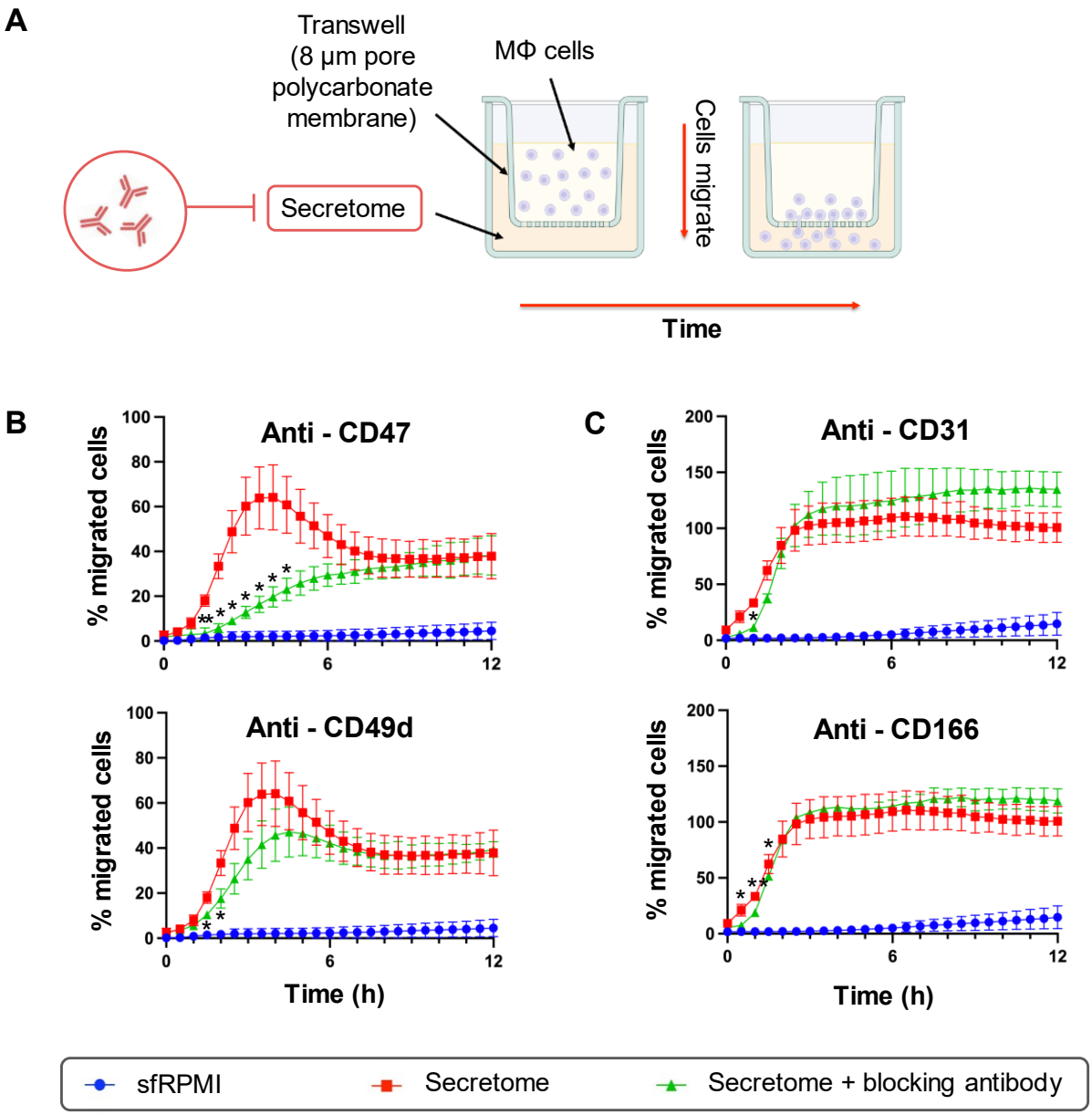

Figure 5.2: Blocking antibodies against CD31, CD47, CD49d and CD166 were incubated with apoptotic secretome to investigate their role in chemotaxis of THP-1 macrophages (MΦs). 8 x 10^4 MΦ cells were seeded into a transwell with apoptotic secretome, SEC-isolated ACdEVs or serum-free RPMI medium plated at the bottom of the wells. The number of MΦs that migrated into the lower chamber of the vertical transwell assay were counted per field of view (FOV) after 12 hours and normalised to a well containing MΦs only (no transwell). Cells were counted by in-built cell segmentation algorithm in the accompanying microscope software (Cytation 5 Cell Imaging Multimode Reader, Biotek). A) Cartoon depiction of vertical transwell migration assay set-up with antibody blockade against apoptotic secretome. B) Migration of MΦs towards Jurkat-derived apoptotic secretome with the addition of anti-CD47 and anti-CD49d blocking antibodies. C) Migration of MΦs towards THP-1-derived apoptotic secretome with the addition of anti-CD31 and anti-CD166 blocking antibodies. (Two-way ANOVA with Dunnett's multiple comparison test comparing secretome (red) to secretome + blocking antibody (green): ns = non-significant, *$p < 0.05$, **$p < 0.01$. mean ± SEM, N = 3). Cytation 5 Cell Imaging Multimode Reader, Biotek.

Typically, we would remove excess unbound antibody by SEC for ACdEV samples. However, as SEC-isolated ACdEVs were not chemoattractive to MΦs (Figure 5.1), it was not possible to test the migratory behaviour of MΦs in response to antibody-blocked ACdEVs cleaned up by SEC. Therefore, no clean up step was implemented so excess unbound blocking antibody was likely to be present in the blocked apoptotic secretome samples. As such, it is possible unbound antibody may have bound directly to the cells within the vertical transwell assay and induced changes in MΦ migration by blocking antigen on the cells rather than the EV. To test this, MΦs were incubated with each blocking antibody before removing unbound antibody through washing and then cell seeding into the upper chamber of the vertical transwell assay, and their ability to migrate towards (unblocked) apoptotic secretome was monitored (Figure 5.3A).

Incubation of anti-CD47 and anti-CD166 blocking antibodies with MΦs resulted in a significantly lower percentage of migrated MΦ cells (Figure 5.3B and 5.3C). In contrast, there was no significant impact on MΦ migration when MΦs were incubated with anti-CD31 or anti-CD49d (Figure 5.3B and 5.3C). Notably, MΦ cells exposed to Jurkat-derived apoptotic secretome did not undergo clumping, as seen in previous experiments (Figure 5.1 and 5.2, supplementary figure 5.3).

The chemoattractive properties of apoptotic secretome derived from Jurkat T cells and THP-1 monocytes had not previously been compared within our research group. Interestingly, apoptotic secretome from THP-1 monocytes promoted migration of MΦs more rapidly, with migrated MΦs plateauing at approximately 3 hours, compared to the percentage of MΦs that migrated towards Jurkat-derived secretome peaking / plateauing at approximately 4-5 hours (Figure 5.1B, 5.2B, 5.2C, 5.3B and 5.3C).

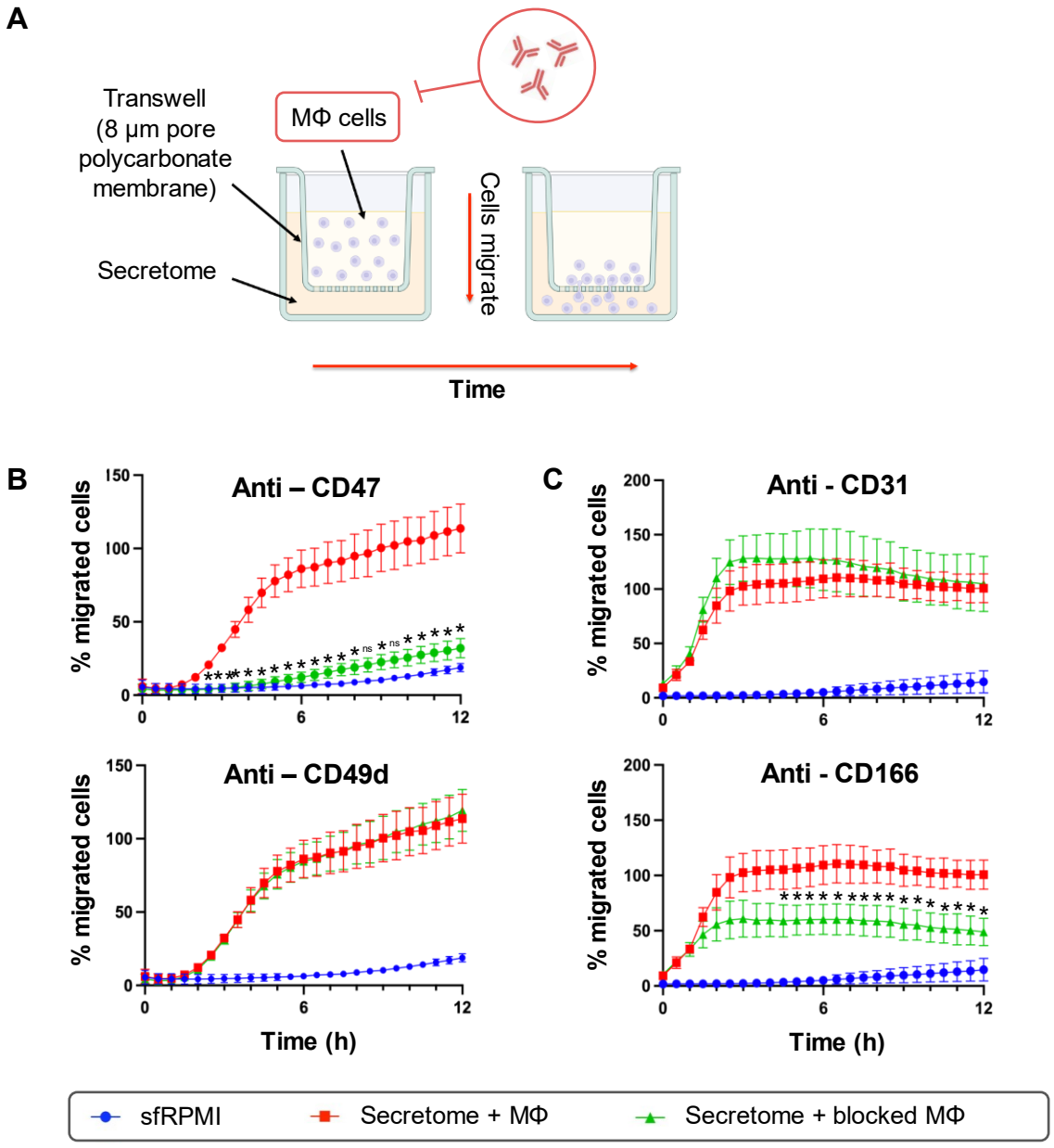

Figure 5.3: Blocking antibodies against CD31, CD47, CD49d and CD166 were incubated with THP-1 macrophages (MΦs) to investigate their role in chemotaxis. 8 x 10^4 MΦ cells were seeded into a transwell with apoptotic secretome, SEC-isolated ACdEVs or serum-free RPMI medium plated at the bottom of the wells. The number of MΦs that migrated into the lower chamber of the vertical transwell assay were counted per field of view (FOV) after 12 hours and normalised to a well containing MΦs only (no transwell). Cells were counted by in-built cell segmentation algorithm in the accompanying microscope software (Cytation 5 Cell Imaging Multimode Reader, Biotek). A) Cartoon depiction of vertical transwell migration assay set-up with antibody blockade against MΦ cells. B) Migration of CD47-blocked and CD49d-blocked MΦ cells towards Jurkat-derived apoptotic secretome. C) Migration of CD31-blocked and CD166-blocked MΦ cells towards THP-1-derived apoptotic secretome. (Two-way ANOVA with Dunnett's multiple comparison test comparing secretome + MΦ (red) to secretome + blocked MΦ (green): ns = non-significant, *p < 0.05, **p < 0.01. mean ± SEM, N = 3). Cytation 5 Cell Imaging Multimode Reader, Biotek.

5.3.2 Investigating interaction of ACdEVs with macrophages

EVs interact with recipient cells by surface EV : cell binding interactions; these may be by specific receptor-ligand interaction or non-specific physicochemical interactions (Buzás *et al.,* 2018). These interactions may then trigger intracellular signalling cascades or lead to EV uptake whereby the recipient cell processes the intraluminal cargo, which can modulate cell phenotype (Buzás *et al.,* 2018; Mulcahy *et al.*, 2014). To investigate the involvement of the candidate proteins (CD31, CD47, CD49d and CD166) in surface-mediated interactions and uptake, it was first necessary to observe the rate of ACdEV uptake by MΦs in the absence of antibody blockade. To do this, MΦs were incubated at different ratios of BODIPY™ FL Maleimide (BODIPY™)-labelled ACdEVs per MΦ cell for 1 hour at 37°C and measured by flow cytometry. An increase in MΦ fluorescence was indicative of MΦs binding or taking up ACdEVs (Figure 5.4).

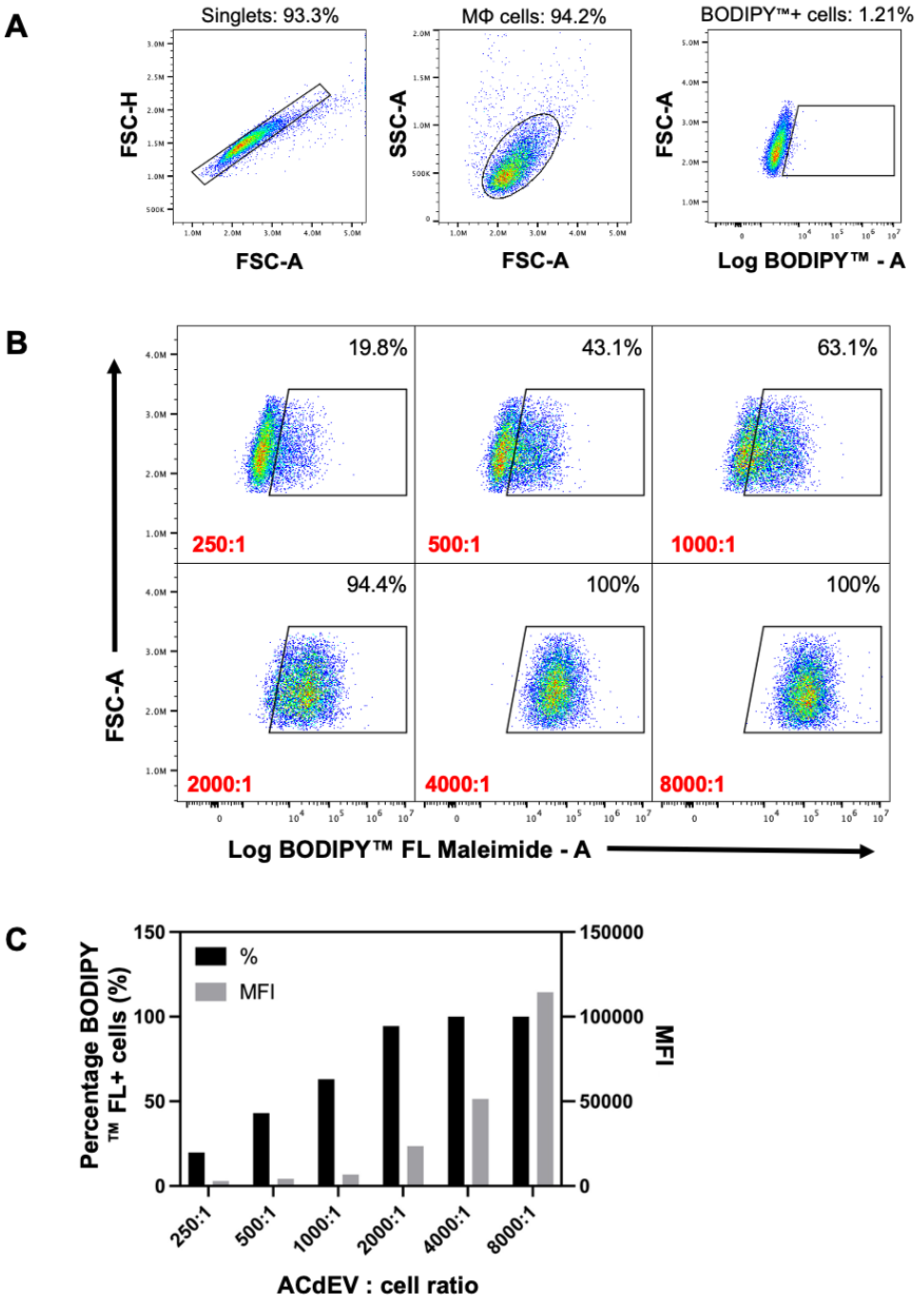

Figure 5.4: Dose-dependent ACdEV interaction with MΦ cells after 1 hour incubation. 1 x 10^5 MΦs were incubated with BODIPY™ FL Maleimide (BODIPY™)-labelled late ACdEVs at different doses, represented as ACdEVs : MΦ cell ratio, for 1 hour at 37°C and measured by flow cytometry (CytoFLEX S, Beckman Coulter). A) Gating strategy for MΦs that became fluorescent upon interaction with BODIPY™ FL Maleimide-labelled ACdEVs. B) Flow plots with percentage MΦs that became fluorescent upon incubation with BODIPY™ FL Maleimide-labelled ACdEVs. ACdEV : cell ratios shown in red. (N = 1). C) Percentage fluorescent MΦs and median fluorescence intensity (MFI) per ACdEV : cell ratio (N = 1).

The concentration of BODIPY™-labelled ACdEVs was measured by nano-flow cytometry and this was used to calculate the ACdEV : cell ratios (Figure 5.4B). As the dose of ACdEVs increased, the percentage MΦs that were fluorescent after 1 hour increased until a 4000:1 ACdEV : cell ratio, upon which 100% MΦs were fluorescent (Figure 5.4B and 5.4C). The median fluorescence intensity (MFI) continued to increase, even at the highest ACdEV dose at an 8000:1 ACdEV : cell ratio (Figure 5.4C). This indicated MΦs continued to interact with more ACdEV in the presence of higher concentrations of ACdEVs.

Next, to identify protein-specific roles in ACdEV interaction with MΦs, blocking antibodies against the candidate proteins (CD31, CD47, CD49d and CD166) were incubated with BODIPY™-labelled ACdEVs. This time excess antibody was removed by SEC, as ACdEV interaction with MΦs was not inhibited by this method (Figure 5.4). The 500:1 ratio of ACdEVs : cells was chosen for testing, as 43.1% MΦs were fluorescent after 1 hour exposure to ACdEVs, allowing flexibility to observe inhibited or promoted interaction of blocked ACdEVs by MΦs in the presence of blocking antibodies (Figure 5.4B and 5.4C). In other words, this ACdEV : cell ratio would not result in oversaturation of the MΦs with ACdEVs, masking any inhibitive or promoting effects.

Additionally, blocked ACdEVs were incubated with MΦ cells at different temperatures: 37°C, 20°C, and 4°C. Previously, ICAM-3 on the surface of apoptotic cells was shown to interact with THP-1 MΦ cells via surface tethering by monitoring their interaction at 37°C, a physiological temperature, and at 20°C, where energy-dependent processes like phagocytosis are inhibited (Torr *et al.,* 2011). The authors found no evidence of phagocytic uptake of apoptotic cells at 20°C, concluding that phagocytosis was effectively blocked at this temperature (Torr *et al.,* 2011). Our experiment used a similar approach; the interaction between ACdEVs and MΦ cells was assessed at 37°C, 20°C, and 4°C. Furthermore, the energy-driven process of endocytosis is also disrupted at 20°C (and therefore, 4°C) (Tomoda *et al.,* 1989). However, electrostatic interactions and surface tethering were expected to still occur at these lower temperatures, allowing us to assess ACdEV binding independently of internalisation.

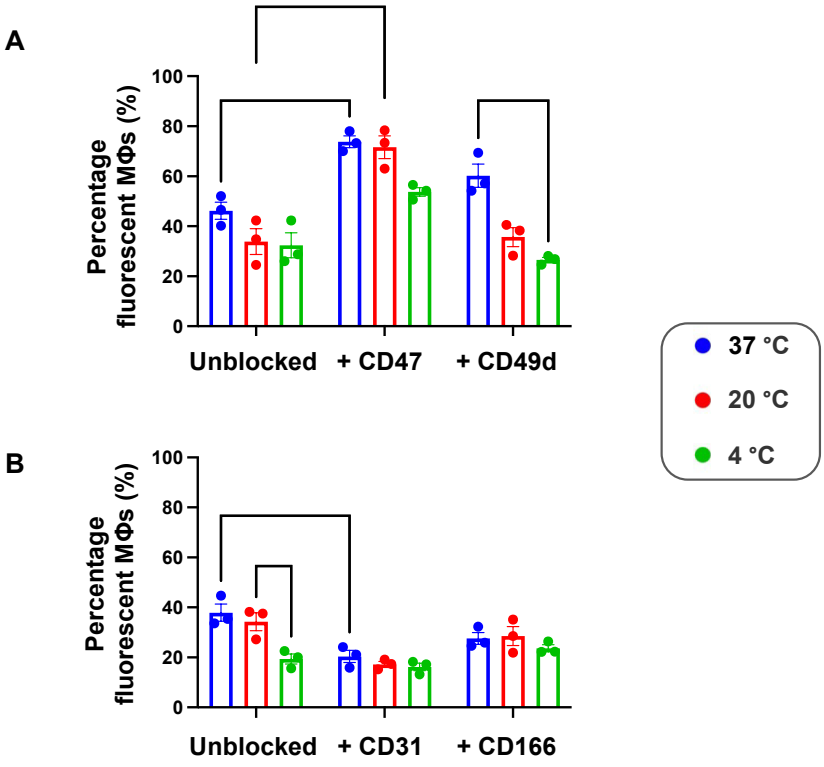

Figure 5.5: Interaction of BODIPY™ FL Maleimide (BODIPY™)-labelled ACdEVs with MΦ cells, indicated by MΦ fluorescence, after a 2 hour incubation at 37°C, 20°C and 4°C with and without the addition of blocking antibodies. MΦ were incubated with late ACdEVs at a 500 ACdEV : 1 cell ratio and measured for fluorescence by flow cytometry (CytoFLEX S, Beckman Coulter). A) Jurkat - derived ACdEVs with blocking antibodies against CD47 and CD49d. B) THP-1 - derived ACdEVs with blocking antibodies against CD31 and CD166. (Two-way ANOVA with Tukey's multiple comparison test, *$p < 0.05$, ** $p < 0.01$. Mean ± SEM, N = 3).

At a 500:1 ACdEV : cell ratio, approximately 40% MΦ cells became fluorescent after a 2 hour incubation (Figure 5.5A). This was consistent with the previous dose-dependent uptake experiment, in which ACdEVs at a 500:1 ratio were incubated for 1 hour (Figure 5.4B and 5.4C). This indicated the majority of ACdEV interaction occurs quickly within 1 hour. Similarly, approximately 40% MΦ cells became fluorescent after a 2 hour exposure to THP-1-derived ACdEVs, suggesting MΦ cell had no preferential interaction with ACdEVs derived from the same cell type (Figure 5.5B). A significantly lower percentage of MΦ cells were fluorescent after incubation with THP-1-derived ACdEVs at 4°C compared to 20°C, highlighting temperature-sensitive changes in ACdEV interaction (Figure 5.5B). Notably, this effect was not observed for Jurkat-derived ACdEVs, suggesting cell-dependent differences in ACdEV interaction.

A significantly higher percentage of MΦ cells became fluorescent upon incubation with CD47-blocked ACdEVs at 37°C and 20°C, compared to unblocked ACdEVs (Figure 5.5A). This suggested CD47 may inhibit active internalisation of ACdEVs by MΦs. In contrast, a significantly lower percentage of MΦ cells became fluorescent upon incubation with CD31-blocked ACdEVs at 37°C, compared to unblocked ACdEVs, suggesting CD31 may promote internalisation of ACdEVs (Figure 5.5B). Finally, a lower percentage of MΦ cells were fluorescent after incubation with CD49d-blocked ACdEVs at 4°C (statistically significant) and 20°C (non-significant) than unblocked ACdEVs, suggesting CD49d may also be involved in the active internalisation of ACdEVs (Figure 5.5A). No significant differences in ACdEV - MΦ interaction was observed upon anti-CD166 antibody blockade (Figure 5.5B).

5.3.3 Macrophage phenotype in response to ACdEVs

Macrophages are a major type of innate immune cell that are highly efficient at engulfing and phagocytosing apoptotic cells (Poon *et al.,* 2014b). Furthermore, macrophages exert anti-inflammatory pro-resolving functions in response to phagocytic clearance of apoptotic cells and apoptotic bodies (Jiang *et al.,* 2023; Fadok *et al.,* 1998). Unpublished work has determined ACdEVs carry anti-inflammatory molecules, including eicosanoids and active lipooxygenases, and these are transferred to recipient macrophages. Therefore, we hypothesised that ACdEVs may contribute to promoting an anti-inflammatory pro-resolving macrophage phenotype.

Macrophages are dynamic immune cells that can exert different pro-inflammatory or anti-inflammatory, pro-resolution functions that modulate the microenvironment, widely referred to as ‘M1’ and ‘M2’ macrophages, respectively (Sica & Mantovani, 2012). To understand how ACdEVs may modulate the activity of macrophages, a macrophage phenotyping assay was adapted from Grant (2022) that measured the cell surface expression of several markers of M1, M2, or unpolarised ‘M0’ cells by flow cytometry. Several adaptations were made to the protocol in an attempt to improve the distinction of M1 versus M2 cell types and improve the workflow efficiency. Firstly, THP-1 monocytes were differentiated into MΦs by treatment with a lower concentration of PMA for just 1 hour (6.16 nM (equivalent to 10 ng/mL) for 1 hour instead of 250 nM for 48 hours) (see Methods) (Grant, L.R., 2022). These MΦ cells were termed ‘M0’ cells. Secondly, M0 cells were polarised by a combination treatment with LPS and IFNγ, or IL-4 and IL-13, to produce M1 and M2 cells, respectively (instead of single treatment with LPS or IL-4, to produce M1 and M2 cells, respectively) (Figure 5.7A) (Grant, L.R., 2022). The inflammatory functions of M0, M1 and M2 cells have been widely reported using similar methods (Vogel *et al.,* 2014).

EV cargo delivery efficiency is reported to be low with an EV dose-dependent increase in cargo detected in recipient cells (Hagey *et al.,* 2023). Therefore, the highest possible ACdEV dose, from the Jurkat-derived late ACdEV sample that was collected for this experiment (5.9E+09 ACdEVs/mL concentration estimated by nano-flow cytometry), was administered. This resulted in an ACdEV : cell ratio of 1180:1 that treated M0 cells for 48 hours. This allowed us to observe whether ACdEVs skew macrophage phenotype to become more M1-like or M2-like. Finally, a new panel of antibodies was designed by Dr Ivana Milic (Aston University), targeting: CD11b, CD14, CD40, CD64, CD86, CD206, CD209 (see Table 2.3 for antibody information). Each antibody was conjugated to a different fluorophore that had minimal spectral overlap (Figure 5.6). With compensation, cells were labelled with all seven antibodies simultaneously allowing for higher throughput multiplexed profiling of MΦs. MΦ cells were treated with ACdEVs and the upregulation or downregulation of M1 or M2-associated cell surface markers was measured by flow cytometry (Figure 5.7).

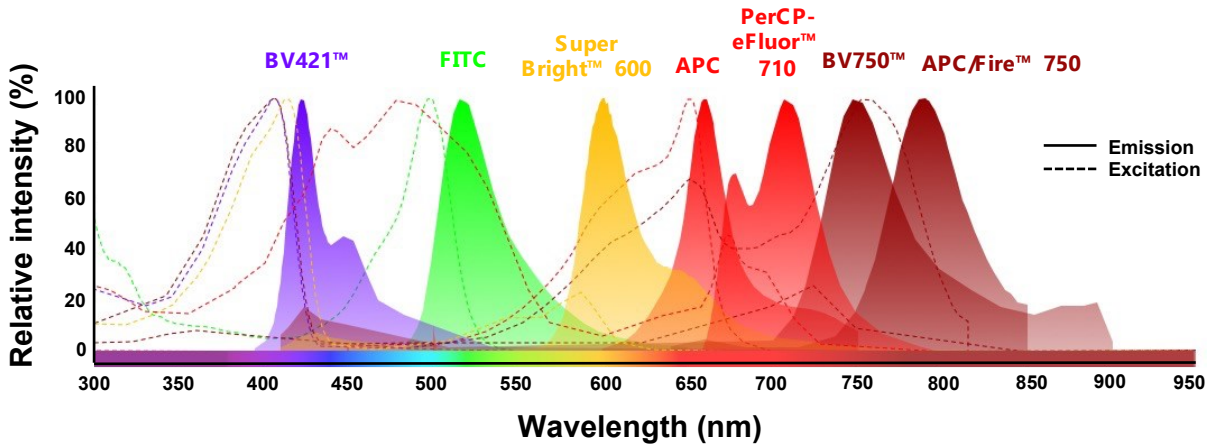

Figure 5.6: Fluorescence spectra of each fluorophore in the macrophage phenotyping antibody panel. Excitation spectra (dashed line) and emission specta (solid line). Figure made using Fluorescence SpectraViewer (ThermoFisher Scientific).

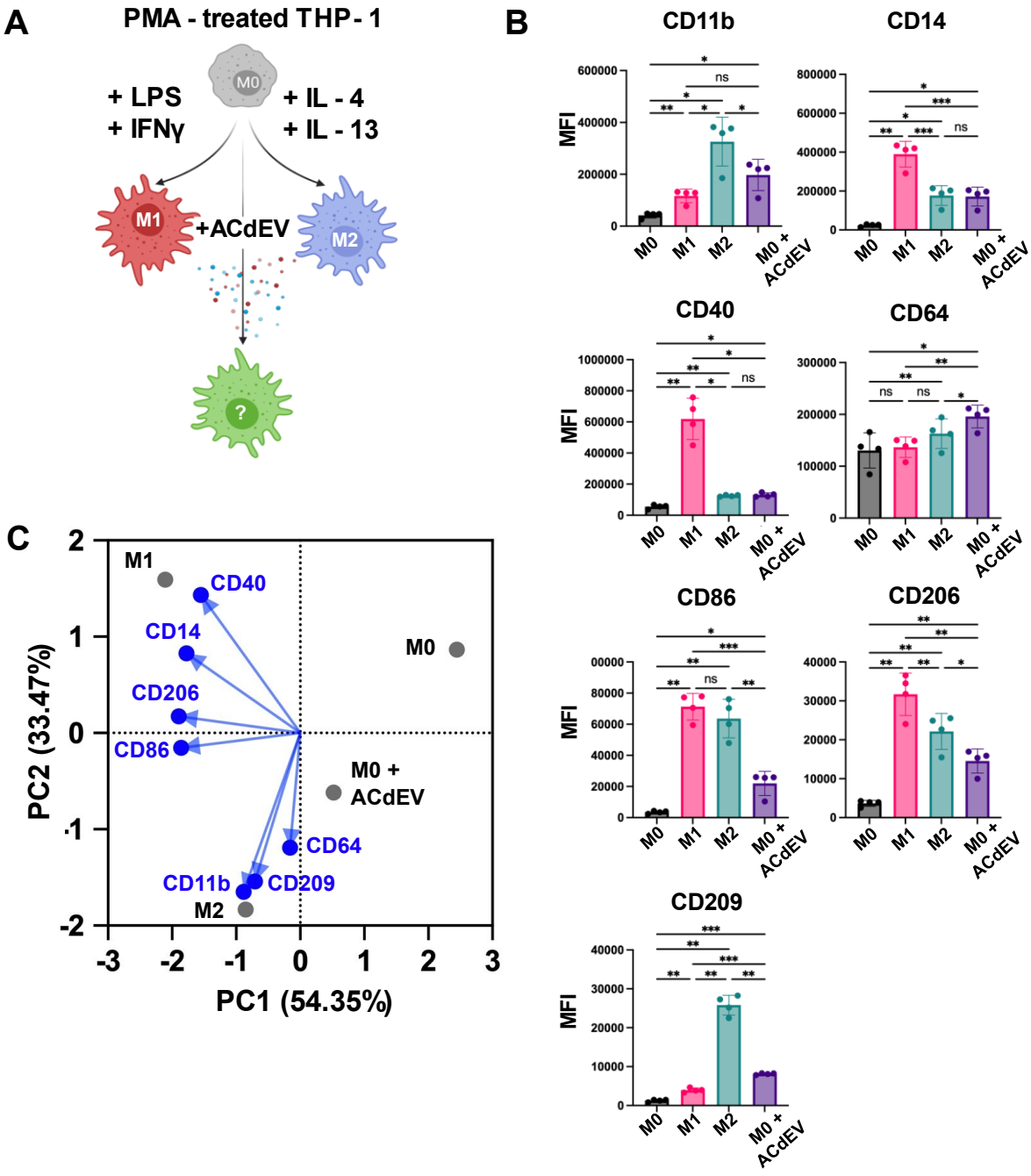

Figure 5.7: The effect of ACdEVs on macrophage phenotype, using a THP-1 cell line model. Changes in surface expression of a panel of macrophage markers were measured by flow cytometry (CytoFLEX S, Beckma Coulter). A) Depiction of macrophage differentiation and polarisation protocol. PMA-differentiated MΦ cells (M0) were treated with LPS and IFNγ, or IL-4 and IL-13, for 48 hours to polarise MΦ cells to M1 or M2 phenotypes, respectively. M0s were also treated with ACdEVs for 48 hours at a ratio of 1180:1 Jurkat-derived late ACdEVs per M0 cell. B) Median fluorescence intensity (MFI) of total cell population with subtraction of isotype control MFI (one-way ANOVA with Tukey's multiple comparison test, ***$p < 0.001$, **$p < 0.01$, *$p < 0.05$, Mean ± SEM, N = 4). C) Principal component analysis (PCA) of macrophage phenotypes corresponding to cell surface marker expression with percentage explain variance per PC (average MFI).

CD14 and CD40, classical M1 markers, were significantly upregulated in M1 polarised cells (Figure 5.7B) (Sica & Mantovani, 2012; Stout *et al*., 1996). Meanwhile, there was no significant difference in expression of CD14 and CD40 between M2 polarised cells and M0 cells treated with ACdEVs. Furthermore, the MFIs of CD14 and CD40 for M2 and ACdEV-treated M0 cells were significantly different to M0 cells, suggesting ACdEV treated M0s cells were most like M2 cells in terms of CD14 and CD40 expression. Surprisingly, CD206 was also significantly upregulated in M1 cells, despite being reported as a marker of M2 cells (Smith *et al.,* 2016).

CD11b and CD209 were significantly upregulated in M2 polarised cells (Figure 5.7B). ACdEV-treated M0 cells had significantly different CD209 expression to M1 and M2 cells, displaying an intermediate level of expression. In contrast, ACdEV-treated M0s had no significant difference in CD11b expression to M1 polarised cells.

There was no significant difference in expression of CD64 and CD86 between M1 and M2 polarised cells (Figure 5.7B). However, CD64 was significantly upregulated in M2 and ACdEV-treated M0s compared to M0 cells. Furthermore, CD64 was significantly upregulated in ACdEV-treated M0 cells compared to M2 polarised cells. In the case of CD86, expression was significantly upregulated in M1 and M2 cells compared to M0s and ACdEV-treated M0s (Figure 5.7B). Furthermore, ACdEV-treated M0s had significantly upregulated expression of CD86 compared to M0 cells. Together, the expression profiles of CD64 and CD86 reveal significant differences in ACdEV-treated M0s compared to M1, M2 and M0 cells.

An average MFI of four biological replicates were represented by principal component analysis (Figure 5.7C). The three macrophage phenotypes M0, M1 and M2 were clearly separated, indicating the adapted protocol achieved three distinctive phenotypes and the panel of surface markers was able to distinguish them. CD209 and CD11b were closely clustered to the M2 phenotype (Figure 5.7C). Notably, the M0 phenotype was not clustered near to any surface markers. ACdEV-treated M0s were skewed away from M1 phenotype and in the middle of the M0 and M2 phenotypes, indicating it represented a unique macrophage phenotype.

Next, using the same antibody panel, the effect of ACdEVs on primary human-derived macrophages was tested to determine if these results could be replicated in a primary cell model (Figure 5.8). Primary human monocytes were collected from four healthy donors and differentiated *ex vivo* into macrophages by *in vitro* treatment with granulocyte-macrophage colony-stimulating factor (GM-CSF) for 6 days. Primary monocyte-derived M0 macrophages (pM0s) were then treated with LPS and IFNγ, or IL-4 and IL-13, for 48 hours to polarise pM0 cells

into primary monocyte-derived M1 (pM1) and M2 (pM2) cells, respectively, as well as treatment with ACdEVs for 48 hours. Furthermore, to investigate the role of the ACdEV surface-expressed candidate proteins in modulation of macrophage phenotype, blocking antibodies against the candidate proteins (CD31, CD47, CD49d and CD166) were incubated with ACdEVs and excess antibody was removed by SEC prior to pM0 treatment. As an EV dose-dependent increase in cargo was previously reported in recipient cells, the highest possible ACdEV : pM0 ratio was implemented in this experiment per condition, to maximise our chances of observing ACdEV-driven phenotypic changes (Hagey *et al.,* 2023). As such, the ACdEV : pM0 ratio varied for each condition; THP-1-derived ACdEVs were more concentrated and therefore had a higher ACdEV : pM0 ratio per condition (see Supplementary Table 5.1 for ACdEV : pM0 ratios) (for full method, refer to section 2.2.1.2).

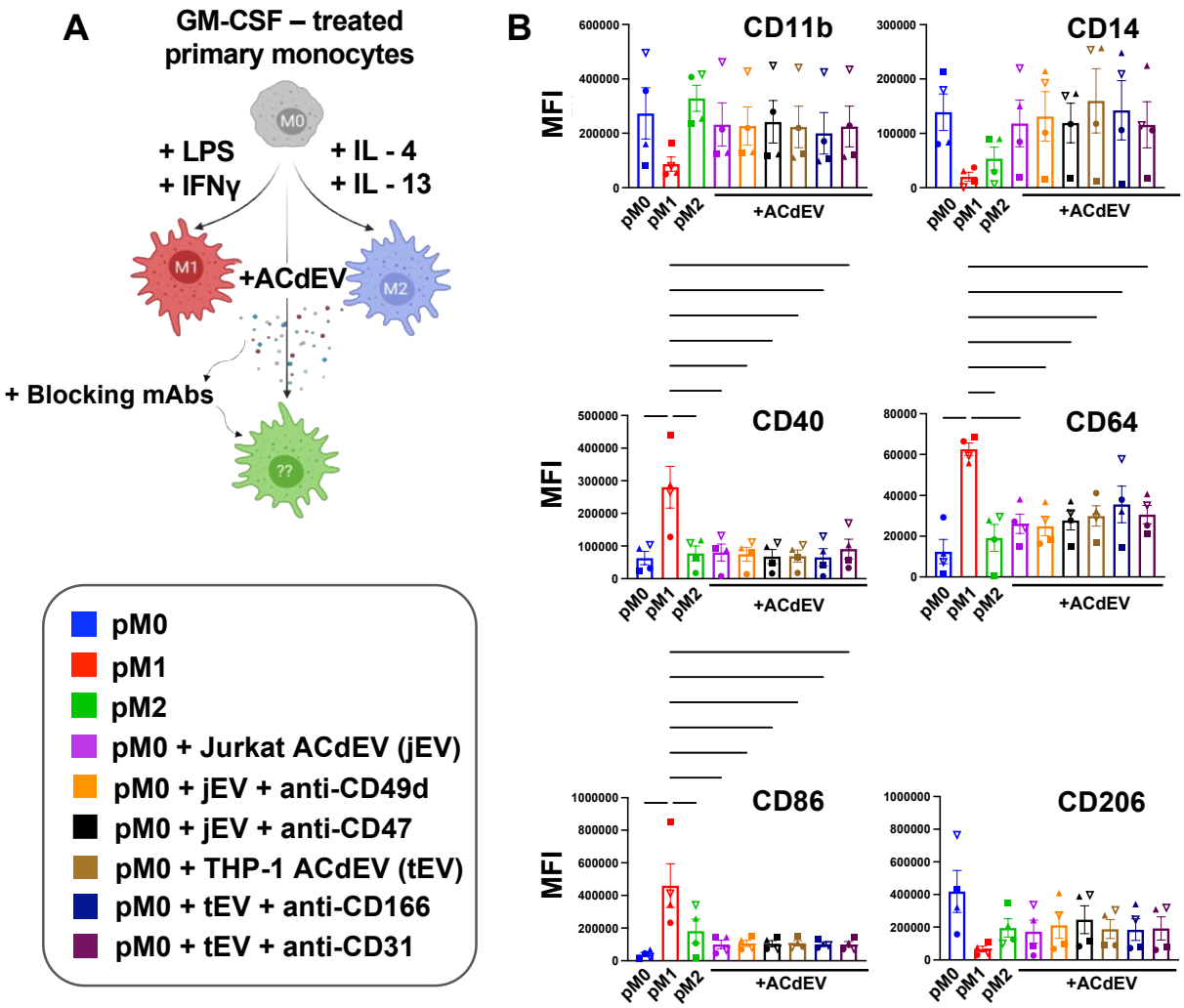

[Figure 5.8 continues onto next page]

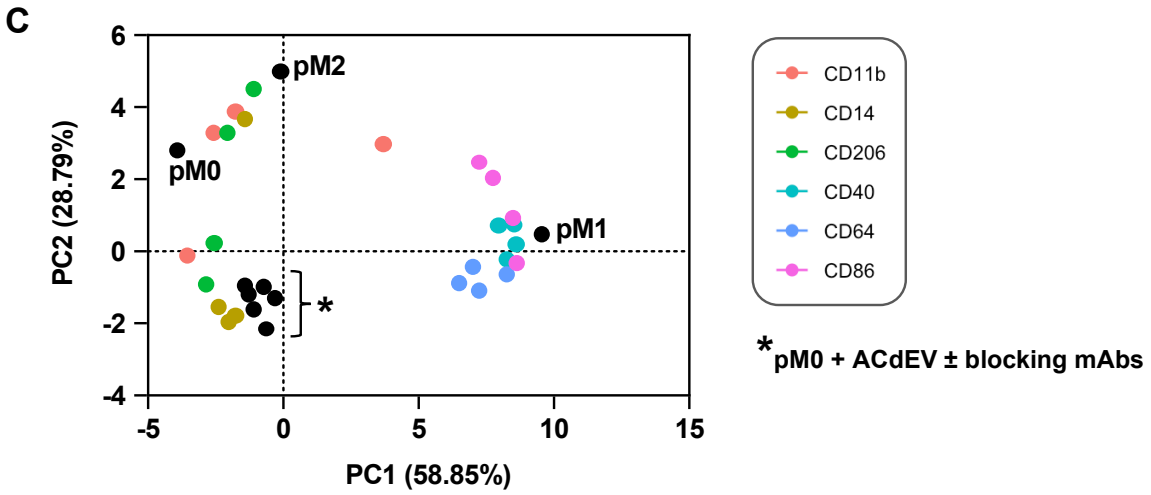

Figure 5.8: The effect of ACdEVs on macrophage phenotype, using a human primary monocyte-derived macrophage model. Changes in surface expression of a panel of macrophage markers were measured by flow cytometry (CytoFLEX S, Beckma Coulter). A) Depiction of macrophage differentiation and polarisation protocol. GM-CSF-differentiated primary monocyte-derived macrophages (pM0) were treated with LPS and IFNγ, or IL-4 and IL-13, to polarise pM0 cells to pM1 or pM2 phenotypes, respectively. pM0 cells were also treated with unblocked or antibody-blocked ACdEVs for 48 hours (see Supplementary Table 5.1 for ACdEV doses). B) Median fluorescence intensity (MFI) of total cell population with subtraction of isotype control MFI. Symbol matched to each donor (one-way ANOVA with Tukey's multiple comparison test, ***$p < 0.001$, **$p < 0.01$, *$p < 0.05$, Mean ± SEM, N = 4). C) Principal component analysis (PCA) of macrophage phenotypes corresponding to cell surface marker expression with percentage explained variance per PC (N4 biological replicates).

Unfortunately, CD209 had to be excluded due to an insufficient compensation control caused by negligible expression (data not shown). Therefore, just the remaining six markers of the antibody panel were analysed. M1 markers CD40, CD64 and CD86 were significantly upregulated in pM1 cells (Figure 5.8B). There was no significant difference in the expression of these markers between any other conditions, including ACdEV-treated pM0s.

Surprisingly, M1 markers CD11b and CD14 appeared to be non-significantly downregulated in pM1 cells compared to every other condition (Figure 5.8B). The donor variability is particularly evident in the graphs displaying these markers, with greatly varying MFI values. There was no significant difference between any conditions.

Expression of CD206, an M2 marker, was also not significantly different between any conditions (Figure 5.8B). However, expression appeared to be non-significantly elevated in pM0s and non-

significantly downregulated in pM1 cells. Furthermore, the expression profiles of pM2 and ACdEV-treated pM0s showed noticeable similarity.

Notably, there was no significant difference between any of the unblocked or blocked ACdEV-treated pM0 conditions for any of the markers (Figure 5.8B).

Because of donor variability, each individual biological replicate was plotted on the PCA (Figure 5.8C). As seen in the THP-1 model, each macrophage phenotype (pM0, pM1 and pM2) were distinctly separated; this was most obvious for the pM1 phenotype, by which M1 markers CD40 (aqua), CD64 (blue) and CD86 (magenta) were clustered together near to the pM1 phenotype, indicating a conserved expression profile across donors. Whereas, M1 marker CD11b (red) was noticeably spread across the PCA plot, indicating CD11b expression relevant to each phenotype was variable across donors. Finally, M1 marker CD14 (mustard) and M2 marker CD206 (green) showed variable clustering localised nearby to the ACdEV-treated pM0 cells and between the pM0 and pM2 phenotypes. Notably, each ACdEV-treated pM0 condition were tightly clustered together, indicating phenotypic similarity, and were skewed away from all three macrophage phenotypes, suggesting they represented a unique phenotype. It also suggested that blockade of each candidate protein had little effect on ACdEV-mediated modulation of macrophage phenotype.

5.4 Discussion

5.4.1 The role of ACdEVs in chemotaxis

ACdEVs are potentially important mediators of apoptotic cell clearance (Caruso & Poon, 2018). Efficient clearance of apoptotic cells is essential for maintaining tissue homeostasis, preventing the release of potentially harmful intracellular contents, and resolving inflammation effectively (Poon *et al.,* 2014b). The ability of phagocytes to migrate towards apoptotic cells is essential for engulfment of apoptotic cells. ACdEVs have previously been shown to promote chemotactic recruitment of immune cells (Torr *et al.,* 2011; Truman *et al.,* 2008; Segundo *et al.,* 1999). Here, apoptotic secretome (containing a mixture of ACdEVs and soluble factors) was chemoattractive to THP-1 MΦs and rapidly induced migration (Figure 5.1B). However, ACdEVs isolated by SEC did not induce migration of MΦs (Figure 5.1B). This effect has previously been reported by Grant (2022) where ACdEVs isolated by ultracentrifugation (UC) retained the ability to induce MΦ migration. This has led to hypothesising the importance of the ACdEV collection method and its potential impact on ACdEV corona, that may be involved in the chemoattraction process of macrophages.

The formation of a corona at the surface of artificial nanoparticles (*e.g.* lipid nanoparticles, liposomes) is well established and implicated in the efficacy of drug delivery (Xiao & Gao, 2018). However, the composition of an EV corona is not well characterised, especially *in vivo* (Buzás, 2022). To date, most studies have characterised the protein content of EV coronas formed by exposure to plasma or serum and therefore, comprise proteins commonly present in plasma, including apolipoproteins and immunoglobulins (Tóth et al., 2021). However, the corona is comprised of a diverse array of molecules, including lipids, glycans and nucleic acids, that is likely to form spontaneously, depending on the microenvironment, by a combination of receptor-ligand interactions and electrostatic interactions (Yerneni *et al.,* 2022; Buzás, 2022). The affinity of these interactions is not reported to date. The importance of EV corona on downstream EV function was first highlighted by E. Tóth *et al.* (2021), where they observed differential cytokine release induced in recipient dendritic cells, when incubated with plasma-coated THP-1-derived EVs versus uncoated THP-1-derived EVs (Tóth *et a*l, 2021). Since *in vivo* cells and EVs are constantly surrounded by soluble factors, it is highly likely that EVs are always naturally coated with some form of corona, with its composition likely influenced by the local microenvironment (Buzás, 2022). Importantly, the tendency to adopt a reductionist approach in research, such as aiming to purify EVs as much as possible, might lead to EV samples that no longer resemble the natural EV in its

native state. Consequently, the process of EV isolation and purification may lose or hide important EV-associated functions.

Interestingly, both UC and SEC have been reported to remove the EV corona, observed by TEM, and impair EV-mediated angiogenesis *in vivo* (Wolf *et al.,* 2022). However, only SEC abolished the chemoattractive properties of ACdEVs in this study (Supplementary Figure 5.1). This may therefore perhaps suggest a non-corona mediated change in EV function following SEC. Furthermore, soluble factors that eluted from the later fractions of the SEC column, or present in the UC supernatant, were chemoattractive and able to induce MΦ migration (Supplementary Figure 5.1). Indeed, fractions 14-28 that eluted from the SEC column were enriched in soluble protein (see Chapter 3, Figure 3.2). It is possible that CX3CL1, a potent chemokine and 'find me' signal that attracts phagocytes towards apoptotic cells, may be a chemoattractive soluble protein that is released into the secretome by apoptotic Jurkat T cells (Truman *et al.,* 2008). There may also have been other soluble factors present, such as LPC or S1P, chemoattractive lipid mediators released by apoptotic cells to recruit phagocytes (Figure 3.2) (Gude *et al.,* 2008; Lauber *et al*., 2003). In addition to chemoattractive soluble factors and UC-isolated ACdEVs, the combination of ACdEVs with soluble factors (*i.e.* crude apoptotic secretome) appeared most chemoattractive to MΦs (Supplementary Figure 5.1). This suggested the presence of both ACdEVs and soluble factors may exert an additive chemoattractive potency. To determine whether the chemoattractive properties of SEC-isolated ACdEVs could be rescued, a preliminary experiment was carried out in which the 'coating' of SEC-isolated ACdEVs with chemoattractive soluble factors, collected by SEC and UC, was attempted. Excess soluble factors were then removed by an additional round of UC. The 'coated' SEC-isolated ACdEVs failed to induce MΦ migration (Supplementary Figure 5.1). This may suggest that a corona of chemoattractive molecules isn't the source of the chemoattractive properties of ACdEVs. Alternatively, the chemoattractive factors may not have been potent enough to induce migration due to dilution during SEC, a functional corona may have assembled as a result of low affinity interactions that were permanently disrupted, or fundamental changes to the ACdEV surface may have permanently impaired function during processing by SEC. For example, SEC may induce conformational changes in corona/ACdEV surface molecules, due to alterations in salt levels or ionic strength of the eluent buffer, which could lead to loss of functional activity. Going forward, refining eluent buffers to maintain the salt concentration, pH and ionic strength of the apoptotic secretome may help to preserve the ACdEV corona and ACdEV surface, and shed light on corona formation. Interestingly, Grant (2022) carried out proteomic compositional analysis of SEC-isolated ACdEVs versus UC-isolated ACdEVs, but no candidate protein was identified responsible

for loss of chemoattractive function (L. R. Grant, 2022). Future work should aim to identify the functional soluble factors that are potently chemoattractive, as well as their functional relationship with ACdEVs, to provide insight into the mechanism of chemoattraction.

Previous data generated in the lab reported early ACdEVs (collected by UC) as more chemoattractive than late ACdEVs (A. Cameron, 2018). However, this project reported no significant difference in the percentage of macrophages that migrated towards early or late Jurkat-derived apoptotic secretome (Figure 5.1B). The reason for the conflicting results remains unclear. As late apoptotic secretome contains an accumulation of ACdEVs and soluble factors released during early and late apoptosis, it is more concentrated than early apoptotic secretome – this was demonstrated in Chapter 3 (Figure 3.3). This could suggest that concentration of ACdEVs or soluble chemoattractive factors isn't directly linked to chemoattractive potency, which would support the findings of Cameron (2018). Alternatively, approximately 100% MΦs had migrated by 3.5 hours, which could suggest the MΦ surface receptors responsive to chemoattractants were fully saturated by the chemoattractive factors present in early apoptotic secretome (Figure 5.1). This could have masked any potential concentration effect. Future work should observe MΦ migration towards titrated early and late apoptotic secretome to determine this. To further clarify the functional differences between early and late ACdEVs/secretome, apoptotic cells could be replenished with fresh medium after the initial harvest at early apoptosis, allowing for the collection of ACdEVs released exclusively between 6-18 hours. However, this approach may introduce uncontrolled changes to the apoptotic cells due to the renewed availability of nutrients.

Blocking antibodies against the candidate proteins (CD31, CD47, CD49d and CD166) were implemented against apoptotic secretome to inhibit protein function and assess any changes in MΦ migration. Antibody blockade impacted MΦ migration indicating that ACdEVs are likely important for inducing chemoattraction in addition to soluble factors (Figure 5.2). Despite previous reports of effective blockade (refer to Table 2.4 for blocking antibody information), it is important to acknowledge that the inhibition of protein function in these experiments was still an assumption relying on epitope accessibility and the ability of bound antibody to render the protein unable to signal normally. It is possible that an antibody can block one particular function but not another; indeed, multiple epitopes could be responsible for different activities, meaning several distinct blocking antibodies might be required to fully confirm a function. Furthermore, blocking antibody concentrations were not titrated so a high concentration (10 µg/ mL) was incubated to increase the likelihood of saturation of ACdEV surface epitopes. This may have led to increased non-

specific binding, which could have affected the function of neighbouring molecules and impacted cell migration.

A significant delay in migration was observed in the presence of all four blocking antibodies (Figure 5.2B). Importantly, the antibodies may have exhibited some level of toxicity that hindered macrophage migration. However, since each antibody elicited a distinct response pattern, it is likely that the effects are antigen specific. The delayed migration was short-lived for apoptotic secretome incubated with anti-CD31, anti-CD49d and anti-CD166, with no significant delay reported by 1.5 hours for anti-CD31 and 2 hours for anti-CD49d and anti-CD166 (Figure 5.2B). This may suggest the role of these proteins in chemoattraction may be quickly compensated for by other chemoattraction factors. Alternatively, this could be due to biological variation between replicates, with additional replicates reducing the observed significant effect. Interestingly, apoptotic secretome blocked by anti-CD47 resulted in significantly delayed migration until 4.5 hours (Figure 5.2B). This was surprising, as CD47 is a well-established 'don't eat me' signal when interacting with SIRPα (Barclay & Van Den Berg, 2014). Notably, SIRPα was not present in the proteomic ACdEV datasets, therefore suggesting this effect is CD47-mediated and not SIRPα-mediated (Grant L. R., 2022). Intuitively, one would assume inhibition of CD47 would inhibit its 'don't eat me' function allowing 'eat me' signals to prevail, thereby promoting the uptake of ACdEVs but not impacting the chemoattraction process that relies on 'find me' signals (Poon e*t al.*, 2014b). This suggested the possibility of a new, undefined role of CD47 in the chemoattraction of MΦs.

In several experiments, MΦs that were exposed to Jurkat-derived apoptotic secretome clumped together which led to inaccurate counting by the in-built cell segmentation algorithm (Figure 5.1 and 5.2, Supplementary Figure 5.3) (Cytation 5, Biotek). This was not observed for antibody-blocked MΦs (Figure 5.3). Therefore, it was not a universal response to Jurkat-derived apoptotic secretome and may indicate the MΦs used in the prior experiments were stressed which may have changed their migratory behaviour. Indeed, a lower percentage of MΦs migrated towards unblocked Jurkat-derived apoptotic secretome in Figure 5.2B than Figure 5.1B which may represent uncontrolled differences in MΦ phenotype.

Blocking antibodies were incubated with apoptotic secretome with no removal of excess antibody which, therefore, may have bound directly to the MΦs and induced changes in migratory behaviour. Therefore, an additional migration assay was set up to determine if antibody blockade of the MΦ cells impacted their migration towards chemoattractive apoptotic secretome (Figure 5.3A). Indeed, migration of CD47-blocked and CD166-blocked MΦs towards apoptotic secretome

was significantly inhibited (Figure 5.3B and 5.3C). In the case of CD47, migration was inhibited in the presence of antibody-blocked apoptotic secretome and MΦs (Figure 5.2B and 5.3B). This suggests CD47 plays an important role in migration, however, we cannot determine with the set-up of this vertical transwell assay if its function is exhibited by CD47-expressing ACdEVs or solely at the surface of MΦs. If CD47 at the surface of ACdEVs does function as a chemoattractive molecule, the data suggested its role is compensated for by other chemoattractive molecules as equivalent migration was eventually achieved over time (Figure 5.2B). A similar observation was made when migration of neutrophils across an epithelial monolayer was delayed in the presence of an anti-CD47 blocking antibody, but the same number of cells as the control eventually migrated (Liu *et al.,* 2001). The role of CD47 in regulating cell adhesion and migration, and the underlying mechanisms, have been recently reviewed in (Polara *et al.,* 2024). CD47 promotes cell adhesion, motility, and migration across various cell types, including cancer cells, by interacting with integrins, thrombospondin-1 and G proteins to trigger intracellular signaling pathways that facilitate cellular mobility processes, such as cell spreading and focal adhesion formation (Polara *et al.,* 2024). However, these studies investigated the role of CD47 in inducing migration of the host CD47-expressing cell, as opposed to exposure at another cell/EV surface promoting the chemotaxis of neighbouring cells towards them. Indeed, there is little evidence to suggest CD47 functions as a chemoattractive factor. With this breadth of information describing the different mechanisms in which CD47 regulates cell migration, it seems likely that the delayed migration observed in this study in response to anti-CD47, was due to excess antibody resulting in blockade of CD47 at the surface of THP-1 MΦs. To investigate this, CD47 knockout cell lines could be utilised to observe the migration of CD47-deficient macrophages or to collect CD47-deficient EVs. This approach ensures that only either the cells or the EVs have CD47 present on their surface at any given time, allowing identification of where CD47 is functioning.

Whilst a significant short-lived delay in migration towards CD166-blocked apoptotic secretome was observed (Figure 5.2C), CD166-blockade of MΦs significantly delayed overall migration over 12 hours (Figure 5.3C). This suggested the role of CD166 in migration was more influential at the MΦ cell surface than at the ACdEV surface. It was not surprising that CD166 at the surface of ACdEV may not play a big role in chemoattraction, given the small proportion of THP-1-derived ACdEVs that displayed CD166 at the surface (Figure 4.6). Cell surface CD166 has many reported roles in mediating adhesion and migration of leukocytes, including across the blood-brain barrier, neuronal migration, epithelial migration and metastasis, (von Lersner *et al.,* 2019; Soto *et al.,* 2013; Cayrol *et al*., 2007; Masedunskas *et al*., 2006). CD166 can bind via homophilic interactions or to CD6 at the surface of cells (Hassan *et al.,* 2004). Therefore, it is possible ACdEV-associated

CD166 also signals via CD6. Monocytes express low levels of CD6, which could explain why migration wasn't prevented in the presence of CD166-blocked apoptotic secretome, as other mechanisms of chemoattraction are likely to dominate (Figure 5.2C) (Hassan *et al.,* 2004). An alternative approach to investigate the role of CD166 signalling could involve blocking CD6 on the surface of ACdEVs. However, CD6 was not present in ACdEVs derived from any of the immune cell lines (Jurkat, THP-1 and Mutu) according to our proteomics datasets (Grant L.R, 2022). Therefore, the immune cell lines used for modelling ACdEV interactions and macrophage responses were suboptimal for investigating the role of CD166. Future work should use ACdEVs from alternative cell sources that highly express CD166 or CD6 and if so, identify its role in CD166-CD6 interactions. Furthermore, the significant inhibition of macrophage upon incubation of macrophages with anti-CD166 blocking antibody suggested CD166 at the macrophage surface may bind an unknown ligand, that may be soluble or at the ACdEV surface, or that antibody incubation altered normal macrophage behaviour. It was important to consider the effect of preservatives present in the antibody preparations. 0.1% sodium azide was present in anti-CD47 and anti-CD166 antibody vials, which is known to impact cell viability (Vaux *et al.,* 1996) (see Table 2.4 for blocking antibody information). As CD166-blockade of apoptotic secretome didn't result in overall inhibition of MΦ migration and resulted in a short-lived delay in MΦ migration comparable CD31 and CD49d blockade (which were preservative-free), it was assumed sodium azide didn't significantly impact MΦ migration (Figure 5.2B). Furthermore, sodium azide has no impact on the phagocytic uptake of apoptotic cells (personal communication, Professor Andrew Devitt).

THP-1-derived apoptotic secretome induced migration of MΦs more rapidly than Jurkat-derived apoptotic secretome (Figure 5.1B, 5.2B, 5.2C, 5.3B and 5.3C). This could indicate that MΦs are more receptive to signals released by the same cell type as MΦs originated from the THP-1 cell line. Trends between EV cargo delivery and EV source have been demonstrated; preferential delivery of EV RNA transcripts to recipient fibroblasts was demonstrated by Jurkat, THP-1, HAEC amnion epithelium and fibroblast-derived EVs to transfer EV transcripts in an EV dose-dependent manner (over EVs derived from several other cell types, including BM-MSC, HEK293, HUVEC cells and others) (Hagey *et al.,* 2023). Therefore, the EV cell source may dictate potency of chemoattraction and efficiency of cargo delivery.

As our *in vitro* migration assay lacked ECM components, such as fibronectin, any ACdEV-ECM interactions related to chemotaxis could not be observed. Future work should observe macrophage migration in the presence of ECM components, such as embedding macrophages

into a 3D gel matrix composed of ECM components like fibronectin, collagen. This type of assay mimics the *in vivo* 3D extracellular matrix environment that monocytes encounter after leaving the 2D circulatory system (Gao *et al.*, 2021). Upon exiting the bloodstream, monocytes migrate into tissues, where they are exposed to signals that guide their movement and differentiation into macrophages, in a complex 3D environment. By simulating these conditions, this set up could provide a more physiologically relevant model for studying how macrophages respond to tissue-specific cues, such as the release of ACdEVs. This may be particularly relevant for the activity of CD49d at the surface of ACdEVs, which when dimerised with integrin subunit beta 1 (ITGB1) (forming VLA-4), has been implicated in the binding of fibronectin (Rieu *et al.,* 2000). Furthermore, EVs that bind fibronectin have been shown to modulate cell mobility and recipient cell interactions (Purushothaman *et al.,* 2016; Sung *et al.,* 2015).

5.4.2 Investigating interaction of ACdEVs with macrophages

To induce phenotypic behavioural changes in recipient cells, EVs interact with recipient cells either directly, by surface binding interactions or a combination of surface binding followed by intracellular uptake, or indirectly, by modulating the extracellular environment (Buzás *et al.,* 2018). Here, ACdEV binding or uptake by MΦ cells, broadly defined as direct 'interaction', was shown to occur rapidly in approximately 1 hour (Figure 5.1 and 5.2). Furthermore, MΦ cells continued to interact with ACdEV as ACdEV dose increased, even when 100% MΦ cells had interacted with ACdEV at lower doses (Figure 5.4C). This highlighted the capacity of MΦs to bind, engulf and process large quantities of ACdEVs. Notably, SEC-isolated ACdEVs retained their ability to interact with recipient MΦs, unlike their ability to chemotactically attractive MΦs, as discussed earlier (Figure 5.1 and 5.4). This suggested different molecules may be involved in mediating chemoattraction and surface binding/internalisation of ACdEVs.

To investigate the involvement of the candidate proteins in governing ACdEV binding or uptake, MΦs were incubated with ACdEVs at different temperatures: 37°C, 20°C and 4°C. Temperature acts as a non-specific inhibitor of endocytic processes, including phagocytosis (Torr *et al.,* 2011; Tomoda *et al.,* 1989). At 20°C, polymerisation of the actin cytoskeleton is disrupted (Almeida & Bolton, 1995; Los & Murata, 2004). Therefore, cytoskeleton-dependent endocytic processes are inhibited (Szewczyk-Roszczenko *et al.,* 2023). Furthermore, EV uptake by membrane fusion is promoted by an increase in temperature (Parolini *et al.,* 2009). Therefore, at lower temperatures, fusion events may be inhibited, possibly by a decrease in membrane fluidity. Interestingly, MΦs were still able to interact with ACdEVs at low temperatures of 20°C and 4°C, though to a lesser extent as temperature decreased, suggesting that these remaining interactions were likely

electrostatic, physicochemical interactions (Figure 5.5). However, kinetic energy is reduced as temperature decreases which may lower the rate of molecular diffusion within membranes or affect molecular conformations, and this may account for the decrease in ACdEV interaction we commonly observed between 20°C and 4°C (Figure 5.5) (Sanderson, 2012). Overall, this may indicate why the presence of a corona has been shown to both promote or inhibit EV uptake, given that the corona can dynamically alter the surface physicochemical properties of EVs (Liam-Or *et al.,* 2024; Dietz *et al.,* 2023; Abarca-Cabrera *et al*., 2021).

Antibody blockade of CD47 promoted the interaction of ACdEVs with MΦ cells at all three temperature conditions compared to unblocked ACdEVs (Figure 5.5A). The increased interaction between CD47-blocked ACdEVs and MΦ cells, compared to unblocked ACdEVs, was statistically significant at 37°C and 20°C (Figure 5.5A). This could suggest in the absence of CD47 signalling, ACdEVs are taken up intracellularly significantly more by recipient MΦ cells. This result supports our hypothesis that CD47 actively functions as an inhibitory 'don't eat me' signal at the surface of ACdEV, allowing 'eat me' signals to prevail in the presence of an anti-CD47 blocking antibody. Therefore, CD47 signalling may act to prevent the phagocytic internalisation of ACdEV by recipient cells. Indeed, inhibition of phagocytic EV uptake via the activity of CD47 and SIRPα has been demonstrated in multiple studies (Wei *et al.,* 2021; Belhadj *et al*., 2020; Kamerkar *et al.,* 2017). It is possible reliance on CD47 may depend on the mechanism of EV uptake. As CD47 is a potent inhibitor of phagocytosis of viable cells, its activity may potently inhibit phagocytic uptake of EVs but not necessarily other mechanisms of EV uptake; multiple mechanisms of EV uptake may occur simultaneously and depend on the recipient cell. Indeed, our experiments showed unblocked ACdEVs were readily taken up by THP-1 MΦ phagocyte cells, therefore, this is likely instigated by other surface molecules (Figure 4 and 5). One such molecule might be CD31, which has been reported to function as a 'don't eat me' signal on viable cells and as an 'eat me' signal on non-viable apoptotic cells (Vernon-Wilson *et al.,* 2006; Brown *et al*., 2002). Antibody blockade of CD31 significantly inhibited interaction of ACdEV with MΦs at 37°C (Figure 5.5B). No significant difference was observed at 20°C and 4°C, indicating that CD31 is likely to be involved in the internalisation of ACdEVs. On a viable cell, homophilic binding of CD31 with a phagocyte induces detachment and prevention of phagocytosis (Vernon-Wilson *et al.,* 2007). During apoptosis, CD31 undergoes a functional switch, whereby homophilic binding of CD31 promotes attachment of phagocytes to apoptotic cells for their integrin-dependent phagocytic removal (Vernon-Wilson *et al.,* 2006). As such, the results of this experiment suggest CD31 at the ACdEV surface, akin to an apoptotic cell, may function as an 'eat me' signal promoting phagocytic uptake of ACdEVs (Figure 5.5B). Furthermore, this suggests that the activity of CD47 is unlikely to completely prevent

phagocytic uptake of ACdEVs; perhaps these molecules are in competition with one another to exert their opposing functions.

Interaction of CD49d-blocked ACdEV with MΦ cells was also significantly inhibited at 4°C compared to 37°C (Figure 5.5A). This suggested CD49d may be involved in the internalisation of ACdEVs by recipient MΦ cells. Indeed, the involvement of integrins in EV uptake has been observed in several scenarios (French *et al.,* 2017; Mulcahy *et al.,* 2014). Specifically, CD49d was reported to be recruited by the tetraspanin, TSPAN8, which together were implicated in the uptake of tumour-derived EVs into recipient endothelial cells (Nazarenko *et al.,* 2010). Notably, TSPAN8 was not identified in our proteomic datasets, and therefore, ACdEVs must have been internalised by alternative mechanisms which appear to involve CD49d (Figure 5.5A) (Grant L. R., 2022). Interestingly, uptake of melanoma-derived EVs has previously been shown to be dependent on VCAM-1, a ligand of VLA-4 which is formed by the dimerisation of CD49d and integrin b1 subunit (ITGB1) (Leary *et al.,* 2022). Therefore, VLA-4 may initiate ACdEV internalisation and act as an 'eat me' signal through this interaction. No significant effect in ACdEV interaction was observed in the presence of anti-CD166 blocking antibody (Figure 5.5B). Notably, CD166 has been reported as a key molecule facilitating the binding and subsequent uptake of colorectal cancer cell-derived EVs and ovarian cancer cell-derived EVs (Cardeñes *et al.,* 2022). Therefore, this supports the previous hypothesis made in Chapter 4 that multiple immunoglobin superfamily (IgSF) members may undertake a level of functional redundancy; CD166 may be essential in mediating certain EV interactions with recipient cells, depending on the cell types involved. Here, our results suggest CD166 is not a key mediator of THP-1-derived ACdEV interactions with THP-1 MΦ cells and given that only a small population of ACdEVs displayed CD166, this is perhaps not surprising (Figure 4.6C and 5.5B). Notably, the authors reported that blocking CD166 at the EV surface in addition to the recipient cell surface further inhibited EV uptake, suggesting CD166 engaged in heterophilic interactions as well as possibly homophilic interactions. This further highlights the versatility of IgSF members that have a wide variety of interaction partners.

A 500 ACdEV : MΦ cell dose was chosen to allow room to observe inhibition or promotion of ACdEV : MΦ interactions in the presence of blocking antibodies (Figure 5.5). Interestingly, one study showed that high doses of EVs (200,000 EV : cell ratio) from several different cell origins, induced a generic cellular response, irrespective of the EV origin (Hagey *et al.,* 2023). This included upregulated lysosomal activity and downregulated exocytosis, suggested to be caused by overwhelming the recipient cell's molecular machinery involved in endocytosis/exocytosis. In

contrast, low EV doses (20 EV : cell ratio), likely to be more physiologically relevant, induced EV-originating cell-specific changes (Hagey *et al.,* 2023). A 2000 EV : cell ratio was also tested and shown to induce changes in gene expression that were more similar to the changes observed upon treatment at a 200,000 EV : cell ratio than at a 20 EV : cell ratio (Hagey *et al.,* 2023). Cells can take up EVs by multiple different mechanisms (Szewczyk-Roszczenko *et al.,* 2023). Therefore, it remains unknown whether the 500 ACdEV : cell dose used in these ACdEV interaction experiments altered the mechanism in which MΦ cells interacted with and endocytosed ACdEVs, something that was not investigated by the authors. For example, an increased concentration of ACdEVs may promote the formation of aggregates, which may be preferentially taken up by phagocytosis, a pathway that can process large cellular debris and even whole cells (Poon *et al.,* 2014b). Phagocytosis actively modulates phagocyte phenotype; therefore, the pathway of ACdEV uptake may alter recipient cell functions as well as the ACdEVs, themselves (Fadok *et al.,* 1998).

As a complete inhibition of interaction between ACdEVs and MΦs was not observed, even at 4°C when active cell processes are disrupted and membrane fluidity is altered, this suggested that the remaining interactions were most likely electrostatic and physicochemical binding. These could have been mediated by the candidate proteins (CD31, CD47, CD49d, CD166), in addition to other molecules, such as phosphatidylserine (PS), a well-defined 'eat me' signal at the surface of apoptotic cells which may have facilitated binding as it is commonly enriched in the outer leaflet of EV membranes (Buzás *et al.,* 2018; Poon *et al.,* 2014b). Indeed, many different molecules have been implicated in EV binding and/or uptake, including tetraspanins, integrins, proteoglycans, lectins and cholesterol (likely due to its enrichment in lipid rafts) (Esmaeili et al., 2022; French et al., 2017). This highlights the complexity of EV uptake and suggests that EV internalisation may be regulated by multiple different molecules facilitating uptake by multiple different pathways. A more targeted inhibition of binding/internalisation processes would be beneficial for deciphering the exact nature of interaction mediated by each candidate protein. Directed inhibition against specific pathways of endocytosis have been proven effective, such as targeting the clathrin terminal domain with 'pitstop' small molecule inhibitors to prevent the recruitment of adaptor proteins and block clathrin-mediated endocytosis, or by mutating the plextrin homology domain of dynamin, a protein that mediates vesicle scission in multiple endocytic pathways (Szewczyk-Roszczenko *et al*., 2023; von Kleist *et al*., 2011; Vallis *et al.,* 1999). Alternatively, disruption of lipid raft assembly, such as by cholesterol depletion (a lipid often enriched in lipid rafts), may provide insight in the contribution of lipid raft-mediated endocytosis to ACdEV uptake. This type of approach may be helpful for discerning between endocytosis versus direct fusion mechanisms

or discerning between different endocytic pathways of ACdEV uptake, as well as the possible involvement of the candidate proteins in regulating these processes. Additionally, multiplexing of blocking antibodies would help us to better understand the relationship between individual protein functions in ACdEV binding – for instance, what mechanism of ACdEV interaction might take place if the activity of both CD47 and CD31 was inhibited?

This experiment utilised flow cytometry to report ACdEV interaction with MΦs, relying on the assumption that an increase in fluorescence was indicative of increased interaction (Figure 5.4 and 5.5). Importantly, some dyes may reversibly bind and result in transfer of fluorescence across biological membranes. For example, MemGlow™ is a lipophilic dye that intercalates lipid bilayers, and has been suggested to transfer from fluorescently labelled EVs to recipient cell membranes upon transient interaction (Loconte *et al*., 2023). For this reason, BODIPY™ FL maleimide was chosen over MemGlow™ 488 to label of ACdEVs in our interaction assay, as maleimide binds to free thiol groups forming a stable thioester bond that is not pH sensitive and therefore, not readily reversible under physiological conditions (Hermanson, 2013). Notably, the choice of labeling technique and method of detection can also indicate the nature of EV interaction, revealing surface binding, internalisation of intact EVs, or delivery of EV cargo. By implementing imaging flow cytometry, Loconte *et al.,* reported that carboxyfluorescein succinimidyl ester (CFSE), a membrane permeable dye which can bind intraluminal EV esterases, could reveal puncatate fluorescence and homogenous fluorescence inside cells, interpreted as intact EVs or released EV cargo, respectively (Loconte *et al.,* 2023). Whereas, EVs labelled by a GFP-tagged reporter system (localised signal to the inner leaflet of the EV membrane by myristoylation and palmitoylation signals) were only detected as a small population of intracellular punctate signals, hypothesised to represent recently internalised intact GFP-tagged EVs, and other signals may have quickly been lost by EV degradation or fluorophore quenching (Loconte *et al.,* 2023). This highlighted that different methods of EV labelling could indicate different types of EV interactions and therefore, must be carefully interpreted. Going forward, multiple methods of labelling and detection used in parallel may provide a broader view of ACdEV interaction with recipient cells.

5.4.3 Macrophage phenotype in response to ACdEVs

Plasticity is an essential feature of macrophages, enabling them to shift from a pro-inflammatory M1 state to an anti-inflammatory or pro-repair M2 state, which is key to resolving inflammation (Hristodorov *et al.,* 2015; Sindrilaru *et al*., 2011). To provide insight into how ACdEVs might modulate the phenotype of macrophages, a flow cytometric macrophage phenotyping assay was set up utilising both an immortalised cell line (THP-1 cells) and primary human monocytes (Figure

5.7 and 5.8). *In vitro* macrophage polarisation aimed to produce typical M1 and M2 phenotypes, that are likely an oversimplification of macrophage phenotype *in vivo* (Ginhoux *et al*., 2015). The aim was to avoid permanent polarisation of the cells so that the *in vitro* M1 and M2 cells maintained a level of plasticity that is physiologically relevant. This was to provide a framework within which to observe whether ACdEVs skewed unpolarised M0 macrophages towards or away from a pro-inflammatory M1 or pro-resolving M2 phenotype. Irrespective of the nomenclature, the ability of ACdEV to impact the surface phenotype is of value when compared to that of *in vitro*-stimulated MØ.

5.4.3.1 THP-1 model of macrophage phenotype

Using the THP-1 monocyte cell line, M0 MØs were defined by differentiation with PMA for 48 hours, followed by polarisation treatments with IFN and LPS or IL-4 and IL-13 for 48 hours, to polarise M0 cells into M1 and M2 cells, respectively (Figure 5.7A). In addition, M0 cells were incubated with Jurkat-derived late ACdEVs for 48 hours to identify whether ACdEVs modulate MØ phenotype to resemble M1 or M2 cells. Firstly, in the THP-1 model, CD14 and CD40 were significantly upregulated in M1 cells (Figure 5.7B). CD14 is a pattern recognition receptor, sensitive to LPS and other microbial molecules, and a receptor for apoptotic cells that triggers phagocytic clearance (Devitt *et al.,* 1998; Ulevitch & Tobias, 1995). It is widely expressed at the surface of macrophages, hence it was used as a marker of differentiated macrophages in this project (Supplementary figure 5.2) (Basu Mallik *et al.,* 2018). Upregulation of CD14 is associated with M1 cells that have known functions in targeting microbial infection (Sica & Mantovani, 2012). Indeed, in this project M1 cells were polarised by treatment with LPS (and IFNγ), a known inducer of CD14 expression (Landmann *et al.,* 1996).

CD40 is expressed on the surface of antigen-presenting cells (APCs), including macrophages, and plays an important role in governing T cell-mediated activation of APCs (Suttles & Stout, 2009). The CD40 ligand (CD154) is expressed at the surface of T-helper cells which upon binding CD40, results in M1 cell activation (Stout *et al.,* 1996). Furthermore, macrophages increase CD40 expression in response to exposure to IFNγ, which further promotes their activation state (Alderson *et al.,* 1993). This likely explains the large significant increase in CD40 expression at the surface of M1 cells observed in this THP-1 macrophage phenotyping assay, as M1 cells were polarised by treatment with IFNγ and LPS (Figure 5.7B). As such, CD40 was a clear marker of M1 cells. Notably, there was no significant difference in the expression of CD14 and CD40 between M2 cells and M0s cell that had been treated with ACdEVs, suggesting ACdEVs don't promote M1 activation (Figure 5.7B). Furthermore, there was a significant increase in CD14 and

CD40 expression comparing M0s to M0s treated with ACdEVs, indicating ACdEVs may promote some level of cell activation resulting in the upregulated expression of receptors.

CD11b is an integrin alpha M subunit that binds to integrin beta 2 subunit (CD18), which together mediate cell adhesion and migration. Activation of CD11b promotes polarisation of primary murine macrophages to an M1 phenotype by inducing transcriptional changes, mediated by microRNA Let7A (Schmid *et al.,* 2018). Therefore, this suggests upregulation of CD11b expression at the cell surface would indicate an M1 phenotype. The complement system facilitates the opsonisation of apoptotic cells, enhancing their clearance by phagocytes through complement receptor 3 (CR3), which is formed by integrins CD11b and CD18 (Mevorach *et al.,* 1998). Schif-Zuck *et al.* showed that primary murine M1-like macrophages exhibited increased cell surface expression of CD11b, whereas, M2-like macrophages, which secreted pro-resolving lipoxygenases, had reduced CD11b expression (Schif‐Zuck *et al.,* 2010). These M2-like macrophages had previously ingested apoptotic material, after which their phagocytic capability was reduced, likely due to the downregulation of CD11b (Schif‐Zuck *et al.,* 2010). However, in the THP-1 model, CD11b was significantly upregulated at the surface of M2 cells (Figure 5.7B). Therefore, the THP-1 M2-polarised cells in this model may exhibit phagocytic behaviour, which may be indicative of pro-inflammatory functions. Therefore, may not be an accurate representation of the M2 phenotype, indicating a limitation of the THP-1 model. Alternatively, CD11b may act differently in murine macrophages to human macrophages; it has been suggested the CD11b is a marker of murine M1 macrophages and murine markers are insufficient for characterisation of human macrophages (Monnier *et al.,* 2022). Furthermore, primary human M2 cells been shown to be more efficient at phagocytosis than M1 cells *in vitro* (Chinetti-Gbaguidi *et al.,* 2011; Leidi *et al.,* 2009). CD11b is an example molecule that highlights the needs for multiple metrics to effectively define macrophage phenotype.

CD206 and CD209 are considered markers of M2 polarised murineand human macrophages (Smith *et al.,* 2016; Puig-Kröger *et al.,* 2004). CD206 is a mannose scavenger receptor that unexpectedly, was significantly upregulated on the surface of M1 polarised cells compared to M2 polarised cells (Figure 5.7B). Interestingly, one study showed that mouse bone marrow derived macrophages treated with IFNγ and LPS to promote M1 activation, as done in this project with human MØ, gradually progressed to an M2 phenotype with increased CD206 expression coinciding with decreased CD86 expression (Smith *et al.,* 2016). CD86 is a co-stimulatory molecule functioning in T cell activation, and its expression is associated with an M1 phenotype in both human and murine cells (Smith *et al.,* 2016; Sharpe, 2009). The authors reported a

significant increase in CD206 expression in M1 compared to M2 cells at 96 hours post treatment and a significant decrease in CD86 expression in M1 compared to M2 cells at 48 hours post treatment (Smith *et al.,* 2016). This could partly explain the expression profile of CD206 as well as CD86, in which there was no significant different between M1 and M2 cells (Figure 5.7B). Notably, ACdEV-treated M0s expressed significantly less CD86 that M1 and M2 cells and significantly more than M0s, which again suggested ACdEVs may contribute to promoting an intermediate phenotype (Figure 5.7B). This further highlights that the MØ polarisation model of M1 and M2 phenotypes is a continuum, allowing us to observe how ACdEVs influence MØ phenotype.

CD209, otherwise known as Dendritic Cell-Specific Intercellular adhesion molecule-3-Grabbing Non-integrin (DC-SIGN), is a C-type lectin receptor which binds mannose-type glycosylation patterns, present on PAMPs, as well as adhesion molecules such as ICAM-3, a molecule implicated in apoptotic cell clearance (Torr *et al.,* 2011; Domínguez-Soto *et al.,* 2011). CD209 expression is driven by IL-4 (used in this THP-1 macrophage model, Figure 5.7A) (Domínguez-Soto *et al*., 2011). In our THP-1 macrophage model, M2 cells had significantly increased CD209 expression, supporting the use of CD209 in the human THP system as a possible marker of M2 MØ as polarised by IL-4/IL-13 (Figure 5.7B). Meanwhile, the expression of CD209 on ACdEV-treated M0 cells was significantly lower than M2 cells but significantly higher than M0 and M1 cells, again indicating that ACdEV-treated M0 cells present as an intermediate phenotype.

CD64 is an Fc γ receptor which binds IgG of antibody-opsonised cells/pathogens to mediate phagocytosis (Fanger *et al.,* 1996). Whilst also expressed on M2 cells, expression is reportedly upregulated on the surface of M1 cells and inhibition of CD64 results in the elimination of M1 cells but has no effect on M2 cells (Hristodorov *et al.,* 2015). As such, it is regarded as a marker of M1 polarisation. However, in this THP-1 model, there was no significant difference in CD64 expression between M0 and M1 or M1 and M2 cells (Figure 5.7B). Furthermore, ACdEV-treated M0s exhibited the highest level of expression which was significantly increased compared to M0, M1 and M2 cells. This provided more evidence that M1 and M2 cells in this model may not be an accurate representation of *in vivo* phenotypes, and ACdEVs may induce pro-inflammatory functions in M0 cells.

Taken together, the THP-1 model revealed varied expression profiles of the macrophage markers, with some in agreement with the literature (CD14, CD40, CD209) and some showing unexpected results (CD11b, CD64, CD86, CD206) (Figure 5.7). Macrophage phenotype is exceptionally complex. This *in vitro* model depended on a multitude of confounding variables that can affect cell

activation, to name a few: the combination of treatments, including the initial differentiation treatment with PMA, the concentration and timing of treatments, potential intrinsic quirks of the THP-1 immortalised cell line, the passage of the cell line, the lot of foetal bovine serum (FBS) and the tissue culture plastic (non-tissue culture treated) (see Chapter 2. Materials and Methods). Nonetheless, PCA revealed the M0, M1 and M2 phenotypes within the experimental system developed and tested here were distinctly separated which provided a framework to assess phenotypic changes induced by ACdEVs (Figure 5.7C). From this, ACdEV-treated M0s appeared to skew away from an M1 phenotype and skewed between an M0 and M2 phenotype (Figure 5.7C). This suggested ACdEVs may induce a unique macrophage phenotype that share properties with both unstimulated M0 and pro-resolving M2 cells.

5.4.3.2 Primary human monocyte model of macrophage phenotype

To use a more physiologically relevant model, a primary human model was established, utilising primary monocytes that underwent *ex vivo* differentiation into M0 macrophages, referred to as 'pM0s' (Figure 5.8). Primary cells are more representative of *in vivo*, as they lack the genetic alterations associated with an immortalised cell line, which may alter cellular behaviours and retain donor heterogeneity. Notably, heterogeneity makes reproducibility and interpretation of results more challenging, often requiring a greater number of donors for biological replicates. Here, due to time limitations, monocytes were isolated from just four healthy donors (Figure 5.8).

Primary monocytes are routinely differentiated by treatment with GM-CSF, a cytokine, as opposed to VD3 or PMA treatment for THP-1s, as VD3 has been shown to induce differentiation of dendritic cells and PMA is a PKC activator that results in non-specific macrophage activation that may not be physiologically relevant (Ferreira *et al.,* 2014). A six day treatment of GM-CSF was used to differentiate primary monocytes into macrophages (pM0s), which is a routine method of differentiation for primary cells (see Chapter 2, section 2.2.1.2) (Vogel *et al.,* 2014). pM0s were polarised by the same method as for the THP-1 model: IFN and LPS or IL-4 and IL-13 for 48 hours, to polarise M0 cells into M1 and M2 cells, respectively. In addition, pM0s were incubated with ACdEVs for 48 hours with or without the addition of blocking antibodies against CD31, CD47, CD49d or CD166. As the resulting polarised macrophages were not tested for functionality, the pM0 cells treated with IFN and LPS will be referred to as primary M1 cells (pM1s) and the pM0 cells treated with IL-4 and IL-13 will be referred to as primary M2 cells (pM2s).

CD209 was excluded from analysis as negligble expression resulted in an insufficient compensation control (data not included). Indeed, GM-CSF treatment has been shown to downregulate CD209 expression, showing the importance in carefully selecting differentiation and

polarisation treatments (Puig-Kröger *et al.,* 2004). Subsequently, the expression of just one M2 marker, CD206, was characterised in the primary model (Figure 5.8B and 5.8C). Due to the complexity of macrophage phenotype, the reliance on one marker for M2 polarisation was suboptimal and future work should aim to optimise the staining for several M2 markers, such as stabilin-1, CD163 or CD180 (Vogel *et al.,* 2014). Furthermore, the use of beads for compensation controls may be more appropriate as they are generally brighter and so should prevent future overcompensation problems.

As each macrophage marker has already been introduced when discussing the THP-1 macrophage model, just the relationship of marker expression with each polarised phenotype and each ACdEV treatment, in relation to the candidate proteins, as well as comparison between the THP-1 and primary cell model, will now be discussed.

M1 markers CD40, CD64 and CD86 were significantly upregulated in the pM1 cells compared to every other condition, unlike the THP-1 model in which just CD14 and CD40 expression was significantly upregulated in M1 cells (Figure 5.7B and 5.8B). Surprisingly, there was no significant difference in CD14 expression across the conditions in the primary cell model, despite exposure of pM0 cells to LPS for M1 polarisation which is known to upregulate CD14 expression (Landmann *et al.,* 1996) (Figure 5.8B). Furthermore, pM1 cells exhibited the lowest expression of CD14 and this was conserved across donors. A similar trend was observed for M1 marker CD11b (Figure 5.8B). The variability between donors was particularly evident for these markers, so more donors are required to characterise their expression. Nevertheless, CD11b and CD14 were not upregulated at the surface of pM1 cells in this primary cell model.

The M2 marker, CD206, was more highly expressed on pM0 cells and less expressed on pM1 cells, although not statistically significant (Figure 5.8B). Whilst characterisation of more donors may reveal statistical significance, this suggested a typical M2 phenotype may not have been induced in this primary model.

All together, the primary macrophage model seemingly induced a M1-like phenotype by significant upregulation of CD40, CD64 and CD86. However, the establishment of an M2-like phenotype was unclear, partly attributed to the lack of M2 markers measured in this experiment. Nonetheless, PCA revealed pM0, pM1 and pM2 cells were phenotypically distinct, with pM0 and pM2 cells spatially located more closely together, indicating some level of similarity (Figure 5.8C). Furthermore, pM0s treated with each ACdEV condition (unblocked or blocked) were closely clustered together, indicating a high level of similarity. Indeed, there was no significant difference

in the expression of any of the macrophage markers between ACdEV conditions to which MØ were exposed (Figure 5.8B). This may suggest that the ACdEV surface-expressed proteins CD31, CD47, CD49d and CD166 are not essential for ACdEV-mediated modulation of macrophage phenotype (though they may be important for chemoattraction or binding of ACdEV to MØ). As inhibition of ACdEV interaction was observed in the presence of anti-CD47 blocking antibody, it is likely uptake was also partially inhibited in the pMΦ model but this had no observed impact on phenotype, perhaps due to the deliberately high ACdEV dose that was administered (Figure 5.6 and 5.8) (Supplementary table 5.1).

Interestingly, the ACdEV-treated pM0s were distinctly separate from pM0, pM1 and pM2 cells, indicating they represented a unique intermediate macrophage phenotype (Figure 5.8C). Murine macrophages have been shown to exhibit 'mixed' M1 and M2 phenotypes *in vitro* when exposed to combination polarisation treatments (*i.e.* MØ exposed to M1 and M2 polarisation treatments simultaneously) (Smith *et al.,* 2016). Furthermore, the expression of M1 markers gradually diminished but M2 marker expression was persistent, suggesting pro-inflammatory stimuli promoted a long-term pro-resolving M2 phenotype (Smith *et al.,* 2016). Future work may benefit from measuring ACdEV-treated human pM0s over multiple days to observe how marker expression changes, and as such, how macrophage phenotype may change over time.

Overall, the macrophage phenotyping models allowed us to make hypotheses about the functional output of ACdEVs in modulating macrophages (Figure 5.7 and 5.8). Importantly, these hypotheses assumed that cell surface expression indicated phenotype, which should be questioned (Murray, 2017). Macrophage phenotype is complex and dynamic, therefore to make these assumptions more robust, multiple methods of phenotyping should be carried out, such as transcriptional profiling, monitoring of metabolic changes or characterisation of the release of soluble factors, such as cytokines. Advancements in single cell profiling have allowed higher resolution multidimensional phenotyping of macrophages which will pave the way to identifying different macrophage subpopulations (Ginhoux *et al.,* 2015). Furthermore, assuming the polarised 'M1' and 'M2' cell types generated *in vitro* are not permanently polarised and retain their plasticity, it would be valuable to investigate whether treating M1-polarised macrophages with ACdEVs could induce a phenotypic shift towards an M2-like phenotype. This may reveal more information of the role of ACdEVs in regulating macrophage plasticity and their transition to an M2 phenotype that is observed during resolution of inflammation (Ortega-Gómez *et al.,* 2013).

5.4.4 Conclusions

This chapter has demonstrated that apoptotic secretome containing apoptotic cell-derived extracellular vesicles (ACdEVs) induce macrophage migration, ACdEVs interact with macrophages in a dose-dependent and temperature-dependent manner and promote a distinct macrophage phenotype in both THP-1 and primary cell macrophage models. Furthermore, these results have identified specific surface proteins that are involved in mediating surface interactions between ACdEVs and recipient macrophages, but don't alter phenotype, according to our macrophage phenotyping assay. CD166 is likely involved in macrophage migration at the cell surface but ACdEV surface-expressed CD166 is not, at least not in the THP-1 cell system where CD166 is lowly expressed at the surface of ACdEVs. The potential involvement of CD47 in macrophage migration was identified but it was hypothesised that excess antibody may have prevent macrophage migration by binding at the cell surface. CD47 was suggested to play an inhibitory role in ACdEV interaction with macrophages, whereas CD31 and CD49d was suggested to promote interaction with ACdEV. Interestingly, CD31, CD47, CD49d, and CD166 did not seem to influence the modulation of macrophage phenotype, suggesting other surface molecules or delivery of intraluminal ACdEV cargo may be responsible instead.

Together, this suggests that macrophage migration, binding/uptake of ACdEVs and macrophage phenotypic changes may be mediated by a variety of molecules as part of distinct processes. Strikingly, SEC abolishes the chemoattractive properties of ACdEVs but not interaction of ACdEVs and macrophages or the ability of ACdEVs to induce a phenotypic change in recipient macrophages. Although the candidate proteins may be involved, we hypothesise the ACdEV corona is crucial for the chemoattraction process. Future work should identify the effect and composition of ACdEV coronas on ACdEV-macrophage interaction and phenotype, given that the presence of a corona has previously been shown to modulate uptake and recipient cell responses (Liam-Or *et al.,* 2024; Dietz *et al.,* 2023; Tóth *et al*, 2021).

It is also important to consider the impact of the ACdEV dose on macrophage phenotype. As the precise mechanisms for inducing phenotypic changes in macrophages remain unclear, lower doses of ACdEVs should be tested to better represent physiological levels and higher doses should be tested to increase the likelihood of ACdEV cargo delivery (Hagey *et al.,* 2023). To better characterise macrophage phenotype in response to ACdEVs, multiple parallel phenotyping techniques should be carried out, including cytokine profiling, metabolomic and transcriptomic analysis. Additionally, further studies should explore the potential effects of the ACdEV corona on signalling, especially since SEC was used in all functional assays (except the transwell migration

assays), possibly affecting the ACdEV surface and its functional implications. Furthermore, to confirm the antibody blockade results observed in this project, alternative methods for protein blockade should also be implemented, such as CRISPR/Cas9 gene editing or siRNA. This would avoid the implications of unbound excess antibody or preservatives and remove the assumptions made of effective protein activity blockade and specificity in binding.

Finally, future work should determine if ACdEVs from different cell sources trigger cell-specific functions, as immune cell-derived EVs has been shown to deliver cell source-specific RNA transcripts (Hagey *et al.,* 2023). Understanding the influence of the cellular source and dose of ACdEVs on macrophage responses will be crucial for increasing our knowledge of ACdEV-mediated modulation of the immune system to advance therapeutic applications.

5.5 Supplementary Data

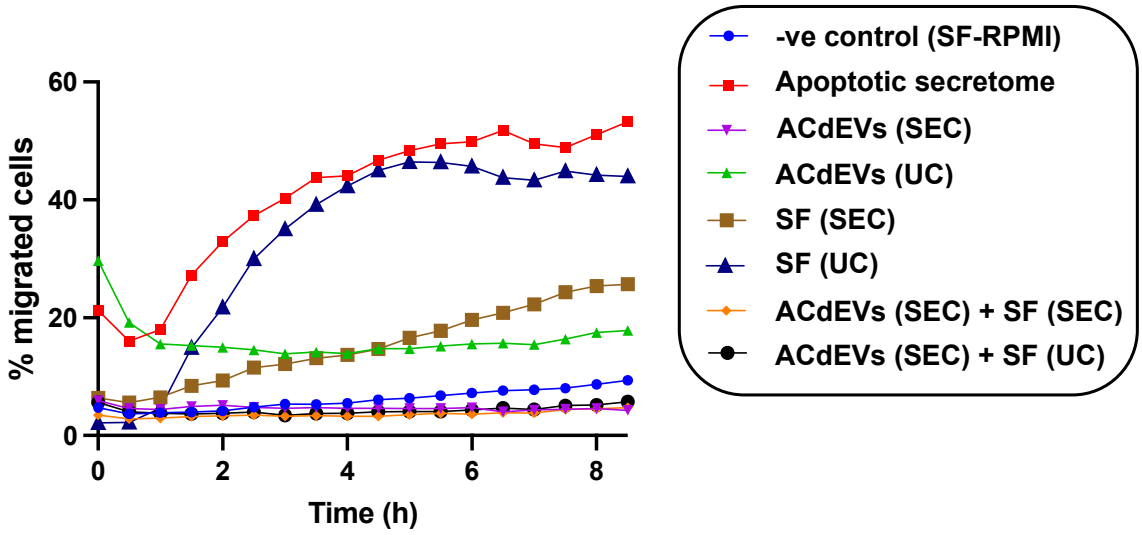

Supplementary Figure 5.1: Evaluation of the chemoattractive properties of different components of the apoptotic secretome processed by size-exclusion chromatography (SEC) or ultracentrifugation (UC). Jurkat T cells (8 x 10^7) in 20 mL of serum-free RPMI medium were induced to undergo apoptosis via UV irradiation (100 mJ/cm^2). The apoptotic secretome was collected 18 hours later (2000 x g, 20 minutes). Equal volumes (4.5 mL) of the Jurkat-derived apoptotic secretome were either concentrated and loaded onto a SEC column or subjected to ultracentrifugation (100,000 x g, 1 hour, 4°C). SEC fractions 7-13 were pooled, containing the ACdEVs in a 3.5 mL volume, and SEC fractions 14-28 were pooled, referred to as soluble factors (SF (SEC)). The ACdEV UC pellet was resuspended in 3.5 mL, and the UC supernatant containing soluble factors was collected (SF (UC)). Additionally, to determine whether the chemoattractive properties of ACdEVs could be restored by 'coating' with chemoattractive soluble factors, equal volumes of SEC-isolated ACdEVs were incubated for 15 minutes at room temperature with SF (SEC) or SF (UC), followed by another ultracentrifugation step (100,000 x g, 1 hour, 4°C). THP-1 macrophages (8 x 10^4) were seeded into a transwell chamber with each SEC or UC sample, along with apoptotic secretome or serum-free RPMI medium placed at the bottom of the wells. The number of macrophages that migrated into the lower chamber of the transwell assay was counted per field of view (FOV) after 8.5 hours and normalized to a control well containing only macrophages (no transwell). Wells were plated in triplicate (N = 1 biological replicate). Imaging was performed using the Cytation 5 Cell Imaging Multimode Reader (Biotek).

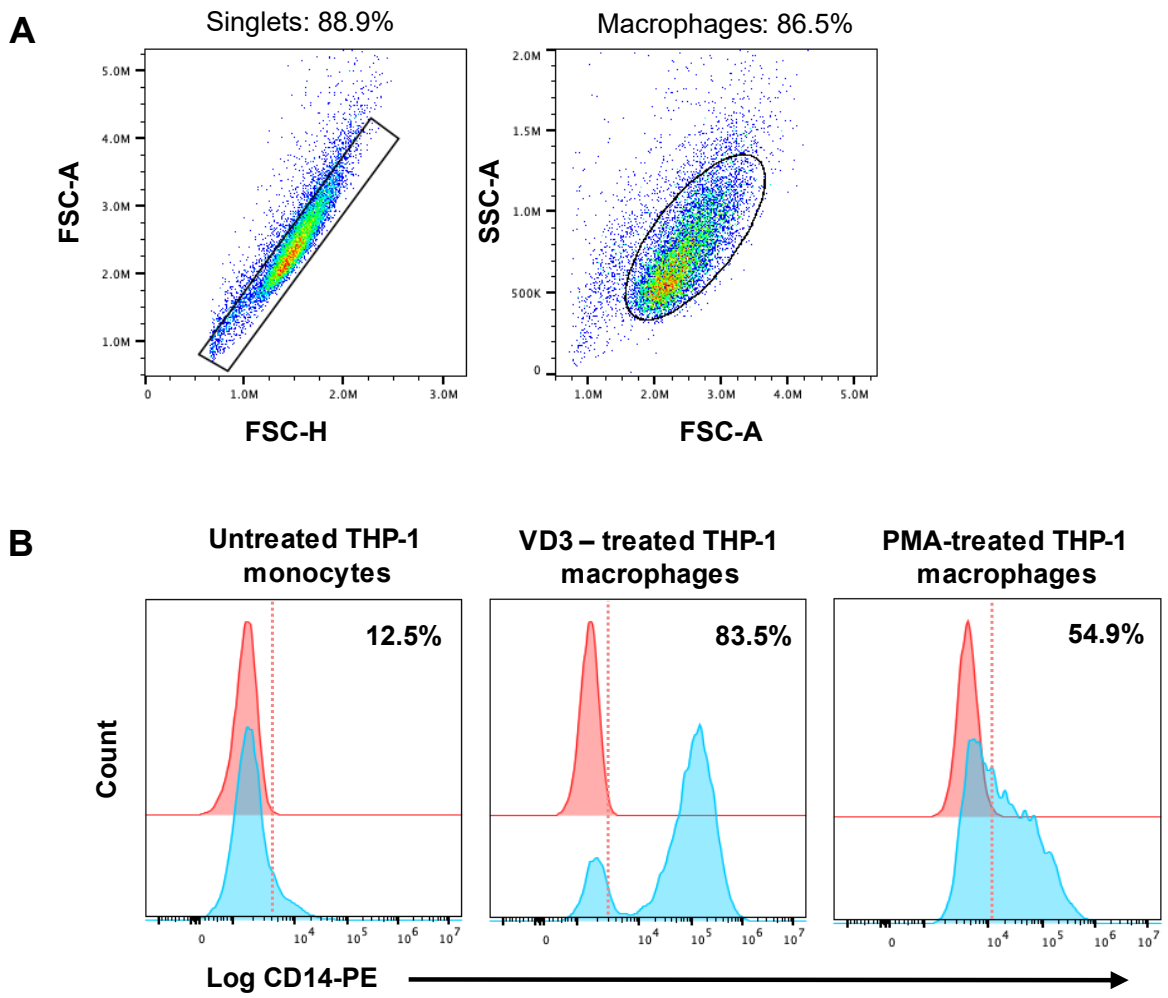

Supplementary figure 5.2: Differentiation of THP-1 macrophages by 1,25-dihydroxyvitamin D3 (VD3) or phorbol 12-myristate 13-acetate (PMA) upregulated the expression of CD14, in line with Thomas (2011). THP-1 monocytes were treated with 100 nM VD3 or 10 ng/mL PMA and measured for CD14 expression 48 hours later. A) Representative flow cytometry gating strategy, gating for singlets (FSC-H vs FCS-A) and live cells (FSC-A vs SSC-A). B) Representative flow cytometry histograms showing percentage THP-1 cells positive for CD14 (blue) upon no treatment, VD3 treatment and PMA treatment (N = 1). Isotype control (IgG1κ-PE) (red) was used to set gate with < 2 % false positive threshold.

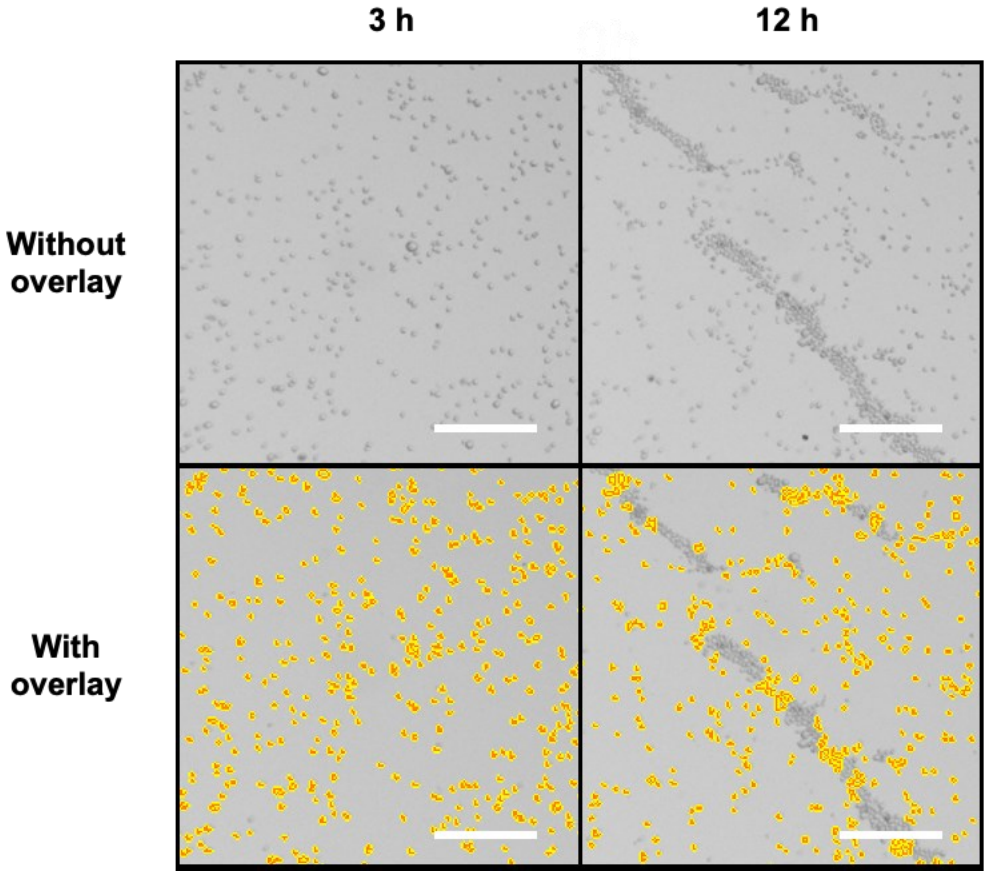

Supplementary Figure 5.3: THP-1 macrophage clumping increased with time and caused an under representation in cell counts. The Cytation 5 software (Gen5) in-built cell segmentation algorithm failed to accurately discriminate cells that had clumped together (segmented cells shown as yellow overlay). Representative images of THP-1 macrophages 3 hours and 12 hours post plating into vertical transwell assay. Images taken at x10 magnification on Cytation 5 Cell Imaging Multimode Reader, Biotek. Scale bar ~300 µm.

ACdEV sample	ACdEV : pM0 ratio
Unblocked Jurkat ACdEV	527:1
CD47-blocked Jurkat ACdEV	691:1
CD49d-blocked Jurkat ACdEV	971:1
Unblocked THP-1 ACdEV	4580:1
CD31-blocked ACdEV	3720:1
CD166-blocked ACdEV	2817:1

Supplementary Table 5.1: ACdEV : primary monocyte-derived macrophage (pM0) ratio for each ACdEV condition. For incubation with blocking antibodies, antibodies were incubated (10µg / mL) with 500 µL concentrated apoptotic secretome (collected from 4 x 10^7 cells in 10 mL sfRPMI medium) for 30 mins at 4°C. Blocked ACdEVs were isolated and excess unbound antibody was removed, simultaneously, by SEC (qEV Original, Izon). ACdEV concentrations were determined by labelling with MemGlow™ 488 and measuring by nano-flow cytometry (NanoAnalyzer, NanoFCM). Ratios represented to the nearest whole number.

Chapter 6 Concluding remarks

EV release is a highly conserved and vital mechanism utilised by cells to communicate and transport complex molecular cargo. This process is fundamental to cellular interaction across various physiological and pathological contexts. Apoptosis is a highly regulated form of cell death that is essential for maintaining tissue homeostasis, during which, apoptotic cells release EVs in large quantities, including large apoptotic bodies (> 1 μm) and small apoptotic cell-derived extracellular vesicles (ACdEVs) (< 1 μm) (Skovronova *et al.,* 2021; Poon *et al*., 2014b). There is growing recognition that ACdEVs may serve as important regulators of inflammation (Grant *et al.,* 2019; Caruso & Poon, 2018). ACdEVs have been shown to potently attract immune cells to promote apoptotic cell clearance (Torr *et al.,* 2011; Truman *et al.,* 2008; Segundo *et al.*, 1999). In addition, multiple groups have shown that ACdEVs modulate the phenotype of immune cells to promote their anti-inflammatory pro-resolving functions, highlighting their ability to control immune responses (Zhu *et al.,* 2023; Li *et al.,* 2022; Liu *et al.,* 2020; Shen *et al.,* 2017; Fehr *et al.,* 2013). Despite being the most abundant type of EV released during apoptosis, remarkably little is understood about their biogenesis or the molecular mechanisms governing interactions of small ACdEVs with recipient cells.

This project aimed to address the significant knowledge gaps surrounding ACdEVs, particularly focusing on the surface proteome which determine their surface properties. The surface of ACdEVs, and EVs in general, is crucial, as it is the first point of contact of an EV to engage with recipient cells. Just two functional proteins at the ACdEV surface have been defined so far; CX3CL1, a chemokine and adhesion molecule that acted to attract phagocytes and ICAM-3, that was chemotactic and also involved in surface tethering of phagocytes (Torr *et al.,* 2011; Truman *et al.,* 2008). However, ICAM-3 was only identified by proteomics analysis in T cell (Jurkat)-derived ACdEVs and B cell (Mutu)-derived ACdEVs, and CX3CL1 was absent from all of the proteomic datasets (Grant L. R., 2022). Therefore, it was hypothesised other unidentified molecules likely contribute chemoattraction or adhesion at the surface of ACdEV.

Both physical characteristics and the molecular composition of ACdEV were compared from different immune cell sources and different apoptotic timepoints, to identify cell-specific features and investigate temporal functions of ACdEVs. Furthermore, the involvement of specific ACdEV surface proteins of interest, CD31, CD47, CD49d and CD166, were investigated. These candidate proteins, identified by previous in-house LC-MS/MS proteomics, are all adhesion proteins with

prior known roles in immunomodulation and cellular communication. Therefore, they were hypothesised to also be important in mediating ACdEV-cell interactions. This study also examined interactions between ACdEVs and macrophages, a major innate immune cell type that have exceptional plasticity allowing them to exert dynamic functions. These properties make macrophages powerful regulators of apoptotic cell clearance and resolution of inflammation (Poon *et al*., 2014b; Sindrilaru *et al.,* 2011). By evaluating the ability of ACdEVs to induce macrophage migration, initiate surface binding and internalisation, and impact macrophage phenotype, this project provided insight on the potential regulatory roles ACdEVs and associated key molecules play in regulating immune system processes and the general molecular mechanisms that may be utilised by EVs to interact with recipient cells.

In line with the MISEV guidelines, a globally accepted framework for defining EVs, ACdEVs from Jurkat T cell and THP-1 monocyte immune cell lines were characterised at early and late apoptosis, revealing unique traits specific to each cell source, as well as some shared characteristics (Welsh *et al.,* 2024). The majority of ACdEVs were below 100 nm in size, highlighting the ongoing need to push the limits of detection of multiple methods in order to better characterise particles below this size (Figure 3.5). An increased presence of larger Jurkat-derived ACdEVs (> 100 nm) was detected at late apoptosis, whilst THP-1-derived ACdEVs remained consistent in size. THP-1 cells also consistently released a higher abundance of ACdEVs and a greater frequency of multilamellar ACdEVs at both apoptotic timepoints compared to Jurkat T cells (Figure 3.4 and 3.6). The tetraspanins CD9, CD63 and CD81, common markers of EVs, were detected at the surface of ACdEVs from both cell lines but revealed differences in expression profiles (Figure 3.7 and 3.8). Whilst CD81 was most readily detected at the surface of ACdEVs from both cell lines, a greater proportion of Jurkat-derived ACdEVs displayed CD9 and a greater proportion of THP-1-derived ACdEVs displayed CD63 (Figure 3.7). Altogether, this highlighted the heterogeneity of ACdEVs with fundamental differences according to the cell source and apoptotic timepoint.

Next, the protein composition of ACdEVs was investigated; proteomic profiling revealed a change in protein composition between early and late ACdEVs, with differentially expressed proteins identified at early versus late apoptosis in all three immune cell lines: Jurkat T cell, THP-1 monocyte and Mutu B cell lines (Figure 4.4) (Grant L.R., 2022). This, coupled with gene ontology analysis, allowed the identification of known immunomodulators CD31, CD47, CD49d and CD166 as novel ACdEV surface-associated proteins (Figure 4.2 and 4.3). Their surface localisation, and therefore accessibility to immune cells, was confirmed by nano-flow cytometry (Figure 4.6).

Macrophages are highly adaptable effectors of inflammation and therefore, how ACdEVs modulate macrophage behaviour may be pivotal to the control of immune responses and resolution of inflammation. ACdEV-containing secretome and ultracentrigation (UC)-isolated ACdEVs were chemoattractive to macrophages, but SEC-isolated ACdEVs lost their chemoattractive properties, which may represent the disruption of a functional ACdEV corona that cannot be rescued (Figure 5.1). Macrophages interacted with ACdEVs in a dose-dependent and temperature-dependent manner (Figure 5.4 and 5.5). This interaction was partially disrupted by decreases in temperature, at which active endocytic and phagocytic processes were considered inhibited (Figure 5.5). This indicated that a significant proportion of ACdEV surface interactions were likely electrostatic physicochemical interactions. ACdEVs were also shown to induce a unique macrophage phenotype, in both the THP-1 cell line and primary human monocyte models, that was distinct from classical M0, M1 or M2 phenotypes, suggesting the capability of ACdEVs to influence macrophage behaviour (Figure 5.7 and 5.8). In addition, the activity of CD31, CD47, CD49d and CD166 was inhibited by antibody-mediated blockade to assess their individual roles at the ACdEV surface in relation to interaction with macrophages.

CD47 is a well-established inhibitory 'don't eat me' signal at the surface of viable cells, that signals with SIRPα at the surface of phagocytes to prevent their inappropriate engulfment (Oldenborg, Gresham, and Lindberg, 2001). During apoptosis, CD47 signalling is disrupted, permitting phagocytic uptake and clearance (Gardai *et al.,* 2005). Reorganisation of CD47 at the cell surface has been observed during apoptosis, from a clustered formation to an evenly distributed formation (Lv *et al.,* 2015). This is thought to be mediated by disassembly of cholesterol-enriched lipid rafts during apoptosis, of which CD47 is reported to be closely associated with (Dufour *et al.,* 2023; Lv *et al.,* 2015). In this project, expression of CD47 at the surface of Jurkat T cells decreased as cells progressed through apoptosis, which may contribute to disrupted CD47-SIRPα signalling (Figure 4.5). In addition, CD47 was detected at the surface of Jurkat-derived ACdEVs (Figure 4.6). Therefore, we hypothesise apoptotic cells may shed CD47 from the surface, in order for them appear more 'edible' to phagocytes to ensure their efficient removal. The next question was whether CD47 maintains the ability to signal as a 'don't eat me' signal at the ACdEV surface, and how this may influence the interaction of ACdEV with macrophages, a professional phagocyte. Antibody blockade of CD47 resulted in significantly increased interaction between ACdEVs and recipient macrophages, suggesting that its functional activity is preserved at the surface of ACdEVs (Figure 6.1 and 5.5). This may protect ACdEVs from internalisation and therefore, preserve their ability to carry out surface-mediated signalling for longer. Indeed, CD47- SIRPα

signalling has been shown by several groups to protect EVs or liposomes from phagocytic removal (Wei *et al.,* 2021; Belhadj *et al*., 2020; Kamerkar *et al.,* 2017). Interestingly, the presence of CD47 at the EV surface may not always indicate its activity; one group found that apoptotic blebs that expressed CD47 did not bind SIRPα and another found that antibody blockade of CD47 at the surface of breast carcinoma-derived EVs did not impact uptake but did alter the activation of signalling pathways in recipient endothelial cells (Dufour *et al.,* 2023; Kaur *et al.,* 2017). Therefore, the regulation of CD47 is complex and its activity may depend on many variables, such as cell source or microenvironmental cues. Most ACdEVs in this project were evenly decorated with CD47, with just a minority population of approximately 7-8% identified by SMLM to exhibit CD47 in a clustered formation (Figure 4.8). Notably, clustering of CD47 is not required for its signalling but association with cholesterol is thought to be essential (Dufour *et al.,* 2023). EVs are known to be enriched in specific lipid classes, including PS, PE, PC, SM, ceramide and cholesterol (Skotland *et al.,* 2020). Therefore, to elucidate the molecular mechanism that CD47 activity is regulated at the ACdEV surface, the localisation of CD47 to cholesterol could be investigated. This may contribute to ongoing efforts to modulate EV uptake by CD47 activity (Belhadj *et al*., 2020). Furthermore, blockade of CD47 resulted in an overall decrease in migrated macrophages, highlighting its potential importance in the chemoattraction process (Figure 5.2 and 5.3). However, due to the constraints of our migration assay, it was undetermined whether this effect was mediated by blockade of CD47 at the ACdEV surface in addition to the THP-1 macrophage surface or just at the macrophage surface. Notably, SIRPa was absent from the proteomic datasets, therefore suggesting this effect is CD47-mediated and not SIRPa-mediated (Grant L. R., 2022).

CD31 is a dynamic adhesion protein that functionally switches during apoptosis, from a ‘don’t eat me’ signal facilitating the detachment and release of viable cells, to an ‘eat me’ signal promoting integrin-mediated phagocytosis (Vernon-Wilson *et al.,* 2006; Brown *et al.,* 2002). Although homophilic CD31 interactions mediate the attachment of both apoptotic and viable cells, it has been demonstrated to specifically promote integrin-mediated phagocytosis of apoptotic cells by prolonging membrane depolarisation in phagocytes (Vernon-Wilson *et al.,* 2007). Membrane depolarisation activates β1 integrins on surface of phagocytes, allowing them to bind fibronectin-opsonised apoptotic cells, thereby facilitating the selective engulfment of apoptotic cells; a similar process could take place with ACdEVs (Figure 6.1) (Vernon-Wilson *et al.,* 2007; Vernon-Wilson *et al.,* 2006). As such, the aim in this project was to understand whether the role of CD31 at the ACdEV surface was involved in promoting recruitment and attachment or repelling phagocytic

interaction. Like CD47, CD31 was lost from the cell surface during apoptosis, where it was detected at the ACdEV surface by nano-flow cytometry (Figure 4.5 and 4.6). In addition, the loss of cell surface CD31 may be accounted for by proteolytic cleavage and release of a soluble CD31 fragment and whilst this was not assessed here, the release of CD31 fragments could be assessed via ELISA. This has previously been suggested to contribute to disassembly of junction complexes leading to detachment of apoptotic endothelial cells which may aid their phagocytic clearance (Llan *et al.,* 2001). Shedding of CD31 from the apoptotic cell surface via the release of ACdEVs may also facilitate disassembly and detachment of apoptotic cells. Antibody blockade of CD31 delayed macrophage migration, hinting that if CD31 plays a role in chemoattraction, any delay may be quickly compensated for by other chemotactic factors (Figure 5.2). CD31 blockade also significantly decreased macrophage interaction with ACdEVs, indicating it functions to promote interaction with macrophages, possibly functioning as an 'eat me' signal at the surface of ACdEVs (Figure 6.1 and 5.5). To confirm this, it would be beneficial to determine whether CD31 specifically promotes the internalisation ACdEVs – this could be achieved by confocal microscopy, which is a lower throughput but high-content, more finetuned method of determining EV uptake as internalisation can be verified by z-stack imaging. Notably, some authors have suggested the role of CD31 in apoptotic cell clearance is negligible in the presence of serum, which contains a complex mixture of opsonins (Potter *et al.,* 2007). It would be insightful to measure CD31 interaction at the surface of ACdEVs in the presence of serum to identify whether a similar trend is observed, in which dependency on CD31 for surface interactions is diminished. As mentioned, the data from this project suggested most ACdEV interactions with recipient macrophages was likely mediated by electrostatic physicochemical surface interactions, which may or may not involve specific receptor-ligand interactions. This again hints at the potential functional importance of EV coronas in governing chemoattraction, binding and uptake. In addition, evidence suggests CD31 homophilic signalling may be enhanced by clustering at membrane surfaces; understanding the effect on binding affinity may be informative for understanding the mechanism of CD31 signalling which is functionally distinct on viable and apoptotic cells (Fornasa *et al.,* 2010; DeLisser *et al.,* 1997). Finally, further understanding of the relationship between CD31 signalling, integrin activation and subsequent interaction with ECM, such as fibronectin, may provide insight into the complex multidimensional pathways of activation that occurs during apoptosis and phagocytosis.

CD49d is an α4 integrin subunit. Integrins are another major family of adhesion proteins that regulate cell mobility by modulating adhesion to neighbouring cells and the ECM (Hynes, 2002).

Integrin activation engages the actin cytoskeleton in cells and triggers intracellular signalling pathways that can promote survival, proliferation and determine the fate of stem cells, suggesting their ability to alter cell phenotype (Kadry & Calderwood, 2020; Koopman *et al.,* 1994; Taichman *et al.,* 1991). CD49d is known to heterodimerise with integrin β1 subunit (ITGB1), forming VLA-4, which facilitates adhesion and extravasation of circulating leukocytes through binding with VCAM-1 and fibronectin (Taichman *et al.,* 1991). Here, CD49d was observed to be lost from the apoptotic cell surface and detected at the surface of ACdEVs (Figure 4.5 and 4.6). Antibody blockade of CD49d did not profoundly impact macrophage migration, with just a short delay in migration observed, but did significantly inhibit ACdEV interaction at lower temperatures, indicating a role in internalisation of ACdEVs (Figure 5.2 and 5.5). Several integrins have been implicated in EV uptake, including CD49d which was shown to induce EV internalisation when in complex with tetraspanin, TSPAN8 (French *et al.,* 2017; Nazarenko *et al.,* 2010). Notably, TSPAN8 was absent from our ACdEV proteomic datasets (Grant L. R., 2022). However, ITGB1 was identified in our proteomics datasets as present in ACdEVs from all three immune cell lines (Table 4.1) In addition, the only other known binding partner of CD49d, ITGB7, was absent from our proteomics datasets. Therefore, we hypothesise that CD49d may heterodimerise with ITGB1 at the surface of ACdEVs to form VLA-4, a known immunomodulatory integrin complex (Figure 6.1). Uptake of melanoma-derived EVs has previously been shown to be partly dependent on VCAM-1 expressed by recipient endothelial cells; VCAM-1 is a ligand for VLA-4 (Leary *et al.,* 2022). Therefore, VLA-4 may act as an 'eat me' signal through this interaction (Figure 6.1). Furthermore, EV surface-associated VLA-4 has been demonstrated to bind fibronectin *in vitro,* suggesting active engagement with the ECM (Rieu *et al.,* 2000). Integrin-fibronectin binding mediated by EVs has also been reported to promote directional migration of the source cells in an autocrine manner (Sung *et al.,* 2015). Therefore, surface-displayed VLA-4 may be important in governing ACdEV interaction with the ECM, a component that was not included in the functional assays performed in this project (Figure 6.1). Determining the co-localisation of these two integrin subunits should therefore be prioritised. In addition, the chemoattractive properties of ACdEVs should be assessed in the presence of various ECM components, to better model the potential interactions between ACdEVs and ECM, which may impact the distribution of ACdEVs *in vivo*. This approach may also provide insight into the relationship between homophilic CD31 binding and integrin activation in mediating EV binding and uptake.

CD166 is an IgSF member that is widely expressed and involved in a variety of diverse immune processes such as leukocyte migration and T cell activation (von Lersner *et al*., 2019; Cayrol *et*

al., 2007; Hassan *et al.*, 2004). CD166 can transmit signals through either homophilic interactions, promoted by clustering and localisation to tetraspanin CD9, or heterophilic interactions with CD6 which is expressed at the surface of T cells and a subset of B cells (von Lersner *et al*., 2019). Strikingly, THP-1 cell surface expression of CD166 significantly decreased during apoptosis but was only displayed at the surface of a small population of approximately 2.53% Jurkat and 5.0% THP-1-derived ACdEVs (Figure 4.6 and 4.6). Therefore, it is likely that most of the decrease in CD166 cell surface expression may be attributed to proteolytic cleavage and the subsequent release of a soluble fragment, that could be confirmed in future work by ELISA analysis of secretome. This process is known to be mediated by α disintegrin and metalloprotease 17 (ADAM17) and metalloproteinase 14 (MMP-14) and is reported to aid cell motility (von Lersner *et al.,* 2019). Apart from observing a short delay in macrophage migration, antibody blockade of CD166 revealed no significant impact on ACdEV function, within the scope of this project (Figure 5.2, 5.5, 5.7, 5.8). Therefore, CD166 may be unimportant in the context of Jurkat and THP-1-derived ACdEV-mediated modulation of THP-1 macrophages. However, CD166 at the surface of colorectal cancer and ovarian cancer-derived EVs has been shown to promote binding and uptake, and therefore, may be a key mediator at the surface of EVs derived from different cell sources (Cardeñes *et al.,* 2022).

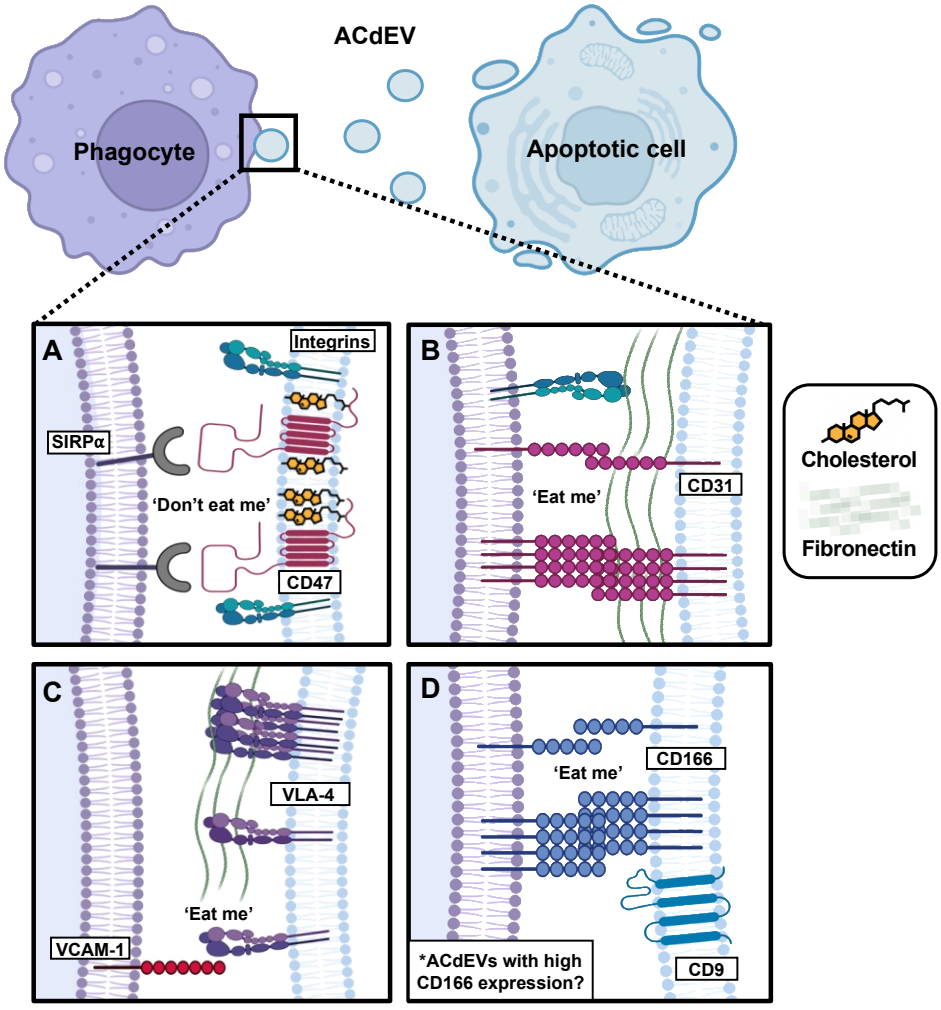

Figure 6.1: Schematic representation of hypothesised signalling between ACdEVs and recipient phagocytes, mediated by [A] CD47, [B] CD31, [C] CD49d and [D] CD166 at the ACdEV surface. A) CD47, known to associate with integrins, may signal with SIRPα to exert a 'don't eat me' signal at the surface of ACdEV, as observed on viable cells (Oldenborg, Gresham, and Lindberg, 2001). This signalling may be dependent on the presence of cholesterol-enriched lipid rafts (Dufour *et al.,* 2023). B) CD31 may promote ACdEV uptake by exerting an 'eat me' signal through homophilic binding, which may be aided by clustering (Fornasa *et al.,* 2010; DeLisser *et al.,* 1997). As seen in cells, CD31 signalling may activate phagocytic integrins to bind fibronectin (Vernon-Wilson *et al.,* 2006). C) CD49d is an α4 integrin subunit that may heterodimerise with integrin β1 subunit (ITGB1), forming VLA-4 at the ACdEV surface, which may function as an 'eat me' signal, promoting uptake through binding of VCAM-1 (Leary *et al.,* 2022). This interaction may be regulated by integrin clustering (Calderwood *et al.,* 2013). EV-associated VLA-4 is also implicated in the binding of fibronectin, promoting cell motility (Sung *et al.,* 2015; Rieu *et al.,* 2000). D) Few ACdEVs (Jurkat and THP-1-derived) in this study displayed CD166 at the surface (≤ 5%) (Figure 4.6). ACdEVs derived from alternative cell sources with high CD166 expression may engage in homophilic binding which may induce an 'eat me' signal and promote uptake, as demonstrated by colorectal cancer and ovarian cancer-derived EVs (Cardeñes *et al.,* 2022). Additionally, clustering of CD166, mediated by CD9, may promote higher affinity binding on ACdEV surface, as seen on cells (Gilsanz *et al.,* 2012). Figure made in Biorender.

Overall, CD47, CD31 and CD49d were identified as potentially important molecules mediating surface interactions between ACdEVs and recipient cells, specifically macrophages. CD166 blockade revealed no unique impact on ACdEV function within the scope of this project, though it is suggested to be important if highly expressed at the ACdEV surface. Antibody blockade of each protein had no apparent impact on macrophage phenotype, as measured in this study, suggesting they are mainly involved in mediating surface interactions between ACdEVs and cells (Figure 5.7 and 5.8). This indicates that the molecular mechanisms governing ACdEV interaction with macrophages differ from the mechanisms responsible for altering macrophage phenotype. This should be explored further by alternative means of characterising macrophage phenotype, such as 'omics methods or cytokine release, given that the presence of CD47 at EV surfaces has previously been implicated in mediating differential recipient cell responses (Kaur *et al.,* 2014). Future efforts should investigate the functional relationship between these different proteins by combining blockade/knockdown strategies. Indeed, CD47 has been shown to regulate the localisation of integrin subunits α4 (CD49d) and β1 with tetraspanin CD81, at the surface of Jurkat-derived EVs, all of which were identified previously and in this project by proteomics analysis (Grant L.R., 2022; Kaur *et al.,* 2022). Additionally, as mentioned, CD31 is involved in the direct activation of β1 integrins (Vernon-Wilson *et al.,* 2006). Therefore, the relationship between molecules implicated in EV binding and uptake is complex and multifaceted; this remains a key challenge in the field of EV research. Given the commonality of Ig-like superfamily members in the human genome and their widespread functions in surface-mediated interactions, we consider whether IgSF members may act as functionally redundant molecules mediating interactions between the surface of ACdEVs, and EVs in general, and recipient cells or the microenvironment (*e.g.* ECM components).

Importantly, this study was limited in that key aspects of the ACdEV surface that are fundamental to ACdEV structure and function were not characterised in this project. These aspects include the lipidomic composition, which affects membrane fluidity, cargo sorting, and serves as another functionally active component of EVs (Fyfe *et al.,* 2023); surface glycosylation patterns, which are known to influence EV signalling and uptake (Buzás, 2019); and compositional analysis of the surface corona, which can dynamically modify the functional state of the EV surfaceome (Buzás, 2022). Integrating these findings with ACdEV surface proteomics would offer a more comprehensive understanding of how ACdEVs interact with recipient cells, which is crucial for harnessing their therapeutic applications.

Furthermore, the use of immortalised cell lines may not fully reflect the diversity and complexity of ACdEVs derived from immune cells that are involved in apoptotic cell clearance *in vivo*. Since different immune cells generate ACdEVs with distinct surface compositions (as shown in this study), using a broader range of primary immune cell types could provide a more physiologically relevant understanding of ACdEV function. Additionally, whilst our *in vitro* work highlighted the role of CD31, CD47, and CD49d, in governing surface interactions with recipient macrophages, their precise function in ACdEV-mediated immunomodulation requires *in vivo* validation. Given the complexity of the immune system, *in vivo* studies may determine how blocking these proteins affects the overall apoptotic cell clearance process and resolution of inflammation, offering potential therapeutic insights for diseases linked to impaired apoptotic cell clearance.

A deeper understanding of EV surface features would offer valuable insights and inform strategies for engineering EV surfaces for drug delivery, such as designing more effective cell-specific targeting and developing methods to avoid or shield EVs from undesired cell or tissue uptake. For instance, researchers are already employing CD47 to deter phagocytic uptake of therapeutic EVs (Wei *et al.,* 2021; Belhadj *et al*., 2020; Kamerkar *et al.,* 2017). This knowledge could also be used to enhance the sensitivity or responsiveness of recipient cells to EV therapeutics, improve EV stability and longevity, and manipulate EVs to promote systemic or localised travel according to therapeutic goals (Iannotta *et al.,* 2023). Moreover, gaining a detailed understanding of the molecular mechanisms by which ACdEVs regulate inflammation would pave the way for the design of EV therapies that actively resolve or modify inflammation. Inflammation is a crucial element of the innate immune system, providing protection during the early stages of an immune challenge. However, if not properly regulated, inflammation can become chronic, contributing to the development of various diseases where clearance of apoptotic cells is impaired. Impaired apoptotic cell clearance is a major contributing factor to several major diseases including atherosclerosis, autoimmune diseases and cancer (Poon *et al.,* 2014b); EV therapies have transformative potential in these disease areas. In particular, ACdEVs possess great therapeutic potential due to their ability to promote pro-resolving functions (Zhu *et al.,* 2023; Li *et al.,* 2022; Liu *et al.,* 2020; Shen *et al.,* 2017; Fehr *et al.,* 2013). Efforts to understand the molecular mechanism of ACdEV-mediated resolution of inflammation will pave the way for the development of therapeutics for chronic inflammatory diseases.

In conclusion, this PhD project has provided valuable insight into how the ACdEV surface proteome, specifically through the roles of adhesion proteins and known immunomodulators such as CD31, CD47, CD49d, and CD166, may interact with macrophages, a key innate immune cell

type. The findings suggest that whilst CD31, CD47, and CD49d are likely involved in the surface-mediated interaction between ACdEVs and macrophages, they do not appear to play a role in inducing phenotypic changes. This highlights the distinct functions of these proteins at the surface of ACdEVs, and suggests mechanisms by which ACdEVs may modulate apoptotic cell clearance and inflammation.

Bibliography

Abarca-Cabrera, L., Fraga-García, P. and Berensmeier, S. (2021) 'Bio-nano interactions: Binding proteins, polysaccharides, lipids and nucleic acids onto magnetic nanoparticles', *Biomaterials Research*, 25(1). doi:10.1186/s40824-021-00212-y.

Alderson, M.R. *et al.* (1993) 'CD40 expression by human monocytes: Regulation by cytokines and activation of monocytes by the ligand for CD40.', *The Journal of experimental medicine*, 178(2), pp. 669–674. doi:10.1084/jem.178.2.669.

Almeida, P.A. and Bolton, V.N. (1995) 'The effect of temperature fluctuations on the cytoskeletal organisation and chromosomal constitution of the human oocyte', *Zygote*, 3(4), pp. 357–365. doi:10.1017/s0967199400002793.

Alvarez-Erviti, L. *et al.* (2011) 'Delivery of sirna to the mouse brain by systemic injection of targeted exosomes', *Nature Biotechnology*, 29(4), pp. 341–345. doi:10.1038/nbt.1807.

Ambrose, A.R. *et al.* (2020) 'Corrected super-resolution microscopy enables nanoscale imaging of Autofluorescent Lung Macrophages', *Biophysical Journal*, 119(12), pp. 2403–2417. doi:10.1016/j.bpj.2020.10.041.

Anderson, H.A. and Roche, P.A. (2015) 'MHC class II association with lipid rafts on the antigen presenting cell surface', *Biochimica et Biophysica Acta (BBA) - Molecular Cell Research*, 1853(4), pp. 775–780. doi:10.1016/j.bbamcr.2014.09.019.

Atkin-Smith, G.K. and Poon, I.K.H. (2017) 'Disassembly of the dying: Mechanisms and functions', *Trends in Cell Biology*, 27(2), pp. 151–162. doi:10.1016/j.tcb.2016.08.011.

Atkin-Smith, G.K. *et al.* (2015) 'A novel mechanism of generating extracellular vesicles during apoptosis via a beads-on-a-string membrane structure', *Nature Communications*, 6(1). doi:10.1038/ncomms8439.

Atsumi, G. *et al.* (1998) 'Fas-induced arachidonic acid release is mediated by ca2+-independent phospholipase A2 but not cytosolic phospholipase A2, which undergoes proteolytic inactivation', *Journal of Biological Chemistry*, 273(22), pp. 13870–13877. doi:10.1074/jbc.273.22.13870.

Atsumi, G. *et al.* (2000) 'Distinct roles of two intracellular phospholipase A2s in fatty acid release in the Cell Death Pathway', *Journal of Biological Chemistry*, 275(24), pp. 18248–18258. doi:10.1074/jbc.m000271200.

Barclay, A.N. (2003) 'Membrane proteins with immunoglobulin-like domains—a master superfamily of interaction molecules', *Seminars in Immunology*, 15(4), pp. 215–223. doi:10.1016/s1044-5323(03)00047-2.

Barclay, A.N. and van den Berg, T.K. (2014) 'The interaction between Signal Regulatory Protein Alpha (SIRPA) and CD47: Structure, function, and therapeutic target', *Annual Review of Immunology*, 32(1), pp. 25–50. doi:10.1146/annurev-immunol-032713-120142.

Basu Mallik, S., Jayashree, B.S. and Shenoy, R.R. (2018) 'Epigenetic modulation of macrophage polarization- perspectives in diabetic wounds', *Journal of Diabetes and its Complications*, 32(5), pp. 524–530. doi:10.1016/j.jdiacomp.2018.01.015.

Beillevaire, D. *et al.* (2022) 'Autolysosomes and caspase-3 control the biogenesis and release of immunogenic apoptotic exosomes', *Cell Death & Disease*, 13(2). doi:10.1038/s41419-022-04591-5.

Belhadj, Z. *et al.* (2020) 'A combined "eat me/don't eat me" strategy based on extracellular vesicles for anticancer nanomedicine', *Journal of Extracellular Vesicles*, 9(1). doi:10.1080/20013078.2020.1806444.

Berezin, A.E. *et al.* (2019) 'Altered signature of apoptotic endothelial cell-derived microvesicles predicts chronic heart failure phenotypes', *Biomarkers in Medicine*, 13(9), pp. 737–750. doi:10.2217/bmm-2018-0449.

Bilyy, R.O. *et al.* (2012) 'Macrophages discriminate glycosylation patterns of apoptotic cell-derived microparticles', *Journal of Biological Chemistry*, 287(1), pp. 496–503. doi:10.1074/jbc.m111.273144.

Blue, M.L., Davis, G. and Kelley, K. (1993) 'Specific cleavage of the alpha 4 integrin associated with activation of peripheral T lymphocytes.', *Immunology*, 78(1), pp. 80–85. doi:PMID: 8436405; PMCID: PMC1421787.

Boucrot, E. *et al.* (2010) 'Roles of AP-2 in clathrin-mediated endocytosis', *PLoS ONE*, 5(5). doi:10.1371/journal.pone.0010597.

Boyer, C. and Zasadzinski, J.A. (2007) ‘Multiple lipid compartments slow vesicle contents release in lipases and Serum’, *ACS Nano*, 1(3), pp. 176–182. doi:10.1021/nn7002025.

Brancolini, C. *et al.* (1997) ‘Dismantling cell–cell contacts during apoptosis is coupled to a caspase-dependent proteolytic cleavage of β-catenin’, *The Journal of Cell Biology*, 139(3), pp. 759–771. doi:10.1083/jcb.139.3.759.

Brennan, F.M. *et al.* (2008) ‘Resting CD4+ effector memory T cells are precursors of bystander-activated effectors: A surrogate model of rheumatoid arthritis synovial T-cell function’, *Arthritis Research & Therapy*, 10(2). doi:10.1186/ar2390.

Broad, K. *et al.* (2023) ‘Unraveling multilayered extracellular vesicles: Speculation on cause’, *Journal of Extracellular Vesicles*, 12(2). doi:10.1002/jev2.12309.

Brown, S. *et al.* (2002) ‘Apoptosis disables CD31-mediated cell detachment from phagocytes promoting binding and engulfment’, *Nature*, 418(6894), pp. 200–203. doi:10.1038/nature00811.

Brumatti, G., Salmanidis, M. and Ekert, P.G. (2010) ‘Crossing paths: Interactions between the cell death machinery and growth factor survival signals’, *Cellular and Molecular Life Sciences*, 67(10), pp. 1619–1630. doi:10.1007/s00018-010-0288-8.

Busatto, S. *et al.* (2019) ‘Organotropic drug delivery: Synthetic nanoparticles and extracellular vesicles’, *Biomedical Microdevices*, 21(2). doi:10.1007/s10544-019-0396-7.

Buzas, E.I. (2022) ‘Opportunities and challenges in studying the extracellular vesicle Corona’, *Nature Cell Biology*, 24(9), pp. 1322–1325. doi:10.1038/s41556-022-00983-z.

Buzás, E.I. *et al.* (2018) ‘Molecular interactions at the surface of extracellular vesicles’, *Seminars in Immunopathology*, 40(5), pp. 453–464. doi:10.1007/s00281-018-0682-0.

Calderwood, D.A., Campbell, I.D. and Critchley, D.R. (2013) ‘Talins and Kindlins: Partners in integrin-mediated adhesion’, *Nature Reviews Molecular Cell Biology*, 14(8), pp. 503–517. doi:10.1038/nrm3624.

Cameron, A. (2018), *Attracted to Death: Apoptotic Cellderived Extracellular Vesicles towards a basic characterisation.* PhD thesis, Aston University.

Cardeñes, B. *et al.* (2022) 'ALCAM/CD166 is involved in the binding and uptake of cancer-derived extracellular vesicles', *International Journal of Molecular Sciences*, 23(10), p. 5753. doi:10.3390/ijms23105753.

Caruso, S. and Poon, I.K. (2018) 'Apoptotic cell-derived extracellular vesicles: More than just debris', *Frontiers in Immunology*, 9. doi:10.3389/fimmu.2018.01486.

Casado-Díaz, A., Quesada-Gómez, J.M. and Dorado, G. (2020) 'Extracellular vesicles derived from mesenchymal stem cells (MSC) in Regenerative Medicine: Applications in Skin Wound Healing', *Frontiers in Bioengineering and Biotechnology*, 8. doi:10.3389/fbioe.2020.00146.

Castle, J.D., Guo, Z. and Liu, L. (2002) 'Function of the t-snare snap-23 and secretory carrier membrane proteins (scamps) in exocytosis in Mast Cells', *Molecular Immunology*, 38(16–18), pp. 1337–1340. doi:10.1016/s0161-5890(02)00084-6.

Castro, M.A. *et al.* (2007) 'Extracellular isoforms of CD6 generated by alternative splicing regulate targeting of CD6 to the immunological synapse', *The Journal of Immunology*, 178(7), pp. 4351–4361. doi:10.4049/jimmunol.178.7.4351.

Cayrol, R. *et al.* (2007) 'Activated leukocyte cell adhesion molecule promotes leukocyte trafficking into the Central Nervous System', *Nature Immunology*, 9(2), pp. 137–145. doi:10.1038/ni1551.

Cha, J.M. *et al.* (2018) 'Efficient scalable production of therapeutic microvesicles derived from human mesenchymal stem cells', *Scientific Reports*, 8(1). doi:10.1038/s41598-018-19211-6.

Chandrasekaran, L. *et al.* (2000) 'Cell contact–dependent activation of α3β1 integrin modulates endothelial cell responses to thrombospondin-1', *Molecular Biology of the Cell*, 11(9), pp. 2885–2900. doi:10.1091/mbc.11.9.2885.

Chaurasiya, A. *et al.* (2021) 'A review on multivesicular liposomes for pharmaceutical applications: Preparation, characterization, and translational challenges', *Drug Delivery and Translational Research*, 12(7), pp. 1569–1587. doi:10.1007/s13346-021-01060-y.

Chekeni, F.B. *et al.* (2010) 'Pannexin 1 channels mediate "find-me" signal release and membrane permeability during apoptosis', *Nature*, 467(7317), pp. 863–867. doi:10.1038/nature09413.

Chinetti-Gbaguidi, G. *et al.* (2011) 'Human atherosclerotic plaque alternative macrophages display low cholesterol handling but high phagocytosis because of distinct activities of the PPARΓ and LXRA PATHWAYS', *Circulation Research*, 108(8), pp. 985–995. doi:10.1161/circresaha.110.233775.

Choi, D. *et al.* (2014) 'Proteomics of extracellular vesicles: Exosomes and ectosomes', *Mass Spectrometry Reviews*, 34(4), pp. 474–490. doi:10.1002/mas.21420.

Choudhuri, K. *et al.* (2014) 'Polarized release of T-cell-receptor-enriched microvesicles at the immunological synapse', *Nature*, 507(7490), pp. 118–123. doi:10.1038/nature12951.

Coleman, M.L. *et al.* (2001) 'Membrane blebbing during apoptosis results from caspase-mediated activation of rock I', *Nature Cell Biology*, 3(4), pp. 339–345. doi:10.1038/35070009.

Colombo, M., Raposo, G. and Théry, C. (2014a) 'Biogenesis, secretion, and intercellular interactions of exosomes and other extracellular vesicles', *Annual Review of Cell and Developmental Biology*, 30(1), pp. 255–289. doi:10.1146/annurev-cellbio-101512-122326.

Crescitelli, R. *et al.* (2013) 'Distinct RNA profiles in subpopulations of extracellular vesicles: Apoptotic bodies, microvesicles and exosomes', *Journal of Extracellular Vesicles*, 2(1). doi:10.3402/jev.v2i0.20677.

Davies *et al.* (1999) 'VCAM-1 contributes to rapid eosinophil accumulation induced by the chemoattractants PAF and LTB₄: Evidence for basal expression of functional VCAM-1 in rat skin', *Immunology*, 97(1), pp. 150–158. doi:10.1046/j.1365-2567.1999.00766.x.

Davis, K.A. *et al.* (1998) 'Determination of CD4 antigen density on cells: Role of antibody valency, avidity, clones, and conjugation', *Cytometry*, 33(2), pp. 197–205. doi:10.1002/(sici)1097-0320(19981001)33:2<197::aid-cyto14>3.0.co;2-p.

DeLisser, H.M., Baldwin, H.S. and Albelda, S.M. (1997) 'Platelet endothelial cell adhesion molecule 1 (PECAM-1/CD31): A multifunctional vascular cell adhesion molecule', *Trends in Cardiovascular Medicine*, 7(6), pp. 203–210. doi:10.1016/s1050-1738(97)00049-2.

Devitt, A. *et al.* (2004) 'Persistence of apoptotic cells without autoimmune disease or inflammation in CD14−/− mice', *The Journal of Cell Biology*, 167(6), pp. 1161–1170. doi:10.1083/jcb.200410057.

Dietz, L. *et al.* (2023) 'Uptake of extracellular vesicles into immune cells is enhanced by the protein Corona', *Journal of Extracellular Vesicles*, 12(12). doi:10.1002/jev2.12399.

Dieudé, M. *et al.* (2015) 'The 20*s* proteasome core, active within apoptotic exosome-like vesicles, induces autoantibody production and accelerates rejection', *Science Translational Medicine*, 7(318). doi:10.1126/scitranslmed.aac9816.

Dive, C. *et al.* (1992) 'Analysis and discrimination of necrosis and apoptosis (programmed cell death) by multiparameter flow cytometry', *Biochimica et Biophysica Acta (BBA) - Molecular Cell Research*, 1133(3), pp. 275–285. doi:10.1016/0167-4889(92)90048-g.

Dixson, A.C. *et al.* (2023) 'Context-specific regulation of extracellular vesicle biogenesis and cargo selection', *Nature Reviews Molecular Cell Biology*, 24(7), pp. 454–476. doi:10.1038/s41580-023-00576-0.

Domínguez-Soto, A. *et al.* (2011) 'Dendritic cell-specific ICAM-3–grabbing nonintegrin expression on m2-polarized and tumor-associated macrophages is macrophage-CSF dependent and enhanced by tumor-derived IL-6 and IL-10', *The Journal of Immunology*, 186(4), pp. 2192–2200. doi:10.4049/jimmunol.1000475.

Dufour, S. *et al.* (2023) 'Nanoscale Imaging of CD47 informs how plasma membrane modifications shape apoptotic cell recognition', *Communications Biology*, 6(1). doi:10.1038/s42003-023-04558-y.

Edwards, J.P. *et al.* (2006) 'Biochemical and functional characterization of three activated macrophage populations', *Journal of Leukocyte Biology*, 80(6), pp. 1298–1307. doi:10.1189/jlb.0406249.

Elliott, M.R. *et al.* (2009) 'Nucleotides released by apoptotic cells act as a find-me signal to promote phagocytic clearance', *Nature*, 461(7261), pp. 282–286. doi:10.1038/nature08296.

Elward, K. *et al.* (2005) 'CD46 plays a key role in tailoring innate immune recognition of apoptotic and necrotic cells', *Journal of Biological Chemistry*, 280(43), pp. 36342–36354. doi:10.1074/jbc.m506579200.

Enari, M. *et al.* (1998) ‘A caspase-activated DNase that degrades DNA during apoptosis, and its inhibitor ICAD’, *Nature*, 391(6662), pp. 43–50. doi:10.1038/34112.

Esmaeili, A. *et al.* (2022) ‘Engineering strategies for customizing extracellular vesicle uptake in a therapeutic context’, *Stem Cell Research & Therapy*, 13(1). doi:10.1186/s13287-022-02806-2.

Fadok, V.A. *et al.* (1998) ‘Macrophages that have ingested apoptotic cells in vitro inhibit proinflammatory cytokine production through autocrine/paracrine mechanisms involving TGF-beta, PGE2, and PAF.’, *Journal of Clinical Investigation*, 101(4), pp. 890–898. doi:10.1172/jci1112.

Fan, S.T. and Edgington, T.S. (1993) ‘Integrin regulation of leukocyte inflammatory functions. CD11B/CD18 enhancement of the tumor necrosis factor-alpha responses of monocytes.’, *The Journal of Immunology*, 150(7), pp. 2972–2980. doi:10.4049/jimmunol.150.7.2972.

Fanger, N.A. *et al.* (1996) ‘Type I (CD64) and type II (CD32) FC gamma receptor-mediated phagocytosis by human blood dendritic cells.’, *The Journal of Immunology*, 157(2), pp. 541–548. doi:10.4049/jimmunol.157.2.541.

Fawcett, J. *et al.* (1995) ‘Mapping the homotypic binding sites in CD31 and the role of CD31 adhesion in the formation of interendothelial cell contacts.’, *The Journal of cell biology*, 128(6), pp. 1229–1241. doi:10.1083/jcb.128.6.1229.

Fehr, E.-M. *et al.* (2013) ‘Apoptotic-cell-derived membrane vesicles induce an alternative maturation of human dendritic cells which is disturbed in Sle’, *Journal of Autoimmunity*, 40, pp. 86–95. doi:10.1016/j.jaut.2012.08.003.

Fenalti, G. *et al.* (2021) ‘Structure of the human marker of self 5-transmembrane receptor CD47’, *Nature Communications*, 12(1). doi:10.1038/s41467-021-25475-w.

Ferreira, G.B. *et al.* (2014) ‘1,25-dihydroxyvitamin D3 promotes tolerogenic dendritic cells with functional migratory properties in Nod mice’, *The Journal of Immunology*, 192(9), pp. 4210–4220. doi:10.4049/jimmunol.1302350.

Fonseca, P. *et al.* (2016) ‘Metabolic and signaling functions of cancer cell-derived extracellular vesicles’, *International Review of Cell and Molecular Biology*, pp. 175–199. doi:10.1016/bs.ircmb.2016.04.004.

Fornasa, G. *et al.* (2010) ‘TCR stimulation drives cleavage and shedding of the ITIM receptor CD31’, *The Journal of Immunology*, 184(10), pp. 5485–5492. doi:10.4049/jimmunol.0902219.

French, K.C., Antonyak, M.A. and Cerione, R.A. (2017) ‘Extracellular vesicle docking at the cellular port: Extracellular vesicle binding and uptake’, *Seminars in Cell & Developmental Biology*, 67, pp. 48–55. doi:10.1016/j.semcdb.2017.01.002.

Frick, M. *et al.* (2007) ‘Coassembly of flotillins induces formation of membrane microdomains, membrane curvature, and vesicle budding’, *Current Biology*, 17(13), pp. 1151–1156. doi:10.1016/j.cub.2007.05.078.

Füllgrabe, J., Hajji, N. and Joseph, B. (2010) ‘Cracking the death code: Apoptosis-related histone modifications’, *Cell Death & Differentiation*, 17(8), pp. 1238–1243. doi:10.1038/cdd.2010.58.

Fyfe, J. *et al.* (2023) ‘Role of lipid signalling in extracellular vesicles-mediated cell-to-cell communication’, *Cytokine & Growth Factor Reviews*, 73, pp. 20–26. doi:10.1016/j.cytogfr.2023.08.006.

Gao, A.G. *et al.* (1996) ‘Integrin-associated protein is a receptor for the C-terminal domain of Thrombospondin’, *Journal of Biological Chemistry*, 271(1), pp. 21–24. doi:10.1074/jbc.271.1.21.

Gao, W.J. *et al.* (2021) ‘Macrophage 3D migration: A potential therapeutic target for inflammation and deleterious progression in diseases’, *Pharmacological Research*, 167, p. 105563. doi:10.1016/j.phrs.2021.105563.

Gardai, S.J. *et al.* (2005) ‘Cell-surface calreticulin initiates clearance of viable or apoptotic cells through Trans-activation of LRP on the phagocyte’, *Cell*, 123(2), pp. 321–334. doi:10.1016/j.cell.2005.08.032.

Gardai S.J., *et al.* (2006) ‘Recognition ligands on apoptotic cells: a perspective.’ J. Leukoc. Biol. 79:896–903. doi:10.1189/jlb.1005550.

Gebara, N. *et al.* (2020) ‘Extracellular vesicles, apoptotic bodies and mitochondria: Stem cell bioproducts for organ regeneration’, *Current Transplantation Reports*, 7(2), pp. 105–113. doi:10.1007/s40472-020-00282-2.

Gilsanz, A. *et al.* (2012) 'ALCAM/CD166 adhesive function is regulated by the Tetraspanin CD9', *Cellular and Molecular Life Sciences*, 70(3), pp. 475–493. doi:10.1007/s00018-012-1132-0.

Ginhoux, F. *et al.* (2015) 'New insights into the multidimensional concept of macrophage ontogeny, activation and function', *Nature Immunology*, 17(1), pp. 34–40. doi:10.1038/ni.3324.

Gioia, L. *et al.* (2018) 'A genome-wide survey of mutations in the Jurkat Cell Line', *BMC Genomics*, 19(1). doi:10.1186/s12864-018-4718-6.

Gordon, S. (2016) 'Phagocytosis: An immunobiologic process', *Immunity*, 44(3), pp. 463–475. doi:10.1016/j.immuni.2016.02.026.

Grant, L.R. (2022) *Characterising the structure-function relationships of apoptotic cell-derived extracellular vesicles in modulation of inflammation*. PhD thesis, Aston University.

Grant, L.R., Milic, I. and Devitt, A. (2019) 'Apoptotic cell-derived extracellular vesicles: Structure–function relationships', *Biochemical Society Transactions*, 47(2), pp. 509–516. doi:10.1042/bst20180080.

Grimmer, S., van Deurs, B. and Sandvig, K. (2002) 'Membrane ruffling and macropinocytosis in A431 cells require cholesterol', *Journal of Cell Science*, 115(14), pp. 2953–2962. doi:10.1242/jcs.115.14.2953.

Gröger, M. *et al.* (1999) 'A standardized, computer-assisted in vitro assay for the assessment of neutrophil transmigration across endothelial monolayers', *Journal of Immunological Methods*, 222(1–2), pp. 101–109. doi:10.1016/s0022-1759(98)00187-2.

Gude, D.R. *et al.* (2008) 'Apoptosis induces expression of sphingosine kinase 1 to release sphingosine-1-phosphate as a "Come-and-get-me" signal', *The FASEB Journal*, 22(8), pp. 2629–2638. doi:10.1096/fj.08-107169.

Gui, Y., Zheng, H. and Cao, R.Y. (2022) 'Foam cells in atherosclerosis: Novel insights into its origins, consequences, and molecular mechanisms', *Frontiers in Cardiovascular Medicine*, 9. doi:10.3389/fcvm.2022.845942.

Hagey, D.W. *et al.* (2023) 'The cellular response to extracellular vesicles is dependent on their cell source and dose', *Science Advances*, 9(35). doi:10.1126/sciadv.adh1168.

Hardy, M.-P. *et al.* (2019) 'Apoptotic endothelial cells release small extracellular vesicles loaded with immunostimulatory viral-like RNAS', *Scientific Reports*, 9(1). doi:10.1038/s41598-019-43591-y.

Hassan, N.J., Barclay, A.N. and Brown, M.H. (2004) 'Frontline: Optimal T cell activation requires the engagement of CD6 and CD166', *European Journal of Immunology*, 34(4), pp. 930–940. doi:10.1002/eji.200424856.

Hebron, K.E. *et al.* (2018) 'Alternative splicing of ALCAM enables tunable regulation of cell-cell adhesion through differential proteolysis', *Scientific Reports*, 8(1). doi:10.1038/s41598-018-21467-x.

Hermanson, G.T. (2013) 'Functional targets for Bioconjugation', *Bioconjugate Techniques*, pp. 127–228. doi:10.1016/b978-0-12-382239-0.00002-9.

Herr, B. *et al.* (2009) 'The supernatant of apoptotic cells causes transcriptional activation of hypoxia-inducible factor–1α in macrophages via sphingosine-1-phosphate and transforming growth factor-β', *Blood*, 114(10), pp. 2140–2148. doi:10.1182/blood-2009-01-201889.

Hmama, Z. *et al.* (1999) '1α,25-dihydroxyvitamin D3–induced myeloid cell differentiation is regulated by a vitamin D receptor–phosphatidylinositol 3-kinase signaling complex', *The Journal of Experimental Medicine*, 190(11), pp. 1583–1594. doi:10.1084/jem.190.11.1583.

Hochreiter-Hufford, A. and Ravichandran, K.S. (2013) 'Clearing the dead: Apoptotic cell sensing, recognition, engulfment, and digestion', *Cold Spring Harbor Perspectives in Biology*, 5(1). doi:10.1101/cshperspect.a008748.

Höög, J.L. and Lötvall, J. (2015) 'Diversity of extracellular vesicles in human ejaculates revealed by Cryo-Electron Microscopy', *Journal of Extracellular Vesicles*, 4(1). doi:10.3402/jev.v4.28680.

Hoshino, A. *et al.* (2015) 'Tumour exosome integrins determine organotropic metastasis', *Nature*, 527(7578), pp. 329–335. doi:10.1038/nature15756.

Hristodorov, D. *et al.* (2015) 'Targeting CD64 mediates elimination of M1 but not M2 macrophages in vitro and in cutaneous inflammation in mice and patient biopsies', *mAbs*, 7(5), pp. 853–862. doi:10.1080/19420862.2015.1066950.

Huang, Y. and Yu, L. (2022) 'Tetraspanin-enriched microdomains: The building blocks of migrasomes', *Cell Insight*, 1(1), p. 100003. doi:10.1016/j.cellin.2021.100003.

Hynes, R.O. (2002) 'Integrins', *Cell*, 110(6), pp. 673–687. doi:10.1016/s0092-8674(02)00971-6.

Iannotta, D. *et al.* (2023) 'Entry and exit of extracellular vesicles to and from the blood circulation', *Nature Nanotechnology*, 19(1), pp. 13–20. doi:10.1038/s41565-023-01522-z.

Ilan, N. *et al.* (2001) 'Pecam-1 shedding during apoptosis generates a membrane-anchored truncated molecule with unique signaling characteristics', *The FASEB Journal*, 15(2), pp. 362–372. doi:10.1096/fj.00-0372com.

Ilic, K. *et al.* (2021) 'Neuroplastin in human cognition: Review of literature and future perspectives', *Translational Psychiatry*, 11(1). doi:10.1038/s41398-021-01509-1.

Imbert, P.R.C. *et al.* (2021) 'An acquired and endogenous glycocalyx forms a bidirectional "don't eat" and "don't eat me" barrier to phagocytosis', *Current Biology*, 31(1). doi:10.1016/j.cub.2020.09.082.

Issekutz, T.B. (1991) 'Inhibition of in vivo lymphocyte migration to inflammation and homing to lymphoid tissues by the TA-2 monoclonal antibody. A likely role for VLA-4 in vivo.', *The Journal of Immunology*, 147(12), pp. 4178–4184. doi:10.4049/jimmunol.147.12.4178.

Janz, R. and Südhof, T.C. (1998) 'Cellugyrin, a novel ubiquitous form of synaptogyrin that is phosphorylated by PP60C-', *Journal of Biological Chemistry*, 273(5), pp. 2851–2857. doi:10.1074/jbc.273.5.2851.

Jeannet, R. *et al.* (2013) 'Alcam regulates long-term hematopoietic stem cell engraftment and self-renewal', *Stem Cells*, 31(3), pp. 560–571. doi:10.1002/stem.1309.

Jensen, H. *et al.* (2017) 'Cutting edge: Il-2–induced expression of the amino acid transporters SLC1A5 and CD98 is a prerequisite for NKG2D-mediated activation of human NK cells', *The Journal of Immunology*, 199(6), pp. 1967–1972. doi:10.4049/jimmunol.1700497.

Jiang, L. *et al.* (2017) 'Determining the contents and cell origins of apoptotic bodies by flow cytometry', *Scientific Reports*, 7(1). doi:10.1038/s41598-017-14305-z.

Jiang, N. *et al.* (2024) 'Multiparametric profiling of HER2-enriched extracellular vesicles in breast cancer using single extracellular vesicle nanoscopy', *Journal of Nanobiotechnology*, 22(1). doi:10.1186/s12951-024-02858-x.

Jiang, T. *et al.* (2023) ‘Apoptotic bodies inhibit inflammation by PDL1–pd1-mediated macrophage metabolic reprogramming’, *Cell Proliferation*, 57(1). doi:10.1111/cpr.13531.

Julian, L. *et al.* (2021) ‘Defective apoptotic cell contractility provokes sterile inflammation, leading to liver damage and tumour suppression’, *eLife*, 10. doi:10.7554/elife.61983.

Kadry, Y.A. and Calderwood, D.A. (2020) ‘Chapter 22: Structural and signaling functions of integrins’, *Biochimica et Biophysica Acta (BBA) - Biomembranes*, 1862(5), p. 183206. doi:10.1016/j.bbamem.2020.183206.

Kajimoto, T. *et al.* (2013) ‘Ongoing activation of sphingosine 1-phosphate receptors mediates maturation of exosomal multivesicular endosomes’, *Nature Communications*, 4(1). doi:10.1038/ncomms3712.

Kamerkar, S. *et al.* (2017) ‘Exosomes facilitate therapeutic targeting of oncogenic kras in pancreatic cancer’, *Nature*, 546(7659), pp. 498–503. doi:10.1038/nature22341.

Kaur, S. *et al.* (2014) ‘CD47-dependent immunomodulatory and angiogenic activities of extracellular vesicles produced by T cells’, *Matrix Biology*, 37, pp. 49–59. doi:10.1016/j.matbio.2014.05.007.

Kaur, S. *et al.* (2017) ‘A function-blocking CD47 antibody modulates extracellular vesicle-mediated intercellular signaling between breast carcinoma cells and endothelial cells’, *Journal of Cell Communication and Signaling*, 12(1), pp. 157–170. doi:10.1007/s12079-017-0428-0.

Kaur, S. *et al.* (2022) ‘Single vesicle analysis of CD47 association with integrins and tetraspanins on extracellular vesicles released by T lymphoblast and prostate carcinoma cells’, *Journal of Extracellular Vesicles*, 11(9). doi:10.1002/jev2.12265.

Kelley, S.M. and Ravichandran, K.S. (2024) ‘No need to “Sugar coat”: Removing glycocalyx on apoptotic blebs promotes phagocytosis’, *Developmental Cell*, 59(7), pp. 827–829. doi:10.1016/j.devcel.2024.02.014.

Kerr, J.F., Wyllie, A.H. and Currie, A.R. (1972) ‘Apoptosis: A basic biological phenomenon with wideranging implications in tissue kinetics’, *British Journal of Cancer*, 26(4), pp. 239–257. doi:10.1038/bjc.1972.33.

Kim, S.-M. and Kim, H.-S. (2017) ‘Engineering of extracellular vesicles as drug delivery vehicles’, *Stem Cell Investigation*, 4(9), pp. 74–74. doi:10.21037/sci.2017.08.07.

King, L.E., Osati-Ashtiani, F. and Fraker, P.J. (2002) ‘Apoptosis plays a distinct role in the loss of precursor lymphocytes during zinc deficiency in mice’, *The Journal of Nutrition*, 132(5), pp. 974–979. doi:10.1093/jn/132.5.974.

Kirchhausen, T. (2012) ‘Bending membranes’, *Nature Cell Biology*, 14(9), pp. 906–908. doi:10.1038/ncb2570.

Koopman, G. *et al.* (1994) ‘Adhesion through the LFA-1 (CD11A/CD18)-ICAM-1 (CD54) and the VLA-4 (cd49d)-vcam-1 (CD106) pathways prevents apoptosis of germinal center B cells.’, *The Journal of Immunology*, 152(8), pp. 3760–3767. doi:10.4049/jimmunol.152.8.3760.

Kulms, D. and Schwarz, T. (2000) ‘Molecular mechanisms of uv-induced apoptosis’, *Photodermatology, Photoimmunology & Photomedicine*, 16(5), pp. 195–201. doi:10.1034/j.1600-0781.2000.160501.x.

Kumar, M.A. *et al.* (2024) ‘Extracellular vesicles as tools and targets in therapy for diseases’, *Signal Transduction and Targeted Therapy*, 9(1). doi:10.1038/s41392-024-01735-1.

Landmann, R. *et al.* (1996) ‘Human monocyte CD14 is upregulated by lipopolysaccharide’, *Infection and Immunity*, 64(5), pp. 1762–1769. doi:10.1128/iai.64.5.1762-1769.1996.

Langnaese, K. *et al.* (1998) ‘Immunoglobulin superfamily members GP65 and GP55: Tissue distribution of glycoforms’, *FEBS Letters*, 429(3), pp. 284–288. doi:10.1016/s0014-5793(98)00616-4.

Lara, P. *et al.* (2020) ‘Exploiting the natural properties of extracellular vesicles in targeted delivery towards specific cells and tissues’, *Pharmaceutics*, 12(11), p. 1022. doi:10.3390/pharmaceutics12111022.

Lauber, K. *et al.* (2003) ‘Apoptotic cells induce migration of phagocytes via caspase-3-mediated release of a lipid attraction signal’, *Cell*, 113(6), pp. 717–730. doi:10.1016/s0092-8674(03)00422-7.

Le, T. *et al.* (2024) ‘Redistribution of the glycocalyx exposes phagocytic determinants on apoptotic cells’, *Developmental Cell*, 59(7). doi:10.1016/j.devcel.2024.01.020.

Leary, N. *et al.* (2022) ‘Melanoma-derived extracellular vesicles mediate lymphatic remodelling and impair tumour immunity in draining lymph nodes’, *Journal of Extracellular Vesicles*, 11(2). doi:10.1002/jev2.12197.

Ledingham, J. (1908) ‘The influence of temperature on phagocytosis’, *Proceedings of the Royal Society of London. Series B, Containing Papers of a Biological Character*, 80(539), pp. 188–195. doi:10.1098/rspb.1908.0019.

Leidi, M. *et al.* (2009) ‘M2 macrophages Phagocytose rituximab-opsonized leukemic targets more efficiently than M1 cells in vitro’, *The Journal of Immunology*, 182(7), pp. 4415–4422. doi:10.4049/jimmunol.0713732.

Lelek, M. *et al.* (2021) ‘Single-molecule localization microscopy’, *Nature Reviews Methods Primers*, 1(1). doi:10.1038/s43586-021-00038-x.

Levkau, B. *et al.* (1998) ‘Caspase-mediated cleavage of focal adhesion kinase pp125FAK and disassembly of focal adhesions in human endothelial cell apoptosis’, *The Journal of Experimental Medicine*, 187(4), pp. 579–586. doi:10.1084/jem.187.4.579.

Levy, B.D. *et al.* (2001) ‘Lipid mediator class switching during acute inflammation: Signals in resolution’, *Nature Immunology*, 2(7), pp. 612–619. doi:10.1038/89759.

Li, J. *et al.* (2022) ‘Apoptotic bodies extracted from adipose mesenchymal stem cells carry microrna-21–5p to induce M2 polarization of macrophages and augment skin wound healing by targeting KLF6’, *Burns*, 48(8), pp. 1893–1908. doi:10.1016/j.burns.2021.12.010.

Li, L.Y., Luo, X. and Wang, X. (2001) ‘Endonuclease G is an apoptotic DNase when released from mitochondria’, *Nature*, 412(6842), pp. 95–99. doi:10.1038/35083620.

Li, Y. *et al.* (2022) ‘CD47 cross-dressing by extracellular vesicles expressing CD47 inhibits phagocytosis without transmitting cell death signals’, *eLife*, 11. doi:10.7554/elife.73677.

Liam-Or, R. *et al.* (2024) ‘Cellular uptake and in vivo distribution of mesenchymal-stem-cell-derived extracellular vesicles are protein corona dependent’, *Nature Nanotechnology*, 19(6), pp. 846–855. doi:10.1038/s41565-023-01585-y.

Linares, R. *et al.* (2015) ‘High-speed centrifugation induces aggregation of extracellular vesicles’, *Journal of Extracellular Vesicles*, 4(1). doi:10.3402/jev.v4.29509.

Liu, J. *et al.* (2020) ‘Apoptotic bodies derived from mesenchymal stem cells promote cutaneous wound healing via regulating the functions of macrophages’, *Stem Cell Research & Therapy*, 11(1). doi:10.1186/s13287-020-02014-w.

Liu, X. *et al.* (2023) 'Macrophage-derived apoptotic bodies impair the osteogenic ability of osteoblasts in periodontitis', *Oral Diseases*, 30(5), pp. 3296–3307. doi:10.1111/odi.14808.

Liu, Y. *et al.* (2001) 'The role of CD47 in neutrophil transmigration', *Journal of Biological Chemistry*, 276(43), pp. 40156–40166. doi:10.1074/jbc.m104138200.

Loconte, L. *et al.* (2023) 'Detection of the interactions of tumour derived extracellular vesicles with immune cells is dependent on ev-labelling methods', *Journal of Extracellular Vesicles*, 12(12). doi:10.1002/jev2.12384.

Los, D.A. and Murata, N. (2004) 'Membrane fluidity and its roles in the perception of environmental signals', *Biochimica et Biophysica Acta (BBA) - Biomembranes*, 1666(1–2), pp. 142–157. doi:10.1016/j.bbamem.2004.08.002.

Lossi, L. (2022) 'The concept of intrinsic versus extrinsic apoptosis', *Biochemical Journal*, 479(3), pp. 357–384. doi:10.1042/bcj20210854.

Luo, B. *et al.* (2016) 'Erythropoeitin signaling in macrophages promotes dying cell clearance and immune tolerance', *Immunity*, 44(2), pp. 287–302. doi:10.1016/j.immuni.2016.01.002.

Luscinskas, F.W. *et al.* (1996) 'L- and P-selectins, but not cd49d (VLA-4) integrins, mediate monocyte initial attachment to TNF-alpha-activated vascular endothelium under flow in vitro.', *The Journal of Immunology*, 157(1), pp. 326–335. doi:10.4049/jimmunol.157.1.326.

Lv, Z. *et al.* (2015) 'Loss of cell surface CD47 clustering formation and binding avidity to sirpα facilitate apoptotic cell clearance by macrophages', *The Journal of Immunology*, 195(2), pp. 661–671. doi:10.4049/jimmunol.1401719.

Maddox, J.F. *et al.* (1997) 'Lipoxin A4 stable analogs are potent mimetics that stimulate human monocytes and THP-1 cells via a G-protein-linked lipoxin A4 receptor', *Journal of Biological Chemistry*, 272(11), pp. 6972–6978. doi:10.1074/jbc.272.11.6972.

Maile, L.A. *et al.* (2008) 'Glucose regulation of integrin-associated protein cleavage controls the response of vascular smooth muscle cells to insulin-like growth factor-I', *Molecular Endocrinology*, 22(5), pp. 1226–1237. doi:10.1210/me.2007-0552.

Martinez, F.O. *et al.* (2006) 'Transcriptional profiling of the human monocyte-to-macrophage differentiation and polarization: New molecules and patterns of gene expression', *The Journal of Immunology*, 177(10), pp. 7303–7311. doi:10.4049/jimmunol.177.10.7303.

Masedunskas, A. *et al.* (2006) 'Activated leukocyte cell adhesion molecule is a component of the endothelial junction involved in transendothelial monocyte migration', *FEBS Letters*, 580(11), pp. 2637–2645. doi:10.1016/j.febslet.2006.04.013.

Mattila, P.K. *et al.* (2013) 'The actin and tetraspanin networks organize receptor nanoclusters to regulate B cell receptor-mediated signaling', *Immunity*, 38(3), pp. 461–474. doi:10.1016/j.immuni.2012.11.019.

McMahon, H.T. and Boucrot, E. (2011) 'Molecular mechanism and physiological functions of clathrin-mediated endocytosis', *Nature Reviews Molecular Cell Biology*, 12(8), pp. 517–533. doi:10.1038/nrm3151.

Mendt, M., Rezvani, K. and Shpall, E. (2019) 'Mesenchymal stem cell-derived exosomes for clinical use', *Bone Marrow Transplantation*, 54(S2), pp. 789–792. doi:10.1038/s41409-019-0616-z.

Mevorach, D. *et al.* (1998) 'Complement-dependent clearance of apoptotic cells by human macrophages', *The Journal of Experimental Medicine*, 188(12), pp. 2313–2320. doi:10.1084/jem.188.12.2313.

Migneault, F. *et al.* (2020) 'Apoptotic exosome-like vesicles regulate endothelial gene expression, inflammatory signaling, and function through the NF-KB signaling pathway', *Scientific Reports*, 10(1). doi:10.1038/s41598-020-69548-0.

Miller, J.R. and Moon, R.T. (1996) 'Signal transduction through beta-catenin and specification of cell fate during embryogenesis.', *Genes & Development*, 10(20), pp. 2527–2539. doi:10.1101/gad.10.20.2527.

Miller, Y.I. *et al.* (2003) 'Minimally modified LDL binds to CD14, induces macrophage spreading via TLR4/MD-2, and inhibits phagocytosis of apoptotic cells', *Journal of Biological Chemistry*, 278(3), pp. 1561–1568. doi:10.1074/jbc.m209634200.

Mitra, P. *et al.* (2006) 'Role of ABCC1 in export of sphingosine-1-phosphate from Mast Cells', *Proceedings of the National Academy of Sciences*, 103(44), pp. 16394–16399. doi:10.1073/pnas.0603734103.

Moffatt, O.D. *et al.* (1999) 'Macrophage recognition of ICAM-3 on Apoptotic leukocytes', *The Journal of Immunology*, 162(11), pp. 6800–6810. doi:10.4049/jimmunol.162.11.6800.

Monleón, I. *et al.* (2001) 'Differential secretion of FAS ligand- or APO2 ligand/TNF-related apoptosis-inducing ligand-carrying microvesicles during activation-induced death of human T cells', *The Journal of Immunology*, 167(12), pp. 6736–6744. doi:10.4049/jimmunol.167.12.6736.

Monnier, M. *et al.* (2022) 'Antitumor strategies targeting macrophages: The importance of considering the differences in differentiation/polarization processes between human and mouse macrophages', *Journal for ImmunoTherapy of Cancer*, 10(10). doi:10.1136/jitc-2022-005560.

Moss, D.K. *et al.* (2006) 'A novel role for microtubules in apoptotic chromatin dynamics and cellular fragmentation', *Journal of Cell Science*, 119(11), pp. 2362–2374. doi:10.1242/jcs.02959.

Mulcahy, L.A., Pink, R.C. and Carter, D.R. (2014) 'Routes and mechanisms of extracellular vesicle uptake', *Journal of Extracellular Vesicles*, 3(1). doi:10.3402/jev.v3.24641.

Muller, W.A. *et al.* (1993) 'Pecam-1 is required for transendothelial migration of leukocytes.', *The Journal of experimental medicine*, 178(2), pp. 449–460. doi:10.1084/jem.178.2.449.

Murakami, N. *et al.* (2004) 'G2a is a proton-sensing G-protein-coupled receptor antagonized by Lysophosphatidylcholine', *Journal of Biological Chemistry*, 279(41), pp. 42484–42491. doi:10.1074/jbc.m406561200.

Murata, M. *et al.* (1995) 'Vip21/caveolin is a cholesterol-binding protein.', *Proceedings of the National Academy of Sciences*, 92(22), pp. 10339–10343. doi:10.1073/pnas.92.22.10339.

Murray, P.J. (2017) 'Macrophage polarization', *Annual Review of Physiology*, 79(1), pp. 541–566. doi:10.1146/annurev-physiol-022516-034339.

Nakaya, M. *et al.* (2014) 'Inflammatory T cell responses rely on amino acid transporter ASCT2 facilitation of glutamine uptake and mtorc1 kinase activation', *Immunity*, 40(5), pp. 692–705. doi:10.1016/j.immuni.2014.04.007.

Nazarenko, I. *et al.* (2010) 'Cell surface tetraspanin TSPAN8 contributes to molecular pathways of exosome-induced endothelial cell activation', *Cancer Research*, 70(4), pp. 1668–1678. doi:10.1158/0008-5472.can-09-2470.

Nelissen, J.M. *et al.* (2000) 'Dynamic Regulation of activated leukocyte cell adhesion molecule–mediated homotypic cell adhesion through the actin cytoskeleton', *Molecular Biology of the Cell*, 11(6), pp. 2057–2068. doi:10.1091/mbc.11.6.2057.

Nourshargh, S. and Alon, R. (2014) 'Leukocyte migration into inflamed tissues', *Immunity*, 41(5), pp. 694–707. doi:10.1016/j.immuni.2014.10.008.

Oberhammer, F.A. *et al.* (1994) 'Chromatin condensation during apoptosis is accompanied by degradation of lamin A+B, without enhanced activation of CDC2 kinase.', *The Journal of cell biology*, 126(4), pp. 827–837. doi:10.1083/jcb.126.4.827.

Ogden, C.A. *et al.* (2001) 'C1Q and mannose binding lectin engagement of cell surface calreticulin and CD91 initiates macropinocytosis and uptake of apoptotic cells', *The Journal of Experimental Medicine*, 194(6), pp. 781–796. doi:10.1084/jem.194.6.781.

Oldenborg, P.-A., Gresham, H.D. and Lindberg, F.P. (2001) 'CD47-signal regulatory protein α (SIRPA) regulates Fcγ and complement receptor–mediated phagocytosis', *The Journal of Experimental Medicine*, 193(7), pp. 855–862. doi:10.1084/jem.193.7.855.

Ortega-Gómez, A., Perretti, M. and Soehnlein, O. (2013) 'Resolution of inflammation: An integrated view', *EMBO Molecular Medicine*, 5(5), pp. 661–674. doi:10.1002/emmm.201202382.

Ozkocak, D.C., Phan, T.K. and Poon, I.K. (2022) 'Translating extracellular vesicle packaging into therapeutic applications', *Frontiers in Immunology*, 13. doi:10.3389/fimmu.2022.946422.

Paddock, C. *et al.* (2016) 'Structural basis for PECAM-1 homophilic binding', *Blood*, 127(8), pp. 1052–1061. doi:10.1182/blood-2015-07-660092.

Park, D. *et al.* (2007) 'Bai1 is an engulfment receptor for apoptotic cells upstream of the elmo/dock180/RAC module', *Nature*, 450(7168), pp. 430–434. doi:10.1038/nature06329.

Park, S.J. *et al.* (2018) 'Molecular mechanisms of biogenesis of apoptotic exosome-like vesicles and their roles as damage-associated molecular patterns', *Proceedings of the National Academy of Sciences*, 115(50). doi:10.1073/pnas.1811432115.

Parolini, I. *et al.* (2009) ‘Microenvironmental Ph is a key factor for exosome traffic in tumor cells’, *Journal of Biological Chemistry*, 284(49), pp. 34211–34222. doi:10.1074/jbc.m109.041152.

Pathan, M. *et al.* (2017) ‘A novel community driven software for functional enrichment analysis of extracellular vesicles data’, *Journal of Extracellular Vesicles*, 6(1). doi:10.1080/20013078.2017.1321455.

Peyret, A. *et al.* (2017) ‘Liposomes in polymersomes: Multicompartment system with temperature-triggered release’, *Langmuir*, 33(28), pp. 7079–7085. doi:10.1021/acs.langmuir.7b00655.

Polara, R. *et al.* (2024) ‘Cell autonomous functions of CD47 in regulating cellular plasticity and metabolic plasticity’, *Cell Death & Differentiation* [Preprint]. doi:10.1038/s41418-024-01347-w.

Pontejo, S.M. and Murphy, P.M. (2021) ‘Chemokines act as phosphatidylserine-bound “Find-me” signals in apoptotic cell clearance’, *PLOS Biology*, 19(5). doi:10.1371/journal.pbio.3001259.

Poon, I.K., Chiu, Y.H., Armstrong A.J., Kinchen, J.M., Juncadella, I.J., Bayliss, D.A., Ravichandran, K.S. (2014a) ‘Unexpected link between an antibiotic, pannexin channels and apoptosis’, *Nature*, 507(7492), pp. 329–334. doi:10.1038/nature13147.

Poon, I.K., Lucas, C.D., Rossi, A.G., Ravichandran, K.S. (2014b) ‘Apoptotic cell clearance: Basic biology and therapeutic potential’, *Nature Reviews Immunology*, 14(3), pp. 166–180. doi:10.1038/nri3607.

Potter, P.K. *et al.* (2007) ‘Efficient clearance of opsonised apoptotic cells in the absence of pecam-1’, *Molecular Immunology*, 44(6), pp. 1135–1140. doi:10.1016/j.molimm.2006.07.002.

Prada, I. and Meldolesi, J. (2016) ‘Binding and fusion of extracellular vesicles to the plasma membrane of their cell targets’, *International Journal of Molecular Sciences*, 17(8), p. 1296. doi:10.3390/ijms17081296.

Privratsky, J.R., Newman, D.K. and Newman, P.J. (2010) ‘Pecam-1: Conflicts of interest in inflammation’, *Life Sciences*, 87(3–4), pp. 69–82. doi:10.1016/j.lfs.2010.06.001.

Puig-Kröger, A. *et al.* (2004) 'Regulated expression of the pathogen receptor dendritic cell-specific intercellular adhesion molecule 3 (icam-3)-grabbing nonintegrin in THP-1 human leukemic cells, monocytes, and macrophages', *Journal of Biological Chemistry*, 279(24), pp. 25680–25688. doi:10.1074/jbc.m311516200.

Purushothaman, A. *et al.* (2016) 'Fibronectin on the surface of myeloma cell-derived exosomes mediates exosome-cell interactions', *Journal of Biological Chemistry*, 291(4), pp. 1652–1663. doi:10.1074/jbc.m115.686295.

Rahman, I. *et al.* (2021) 'L-selectin regulates human neutrophil transendothelial migration', *Journal of Cell Science*, 134(3). doi:10.1242/jcs.250340.

Raja, M.K. *et al.* (2019) 'Elevated synaptic vesicle release probability in synaptophysin/gyrin family quadruple knockouts', *eLife*, 8. doi:10.7554/elife.40744.

Ramos-Zaldívar, H.M. *et al.* (2022) 'Extracellular vesicles through the blood–brain barrier: A Review', *Fluids and Barriers of the CNS*, 19(1). doi:10.1186/s12987-022-00359-3.

Raposo, G. *et al.* (1996) 'B lymphocytes secrete antigen-presenting vesicles.', *The Journal of experimental medicine*, 183(3), pp. 1161–1172. doi:10.1084/jem.183.3.1161.

Reed-Geaghan, E.G. *et al.* (2009) 'CD14 and toll-like receptors 2 and 4 are required for fibrillar AB-stimulated microglial activation', *The Journal of Neuroscience*, 29(38), pp. 11982–11992. doi:10.1523/jneurosci.3158-09.2009.

Renard, H.-F. *et al.* (2020) 'Endophilin-A3 and galectin-8 control the clathrin-independent endocytosis of CD166', *Nature Communications*, 11(1). doi:10.1038/s41467-020-15303-y.

Richter, M., Vader, P. and Fuhrmann, G. (2021) 'Approaches to surface engineering of extracellular vesicles', *Advanced Drug Delivery Reviews*, 173, pp. 416–426. doi:10.1016/j.addr.2021.03.020.

Rieu, S. *et al.* (2000) 'Exosomes released during reticulocyte maturation bind to fibronectin via integrin α4β1', *European Journal of Biochemistry*, 267(2), pp. 583–590. doi:10.1046/j.1432-1327.2000.01036.x.

Rivoltini, L. *et al.* (2016) 'TNF-related apoptosis-inducing ligand (trail)–armed exosomes deliver proapoptotic signals to tumor site', *Clinical Cancer Research*, 22(14), pp. 3499–3512. doi:10.1158/1078-0432.ccr-15-2170.

Robbins, C.S. *et al.* (2013) 'Local proliferation dominates lesional macrophage accumulation in atherosclerosis', *Nature Medicine*, 19(9), pp. 1166–1172. doi:10.1038/nm.3258.

Rodriguez-Pinto, D. *et al.* (2008) 'Identification of novel tumor antigens with patient-derived immune-selected antibodies', *Cancer Immunology, Immunotherapy*, 58(2), pp. 221–234. doi:10.1007/s00262-008-0543-0.

Roos, W.P., Thomas, A.D. and Kaina, B. (2015) 'DNA damage and the balance between survival and death in cancer biology', *Nature Reviews Cancer*, 16(1), pp. 20–33. doi:10.1038/nrc.2015.2.

Sakaguchi, M. *et al.* (2016) 'Identification of an S100A8 receptor Neuroplastin-β and its heterodimer formation with Emmprin', *Journal of Investigative Dermatology*, 136(11), pp. 2240–2250. doi:10.1016/j.jid.2016.06.617.

Salucci, S. *et al.* (2012) 'Ultraviolet B (UVB) irradiation-induced apoptosis in various cell lineages in vitro', *International Journal of Molecular Sciences*, 14(1), pp. 532–546. doi:10.3390/ijms14010532.

Sánchez-Alcázar, J.A. *et al.* (2007) 'The apoptotic microtubule network preserves plasma membrane integrity during the execution phase of apoptosis', *Apoptosis*, 12(7), pp. 1195–1208. doi:10.1007/s10495-006-0044-6.

Sanderson, J.M. (2012) 'Resolving the kinetics of lipid, protein and peptide diffusion in membranes', *Molecular Membrane Biology*, 29(5), pp. 118–143. doi:10.3109/09687688.2012.678018.

Sapoń, K. *et al.* (2023) 'The role of lipid rafts in vesicle formation', *Journal of Cell Science*, 136(9). doi:10.1242/jcs.260887.

Schenkel, A.R., Chew, T.W. and Muller, W.A. (2004) 'Platelet endothelial cell adhesion molecule deficiency or blockade significantly reduces leukocyte emigration in a majority of mouse strains', *The Journal of Immunology*, 173(10), pp. 6403–6408. doi:10.4049/jimmunol.173.10.6403.

Schif-Zuck, S. *et al.* (2010) 'Saturated-efferocytosis generates pro-resolving CD11B^{low} macrophages: Modulation by resolvins and glucocorticoids', *European Journal of Immunology*, 41(2), pp. 366–379. doi:10.1002/eji.201040801.

Schildberger, A. *et al.* (2013) 'Monocytes, peripheral blood mononuclear cells, and THP-1 cells exhibit different cytokine expression patterns following stimulation with lipopolysaccharide', *Mediators of Inflammation*, 2013, pp. 1–10. doi:10.1155/2013/697972.

Schlichting, C.L., Schareck, W.D. and Weis, M. (2005) 'Dendritic cell adhesion is enhanced on endothelial cells preexposed to calcineurin inhibitors', *Journal of Cardiovascular Pharmacology*, 46(3), pp. 250–254. doi:10.1097/01.fjc.0000175233.88207.de.

Schmid, M.C. *et al.* (2018) 'Integrin CD11B activation drives anti-tumor innate immunity', *Nature Communications*, 9(1). doi:10.1038/s41467-018-07387-4.

Scott, R.S. et al. (2001) 'Phagocytosis and clearance of apoptotic cells is mediated by Mer', *Nature*, 411(6834), pp. 207–211. doi:10.1038/35075603.

Sebbagh, M. *et al.* (2001) 'Caspase-3-mediated cleavage of rock I induces MLC phosphorylation and apoptotic membrane blebbing', *Nature Cell Biology*, 3(4), pp. 346–352. doi:10.1038/35070019.

Segawa, K., Kurata, S. and Nagata, S. (2016) 'Human type IV p-type atpases that work as plasma membrane phospholipid Flippases and their regulation by caspase and calcium', *Journal of Biological Chemistry*, 291(2), pp. 762–772. doi:10.1074/jbc.m115.690727.

Segundo, C. *et al.* (1999) 'Surface molecule loss and Bleb Formation by human germinal center B cells undergoing apoptosis: Role of apoptotic blebs in monocyte chemotaxis', *Blood*, 94(3), pp. 1012–1020. doi:10.1182/blood.v94.3.1012.415k05_1012_1020.

Seong, J.S., Yun, M.E. and Park, S.N. (2018) 'Surfactant-stable and ph-sensitive liposomes coated with N-succinyl-chitosan and chitooligosaccharide for delivery of quercetin', *Carbohydrate Polymers*, 181, pp. 659–667. doi:10.1016/j.carbpol.2017.11.098.

Sharpe, A.H. (2009) 'Mechanisms of costimulation', *Immunological Reviews*, 229(1), pp. 5–11. doi:10.1111/j.1600-065x.2009.00784.x.

Shen, G. *et al.* (2017) 'Microvesicles released by apoptotic human neutrophils suppress proliferation and IL-2/IL-2 receptor expression of resting T helper cells', *European Journal of Immunology*, 47(5), pp. 900–910. doi:10.1002/eji.201546203.

Sheng, L., Luo, Q. and Chen, L. (2022) ‘Amino acid solute carrier transporters in inflammation and autoimmunity’, *Drug Metabolism and Disposition*, 50(9), pp. 1228–1237. doi:10.1124/dmd.121.000705.

Sica, A. and Mantovani, A. (2012) ‘Macrophage plasticity and polarization: In vivo veritas’, *Journal of Clinical Investigation*, 122(3), pp. 787–795. doi:10.1172/jci59643.

Sindrilaru, A. *et al.* (2011) ‘An unrestrained proinflammatory M1 macrophage population induced by iron impairs wound healing in humans and mice’, *Journal of Clinical Investigation*, 121(3), pp. 985–997. doi:10.1172/jci44490.

Skotland, T. *et al.* (2020) ‘An emerging focus on lipids in extracellular vesicles’, *Advanced Drug Delivery Reviews*, 159, pp. 308–321. doi:10.1016/j.addr.2020.03.002.

Skovronova, R. *et al.* (2021) ‘Surface marker expression in small and medium/large mesenchymal stromal cell-derived extracellular vesicles in naive or apoptotic condition using orthogonal techniques’, *Cells*, 10(11), p. 2948. doi:10.3390/cells10112948.

Smith, T.D. *et al.* (2016) ‘Regulation of macrophage polarization and plasticity by complex activation signals’, *Integrative Biology*, 8(9), pp. 946–955. doi:10.1039/c6ib00105j.

Soehnlein, O. and Lindbom, L. (2010) ‘Phagocyte partnership during the onset and resolution of inflammation’, *Nature Reviews Immunology*, 10(6), pp. 427–439. doi:10.1038/nri2779.

Soto, M.S. *et al.* (2013) ‘Functional role of endothelial adhesion molecules in the early stages of brain metastasis’, *Neuro-Oncology*, 16(4), pp. 540–551. doi:10.1093/neuonc/not222.

Stachowiak, J.C. *et al.* (2012) ‘Membrane bending by protein–protein crowding’, *Nature Cell Biology*, 14(9), pp. 944–949. doi:10.1038/ncb2561.

Stout, R.D. *et al.* (1996) ‘Impaired T cell-mediated macrophage activation in CD40 ligand-deficient mice.’, *The Journal of Immunology*, 156(1), pp. 8–11. doi:10.4049/jimmunol.156.1.8.

Stunault, M.I. *et al.* (2018) ‘Metabolism plays a key role during macrophage activation’, *Mediators of Inflammation*, 2018, pp. 1–10. doi:10.1155/2018/2426138.

Sugita, S., Janz, R. and Südhof, T.C. (1999) ‘Synaptogyrins regulate ca2+-dependent exocytosis in PC12 cells’, *Journal of Biological Chemistry*, 274(27), pp. 18893–18901. doi:10.1074/jbc.274.27.18893.

Sumardika, I.W. *et al.* (2019) 'Neuroplastin-β mediates S100A8/a9-induced lung cancer disseminative progression', *Molecular Carcinogenesis*, 58(6), pp. 980–995. doi:10.1002/mc.22987.

Sun, J. *et al.* (2024) 'The potential of bacterial anti-phagocytic proteins in suppressing the clearance of extracellular vesicles mediated by host phagocytosis', *Frontiers in Immunology*, 15. doi:10.3389/fimmu.2024.1418061.

Sun, Y. *et al.* (2023) 'Engineered extracellular vesicles as a targeted delivery platform for precision therapy', *Tissue Engineering and Regenerative Medicine*, 20(2), pp. 157–175. doi:10.1007/s13770-022-00503-y.

Sung, B.H. *et al.* (2015) 'Directional cell movement through tissues is controlled by exosome secretion', *Nature Communications*, 6(1). doi:10.1038/ncomms8164.

Suttles, J. and Stout, R.D. (2009) 'Macrophage CD40 signaling: A pivotal regulator of disease protection and pathogenesis', *Seminars in Immunology*, 21(5), pp. 257–264. doi:10.1016/j.smim.2009.05.011.

Suzuki, J., Imanishi, E. and Nagata, S. (2014) 'Exposure of phosphatidylserine by XK-related protein family members during apoptosis', *Journal of Biological Chemistry*, 289(44), pp. 30257–30267. doi:10.1074/jbc.m114.583419.

Suzuki, J., Imanishi, E. and Nagata, S. (2016) 'XKR8 phospholipid scrambling complex in apoptotic phosphatidylserine exposure', *Proceedings of the National Academy of Sciences*, 113(34), pp. 9509–9514. doi:10.1073/pnas.1610403113.

Szewczyk-Roszczenko, O.K. *et al.* (2023) 'The chemical inhibitors of endocytosis: From mechanisms to potential clinical applications', *Cells*, 12(18), p. 2312. doi:10.3390/cells12182312.

Taichman, D.B. *et al.* (1991) 'Tumor cell surface alpha 4 beta 1 integrin mediates adhesion to vascular endothelium: Demonstration of an interaction with the N-terminal domains of INCAM-110/VCAM-1.', *Cell Regulation*, 2(5), pp. 347–355. doi:10.1091/mbc.2.5.347.

Teixidó, J. *et al.* (1992) 'Functional and structural analysis of VLA-4 integrin alpha 4 subunit cleavage.', *Journal of Biological Chemistry*, 267(3), pp. 1786–1791. doi:10.1016/s0021-9258(18)46014-0.

Teng, F.Y., Wang, Y. and Tang, B.L. (2001) 'The Syntaxins', *Genome Biology*, 2(11). doi:10.1186/gb-2001-2-11-reviews3012.

Than, U.T.T. *et al.* (2018) 'Differential expression of keratinocyte-derived extracellular vesicle mirnas discriminate exosomes from apoptotic bodies and microvesicles', *Frontiers in Endocrinology*, 9. doi:10.3389/fendo.2018.00535.

Thomas, L. (2011) *The role of the innate immune system in the clearance of apoptotic cells*. thesis. Aston University.

Tixeira, R. *et al.* (2019) 'ROCK1 but not LIMK1 or pak2 is a key regulator of apoptotic membrane blebbing and cell disassembly', *Cell Death & Differentiation*, 27(1), pp. 102–116. doi:10.1038/s41418-019-0342-5.

Tomoda, H., Kishimoto, Y. and Lee, Y.C. (1989) 'Temperature effect on endocytosis and exocytosis by rabbit alveolar macrophages', *Journal of Biological Chemistry*, 264(26), pp. 15445–15450. doi:10.1016/s0021-9258(19)84849-4.

Torr, E.E. *et al.* (2011) 'Apoptotic cell-derived ICAM-3 promotes both macrophage chemoattraction to and tethering of apoptotic cells', *Cell Death & Differentiation*, 19(4), pp. 671–679. doi:10.1038/cdd.2011.167.

Tóth, E. *et al.* (2021) 'Formation of a protein corona on the surface of extracellular vesicles in blood plasma', *Journal of Extracellular Vesicles*, 10(11). doi:10.1002/jev2.12140.

Trajkovic, K. *et al.* (2008) 'Ceramide triggers budding of exosome vesicles into multivesicular endosomes', *Science*, 319(5867), pp. 1244–1247. doi:10.1126/science.1153124.

Truman, L.A. *et al.* (2008) 'CX3CL1/Fractalkine is released from apoptotic lymphocytes to stimulate macrophage chemotaxis', *Blood*, 112(13), pp. 5026–5036. doi:10.1182/blood-2008-06-162404.

Tucher, C. *et al.* (2018) 'Extracellular vesicle subtypes released from activated or apoptotic T-lymphocytes carry a specific and stimulus-dependent protein cargo', *Frontiers in Immunology*, 9. doi:10.3389/fimmu.2018.00534.

Ulevitch, R.J. and Tobias, P.S. (1995) 'Receptor-dependent mechanisms of cell stimulation by bacterial endotoxin', *Annual Review of Immunology*, 13(1), pp. 437–457. doi:10.1146/annurev.iy.13.040195.002253.

Vallis, Y. *et al.* (1999) 'Importance of the pleckstrin homology domain of dynamin in clathrin-mediated endocytosis', *Current Biology*, 9(5), pp. 257–263. doi:10.1016/s0960-9822(99)80114-6.

Vaux, D.L., Whitney, D. and Weissman, I.L. (1996) 'Activation of physiological cell death mechanisms by a necrosis-causing agent', *Microscopy Research and Technique*, 34(3), pp. 259–266. doi:10.1002/(sici)1097-0029(19960615)34:3<259::aid-jemt8>3.0.co;2-k.

Vernon-Wilson, E.F. *et al.* (2007) 'CD31 delays phagocyte membrane repolarization to promote efficient binding of apoptotic cells', *Journal of Leukocyte Biology*, 82(5), pp. 1278–1288. doi:10.1189/jlb.0507283.

Vernon-Wilson, E.F., Auradé, F. and Brown, S.B. (2006) 'CD31 promotes β1 integrin-dependent engulfment of apoptotic Jurkat T lymphocytes opsonized for phagocytosis by fibronectin', *Journal of Leukocyte Biology*, 79(6), pp. 1260–1267. doi:10.1189/jlb.1005571.

Vogel, D.Y.S. *et al.* (2014) 'Human macrophage polarization in vitro: Maturation and activation methods compared', *Immunobiology*, 219(9), pp. 695–703. doi:10.1016/j.imbio.2014.05.002.

Vogt, A.B., Spindeldreher, S. and Kropshofer, H. (2002) 'Clustering of MHC–peptide complexes prior to their engagement in the immunological synapse: Lipid raft and Tetraspan Microdomains', *Immunological Reviews*, 189(1), pp. 136–151. doi:10.1034/j.1600-065x.2002.18912.x.

von Kleist, L. *et al.* (2011) 'Role of the clathrin terminal domain in regulating coated pit dynamics revealed by small molecule inhibition', *Cell*, 146(3), pp. 471–484. doi:10.1016/j.cell.2011.06.025.

von Lersner, A., Droesen, L. and Zijlstra, A. (2019) 'Modulation of cell adhesion and migration through regulation of the Immunoglobulin Superfamily member ALCAM/CD166', *Clinical & Experimental Metastasis*, 36(2), pp. 87–95. doi:10.1007/s10585-019-09957-2.

Vorselen, D. (2022) 'Dynamics of phagocytosis mediated by phosphatidylserine', *Biochemical Society Transactions*, 50(5), pp. 1281–1291. doi:10.1042/bst20211254.

Wang, H. and Zúñiga-Pflücker, J.C. (2022) 'Thymic microenvironment: Interactions between innate immune cells and developing thymocytes', *Frontiers in Immunology*, 13. doi:10.3389/fimmu.2022.885280.

Wang, L. *et al.* (2023) 'Engineering extracellular vesicles as delivery systems in therapeutic applications', *Advanced Science*, 10(17). doi:10.1002/advs.202300552.

Wang, X.-Q. and Frazier, W.A. (1998) 'The thrombospondin receptor CD47 (IAP) modulates and associates with A2B1 Integrin in vascular smooth muscle cells', *Molecular Biology of the Cell*, 9(4), pp. 865–874. doi:10.1091/mbc.9.4.865.

Wei, Z. *et al.* (2021) 'Mononuclear phagocyte system blockade using extracellular vesicles modified with CD47 on membrane surface for myocardial infarction reperfusion injury treatment', *Biomaterials*, 275, p. 121000. doi:10.1016/j.biomaterials.2021.121000.

Welsh, J.A. *et al.* (2023) 'A compendium of single extracellular vesicle flow cytometry', *Journal of Extracellular Vesicles*, 12(2). doi:10.1002/jev2.12299.

Welsh, J.A. *et al.* (2024) 'Minimal information for studies of extracellular vesicles (MISEV2023): From basic to advanced approaches', *Journal of Extracellular Vesicles*, 13(2). doi:10.1002/jev2.12404.

Wijeyesakere, S.J. *et al.* (2016) 'The C-terminal acidic region of calreticulin mediates phosphatidylserine binding and apoptotic cell phagocytosis', *The Journal of Immunology*, 196(9), pp. 3896–3909. doi:10.4049/jimmunol.1502122.

Williams, A.F. and Barclay, A.N. (1988) 'The immunoglobulin superfamily—domains for cell surface recognition', *Annual Review of Immunology*, 6(1), pp. 381–405. doi:10.1146/annurev.iy.06.040188.002121.

Williams, C. *et al.* (2019) 'Assessing the role of surface glycans of extracellular vesicles on cellular uptake', *Scientific Reports*, 9(1). doi:10.1038/s41598-019-48499-1.

Williams, M.R. *et al.* (2009) 'Transmigration across activated endothelium induces transcriptional changes, inhibits apoptosis, and decreases antimicrobial protein expression in human monocytes', *Journal of Leukocyte Biology*, 86(6), pp. 1331–1343. doi:10.1189/jlb.0209062.

Witasp, E. *et al.* (2007) 'Bridge over troubled water: Milk fat globule epidermal growth factor 8 promotes human monocyte-derived macrophage clearance of non-blebbing

phosphatidylserine-positive target cells', *Cell Death & Differentiation*, 14(5), pp. 1063–1065. doi:10.1038/sj.cdd.4402096.

Wolf, M. *et al.* (2022) 'A functional corona around extracellular vesicles enhances angiogenesis, skin regeneration and immunomodulation', *Journal of Extracellular Vesicles*, 11(4). doi:10.1002/jev2.12207.

Xiao, W. and Gao, H. (2018) 'The impact of protein corona on the behavior and targeting capability of nanoparticle-based Delivery System', *International Journal of Pharmaceutics*, 552(1–2), pp. 328–339. doi:10.1016/j.ijpharm.2018.10.011.

Yang, M. *et al.* (2022) 'Extracellular vesicle glucose transporter-1 and glycan features in monocyte-endothelial inflammatory interactions', *Nanomedicine: Nanotechnology, Biology and Medicine*, 42, p. 102515. doi:10.1016/j.nano.2022.102515.

Yang, M. *et al.* (2022) 'Extracellular vesicle glucose transporter-1 and glycan features in monocyte-endothelial inflammatory interactions', *Nanomedicine: Nanotechnology, Biology and Medicine*, 42, p. 102515. doi:10.1016/j.nano.2022.102515.

Yerneni, S.S. *et al.* (2022) 'Radioiodination of extravesicular surface constituents to study the BIOCORONA, cell trafficking and storage stability of extracellular vesicles', *Biochimica et Biophysica Acta (BBA) - General Subjects*, 1866(2), p. 130069. doi:10.1016/j.bbagen.2021.130069.

Yoon, B.R. *et al.* (2018) 'Role of SLC7A5 in metabolic reprogramming of human monocyte/macrophage immune responses', *Frontiers in Immunology*, 9. doi:10.3389/fimmu.2018.00053.

Yu, J. *et al.* (2024) 'Biogenesis and delivery of extracellular vesicles: Harnessing the power of evs for diagnostics and Therapeutics', *Frontiers in Molecular Biosciences*, 10. doi:10.3389/fmolb.2023.1330400.

Yuan, Z. *et al.* (2017) 'Trail delivery by msc-derived extracellular vesicles is an effective anticancer therapy', *Journal of Extracellular Vesicles*, 6(1). doi:10.1080/20013078.2017.1265291.

Zacharia, E. *et al.* (2020) 'Plasma signature of apoptotic microvesicles is associated with endothelial dysfunction and plaque rupture in acute coronary syndromes', *Journal of Molecular and Cellular Cardiology*, 138, pp. 110–114. doi:10.1016/j.yjmcc.2019.11.153.

Zhang, S. *et al.* (2019) 'EFFEROCYTOSIS fuels requirements of fatty acid oxidation and the electron transport chain to polarize macrophages for tissue repair', *Cell Metabolism*, 29(2). doi:10.1016/j.cmet.2018.12.004.

Zhang, T. *et al.* (2024) 'Structural–functional diversity of CD47 proteoforms', *Frontiers in Immunology*, 15. doi:10.3389/fimmu.2024.1329562.

Zhu, Y., Chen, X. and Liao, Y. (2023) 'Mesenchymal stem cells-derived apoptotic extracellular vesicles (ApoEVs): Mechanism and application in tissue regeneration', *Stem Cells*, 41(9), pp. 837–849. doi:10.1093/stmcls/sxad046.

Zimmerman, B. *et al.* (2016) 'Crystal structure of a full-length human tetraspanin reveals a cholesterol-binding pocket', *Cell*, 167(4). doi:10.1016/j.cell.2016.09.056.

Zindel, J. and Kubes, P. (2020) 'Damps, pamps, and lamps in immunity and sterile inflammation', *Annual Review of Pathology: Mechanisms of Disease*, 15(1), pp. 493–518. doi:10.1146/annurev-pathmechdis-012419-032847.

Zuidscherwoude, M. *et al.* (2015) 'The tetraspanin web revisited by super-resolution Microscopy', *Scientific Reports*, 5(1). doi:10.1038/srep12201.

Appendix

Cell	Time (h)	filename	Spherical	Oval	Tubular	Irregular
THP-1	18	THP1_18h_20kX_2594.tif	1	0	0	0
THP-1	18	THP1_18h_20kX_2592.tif	1	1	2	0
THP-1	18	THP1_18h_20kX_2590.tif	0	0	0	1
THP-1	18	THP1_18h_20kX_2588.tif	1	0	0	0
THP-1	18	THP1_18h_20kX_2586.tif	1	1	1	0
THP-1	18	THP1_18h_20kX_2584.tif	1	0	1	0
THP-1	18	THP1_18h_20kX_2582.tif	0	0	0	1
THP-1	18	THP1_18h_20kX_2580.tif	0	0	0	1
THP-1	18	THP1_18h_20kX_2578.tif	1	0	0	0
THP-1	18	THP1_18h_20kX_2575.tif	2	0	1	0
THP-1	18	THP1_18h_20kX_2573.tif	2	0	0	0
THP-1	18	THP1_18h_20kX_2571.tif	2	0	1	0
THP-1	18	THP1_18h_20kX_2568.tif	0	0	1	0
THP-1	18	THP1_18h_20kX_2566.tif	0	0	1	0
THP-1	18	THP1_18h_20kX_2564.tif	1	0	1	0
THP-1	18	THP1_18h_20kX_2562.tif	0	0	0	2
THP-1	6	THP1_6h_20kX_2534.tif	0	0	1	0
THP-1	6	THP1_6h_20kX_2559.tif	1	0	0	4
THP-1	6	THP1_6h_20kX_2556.tif	0	2	0	0
THP-1	6	THP1_6h_20kX_2554.tif	0	0	1	0
THP-1	6	THP1_6h_20kX_2552.tif	0	0	1	0
THP-1	6	THP1_6h_20kX_2550.tif	0	0	2	1
THP-1	6	THP1_6h_20kX_2548.tif	2	0	0	1
THP-1	6	THP1_6h_20kX_2547.tif	1	2	0	0
THP-1	6	THP1_6h_20kX_2544.tif	0	0	1	0
THP-1	6	THP1_6h_20kX_2542.tif	1	0	0	0
THP-1	6	THP1_6h_20kX_2540.tif	0	1	0	2
THP-1	6	THP1_6h_20kX_2538.tif	1	0	0	0
THP-1	6	THP1_6h_20kX_2536.tif	0	0	0	3
THP-1	6	THP1_6h_20kX_2532.tif	1	0	0	0
THP-1	6	THP1_6h_20kX_2530.tif	0	0	1	0
THP-1	6	THP1_6h_20kX_2528.tif	0	0	1	0
1° T cell	18	primaryEV_20kX_2636.tif	1	1	0	0
1° T cell	18	primaryEV_20kX_2634.tif	0	0	0	0

1° T cell	18	primaryEV_20kX_2632.tif	1	0	0	0
1° T cell	18	primaryEV_20kX_2630.tif	0	1	0	0
1° T cell	18	primaryEV_20kX_2628.tif	1	0	0	0
1° T cell	18	primaryEV_20kX_2626.tif	1	0	0	1
1° T cell	18	primaryEV_20kX_2624.tif	0	0	0	0
1° T cell	18	primaryEV_20kX_2622.tif	1	0	0	0
1° T cell	18	primaryEV_20kX_2620.tif	1	0	0	0
1° T cell	18	primaryEV_20kX_2618.tif	1	0	0	0
1° T cell	18	primaryEV_20kX_2615.tif	1	0	0	0
1° T cell	18	primaryEV_20kX_2613.tif	1	0	0	0
1° T cell	18	primaryEV_20kX_2611.tif	2	0	0	0
1° T cell	18	primaryEV_20kX_2609.tif	1	0	0	0
1° T cell	18	primaryEV_20kX_2607.tif	1	0	0	0
1° T cell	18	primaryEV_20kX_2605.tif	1	0	0	0
1° T cell	18	primaryEV_20kX_2603.tif	0	0	0	0
1° T cell	18	primaryEV_20kX_2601.tif	0	0	0	0
1° T cell	18	primaryEV_20kX_2600.tif	1	0	0	0
1° T cell	18	primaryEV_20kX_2597.tif	1	0	0	0
1° T cell	18	PrimaryEV_20_1.tif	1	0	0	0
Jurkat	18	Jurkat18h_20kX_2525.tif	0	0	0	0
Jurkat	18	Jurkat18h_20kX_2521.tif	0	1	0	0
Jurkat	18	Jurkat18h_20kX_2519.tif	1	0	0	0
Jurkat	18	Jurkat18h_20kX_2518.tif	1	1	0	0
Jurkat	18	Jurkat18h_20kX_2515.tif	0	0	0	1
Jurkat	18	Jurkat18h_20kX_2513.tif	0	0	0	0
Jurkat	18	Jurkat18h_20kX_2511.tif	0	0	1	4
Jurkat	18	Jurkat18h_20kX_2509.tif	0	0	0	2
Jurkat	18	Jurkat18h_20kX_2507.tif	1	1	0	1
Jurkat	18	Jurkat18h_20kX_2505.tif	0	0	0	2
Jurkat	18	Jurkat18h_20kX_2503.tif	0	0	0	0
Jurkat	18	Jurkat18h_20kX_2501.tif	0	2	1	0
Jurkat	18	Jurkat18h_20kX_2499.tif	2	0	1	0
Jurkat	18	Jurkat18h_20kX_2498.tif	1	1	1	1
Jurkat	18	Jurkat18h_20kX_2495.tif	0	1	0	3
Jurkat	18	Jurkat18h_20kX_2493.tif	2	1	1	0
Jurkat	18	Jurkat18h_20kX_2491.tif	1	1	0	0
Jurkat	6	Jurkat6h_20kX_2489.tif	1	0	0	0
Jurkat	6	Jurkat6h_20kX_2487.tif	0	0	0	0

Jurkat	6	Jurkat6h_20kX_2485.tif	2	0	0	0
Jurkat	6	Jurkat6h_20kX_2483.tif	3	1	0	0
Jurkat	6	Jurkat6h_20kX_2481.tif	0	2	0	0
Jurkat	6	Jurkat6h_20kX_2478.tif	0	1	0	0
Jurkat	6	Jurkat6h_20kX_2476.tif	0	0	0	0
Jurkat	6	Jurkat6h_20kX_2474.tif	0	0	0	0
Jurkat	6	Jurkat6h_20kX_2472.tif	0	0	0	1
Jurkat	6	Jurkat6h_20kX_2470.tif	0	0	0	1
Jurkat	6	Jurkat6h_20kX_2468.tif	0	0	1	0
Jurkat	6	Jurkat6h_20kX_2465.tif	2	0	1	0
Jurkat	6	Jurkat6h_20kX_2462.tif	0	1	0	0
Jurkat	6	Jurkat6h_20kX_2460.tif	1	1	0	0
Jurkat	6	Jurkat6h_20kX_2458.tif	1	0	0	0
Jurkat	6	Jurkat6h_20kX_2456.tif	0	2	1	0
Jurkat	6	Jurkat6h_20kX_2453.tif	0	1	0	0
Jurkat	6	Jurkat6h_20kX_2451.tif	1	0	0	0

Table 7.1: Raw counts of ACdEVs categorised by shape using cryoTEM images. (1° T cell = primary human T cell).

			Multilamellar (number of bilayers)		
Cell type	**Timepoint (h)**	**filename**	**2**	**3**	**4+**
THP-1	18	THP1_18h_20kX_2594.tif	0	0	0
THP-1	18	THP1_18h_20kX_2592.tif	0	0	0
THP-1	18	THP1_18h_20kX_2590.tif	1	0	0
THP-1	18	THP1_18h_20kX_2588.tif	1	0	0
THP-1	18	THP1_18h_20kX_2586.tif	0	1	0
THP-1	18	THP1_18h_20kX_2584.tif	0	0	0
THP-1	18	THP1_18h_20kX_2582.tif	0	0	0
THP-1	18	THP1_18h_20kX_2580.tif	0	0	0
THP-1	18	THP1_18h_20kX_2578.tif	0	1	0
THP-1	18	THP1_18h_20kX_2575.tif	1	1	0
THP-1	18	THP1_18h_20kX_2573.tif	1	0	0
THP-1	18	THP1_18h_20kX_2571.tif	0	0	0
THP-1	18	THP1_18h_20kX_2568.tif	0	0	0
THP-1	18	THP1_18h_20kX_2566.tif	0	0	0
THP-1	18	THP1_18h_20kX_2564.tif	0	0	0
THP-1	18	THP1_18h_20kX_2562.tif	0	0	0
THP-1	6	THP1_6h_20kX_2534.tif	0	0	0
THP-1	6	THP1_6h_20kX_2559.tif	0	0	0
THP-1	6	THP1_6h_20kX_2556.tif	0	0	0
THP-1	6	THP1_6h_20kX_2554.tif	0	0	0
THP-1	6	THP1_6h_20kX_2552.tif	0	0	0
THP-1	6	THP1_6h_20kX_2550.tif	0	0	0
THP-1	6	THP1_6h_20kX_2548.tif	0	1	0
THP-1	6	THP1_6h_20kX_2547.tif	0	1	0
THP-1	6	THP1_6h_20kX_2544.tif	0	0	0
THP-1	6	THP1_6h_20kX_2542.tif	1	0	0
THP-1	6	THP1_6h_20kX_2540.tif	0	0	0
THP-1	6	THP1_6h_20kX_2538.tif	1	0	0
THP-1	6	THP1_6h_20kX_2536.tif	0	0	0
THP-1	6	THP1_6h_20kX_2532.tif	1	0	0
THP-1	6	THP1_6h_20kX_2530.tif	0	0	0
THP-1	6	THP1_6h_20kX_2528.tif	0	0	0
1° T cell	18	primaryEV_20kX_2636.tif	0	0	0
1° T cell	18	primaryEV_20kX_2634.tif	0	0	0
1° T cell	18	primaryEV_20kX_2632.tif	0	0	0

1° T cell	18	primaryEV_20kX_2630.tif	0	0	0
1° T cell	18	primaryEV_20kX_2628.tif	0	0	0
1° T cell	18	primaryEV_20kX_2626.tif	0	0	0
1° T cell	18	primaryEV_20kX_2624.tif	0	0	0
1° T cell	18	primaryEV_20kX_2622.tif	0	0	0
1° T cell	18	primaryEV_20kX_2620.tif	0	0	0
1° T cell	18	primaryEV_20kX_2618.tif	0	0	0
1° T cell	18	primaryEV_20kX_2615.tif	0	0	0
1° T cell	18	primaryEV_20kX_2613.tif	0	0	0
1° T cell	18	primaryEV_20kX_2611.tif	0	0	0
1° T cell	18	primaryEV_20kX_2609.tif	0	0	0
1° T cell	18	primaryEV_20kX_2607.tif	0	0	0
1° T cell	18	primaryEV_20kX_2605.tif	0	0	0
1° T cell	18	primaryEV_20kX_2603.tif	0	0	0
1° T cell	18	primaryEV_20kX_2601.tif	0	0	0
1° T cell	18	primaryEV_20kX_2600.tif	0	0	0
1° T cell	18	primaryEV_20kX_2597.tif	0	0	0
1° T cell	18	PrimaryEV_20_1.tif	0	0	0
Jurkat	18	Jurkat18h_20kX_2525.tif	0	0	0
Jurkat	18	Jurkat18h_20kX_2521.tif	1	0	0
Jurkat	18	Jurkat18h_20kX_2519.tif	0	0	0
Jurkat	18	Jurkat18h_20kX_2518.tif	0	0	0
Jurkat	18	Jurkat18h_20kX_2515.tif	0	0	0
Jurkat	18	Jurkat18h_20kX_2513.tif	0	0	0
Jurkat	18	Jurkat18h_20kX_2511.tif	0	0	0
Jurkat	18	Jurkat18h_20kX_2509.tif	0	0	0
Jurkat	18	Jurkat18h_20kX_2507.tif	0	0	0
Jurkat	18	Jurkat18h_20kX_2505.tif	0	0	0
Jurkat	18	Jurkat18h_20kX_2503.tif	0	0	0
Jurkat	18	Jurkat18h_20kX_2501.tif	0	0	0
Jurkat	18	Jurkat18h_20kX_2499.tif	0	0	0
Jurkat	18	Jurkat18h_20kX_2498.tif	0	0	0
Jurkat	18	Jurkat18h_20kX_2495.tif	0	0	0
Jurkat	18	Jurkat18h_20kX_2493.tif	1	0	0
Jurkat	18	Jurkat18h_20kX_2491.tif	0	0	0
Jurkat	6	Jurkat6h_20kX_2489.tif	0	0	0
Jurkat	6	Jurkat6h_20kX_2487.tif	0	0	0
Jurkat	6	Jurkat6h_20kX_2485.tif	0	0	0

Jurkat	6	Jurkat6h_20kX_2483.tif	0	0	0
Jurkat	6	Jurkat6h_20kX_2481.tif	0	0	0
Jurkat	6	Jurkat6h_20kX_2478.tif	0	0	0
Jurkat	6	Jurkat6h_20kX_2476.tif	0	0	0
Jurkat	6	Jurkat6h_20kX_2474.tif	0	0	0
Jurkat	6	Jurkat6h_20kX_2472.tif	0	0	0
Jurkat	6	Jurkat6h_20kX_2470.tif	0	0	0
Jurkat	6	Jurkat6h_20kX_2468.tif	0	0	0
Jurkat	6	Jurkat6h_20kX_2465.tif	0	0	0
Jurkat	6	Jurkat6h_20kX_2462.tif	0	0	0
Jurkat	6	Jurkat6h_20kX_2460.tif	0	0	0
Jurkat	6	Jurkat6h_20kX_2458.tif	0	0	0
Jurkat	6	Jurkat6h_20kX_2456.tif	0	0	0
Jurkat	6	Jurkat6h_20kX_2453.tif	0	0	0
Jurkat	6	Jurkat6h_20kX_2451.tif	0	0	0

Table 7.2: Raw counts of ACdEVs categorised by number of bilayers using cryoTEM images. (1° T cell = primary human T cell).

TRAPPC5	KHDRBS3	RGS12	DCK	EVL	MAGOH	MT-CO2
ELANE	CDC73	PIBF1	CYBB	LUC7L3	MT-ATP6	RTCB
HCLS1	DHPS	ARHGEF4	P2RY8	UQCRFS1P1	OR8H2	SETSIP
GAPT	HNRNPDL	NCF2	EIF4E2	THUMPD1	ADGRE5	ZNF500
FCGR2A	RNASEH2B	WDR54	CD38	DCTN3	HDDC2	NEK9
SRGAP2B	HNRNPUL1	HLA-F	FAM234A	FANCI	CCAR2	RACK1
TMEM41A	BTAF1	RASGEF1B	ASF1B	INPP4A	PCNP	HBS1L
ITGAX	COPS7B	TTC24	TIGAR	CMSS1	EIF1AD	SIRPB1
UBA7	LARP1B	ZDBF2	GTF3C4	NUP85	VN1R5	TYMP
COLGALT1	RPA3	BCAT1	MAP1S	RB1	MAD2L1	PTGER4
AMPD3	MRPL44	CTCFL	CNOT11	TSPAN7	STX11	
P3H1	THOC7	OAS2	RTRAF	ELP3	PPM1F	
C17orf62	PLRG1	GON4L	UCRIL	TRRAP	C1orf50	
GGACT	ABL2	CD180	BABAM2	TERF2IP	GARS1	
LGALS9B	MAEA	SLC7A3	PUM3	ITK	GCN1	
PRKCD	HIVEP3	HSDL1	CNOT9	CPSF2	ERBIN	
FAM50A	PNMA2	KIAA0586	SNRPGP15	JAM3	PLPBP	
CTSS	ZBED6CL	S1PR2	MYG1	VPS52	EMP3	
FCGR1A	LARS2	CD79A	CARMIL2	MDC1	LILRA2	
CYBA	SPC24	FKBP5	TRBC1	SPATA5L1	SSSCA1	
RCSD1	CNOT7	MLX	HDHD5	POGZ	DNPH1	
MTM1	GID8	CCDC176	WASHC4	ANAPC1	EIF2D	
NR4A3	NDUFA7	FREM1	RBM15	RNASEH2A	TRPV2	
UFC1	NUBP2	GPM6A	RNASET2	DNAH9	EMB	
GPSM3	CD3E	ISG20	SAMSN1	CNTRL	VPS13D	
RBMXL1	XYLB	RPL13AP3	RGS19	NHLRC1	FBXL7	
ERC2	ALMS1	EIF2S3B	TMEM206	TYMS	ADGRL2	
DTD1	MDN1	ATP5F1C	RAB7B	PPP4R3A	ITGA10	
GIF	SF1	NME2P1	SLC2A9	EXOSC7	ATAD1	
CSF2RA	AQR	NAPRT	C11orf73	ACAP1	TAPBP	
ASCC2	SPATA5	LCP2	PGP	LAGE3	FCGR1B	
IFI35	DCTN4	BYSL	RMDN1	VAV1	LZIC	
LSM1	COPS7A	NOP53	MARVELD1	RFC2	KYNU	
NINJ1	GATAD2A	FAM220BP	CALML3	ELP5	GMIP	
TLR2	HAUS1	ABRAXAS2	CD36	ABCA13	PDZD8	
NDUFB11	MAP4K1	TKFC	NUDT16	KIAA1524	MCEMP1	
AZU1	TELO2	IGL1	TMEM164	COG7	CA11	
XPO4	MYO7B	HGH1	DNAH8	NTPCR	APMAP	

Table 7.3: List of 232 proteins not previously reported in T cells, B cells or Monocytes by Vesiclepedia. Proteins represented as gene symbol. Analysis performed in FunRich v3.1.4 on 1.07.24

TRAPPC5	ECHDC1	COPS5	RPL34	RAB5B
ELANE	PPP2R5C	STUB1	S100A11	HSPB1
HCLS1	ATP6V1D	DPP7	ITGAL	EHD4
GAPT	ATP6V1C1	RAB22A	ERP44	KRT10
FCGR2A	PCYOX1	SSR3	QSOX1	RDX
SRGAP2B	PPA2	SLC25A1	NAPG	KRT9
TMEM41A	KDELR2	SEC23B	CD58	RAB11B
ITGAX	ZMPSTE24	OSTF1	HBB	KRT2
UBA7	CTSZ	MMP14	RPS19	RAB5A
COLGALT1	IL4I1	ERLIN1	IPO7	FSCN1
AMPD3	NLN	RAB9A	FH	BROX
P3H1	NRD1	PTP4A1	PTPRJ	IST1
C17orf62	IFITM1	GNAL	ALDH9A1	RAB6A
GGACT	SOD2	FAH	AK1	VASP
LGALS9B	BIN2	GYS1	ACSL4	RRAS
PRKCD	LACTB2	IDI1	RPL28	CBR1
FAM50A	STX6	SAR1A	NANS	CAPN1
CTSS	GGT1	CKB	AHNAK	CHMP2A
FCGR1A	FCER1G	SNRPA	TTYH3	MVP
CYBA	CHI3L1	TRIM25	SEC22B	RALB
RCSD1	SFT2D1	NUCB2	FAM129B	GSN
MTM1	PYCARD	GPX1	POTEF	PGLS
NR4A3	ATG7	CNN2	RNPEP	HRAS
UFC1	S100A4	RTCA	GGCT	CHMP4B
GPSM3	TOR1AIP1	UBE2V2	ITGB2	OTUB1
RBMXL1	SWAP70	ARL6IP5	LMNA	PLOD3
ERC2	LAIR1	BLVRB	HCK	PYGL
DTD1	ITGAM	CYBRD1	TSTA3	IDH1
GIF	CES1	YKT6	LGALS1	CAB39
CSF2RA	TMCO1	TMX1	LASP1	CAPN2
ASCC2	SAR1B	TMED5	TMED2	COTL1
IFI35	MTCH2	HDGF	NDRG1	TSPAN14
LSM1	ASNA1	NAGK	LMAN2	HSD17B4
NINJ1	PPIH	ZDHHC5	MYADM	DNM2
TLR2	PVR	RNF123	AP3B1	RHOC
NDUFB11	TMEM30A	MYO1F	SSR4	CD99
AZU1	SNX1	TXNDC12	CHP1	PLXNB2
XPO4	RAB32	ALDH2	VAMP8	BLVRA
RBM15	SRP72	TMEM33	S100A9	SERPINB1
RNASET2	SNX3	SSR1	PLSCR1	RAB13
SAMSN1	PLEK	PTGES2	RAB18	ATP1B1
RGS19	LMNB2	SEC11A	ERLIN2	DLST
TMEM206	GMFB	CORO1B	UBE2V1	AKR1A1
RAB7B	VKORC1L1	ARHGAP1	ANPEP	KRT1
SLC2A9	SART1	PPP3CA	SKP1	CREG1
C11orf73	SH3KBP1	FAM129A	STAT1	APOA1BP
PGP	TCEB2	TNFAIP2	CPNE2	HIST1H2BA
RMDN1	SAE1	DPP9	RRAS2	HSPA1B
MARVELD1	MRPL12	DTYMK	CD276	LGALS8
CALML3	SAMHD1	API5	RAB4A	RAB27A
CD36	MESDC2	RAB23	EFHD2	CD44
NUDT16	ADRBK1	UROD	S100A8	SLC30A1
TMEM164	SDF2L1	OSBP	ITGA5	TIMP3

EMP3	TPCN1	ME1	UGGT1	HSPA1A
LILRA2	UCHL5	SEC61A1	RPL32	MFSD10
SSSCA1	DUSP3	MPP1	UBE2M	
DNPH1	SLC8A1	G3BP1	SERPINB6	
EIF2D	DDX3Y	PPT1	STXBP2	
TRPV2	PSMB10	SPCS2	STT3A	
EMB	KCMF1	SLC19A1	NSF	
VPS13D	ITPA	PRCP	EFR3A	
FBXL7	DIRAS2	SH3BGRL	MOGS	
ADGRL2	ARGLU1	PSMD4	TMED9	
ITGA10	MEF2D	EML4	GFAP	
ATAD1	PPP2R5D	CD14	PITPNB	
TAPBP	ARL8B	IMPA1	HMBS	
HBS1L	PABPC3	AP1M1	RAB31	
SIRPB1	EIF1AX	EIF4B	LIMS1	
TYMP	PAK2	NAGA	STK24	
PTGER4	AGTRAP	CPM	SPCS3	
CA11	NUCKS1	OPA1	RHEB	
APMAP	MAN2B1	GNS	CKAP4	
FCGR1B	CPPED1	FCGRT	CLEC11A	
LZIC	PPCS	QPRT	PIK3R1	
KYNU	FN3KRP	SEC24A	PTPN6	
GMIP	P2RY2	TIPRL	SNX6	
PDZD8	GPX4	TPP1	GPC1	
MCEMP1	THBD	GBA	HIST3H3	
DNAH8	CDC42BPA	INSR	DNASE1L1	
HGH1	MMP9	HTATIP2	TFG	
NAPRT	ABHD8	BRI3BP	CD70	
LCP2	BST1	DECR1	SCAMP3	
BYSL	RPE	CTSG	SERBP1	
NOP53	TK1	DNAJC5	THOP1	
FAM220BP	PRTN3	APLP2	CD109	
ABRAXAS2	DCPS	GAA	MYOF	
TKFC	DERL1	ZYX	CA2	
IGL1	CPSF7	EIF2A	TMEM189-UBE2V1	

Table 7.4: List of 407 THP-1 monocyte cell line-specific proteins. Proteins represented as gene symbol.

KHDRBS3	PMPCA	PDCD10	ARID1A	UCRIL
CDC73	NUDT5	HIST1H1A	PPIL1	BABAM2
DHPS	IPO11	GOT2	COX5A	PUM3
HNRNPDL	U2AF2	CARS	RNPS1	CNOT9
RNASEH2B	RBMX	PCMT1	ZZEF1	SNRPGP15
HNRNPUL1	MMS19	MYO1B	ALYREF	MYG1
BTAF1	TNPO3	ABCE1	PRAF2	CARMIL2
COPS7B	H1FX	KPNA2	DLAT	TRBC1
LARP1B	AP2S1	ASNS	NOP58	HDHD5
RPA3	SRSF10	MAP4K4	KIAA2013	WASHC4
MRPL44	PDCD5	MTOR	ZAP70	RAP1B
THOC7	GALNT2	PPP1CB	ZC3HAV1L	HLA-A
PLRG1	NCBP1	SSRP1	HDHD2	TXN
ABL2	EXOC7	HSPE1	DENND2D	FLNA
MAEA	CYB5B	PLS1	VAMP1	CPNE3
HIVEP3	ACOX1	BUB3	EPHX2	ENO2
PNMA2	NXN	GNB4	PDS5B	ACTR1A
ZBED6CL	BAG6	MATR3	VPS13A	RPL30
LARS2	HDAC2	SNRPD2	UBE4A	MYH10
SPC24	ACADM	DLD	HS2ST1	MFGE8
CNOT7	HAT1	PYCRL	SMARCC1	PSMC2
GID8	FUBP1	HSD17B10	ADAR	PLEC
NDUFA7	EFHD1	NCKAP1L	RFC5	DIP2B
NUBP2	RSL1D1	DDAH2	RFC3	PFKP
CD3E	HAGH	MYO1G	PRKAG1	CORO1C
XYLB	STK25	PRKAR1A	CELF1	PSMD5
ALMS1	RPL36A	NMT1	FKBP15	TUBB4A
MDN1	VAMP5	DCTN1	PSPC1	PSMC5
SF1	ICAM2	TOP2B	CPD	SHMT2
AQR	COPS2	SLC4A7	PPM1G	ACOT7
SPATA5	HPCAL1	LYPLA2	IKBKAP	LCK
DCTN4	WDR82	KTN1	ASPM	HNRNPF
COPS7A	SPTLC1	CSNK2B	TARBP1	PPP1CA
GATAD2A	MCM7	COPG2	FBL	PSMG1
HAUS1	GSTM1	FKBP1A	PYCR1	DRG1
MAP4K1	U2AF1	XPOT	PAPSS1	AGL
TELO2	ATP6V1H	STRAP	RPP30	ADA
MYO7B	COX5B	MPST	KDM1A	TRIM28
THUMPD1	SHPK	IPO4	HLA-H	UBA6
DCTN3	NAT10	DCTN2	CD2	MPZL1
FANCI	CARHSP1	PPID	SNRPF	SORT1
INPP4A	ARL8A	ROCK2	MTA1	PFDN4
CMSS1	GNAO1	NAA15	IGF2BP1	
NUP85	CDK5	UPF1	GTPBP4	
RB1	STRBP	ALDH18A1	RFC1	
TSPAN7	SRRT	SHMT1	EXOSC6	
ELP3	TBCD	YARS	DPY30	
TRRAP	RAD50	CUL2	MRPS26	
TERF2IP	CTH	NOP56	RBM8A	
ITK	PML	WDR77	MOV10	
CPSF2	PRPSAP1	RPA1	FAM98B	
JAM3	DDX23	MACF1	PRPF4B	
VPS52	USP39	SFXN1	NOLC1	

MDC1	SNRNP40	DOCK2	SUPT16H	
SPATA5L1	TRA2A	MYO18A	CUTA	
POGZ	THOC2	MPP6	KIF23	
ANAPC1	PANX1	GNPNAT1	SNRPD1	
RNASEH2A	DDX47	TUBG1	ANXA3	
DNAH9	XPO5	DDX5	PIP4K2A	
CNTRL	WDR12	LRRC59	EIF2S3	
NHLRC1	SYNGR1	SNRPE	CLINT1	
TYMS	PLCG1	RPIA	C7orf50	
PPP4R3A	PRPSAP2	ATP5J2	TSR1	
EXOSC7	CXCR4	GOLGA3	CCDC47	
ACAP1	SRPK1	IMMT	TCEA1	
LAGE3	SRSF6	COPS6	THOC5	
VAV1	POLR2H	TARDBP	TRIP13	
RFC2	RALYL	DNAJB1	PAFAH1B2	
ELP5	THOC6	TMEM109	PEF1	
ABCA13	FXR1	RAD23A	ETFA	
KIAA1524	PPP2R5E	TSN	DDX3X	
COG7	TAF15	PI4KA	GLG1	
NTPCR	ISOC1	SLC38A2	RAC3	
ASF1B	SIT1	LETM1	HNRNPL	
TIGAR	FKBP3	FMNL1	NF1	
GTF3C4	STAU1	BTF3	CHD4	
MAP1S	HTATSF1	RNF213	TOMM22	
CNOT11	DIABLO	GNE	CDK2	
RTRAF	ACTL6A	DOCK7	TUFM	

Table 7.5: List of 358 Jurkat T cell line-specific proteins. Proteins represented as gene symbol.

RGS12	HIST1H3H	MC1R
PIBF1	HIST1H3B	IGHM
ARHGEF4	HIST1H3E	HLA-DRB3
NCF2	HIST1H3C	SLC6A6
WDR54	HIST1H3I	TEX10
HLA-F	FGB	CD86
RASGEF1B	MYL6B	MAT2B
TTC24	RAP2A	CD79B
ZDBF2	HIST1H3D	PELP1
BCAT1	GSS	IGKC
CTCFL	FGG	MME
OAS2	FGA	NDRG3
GON4L	ACTR1B	CD19
CD180	HMGCS1	CD22
SLC7A3	TUBA4A	ECE1
HSDL1	TUBB3	SLC38A5
KIAA0586	ST13	SORL1
S1PR2	ATP2B1	PODXL
CD79A	HIST1H1C	LSP1
FKBP5	HLA-DRB1	CD74
MLX	SLC44A2	HLA-DQB1
CCDC176	BASP1	FAS
FREM1	HIST1H1D	MS4A1
GPM6A	STX7	H3F3C
ISG20	HIST1H2AD	HLA-DPB1
RPL13AP3	HIST1H3A	HLA-DQA1
EIF2S3B	GLUD1	CD37
ATP5F1C	SLC25A6	BCAP31
NME2P1	HIST1H3J	RFTN1
HIST1H3F	HIST1H3G	

Table 7.6: List of 89 Mutu B cell line-specific proteins. Proteins represented as gene symbol.

GAPDH	ABCC1	EIF3B	CCT4	RPL4	ITGB1
ACTB	CDC37	PSMB4	RPS3	XRCC5	PSMB3
CD81	EPB41L2	RPS9	TLN1	RAB11A	UBA1
HSPA8	CNDP2	RPS27A	SLC1A5	SLC16A1	GNAI2
CLTC	SF3B3	DYNC1H1	RUVBL1	WDR1	SLC2A1
LDHA	PSMD1	HNRNPA2B1	CAP1	EEF1D	CCT6A
HSP90AA1	DDB1	ALDOC	RPS18	LNPEP	GNB1
ENO1	ECH1	RHOG	HSP90B1	SLC44A1	HSPA5
YWHAZ	EIF3F	RPL6	PDCD6	2-Sep	ARF1
PKM	SSB	EPRS	HNRNPK	HPRT1	KPNB1
HIST2H4A	PRMT1	RPS13	ARPC4	ATP5A1	SLC3A2
HIST1H4I	HADH	IARS	ANXA11	ARHGDIA	RALA
EZR	RPL10	RAC1	PEBP1	SPTAN1	CAND1
ALB	AKR1B1	PA2G4	OLA1	RPL18	CCT8
CFL1	NACA	HSPA4	EEF1G	TPP2	HSPD1
AHCY	EIF3K	RPS15A	GANAB	MTHFD1	GDI2
TFRC	LARS	RPL9	RAC2	IPO5	PSMB6
RAB5C	TNPO1	EIF2S1	PPIB	RPS6	RUVBL2
HIST4H4	NAP1L4	SLC1A4	PSMD2	STIP1	TAGLN2
YWHAE	SFPQ	RPS7	ACTR3	TALDO1	PSMA4
PRDX1	ATP5O	NAP1L1	FLNB	CYFIP1	RAB7A
HIST1H4H	EFTUD2	EIF3I	PSMA1	DHX9	RHOA
HIST1H4F	VDAC2	CS	ARPC2	P4HB	RPS16
HIST1H4A	ADSS	GLO1	NME1	RPS24	RPS8
LDHB	DPP3	VARS	PDIA3	MYL6	PRDX2
HIST1H4D	DDX17	ATP1B3	GNAI3	CSE1L	EIF4A1
PGK1	PSMD14	EIF4A2	RPL15	HNRNPR	YWHAB
HIST1H4C	F5	RPL17	NAPA	SOD1	RPSA
ATP1A1	PRPF8	HNRNPD	RPL12	PSMC6	PGD
HIST2H4B	FDPS	RPL19	RPL7A	SYNCRIP	GSTP1
HIST1H4B	NPTN	RPL27	PDIA6	ARF6	ATP5B
HIST1H4L	SF3B1	PPA1	ATIC	PARK7	CCT7
HIST1H4J	SLC25A3	RPL8	LCP1	NPM1	CCT3
HIST1H4K	MCM4	RPL10A	PPP2R1A	APRT	PSMB2
ACLY	PGM1	PECAM1	PSMB1	NCL	RAB2A
CCT2	ITGA4	PCNA	ATP6V1A	RPS25	PGAM1
HIST1H4E	APEX1	PSME2	DARS	PSMD6	MDH1
EEF1A1	ALCAM	RPL11	ACTR2	RPL13	SNAP23
MYH9	PAFAH1B3	HNRNPH1	HNRNPC	RPL7	NRAS
TCP1	YBX1	CALR	MDH2	PARP1	PRDX6
FASN	TMED10	ARHGDIB	EHD1	PNP	TKT
MSN	RPS15	RPL5	RPS3A	XRCC6	PSMA5
TPI1	PSME3	VTN	CAPZB	CAPZA1	IQGAP1
ANXA5	DHX15	ARPC3	RPS2	IMPDH2	RPLP0
HSP90AB1	PRDX3	EIF3A	RPS4X	ACAT2	TUBB4B
PSMA7	NUDC	SYNGR2	STX4	ATP6V1B2	PSME1
BSG	PRMT5	H2AFY	VDAC1	NUMA1	DCTPP1
PAICS	FARSB	APEH	EIF3M	HNRNPA0	MCM2
TUBB	RPLP1	SLC7A5	RPS17	DDX1	DKC1
VCP	PLIN3	SND1	COPS4	SCAMP2	TPR
ALDOA	EIF3H	PSMD11	RPS10	ATP5F1	KHDRBS1
GNAS	AIMP1	HSPH1	PDIA4	ATP5H	SNRPB
RAB1B	RPS23	SLC29A1	HNRNPA1	NONO	PSMG2

YWHAQ	PPP1R7	SLC25A5	ADSL	RRM1	SF3A1
GPI	SNRNP70	PSMD13	CORO1A	HMGB2	RPLP0P6
EEF2	RPS12	AK2	PRDX4	TSNAX	DUT
ACTN4	RCC2	RPS20	PTPRC	ELAVL1	EEA1
YWHAG	MOB1A	ACTA2	RPL14	NASP	ATP5C1
PSMA6	STMN1	PPP2CA	KARS	CAPRIN1	ILF3
CCT5	ARPC5	RAB21	SNRNP200	PFDN2	FUS
RAB14	HNRNPA3	PSMD7	PTBP1	EIF3CL	UBE2L3
CLIC1	RBBP4	ILF2	RPS26	TNFAIP8	**MT-CO2**
RAB10	BLMH	RPL27A	PSMB8	ELMO1	**RTCB**
CDC42	CD47	CPNE1	7-Sep	SLC43A3	**SETSIP**
PPIA	SLC7A1	XPO1	RPL22	NUDT21	**ZNF500**
PFN1	PLP2	NPEPPS	ARPC1B	ANP32B	**NEK9**
RAN	HMGA1	RARS	EIF3E	MCM3	**RACK1**
ANXA6	PHB2	PRKDC	EIF3L	EIF4E	
PSMA2	RPL29	EEF1B2	SYPL1	LMNB1	
PSMA3	COPS8	MARCKSL1	RPL26L1	MAPRE1	

Table 7.7: List of 417 proteins conserved in ACdEVs from immune cell lines: Jurkat T cells, THP-1 monocytes and Mutu B cells. All proteins, except six (highlighted in bold), were previously reported in Vesiclepedia (Pathan *et al.,* 2017). Proteins represented as gene symbol.

Gene symbol	Protein	Protein family
ANXA11	Annexin A11	Annexin family
ANXA5	Annexin A5	Annexin family
ANXA6	Annexin A6	Annexin family
BSG	Basigin	Basigin family
CDC42	Cell division control protein 42 homolog	Small GTPase superfamily, Rho family
GDI2	Rab GDP dissociation inhibitor beta	Rab GDI family
GNAI2	Guanine nucleotide-binding protein G(i) subunit alpha-2	G-alpha family, G(i/o/t/z) subfamily
GNAS	Neuroendocrine secretory protein 55	Chromogranin / NESP55 family
GNB1	Guanine nucleotide-binding protein subunit beta-like protein 1	G-beta family
HSP90AB1	Heat shock protein HSP 90-beta	Heat-shock protein 90 family
IQGAP1	Ras GTPase-activating-like protein IQGAP1	IQGAP family
KPNB1	Importin subunit beta-1	Karyopherin / importin beta family
RALA	Ras-related protein Ral-A	Small GTPase superfamily, Ras family
RHOA	Transforming protein RhoA	Small GTPase superfamily, Rho family
SLC3A2	Amino acid transporter heavy chain SLC3A2	SLC3A transporter family
TFRC	Transferrin receptor protein 1	Peptidase M28 family

Table 7.8: 16 proteins listed in the top 100 most reported proteins in Vesiclepedia that were also identified in the list of proteins narrowed down by cellular component and biological process gene ontology analysis. Analysis performed in FunRich v3.1.4 on 1.07.24.

Gene symbol	Protein	Protein family
ALB	Albumin	ALB/AFP/VDB family
ARF1	ADP-ribosylation factor 1	Small GTPase superfamily, Arf family
ARF6	ADP-ribosylation factor 6	Small GTPase superfamily, Arf family
ATP1A1	Sodium/potassium-transporting ATPase subunit alpha-1	Cation transport ATPase (P-type) family
ATP1B3	Sodium/potassium-transporting ATPase subunit beta-3	Potassium ATPases subunit beta family
CLIC1	Chloride intracellular channel protein 1	Chloride channel CLIC family
EHD1	EH domain-containing protein 1	TRAFAC class dynamin-like GTPase superfamily
GNAI3	Guanine nucleotide-binding protein G(i) subunit alpha-3	G-alpha family, G(i/o/t/z) subfamily
HSPD1	60 kDa heat shock protein, mitochondrial	HSP60 chaperonin family
NRAS	GTPase NRas	Small GTPase superfamily, Ras family
RAC1	Ras-related C3 botulinum toxin substrate 1	Small GTPase superfamily, Rho family
RAC2	Ras-related C3 botulinum toxin substrate 2	Small GTPase superfamily, Rho family
RHOG	Rho-related GTP-binding protein RhoG	Small GTPase superfamily, Rho family
SEPT2	Septin-2	Septin GTPase family
SLC43A3	Equilibrative nucleobase transporter 1	SLC43A transporter family
RAB14	Ras-related protein Rab-14	Small GTPase superfamily, Rab family

Table 7.9: 16 proteins that are members of the same protein families as the top 100 most reported proteins in Vesiclepedia were also identified in the list of proteins narrowed down by cellular component and biological process gene ontology analysis. Analysis performed on 1.07.24.

Gene symbol	Protein	Protein family	UniProt subcellular location
AIMP1	Aminoacyl tRNA synthase complex-interacting multifunctional protein 1	AIMP family	'Nucleus' 'Cytoplasm, cytosol' 'Secreted' 'Endoplasmic reticulum' 'Golgi apparatus'
CAPRIN1	Cell cycle associated protein 1	Caprin family	'Cytoplasm' 'Cytoplasm, cytosol'
CSE1L	Exportin-2	XPO2/CSE1 family	'Cytoplasm' 'Nucleus'
EEA1	Early endosome antigen 1		'Cytoplasm'
PEBP1	Phophatidylethanolamine-binding protein 1	PEBP family	'Cytoplasm'
PLIN3	Perilipin 3	Perilipin family	Cytoplasm' 'Lipid droplet' 'Endosome membrane'
PPP2CA	Serine/threonine-protein phosphatase 2A catalytic subunit alpha isoform	PPP Phosphatase family	'Cytoplasm' 'Nucleus' 'Chromosome' 'Centromere' 'Cytoskeleton' 'Spindle pole'
PPP2R1A	PPP2R1A-PPP2R2A-interacting phosphatase regulator 1	FAM122 family	'Cytoplasm' 'Nucleus'
SCAMP2	Secretory carrier-associated membrane protein 2	SCAMP family	'Golgi apparatus' 'Recycling endosome membrane'
SLC25A3	Solute carrier family 25 member 3	Mitochondrial carrier (TC 2.A.29) family	'Mitochondrion inner membrane'

Table 7.10: 10 proteins were excluded based on their predicted cellular localisation being reported intracellular only.

Jurkat T cell	THP-1 monocyte	Mutu B cell
ICAM1	CD276	CD19
IGSF8	PECAM1 (CD31)	BSG
BSG	FCGR2A	ALCAM (CD166)
ALCAM (CD166)	CD58	NPTN
JAM3	FCGR1A	ICAM3
NPTN	NPTN	CD79B
PECAM1 (CD31)	ICAM1	CD22
ICAM3	ALCAM (CD166)	IGSF8
CD47	LAIR1	PECAM1 (CD31)
	LILRA2	CD47
	BSG	
	EMB	
	SIRPB1	
	FCGR1B	
	CD47	
	PVR	
	TAPBP	

Table 7.11: List of proteins identified in ACdEVs derived from each cell line that are members of the Immunoglobulin superfamily (IgSF) (L. R. Grant, 2022). According to gene ontology analysis for protein domains using annotations ‘IG’ and ‘IG-like’. Proteins represented as gene symbol.